UNIVERSITE DE LIEGE

FACULTES DES SCIENCES

DEPARTEMENT DE GEOLOGIE

Early Life Traces & Evolution-Astrobiology Lab

UR ASTROBIOLOGY

Biostratigraphie, paléoécologie et évolution thermique du Supergroupe Mésoprotérozoïque de Mbuji-Mayi, RdCongo.

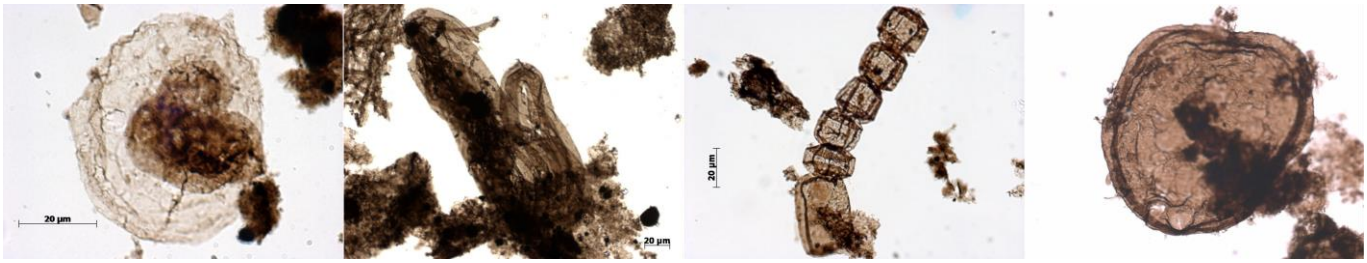

Thèse de doctorat

présentée pour l'obtention du grade de docteur en sciences

Par

B. KABAMBA BALUDIKAY

Février 2019

UNIVERSITE DE LIEGE

FACULTES DES SCIENCES

DEPARTEMENT DE GEOLOGIE

Early Life Traces & Evolution-Astrobiology lab

UR ASTROBIOLOGY

Biostratigraphie, paléoécologie et évolution thermique du Supergroupe Mésoprotérozoïque de Mbuji-Mayi, RdCongo.

Thèse de doctorat

présentée pour l'obtention du grade de docteur en sciences

Par

B. KABAMBA BALUDIKAY

Soutenance publique du 07 Février 2019 devant le jury composé de :

Prof. Frédéric BOULVAIN (Université de Liège)	Président
Dr. Camille FRANÇOIS (Université de Liège)	Secrétaire
Prof. Emmanuelle JAVAUX (Université de Liège)	Promotrice
Dr. Max FERNANDEZ-ALONSO (MRAC, Tervuren)	Membre
Prof. Valentin KANDA NKULA (Université de Kinshasa)	Membre
Dr. Marc VANZUILEN (Institut de Physique du Globe de Paris)	Membre

Cette recherche a reçu le financement de :

Conseil Européen de la Recherche, ERC StG ELITE.

Belgian Science Policy, projet PAI PLANET TOPERS.

Research Fondation Flanders et Fonds National de la Recherche Scientifique, projet EOS ET-HOME.

« *La nature réelle d'une forme de vie ne se trouve pas dans la vie elle-même mais plutôt dans le pourquoi de cette forme de vie* »

Sagesse africaine.

Aux ancêtres, aux loas, je dédie ce travail.

Shikamoo !

Remerciements

À vous chers lecteurs qui vous apprêtez à lire ce document. Que vous le survoliez, le décortiquiez avec minutie, ou que vous vous arrêtiez à cette section, je vous remercie de l'intérêt que vous lui portez.

Je tiens à remercier tous ceux qui, de près ou de loin, ont pu contribuer à l'aboutissement de cette oeuvre.

Avant toute chose, je tiens à remercier ma promotrice, Professeur Emmanuelle Javaux qui est à l'initiative de l'ébauche du projet de recherche développé dans cette thèse. Emmanuelle, avec toi, j'ai découvert que le doctorat c'est avant tout une expérience professionnelle, dans une équipe et avec un projet de recherche. J'ai appris bien plus, tant professionnellement que personnellement. Je te remercie pour la confiance que tu m'as accordée aux prémices de cette thèse. Tu as su croire en moi, quand tout n'était encore qu'une idée vague. Tu m'as offert l'opportunité de grandir scientifiquement en me permettant d'évoluer au sein d'une une équipe pétrie des compétences. Pour tout ça, je te suis reconnaissant. Merci pour ton humanité et pour tous ces colloques à l'étranger qui m'ont permis non seulement d'accroître mes compétences transversalles, mais aussi de découvrir le monde.

Ma gratitude va également à l'endroit du Professeur Valentin Kanda pour l'estime qu'il a porté à ma personne, en permettant le contact avec Madame Javaux, via ses connections avec le Musée Royal d'Afrique Centrale (MRAC). Au travers de sa personne, je remercie tous mes formateurs. Sans eux, je suis persuadé que je n'allais pas réussir ce que j'ai réussi aujourd'hui. On dit chez moi « La force d'un baobab se trouve dans ses racines ».

Je remercie le MRAC (Musée Royal d'Afrique Centrale) pour avoir permis l'accès aux sondages d'où proviennent les roches étudiées. Un merci particulier à Daniel Baudet pour son accompagnement lors de différentes séries d'échantillonnage et surtout pour toutes les informations nécessaires fournies pendant nos multiples échanges.

Merci aux membres de mon comité de thèse, Emmanuelle Javaux, Daniel Baudet, Jean-Yves Storme, Camille François et Marie Catherine Sforna, pour leur suivi et leurs précieux conseils durant des multiples discussions, lesquelles d'année en année ont conduit à l'amélioraton de mes travaux de recherche. Mais aussi pour la lecture de ce manuscrit ainsi que

les conseils qui ont permis d'affiner sa rédaction. Et merci à mon jury de thèse qui permettra l'aboutissement de cette rédaction.

La réalisation de ce doctorat n'aurait pas été possible sans le soutien financier du Conseil Européen de la Recherche via les fonds alloués aux projets du Prof. E. Javaux ERC StG ELITE (Early Life Traces, Evolution, and Implications for Astrobiology), BELSPO PAI PLANET TOPERS et FRS-FNRS-FWO EOS ET-HOME, que je remercie.

Ce travail a nécéssité la participation de plusieurs personnes lors des différents travaux en laboratoire. Ainsi, que Marcella Giraldino, Joël Laval, Dan Asael, Nathalie Fagel, François Fontaine, Elisa Peugler (Université de Liège), Romain Guilbaud (University of Leeds), Vinciane Debaille (Université Libre de Bruxelles), Olivier Rouxel (Institut Français de Recherche pour l'Exploitation de la Mer, IFREMER), Donka Macherey, Bernhard Krooss et Ralph Littke (Aachen University), trouvent ici, l'expression de ma reconnaissance pour leurs interventions dans la préparation des échantillons, la confection des lames (palynologiques et pétrographiques) et dans différentes analyses géochimiques.

Je tiens particulièrement à remercier l'ensemble du personnel (retraités et actifs) des laboratoires « Eddy Lab » et « Early Life Lab » sans qui l'ambiance agréable de travail dans laquelle j'ai évolué ne serait pas ce qu'elle est, notamment grâce à l'humour de Joël Laval qui égaie les pauses-café. Je remercie également les charmantes et joviales secrétaires du Département (Joëlle Schmetz et Mariella Guadagnano) pour m'avoir accompagné dans des multiples démarches adminstratives, tant au niveau de l'Université que de l'Office des étrangers. Merci à Yohan Cornet, avec qui j'ai partagé le bureau pendant cinq ans, pour avoir supporté mon caractère flégmatique et ennuyeux à la fois.

Enfin, à tous mes amis et proches parents, merci pour vos encouragements et assistance. À ma famille, mon épouse et mes deux filles, merci de colorer ma vie. Sans vous, la vie n'aurait aucun sens. Lubanda, merci d'être toujours à mes côtés et de me comprendre tellement bien. Merci pour tes encouragements, ton dévouement, ta patience, pour avoir rendu cette thèse réalisable, et pour tout ce que tu m'apportes au quotidien. Meji-Jade et Afya, merci pour toute la joie infinie que vous m'apportez chaque jour. À tous, merci d'embellir ma vie et déjà merci pour les merveilleuses années à venir !

Résumé

Comprendre l'origine, l'évolution et la distribution de la vie dans l'Univers – objet d'étude de l'astrobiologie – nécessite une connaissance sans équivoque des différentes étapes de l'évolution de la vie sur Terre, la seule planète dans laquelle, pour l'instant, l'existence de la vie est une évidence absolue. Cela requiert l'apport de plusieurs disciplines scientifiques (biologie, géologie, géochimie, géophysique, micropaléontologie, …) dans la production des données relatives au Précambrien, période dans laquelle la vie est apparue sur Terre et a connu ses premières étapes d'évolution.

Cette étude est focalisée sur une période clé de la diversification d'un des trois domaines de la vie, les eucaryotes, au Protérozoïque. Elle présente les résultats sur la micropaléontologie, la paléoécologie, la chimiostratigraphie et la géothermométrie du Supergroupe de Mbuji-Mayi, situé en République Démocratique du Congo. Cette séquence sédimentaire est datée entre 1065 et 1000 Ma (fin du Mésoprotérozoïque).

Les résultats obtenus à l'aide de diverses analyses (microscopie optique, spectrométrie de masse, microspectroscopie Raman, XRD, réflectance du bitume solide et TAI) révèlent : (1) un assemblage bien préservé et diversifié de microfossiles à paroi organique, constitué de 49 taxa dont 11 eucaryotes unicellulaires et multicellulaires. Cet assemblage est semblable à d'autres assemblages contemporains connus ailleurs dans le monde, ce qui implique une connexion avec les autres bassins océaniques et permet de préciser la biostratigraphie du Protérozoïque ; (2) une stratification des eaux en zones oxique, anoxique ferrugineux et anoxique sulfidique (euxinique) pendant le dépôt du Supergroupe de Mbuji-Mayi ; (3) une abondance des eucaryotes et une meilleure préservation et peut-être habitats dans les environnements proximaux anoxiques et ferrugineux ; (4) des variations de $\delta^{13}C_{carb}$ semblables aux variations contemporaines enregistrées ailleurs dans le monde ; (5) une similarité entre les différentes gammes d'estimation de températures issues des géothermomètres Raman, de la réflectance du bitume solide ou de l'indice de Kübler des argiles. Ceci a permis de montrer que l'extraction du kérogène par attaque acide ne modifie pas son signal chimique. Cette diversité modérée des eucaryotes à ~ 1065 Ma permet de reculer la grande diversification des premiers eucaryotes généralement estimée à 800 Ma, et de montrer qu'elle a eu lieu aussi en Afrique.

Abstract

Understanding the origin, evolution and distribution of life in Universe - the subject of astrobiology - requires unambiguous knowledge of the different stages of evolution of life on Earth, the only planet where, for the moment, the existence of life is an absolute evidence. This requires the contribution of several scientific disciplines (biology, geology, geochemistry, geophysics, micropaleontology ...) in the production of data relating to the Precambrian, period during which life appeared on Earth and knew its first stages of evolution.

This study focusses on a key period of life evolution, and in particular the diversification of early eukaryotes, during the Proterozoic. It presents the results on the micropaleontology, palaeoecology, chemostratigraphy and geothermometry of the Mbuji-Mayi Supergroup, located in the Democratic Republic of Congo. This sedimentary sequence is dated between 1065 and 1000 Ma (late Mesoproterozoic).

The results obtained using conventional analyzes (optical microscopy, mass spectrometry, Raman microspectroscopy, XRD, solid bitumen reflectance and TAI) reveal: (1) a well-preserved assemblage of organic-walled microfossils, consisting of 49 taxa of which 11 unicellular and multicellular eukaryotes. This assemblage is similar to other contemporaneous assemblages known elsewhere in the world, impliyng a connection with the other oceanic basins, and permitting to improve Proterozoic biostratigraphy ; (2) a redox stratification of ocean water into oxic, anoxic iron-rich and anoxic sulfidic-rich zones during the deposition of the Mbuji-Mayi Supergroup; (3) an abundance and better preservation and perhaps habitats of eukaryotes in proximal anoxic and iron-rich environments; (4) $\delta^{13}C_{carb}$ variations similar to contemporaneous variations elsewhere in the world; (5) a similarity between the different ranges of temperature estimates from Raman geothermometers, solid bitumen reflectance or Kübler index obtain on clays. This has shown that extraction of kerogen by acid attack does not alter its chemical signal. This moderate diversity of eukaryotes at ~ 1065 Ma makes it possible to set back the great diversification of the first eukaryotes which is generally estimated at 800 Ma, and to show that it also happened in Africa.

Table des matières

Avant-propos

Depuis la nuit des temps, l'homme a toujours été fasciné par des questions existentielles. Parmi celles-ci, il y en a qui ramènent aux questionnements sur l'origine de la vie : **d'où vient la vie ? Comment et quand est-elle apparue sur Terre ?** Dans sa quête, nombre de réponses furent alors proposées allant du créationnisme (empreint des religions) à l'évolutionnisme (basé sur des vérités factuelles observables dans la nature). Force est de constater que l'homme n'est toujours pas capable de dire avec certitude quand la vie est apparue sur Terre ni où et comment. Néanmoins, grâce aux multiples traces de vie récupérées dans des roches bien datées provenant des différents endroits de la Terre, l'homme est capable de reconstituer le puzzle permettant de comprendre l'évolution de la vie et le contexte dans lequel cela s'est opéré. La reconstitution de ce fameux puzzle requiert une part importante des données relatives aux premières formes de vie. Car on sait que la vie s'est transformée au cours du temps et qu'elle n'a pas toujours été semblable à ce qu'elle est aujourd'hui.

Les traces laissées par les premières formes de vie, révèlent que la vie, dans sa forme cellulaire la plus simple, est apparue au Précambrien. Le Précambrien est un intervalle des temps compris entre la fin de l'accrétion de la Terre (4,56 Ga) et l'explosion de la vie macroscopique cambrienne (0,54 Ga). Cependant, retracer l'évolution de la vie précambrienne constitue un réel défi. C'est pourquoi plusieurs disciplines scientifiques sont mises à contribution et un panel d'outils a été établi pour permettre d'identifier les traces de vie précambrienne. Ces outils sont repartis en quatre catégories : (i) le fractionnement isotopique de certains éléments essentiels à la vie (C, S, N, Fe) ; (ii) les biomarqueurs lipidiques (molécules fossiles) ; (iii) les structures biosédimentaires et (iv) les microfossiles. Toutefois, l'usage, même combiné, de ces outils n'est pas toujours gage des interprétations univoques, surtout dans des roches précédant le Protérozoïque (> 2,5 Ga).

En effet, la biosphère de l'Archéen est très discutée contrairement à celle du Protérozoïque. Mojzsis et al., (*1996*) ont avancé que la vie serait apparue vers 3,85 Ga, après le bombardement tardif intense, en se basant sur la composition isotopique du carbone des roches d'Isua (~3,8 Ga, Groenland) et d'Akilia (3,85 Ga, Groenland). Ces interprétations sont actuellement contestées, car la nature sédimentaire de ces roches fortement métamorphisées est très discutée ; d'autant plus que les processus métasomatiques, liés au métamorphisme, sont à

mêmes de produire la même signature isotopique par décrépitation de la sidérite (*Lepland et al., 2002; Van Zuilen et al., 2002*). Il y a également les cas de structures biosédimentaires et autres microfossiles putatifs, rencontrés dans les Cherts du Strelley Pool (Australie) et de la ceinture de roches verste de Barberton (Afrique du Sud) datés de ~3,54 à 3,2 Ga (*Allwood et al., 2006, 2007; Duda et al., 2016; Sugitani et al., 2010; Tice and Lowe, 2004*), pour lesquels la nature biogénique est loin de faire l'unanimité (*Garcia-Ruiz et al., 2003, 2009; Kerr, 2003*). Des biomarqueurs provenant des roches datées de ~2,7 à 2,5 Ga, et attribués à des bactéries et à des eucaryotes (*Brocks et al., 2003*) ont également été remis en question (*Rasmussen et al., 2008*).

De tous ces outils, seuls les microfossiles (ou fossiles) fournissent des preuves directes des premières formes de vie. Ils permettent également de suivre dans le temps, les différentes étapes des innovations biologiques et biochimiques de ces premières formes de vie. Toutefois, l'usage des microfossiles comme outil d'investigation de la vie précambrienne exige la prise en compte d'autres critères permettant de s'assurer de sa nature biogénique. Il s'agit notamment de (i) la compatibilité de l'environnement de dépôt de la roche avec l'existence des micro-organismes ; (ii) l'endogénicité et la syngénicité entre la roche et le microfossile et (iii) les évidences de la biogénicité du microfossile (*Westall et al., 2006*). L'environnement de dépôt ne doit souffrir d'aucune ambiguïté, d'autant plus qu'un environnement hydrothermal peut, par une chimie abiotique, produire des morphologies ressemblant aux microfossiles. C'est le cas dans la Formation d'Apex Chert âgée de 3,5 Ga (*Brasier et al., 2002*) dont les formes recueillies ont été jadis considérées comme les plus anciennes traces de vie dans le registre fossile, du fait de leur ressemblance aux cyanobactéries modernes (*Schopf, 1993; Schopf and Packer, 1987*).

Une chose est d'établir la biogénicité du microfossile, une autre est de déterminer s'il s'agit d'un procaryote ou d'un eucaryote. Pour y arriver, les microfossiles constituent à nouveau un outil privilégié ; non seulement pour identifier avec certitude les premiers eucaryotes mais également pour suivre leur évolution et leur diversification. Certes, les biomarqueurs sont largement mis à contribution pour spéculer sur la présence des eucaryotes dans les roches précambriennes. Mais, il ne s'agit là, que des preuves indirectes sans détail sur les transformations subies par ces premiers eucaryotes au cours du temps. De plus, il y a débat concernant le stérane, biomarqueur utilisé à cet effet (*Rasmussen et al., 2008; Waldbauer et al., 2009*). Car, certaines bactéries synthétisent également le stérol, précurseur du stérane (*Pearson*

et al., 2003) tandis que quelques eucaryotes modernes adaptés à des environnements anoxiques ne produisent pas non plus du stérol (*Porter et al., 2018; Summons et al., 2006*).

Dans le registre du microfossile, les premiers eucaryotes acceptés de tous, sont connus depuis 1,7–1,8 Ga (*Lamb et al. 2009; Peng et al., 2009*) et ont enregistré une diversification majeure à partir de 0,8 Ga (*Cohen and Riedman 2018; Knoll, 2014; Knoll et al. 2006; Javaux and Knoll 2016; Xiao and Tang 2018*). Cette thèse s'inscrit donc dans ce processus de reconstitution du fameux puzzle sur l'évolution de la vie, en ce qu'elle apporte des informations permettant de raffiner davantage, en association avec des données provenant des autres coins du globe, notre compréhension sur l'évolution et la diversification des eucaryotes. En effet, le Supergroupe Protérozoïque de Mbuji-Mayi, d'âge supérieur à 1 Ga (*François et al. 2017 and submitted*) et reposant sur le Craton Archéen à Protérozoïque du Congo-Kasaï (3,1–1,9 Ga), contient des roches renfermant une large diversité de microfossiles dont une présence modérée d'eucaryotes. Ces nouvelles données sur la paléobiologie, d'une partie du continent africain en l'occurrence l'Afrique Centrale, constitue également une autre plus-value à l'actif de cette étude. En effet, excepté le sud de l'Afrique, le continent souffre d'une insuffisance des données sur la paléobiologie alors que les roches précambriennes sont distribuées sur près de 3/4 de la superficie actuelle du continent (Fig. i ; *Merdith et al., 2017*).

Ce manuscrit est constitué de 7 chapitres et d'annexes. Les chapitres 3, 4, 5 et 6 sont publiés, soumis ou en cours de soumission.

Le Chapitre 1 constitue l'introduction générale. Il présente en premier lieu, de manière succincte, l'état des connaissances actuelles sur le Précambrien ; avec un accent particulier sur les conditions environnementales au Précambrien ainsi que sur l'évolution et la diversification des premiers eucaryotes. Il présente ensuite les objectifs de la thèse.

Le Chapitre 2 donne un aperçu de la zone d'étude et de la séquence sédimentaire étudiée : sa localisation et son contexte géologique (stratigraphie, paléoenvironnements et géochronologie). Il décrit également les sondages et roches échantillonnés et présente les différentes approches utilisées pour atteindre les objectifs assignés.

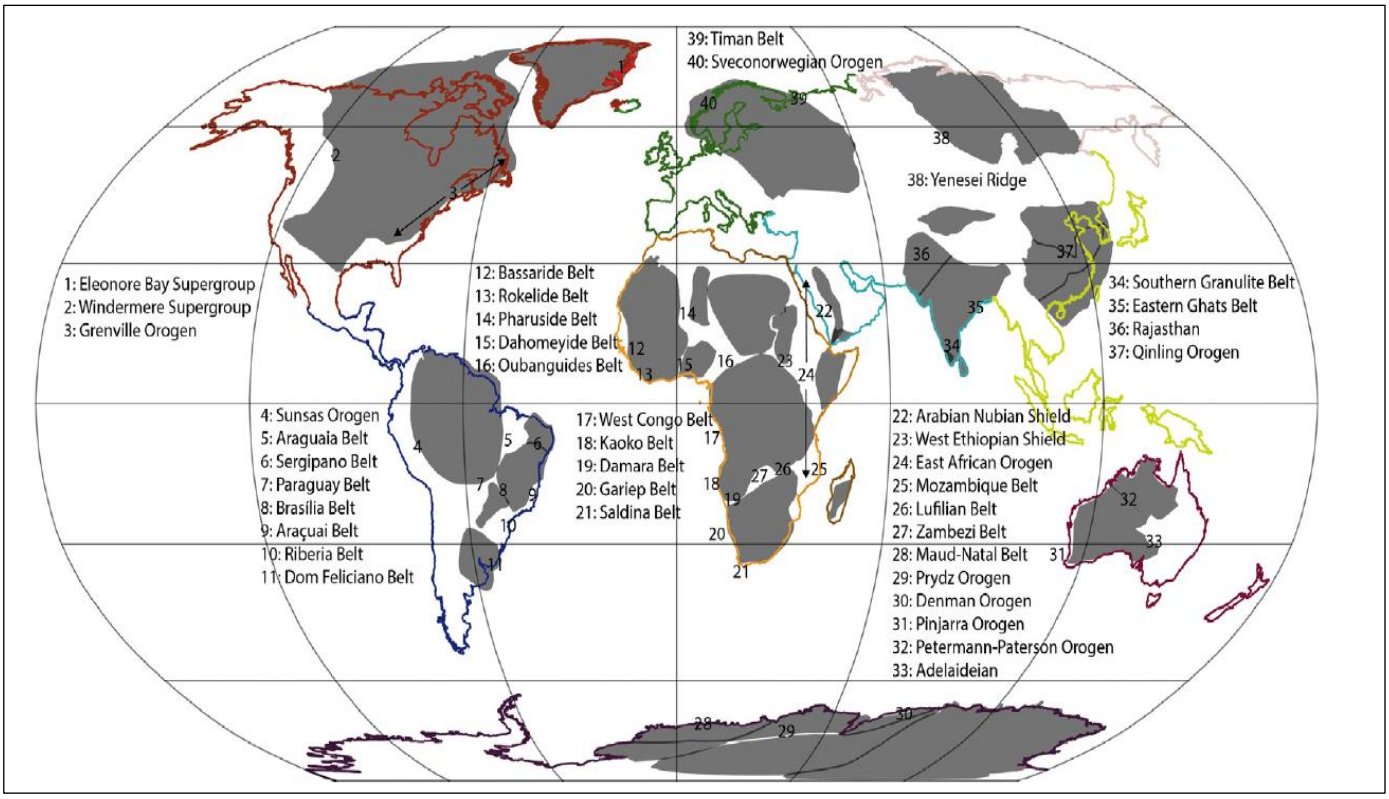

Fig. i. Carte montrant la distribution géographique actuelle des Cratons et ceintures précambriens (en gris). Modifiée d'après *Merdith et al., 2017*.

Le Chapitre 3 présente les résultats sur la diversité, la paléobiologie et la paléontologie systématique des microfossiles étudiés. Il établit la biostratigraphie du Supergroupe de Mbuji-Mayi et discute également des implications pour la biostratigraphie générale du Protérozoïque. Il comprend une introduction, un résumé et le manuscrit du premier article publié dans *Precambrian research* (2016) : « **A diverse and exquisitely preserved organic-walled microfossil assemblage from the Meso–Neoproterozoic Mbuji-Mayi Supergroup (Democratic Republic of Congo) and implications for Proterozoic biostratigraphy** », ainsi que la systématique des microfossiles, également publiée en annexe.

Le Chapitre 4 établit une chimiostratigraphie basée sur des analyses isotopes du carbone, d'oxygène et du souffre ; discute de leurs implications sur les paléoenvironnements et altérations. Cette chimiostratigraphie est contrainte par les nouveaux cadres biostratigraphique et géochronologique établi lors de cette thèse et dans des travaux connexes en collaboration.

Le Chapitre 5 est consacré à la paléoécologie, il présente la distribution temporelle et spatiale des microfossiles dans le Supergroupe de Mbuji-Mayi, en mettant en exergue le lien possible entre la productivité primaire, la préservation (palynofacies) et les conditions redox

dominantes dans les différents paléoenvironnements reconnus. Il est composé d'une introduction et du draft du troisième article (en préparation) pour être soumis à *Precambrian research* : « **Palaeoecology of Mesoproterozoic organic-walled microfossil assemblages from the Mbuji-Mayi Supergroup, DRC** ».

Le Chapitre 6 porte sur la géothermométrie des roches étudiées et plus particulièrement sur la matière organique. Il présente les techniques mises en place pour l'évaluation de la maturité thermique des kérogènes du Supergroupe de Mbuji-Mayi via la spectroscopie Raman. Il présente aussi les différentes autres techniques utilisées en vue de valider les résultats obtenus à l'aide des paramètres Raman. Il est constitué d'une introduction et du manuscrit du deuxième article publié dans *International Journal of Coal Geology* (2018) : « **Raman microspectroscopy, bitumen réflectance and illite crystallinity scale : comparison of different geothermometry methods on fossiliferous Proterozoic sedimentary basins (DR Congo, Mauritania and Australia)** », lequel inclut également les données des deux bassins Protérozoïques contenant des microfossiles, bassins du Taoudeni (Mauritanie) et de l'Officer (Australie). Une discussion des implications de ces résultats sur l'évolution thermique du bassin du Congo conclut ce chapitre.

Le Chapitre 7 reprend les conclusions générales. Un résumé de tous les acquis et implications de la recherche est présenté, suivi des perspectives.

Des annexes reprennent des données détailles des toutes les analyses effectuées et des études géochronologiques auxquelles j'ai participé et qui ont fait l'objet de deux articles. L'un concerne la partie inférieure de la séquence publié dans *Precambrian research* (2017) sous le titre de : « **Contributions of U-Th-Pb dating on the diagenesis and sediment sources of the lower group (BI) of the Mbuji-Mayi Supergroup (Democratic Republic of Congo)** ». L'autre s'intéresse à la partie supérieure, et plus précisement aux roches éffusives qui surplombent le Groupe BII : « **Mesoproterozoic doleritic emplacement in the Sankuru-Mbuji-Mayi-Lomami-Lovoy basin (DRCongo) and implications on the diversification of early eukaryotes and geodynamics in Central Africa** (*in prep*) ».

Chapitre 1 : Introduction générale

En géologie, l'histoire de la Terre est subdivisée suivant un système de classement chronologique dénommé « **échelle des temps géologiques** » (Fig. 1.1). L'histoire géologique de la Terre est subdivisée en quatre intervalles géochronologiques, appelés « Eons ». Du plus anciens au plus récent, nous distinguons (*Ogg et al., 2008*) :

Hadéen (4.6 – 4 Ga), terme dérivé du grec en référence au dieu de l'enfer « Hadès » ;

Archéen (4 – 2.5 Ga), signifiant « origine ou commencement » en grec ;

Protérozoïque (2.5 – 0.54 Ga), du grec « avant la vie animale » et

Phanérozoïque (0.54 Ga à aujourd'hui), du grec « vie animale visible ».

Les trois premiers éons constituent le Précambrien, lequel n'est pas un intervalle géochronologique formel mais se réfère simplement à tout événement qui s'est produit depuis la fin de l'accrétion de la Terre (~ 4,6 Ga) jusqu'à l'explosion biologique cambrienne (0,54 Ga). Il est par ce fait l'intervalle de temps le plus long de l'histoire de la Terre (environ 4 Ga). A l'exception de l'Hadéen, l'Archéen et le Protérozoïque sont subdivisés en quatre et trois ères respectivement (Fig. 1.1).

1.1. Conditions environnementales du Précambrien

Durant l'Hadéen, la Terre subit des événements qui assurent sa transformation après sa formation par accrétion de planétésimaux (*Goldblatt et al., 2010*). C'est durant cette période que se produit la différenciation du noyau et du manteau terrestres, le développement de l'atmosphère primordiale (riche en CH_4, H_2, N_2, CO_2, vapeurs d'eau et gaz rares) ainsi que la formation des océans, de la Lune et de la croûte terrestre (*Lunine, 1998; Trail et al., 2007; Wilde et al., 2001; Wood and Halliday, 2005*). Les plus vieux témoins directs de cette formation des océans et de la croûte terrestre sur Terre sont les zircons de Jack Hills préservés dans le Craton du Yilgran en Australie Occidentale et datés majoritairement entre 4,0 et 4,4 Ga. Ils fournissent l'évidence de la formation des océans sur la Terre et d'une protocroûte de type felsique dès 4,0–4,4 Ga (*Russel and Arndt, 2005; Valley et al.,2005; Valley et al., 2014; Wilde et al., 2001*). L'Hadéen est également marqué par une période des bombardements météoritiques intenses (connu sous le nom de Late Heavy Bombardment – LHB) entre 4,1 et

3,9 Ga (*Bhandari, 2002; Koeberl, 2003; O'Neil et al., 2008; Van Kranendonk et al., 2012*). Les traces du LHB sont uniquement observables sur la surface de la Lune ; leur absence sur la surface terrestre est expliquée par la tectonique des plaques très active sur Terre (*Ryder, 2003*). A la fin de l'Hadéen, toutes les conditions nécessaires à l'apparition de la vie sont présentes, néanmoins, en l'absence de roches, aucune trace n'a pu être preserver pour prouver sa potentielle apparition à cette époque.

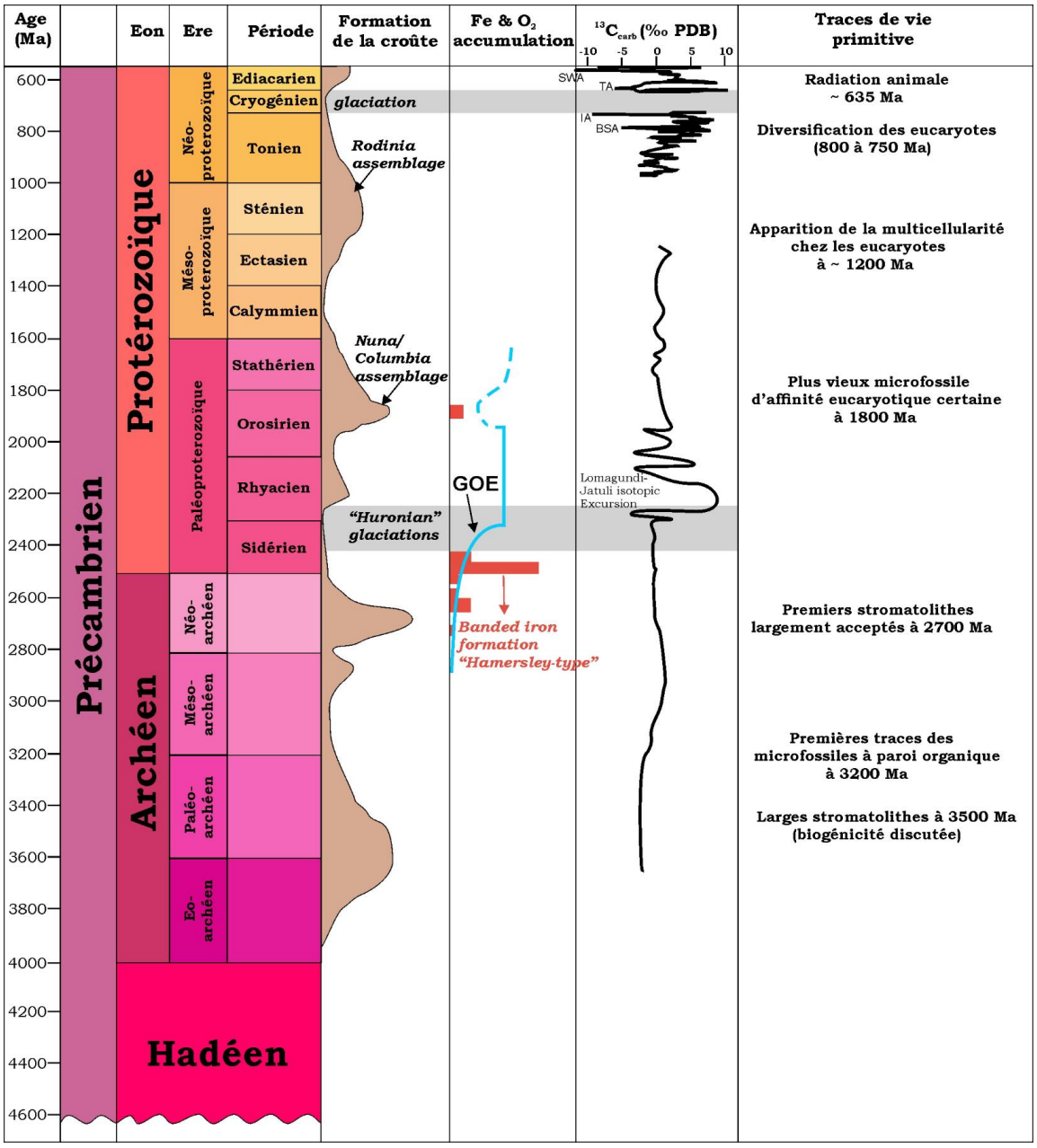

Fig. 1.1. Echelle stratigraphique du Précambrien associée à quelques événements géologiques et biologiques majeurs intervenus au cours de cet intervalle de temps. Modifié d'après *Gradstein et al., 2012*. BSA: Bitter Spring anomaly; IA: Islay anomaly; TA: Trezoma anomaly; SWA: Shuram-Wonoka anomaly; et GOE: Great oxygenation event.

L'Archéen, subdivisé en quatre ères (Eo-, Paléo-, Méso- et Néoarchéen), est la période d'intenses processus géodynamiques, qui ont permis l'extraction de la croûte continentale dont les plus vieilles roches connues sont datées entre 4,0 et 3,9 Ga (*Bowring & Housh 1995; Bowring & Williams 1999; Stern & Bleeker 1998*). Il s'agit du complexe gneissique d'Acasta au nord-ouest du bouclier Canadien. La croûte continentale archéenne est constituée essentiellement de trois grands ensembles. Il s'agit : (1) d'un socle granito-gneissique appelé TTG (pour Tonalite–Trondhjémite–Granodiorite) qui représentent près de 80% de la croûte continentale actuelle; (2) des ceintures de roches vertes fortement déformées comprenant des komatiites (roches ultramafiques), des roches métamorphiques (amphibolites, métasédiments) associées à de rares roches sédimentaires (comprenant les BIF) ; et (3) des granites tardifs, intrusifs dans le socle granito-gneissique et les ceintures de roches vertes (*Goodwin, 1991; Lowe, 1994; Martin, 1994*). Les formations ferrifères rubanées ou BIF (Banded Iron Formation) commencent à se mettre en place en petits dépôts vers 3.2 Ga (*Poulton & Canfeld, 2011*) puis forment des grands gisements à la transition Archéen–Protérozoïque (~2,5 Ga, Fig. 1.1), dont le bassin de Hamersley en Australie occidentale constitue l'exemple-type (*Van Kranendonk et al., 2012*).

L'atmosphère archéenne était extrêmement pauvre en O_2 (*Pavlov & Kasting, 2002*), avec des concentrations élevées en gaz à effet de serre, notamment CO_2 et CH_4 (*Kasting, 1993*). Les traces de vie archéenne sont rares et sont, pour la plupart, l'objet des interprétations controversées. C'est le cas notamment de l'assemblage décrits dans la formation Strelley Pool (~3.4 Ga) du Craton de Pilbara (Australie), dont certains microfossiles pourraient être biogéniques tandis que d'autres pourraient être des pseudofossiles crées par le déplacement de la matière organique sur des fragements de verres volcaniques (*Sugitani et al. 2010; Wacey et al., 2018*). Quelques-unes sont, néanmoins, largement acceptées. Il s'agit des larges vésicules à parois organiques datées de 3,2 Ga, provenant du Groupe du Moodies en Afrique du Sud et qui pourraient correspondre soit à des eucaryotes, soit a des procaryotes – une cellule ou une enveloppe de colonie – (*Javaux et al., 2010*). Dans le registre des biomarqueurs, il y a ceux attribués aux bactéries dans le Supergroupe du Transvaal (~2,67 à 2,46 Ga) en Afrique du Sud (*Waldbauer et al., 2009*) bien que ce soit très discuté. Les stromatolithes non contestés de la Formation de Tumbiana en Australie témoignent de l'activité photosynthétique à ~2,7 Ga (*Lepot et al., 2008*). Bien qu'il y en ait de plus anciens datés à 3,45 Ga dans la Formation Strelley Pool en Australie (Allwood et al. 2006; Allwood et al. 2009) pour lesquels, seules les formes coniques sont acceptées comme biogéniques (*Bosak et al., 2013*). Dans la formation de

Tumbiana, des valeurs de $\delta^{13}C$ descendant jusqu'à –60‰ indiqueraient la présence des Archées méthanogènes (produisant du CH4), et de bactéries méthanotrophes (consommant du CH4 ; *Hayes, 1994; Thomazo et al., 2009*). Ces indices isotopiques du carbone et du soufre (*Arndt & Nisbet, 2012; Nisbet et al., 2007*) mais également de l'uranium, du chrome et du molybdène (*Diamond and Lyons 2018; Lyons et al., 2014*) permettent également de mettre en évidence le développement de la photosynthèse oxygénique à la fin de l'Archéen.

Au Protérozoïque, différents indicateurs géologiques et géochimiques suggèrent une accumulation brutale de la teneur en oxygène (O_2) entre 2,45 et 2,3 Ga ; événement connu sous le nom de GOE (pour Great Oxygenation Event, en anglais ; *Bekker et al. 2004; Lyons et al., 2014*). L'éon Protérozoïque (2,5 à 0,54 Ga) est subdivisé en trois ères (Paléo-, Méso-, et Néoprotérozoique) et dix périodes (Fig. 1.1). Hormis le GOE qui, d'un point de vue géobiologique, constitue le changement le plus significatif du Protérozoïque, cet éon a enregistré d'autres bouleversements importants. C'est le cas des glaciations majeures (huronienne, sturtienne et marinoenne), témoins d'une situation où la Terre était recouverte de glaces (*Fairchild & Kennedy, 2007; Hoffman & Li, 2009; Sansjofre et al., 2011; Tang & Chen, 2013*). Lapparition de la tectonique des plaques moderne à au moins 2,1–2,2 (*François et al.,, 2018*) avec laquelle on note, le développement d'importantes orogenèses qui ont conduit à la formation et à dislocation des supercontinents Columbia (ou Numa) et Rodina (*Li et al., 2008; Merdith et al., 2017; Van Kranendonk et al., 2012*). Il y a l'arrêt des dépôts majeurs de BIF à ~1,8 Ga (*Isley & Abbott, 1999; Poulton & Canfeld, 2011*). Il s'en est suivi une stratification de l'hydrosphère avec une prédominance des conditions ferrugineuses et/ou sulfidiques dans les zones profondes bien avant l'oxygénation des océans profonds à 0,58 Ga (*Anbar & Knoll, 2002; Bekker et al., 2005; Canfield, 2005; Canfield et al., 2007, 2008; Diamond and Lyons, 2018; Johnston et al. 2010; Li et al., 2010; Lyons et al., 2014; Poulton et al., 2004; Rouxel et al., 2005*). Les eaux ferrugineuses peu profondes ont permis la mise en disponibilité des bioéléments (Fe, Mo, Co, Cu,…) essentiels au métabolisme des eucaryotes, facilitant ainsi leur évolution, ce qui n'était le cas dans des eaux sulfidiques où leur évolution était limité par la rareté ou l'absence de ces bioéléments (*Anbar and Knoll 2002; Guilbaud et al. 2015; Planavsky et al. 2011; Poulton and Canfield 2011*). Des larges excursions négatives (Bitter Spring, Islay et Shuram–Wonoka) dans les valeurs de $\delta^{13}C_{carb}$ sont également enregistrées au Néoprotérozoïque (*Halverson et al. 2005, 2010; Swanson-Hysell et al. 2015*). Tous ces changements environnementaux, que la Terre a connus durant le Protérozoïque, ont permis l'évolution et la diversification du vivant et ont influencé l'évolution des eucaryotes.

1.2. Evolution et diversification des premiers eucaryotes

La biologie cellulaire et moléculaire subdivisent la vie en trois domaines différents : les Bactéries, les Archées et les Eucaryotes (*Woese et al., 1990*). Les bactéries et les archées sont des procaryotes, c'est-à-dire des organismes vivants à structure cellulaire simple et dépourvue d'un noyau, mais avec des métabolismes très diversifiés. Alors que les eucaryotes regroupent des organismes à structure cellulaire complexe et possédant un noyau bien défini, un cytosquelette (ensemble des constituants organisés en réseau de filaments et de tubules, qui assurent la permanence et le maintien de la structure cellulaire) ainsi que des organites tels que la mitochondrie et le chloroplaste. Parmi les eucaryotes, sont regroupés les protistes (unicellulaires), les animaux, les végétaux ainsi que les champignons (*Cavalier-Smith, 1998*). Plusieurs modèles (au moins une dizaine) sont avancés pour expliquer l'origine de la cellule eucaryote ; ceci atteste que cette origine reste encore non résolue. Cependant, de tous les modèles, celui suggérant la symbiose entre deux procaryotes (une bactérie et un archée) semble le plus probable (*Lopez-Garcia & Moreira, 2006; López-García et al., 2017*). Ce modèle a été également soutenu avec la découverte d'un groupe d'archées plus proches des eucaryotes (*Spang et al. 2015*) .

Dans le registre du microfossile, l'identification des eucaryotes précambriens repose sur quelques caractéristiques morphologiques et chimiques indiquant un niveau de complexité inconnu chez les microfossiles procaryotes (*Javaux et al., 2003, 2004*). Ces critères sont : (i) l'ornementation de la paroi, (ii) les processus s'étendant depuis la paroi, (iii) les structures de désenkystement, (iv) l'ultrastructure de la paroi et (v) la chimie de la paroi. Les trois premiers peuvent être mis en évidence par la microscopie optique alors que les deux derniers nécessitent l'emploi de la microscopie électronique à balayage (MEB), à transmission (MET) et de la microspectroscopie à infrarouge et Raman.

Les plus vieux microfossiles, dont l'affinité eucaryotique est sans ambiguïté, sont connus au Paléoprotérozoïque (entre 1,8 et 1,65 Ga). Ces microfossiles révèlent une morphologie complexe avec des ornementations de la paroi cellulaire, des processus hétéromorphes, des structures de désenkystement par rupture partielle ou médiane et des biopolymères résistants. Il s'agit de : *Valeria lophostriata*, *Tappania plana*, *Dictyosphaera delicata*, *Shuiyousphaeridium macroreticulum* récupérés dans les Groupes Changcheng et Ruyang (quoique la datation du Groupe Ruyang soit débatue) en Chine septentrionale ainsi que dans le Groupe McArthur en Australie *(Agić et al., 2017; Hofmann, 1999; Javaux, 2011;*

Javaux, et al., 2001, 2003, 2004; Javaux & Marshal, 2006; Javaux and Knoll, 2016; Knoll, 1994; Knoll et al., 2006a; Lamb et al., 2009; Leiming et al., 2005; Pang et al., 2015). Hormis ces microfossiles à morphologies bien distinctes, on note également, la présence des compressions macroscopiques carbonées sous forme de larges filaments enroulés en spirale « *Grypania spiralis* » (*Han & Runnegar, 1992*) retrouvées dans la Formation de Negaunee (1,87 Ga, *Schneider et al., 2002*) aux Etats-Unis. Cependant, leur affinité eucaryotique est encore controversée (*Knoll et al., 2006a; Samuelsson & Butterfield, 2001; Sharma & Shukla, 2009; Xiao & Dong, 2006*).

Au Mésoprotérozoïque (1,6–1 Ga), l'évolution se poursuit avec une diversité et une abondance modérées des eucaryotes (*German & Podkovyrov, 2009; Hofmann & Jackson, 1994; Javaux et al., 2001; Knoll et al., 2006a; Leiming et al., 2005; Nagovitsin, 2009*), bien que localement plus élevée en Afrique (*Baludikay et al., 2016; Beghin et al., 2017*) et au Canada arctique (*Loron et al. 2018a, 2018b*). C'est au cours de cette périonde que l'on note l'acquisition des nouveaux caractères dont la multicellularité, la différenciation cellulaire et la reproduction sexuée, observées notamment chez l'espèce *Bangiomorpha pubescens* (*Butterfield, 2001, 2009*) dans la Formation de Hunting au Canada (1,05 Ga ; *Gibson et al. 2018*). Il y a également l'espèce *Trachyhystrichosphaera aimika*, acritarche portant des processus sur la paroi, considérée comme caractéristique de la transition Méso–Néoprotérozoïque (*Baludikay et al,. 2016; Beghin, et al., 2017; Butterfield et al., 1994; Sergeev, 2009; Tang et al., 2013; Vorob'eva et al., 2009*).

Le Néoprotérozoïque (1–0,54 Ga) est caractérisée par une plus grande diversité de microfossiles d'affinité eucaryotique (10 à 25 espèces) ayant une morphologie des plus en plus complexe conduisant à un nouvel environnement biologique surtout dans sa partie supérieure, l'Ediacarien (*Javaux, 2011; Knoll et al., 2006a; Vorob'eva et al., 2009; Xiao & Dong, 2006*). A côté du genre *Trachyhystrichosphaera*, certaines espèces sont restreintes aux roches pré-sturtiennes (~0,87–0,72 Ga) telles que *Cerebrosphaera buickii*, *Cymatiosphaeroides kullingii*, *Eotylotopalla grandis*, *Vandalosphaeridium reticulatum* et les « *Vase-shaped microfossils* » (*Allison & Awramik, 1989; Butterfield & Rainbird, 1998; Butterfield et al., 1998; Knoll, 1984; Nagy et al., 2009; Prasad et al., 2005; Srivastava, 2009; Tang et al., 2013; Zang, 1995*). Comparés aux tests d'amibes actuels, les VSMs (vase-shaped microfossils) témoignent du développement d'une écologie complexe caractérisée par l'hétérotrophie et la prédation à partir de 0,8 Ga (*Cohen and Riedman 2018; Porter & Knoll, 2000; Porter et al., 2003*). Récemment, des preuves de prédation ont été mises en évidence sur des microfossiles du Supergroupe Shaler, Canada arctique, faisant reculer l'âge de la prédation des protistes par les eucaryotes

(eukaryovory) à 1,1–0,9 Ga (*Loron et al., 2018a*). Il y également plusieurs espèces en formes de filaments ramifiés qui sont comparées soit aux algues (*Jacutianema, Proterocladus, Palaeovaucheria* ; *Butterfield, 2004; Butterfield et al., 1994*) soit aux champignons (*Cheilofilum ; Butterfield, 2005, 2009*). La fin du Néoprotérozoïque est marquée par deux événements biologiques majeurs. Le premier concerne l'extinction de nombre de microfossiles cités ci-dessus durant la période interglaciaire (Cryogénien) et qui sont remplacés par un nouvel assemblage des larges acanthomorphes dénommé ECAP (pour Ediacaran Complex Acritarch Palynoflora ; *Grey, 2005; Grey et al., 2003; Riedman et al. 2014; Sergeev et al., 2011; Veis et al., 2006; Willman et al., 2006; Willman & Moczydłowska 2008*). Le deuxième événement fait référence à la radiation post-marinoenne des premiers métazoaires bilatéraux dont les ichnofossiles constituent la « faune d'Ediacara ». Cette faune caractéristique de la limite terminale du Protérozoïque (*Fedonkin, 2003; Narbonne, 2005; Narbonne et al., 2003*) est connue dans vingt-cinq localités différentes (ex : Mistaken Point au Canada, Ediacara Hills en Australie et Nama en Namibie) à travers le globe et sous des conditions de dépôt variées *(Knoll et al., 2006b*). Cependant, elle pose encore de nombreux problèmes et controverses en partie à cause de l'absence d'un consensus sur une taxonomie claire (*van Loon, 2007*). Très récemment cependant, un des fossiles emblémantiques à symétrie bilatérale, Dickinsonia, a révélé son identité animale grâce à la préservation de biomarqueurs (*Bobrovskiy et al. 2018*).

1.3. Objectifs de la thèse

Les objectifs de cette étude focalisée sur les dépôts sédimentaires du Supergroupe Mésoprotérozoïque de Mbuji-Mayi, RDCongo, consistent à :

- Caractériser en détail la diversité et l'abondance des assemblages de microfossiles à paroi organique contenus dans le Supergroupe de Mbuji-Mayi (Chapitre 3) ;
- Préciser la biostratigraphie du Supergroupe de Mbuji-Mayi (Chapitre 3) ;
- Etablir une chimiostratigraphie dans un nouveau cadre géochronologique et biostratigraphique (Chapitre 4) ;
- Déchiffrer la paléoécologie des assemblages de microfossiles en rapport avec les conditions paléoenvironementales (palynofacies, sédimentologie et conditions paléoredox ; Chapitre 5) ;
- Evaluer la maturité thermique du kérogène contenu dans des roches composant le Supergroupe de Mbuji-Mayi (Chapitre 6) ;

- Discuter les implications des travaux réalisés pour l'évolution des eucaryotes au Protérozoïque (Chapitre 7).

Chapitre 2 : Matériels et méthodes

2.1. Introduction

Cette étude se focalise sur le Supergroupe de Mbuji-Mayi (anciennement dénommé « *Système de la Bushimay* » ; (*Raucq, 1957, 1970*). Il affleure dans les provinces du Kasaï Orientale et du Katanga – d'après l'ancienne subdivision territoriale – en République Démocratique du Congo ; et est considéré comme étant la série basale de la marge Sud-Est du Bassin du Congo (Fig. 2.1 ; *Delvaux and Fernandez-Alonso, 2015).*

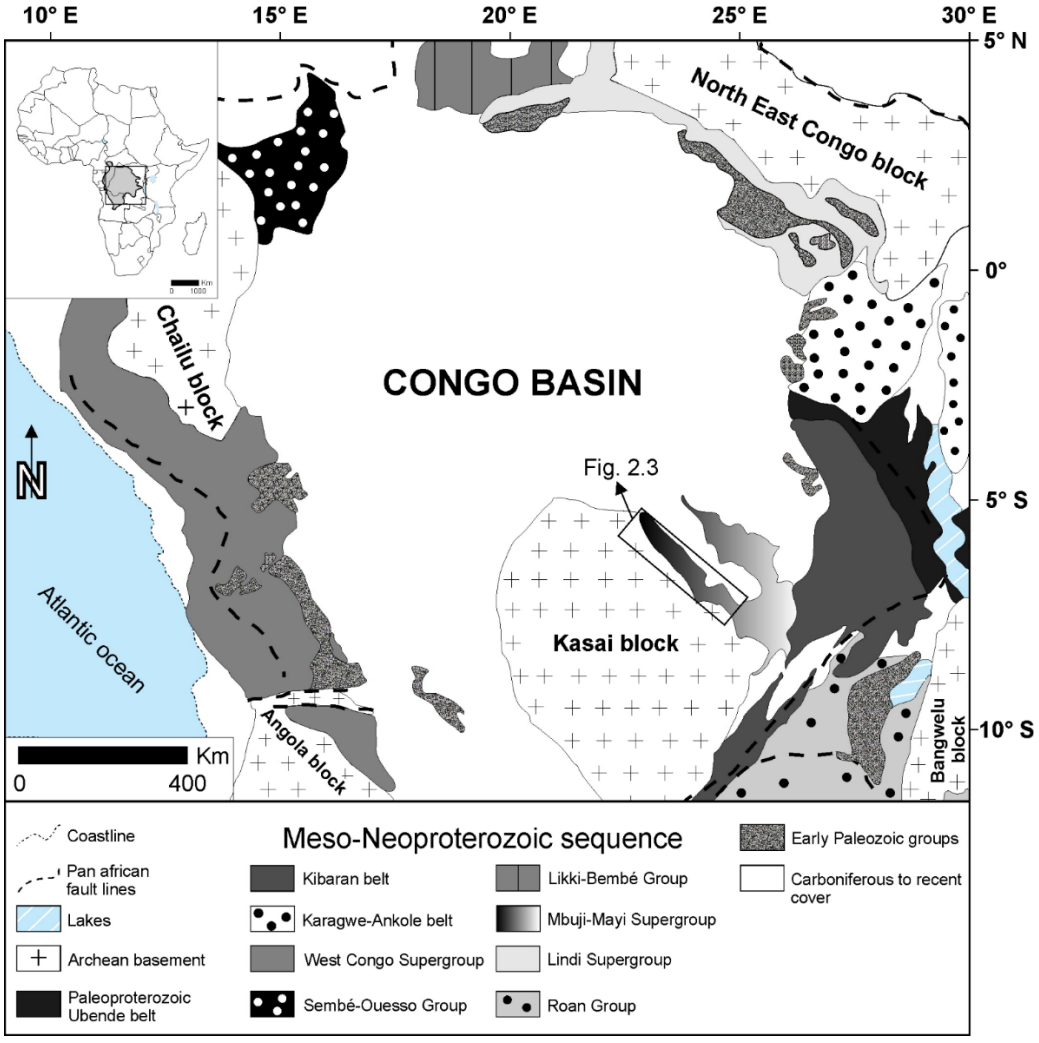

Fig. 2.1. Carte géologique simplifiée du bassin du Congo. Modifiée d'après *Kadima et al., 2010a*

Je me suis particulièrement intéressé à la partie Ouest du Supergroupe de Mbuji-Mayi, dans la zone située entre 5° et 8° de latitude Sud et, 22° et 25° de longitude Est (Fig. 2.3). Une

brève présentation de la situation géographique et du contexte géologique du Bassin du Congo est suivie d'une description détaillée du Supergroupe de Mbuji-Mayi.

2.2. Situation géographique et contexte géologique du Bassin du Congo

Localisé au cœur de l'Afrique (Fig. 2.1), le Bassin du Congo (aussi connu sous l'appellation de « Cuvette Congolaise ») est une dépression intraCratonique, épaisse au centre et s'amincissant uniformément vers les marges, avec une superficie de 1.800.000 km^2 (*Giresse, 2005; Kadima et al., 2011a*). Il s'étend sur cinq pays (RDC, Angola, République Centre Africaine, Congo et Gabon) et contient jusqu'à 9 km d'épaisseur de séquences sédimentaires dont les âges varient du Mésoprotérozoïque tardif (ou terminal) au Néogène, tout en présentant une structure et une évolution géologique complexes (*Delvaux & Fernandez-Alonso 2015; Kadima et al., 2011a, 2011a*). En effet, sa partie centrale est occupée par des sédiments datant du Carbonifère au récent alors que des sédiments d'âge Méso–Néoprotérozoïque et Paléozoïque affleurent à la périphérie (Fig. 2.1). Tous ces sédiments recouvrent le Craton du Congo qui est composé de plusieurs blocs (ou noyaux) d'âge Archéen–Paléoprotérozoïque (Angola, Kasaï, NE Congo, Chailu et Bangwelu). Ces différents blocs furent soudés ensemble au cours du Paléoprotérozoïque lors de l'orogenèse Eburnéenne (*De Waele et al., 2008*). Au Mésoprotérozoïque (~1,1 Ga), suite à l'orogenèse Kibarienne (~1,4 Ga) associée à la formation du supercontinent Rodinia (Fig. 2.2), la marge orientale du Craton du Congo subit une tectonique importante qui conduisit à la mise en place des chaînes de montagne Kibarienne et Irumide (vers 1100 Ma, *De Waele et al., 2008; Kampunzu et al., 2000; Pedreira & De Waele 2008)*. A La fin du Néoprotérozoïque/début du Paléozoïque, l'orogenèse Panafricaine (0,65 à 0,45 Ga) affecta significativement le Craton du Congo et conduisit à la mise en place des chaînes West Congo et Lufilienne le long de marges occidentale et méridionale (*Pedreira & De Waele 2008*).

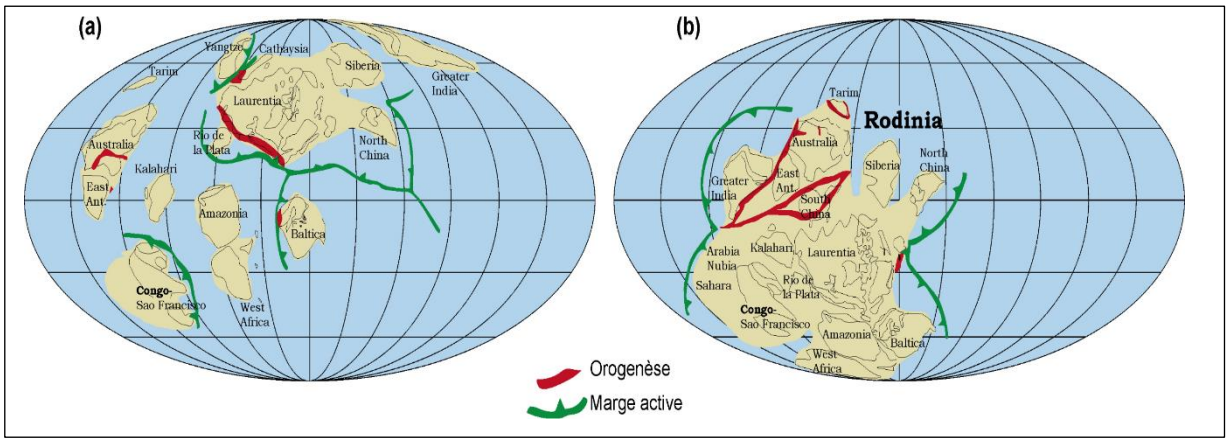

Fig. 2.2. Position du Craton du Congo lors de l'assemblage du Rodinia. (a) à 1,1 Ga ; (b) à 0,9 Ga. Modifiée d'après *Li et al., 2008*.

2.3. Le Supergroupe de Mbuji-Mayi

Le Supergroupe de Mbuji-Mayi est une séquence sédimentaire non affectée par le métamorphisme régional (*Raucq, 1957, 1970*; *Baludikay et al. 2018*). Il s'étend sur un axe NW-SE le long des rivières Sankuru, Mbuji-Mayi (au Kasaï Oriental) et Lomami, Lovoy (au Nord-Ouest du Katanga). Il repose en discordance sur le bloc du Kasaï à l'Ouest et à l'Est sur la ceinture de Kibara (Fig. 2.1). Les datations obtenues sur ces deux blocs permettent d'établir un âge Mesoprotérozoïque pour ces sédiments. En effet, La partie nord du bloc du Kasaï est composée du Complexe granulitique de Musefu (2,6 – 3,1 Ga ; *Fernandez-Alonso et al., 2017*) et du Complexe migmatitique de Dibaya (2,6 – 2,8 Ga ; *Cahen et al., 1984; Fernandez-Alonso et al., 2017*). Ce bloc Archéen a été marqué par l'orogenèse Eburnéo –Transamazonienne (2,2 – 1,98 Ga), qui a résulté à l'accrétion des Cratons du Congo et de São Francisco (*Ledru et al., 1994*). Au cours du Paléoprotérozoïque, la zone a enregistré la mise en place du Complexe gabbro-noritique de Luena (2,3–2,5 Ga) et du Supergroupe de Lusanza (2,2 – 1,9 Ga ; *Ledru et al. 1994 ; Fernandez-Alonso et al., 2017*). L'âge maximum des successions sédimentaires de la ceinture de Kibara a donné 1,15 ± 15 Ga grâce à la méthode K-Ar (*Delhal et al., 1966*).

Les données radiométriques du Supergroupe de Mbuji-Mayi peuvent être regroupées en deux séries : les anciennes et les nouvelles. En effet, la méthode $^{207}Pb/^{206}Pb$ sur galène avait donné un âge moyen de 1055 Ma pour le sommet du Group BI (*Cahen, 1954, 1974; Holmes & Cahen, 1955*), tandis que la méthode K/Ar sur les roches volcaniques surplombant le Groupe BII avait fourni un âge de 948 ± 20 Ma (*Cahen, 1974; Cahen et al., 1984*). Cependant, de nouvelles investigations géochronologiques (U-Th-Pb sur monazite et xénotime diagénétiques

ainsi que Ar-Ar sur feldspath et clinopyroxène), menées parallèlement à cette étude, datent le Supergroupe de Mbuji-Mayi entre 1065 et 1000 Ma (*François et al., 2017 ; François et al., in prep*). Les détails sur ces nouvelles données radiométriques sont repris dans les annexes (A1–A2) du présent manuscrit.

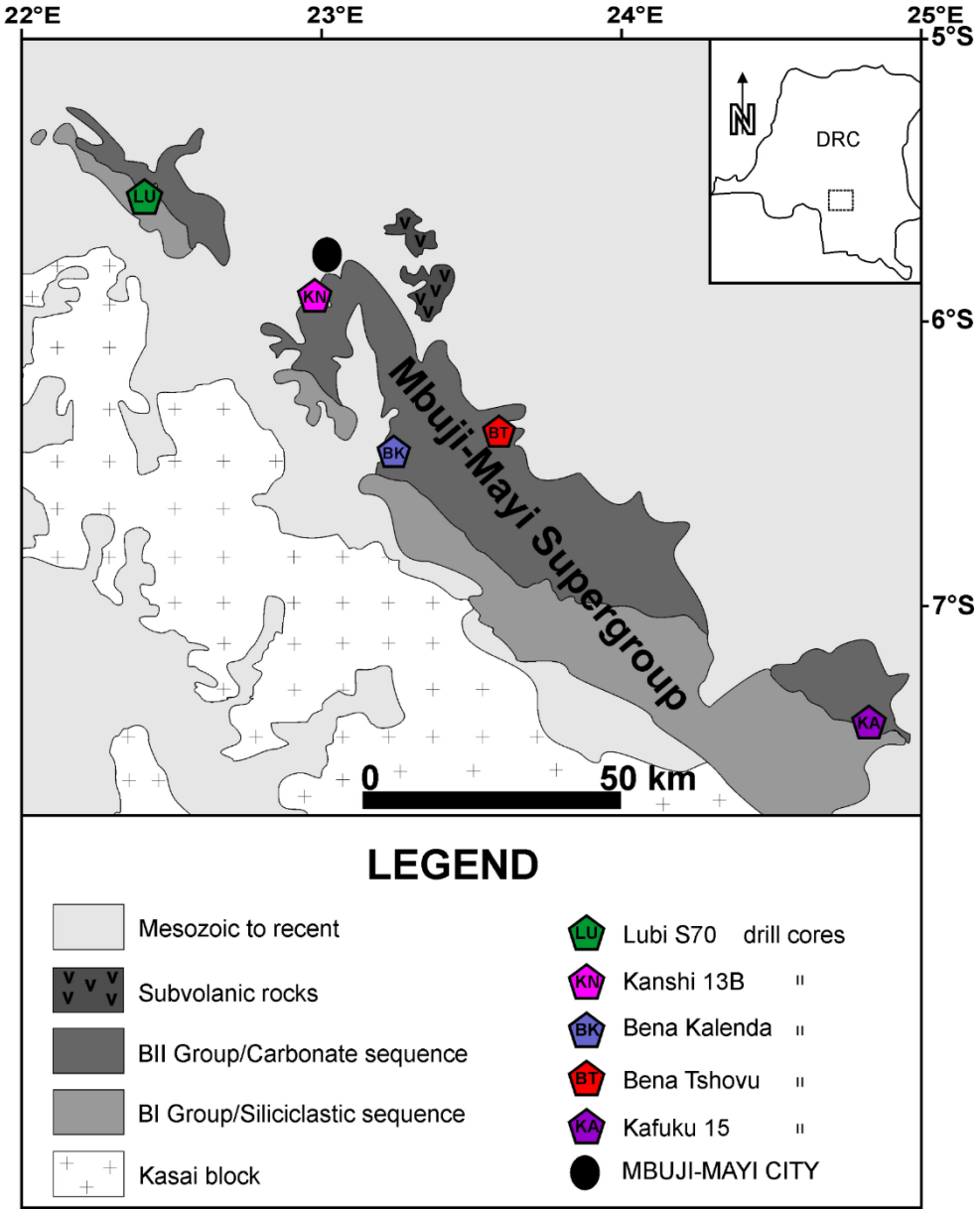

Fig. 2.3. Carte géologique simplifiée du Supergroupe de Mbuji-Mayi dans sa partie Ouest et localisation des sondages étudiés. Modifiée d'après *Baludikay et al., 2016.*

Le Supergroupe de Mbuji-Mayi est constitué de deux Groupes (Figs. 2.3–2.4) : le Groupe inférieur BI, à dominance silico-clastique, reposant sur le socle Archéen et le Groupe supérieur BII ; lequel est constitué principalement des roches carbonatées.

De la base au sommet de ce Supergroupe, nous avons la constitution suivante (*Raucq, 1970*) :

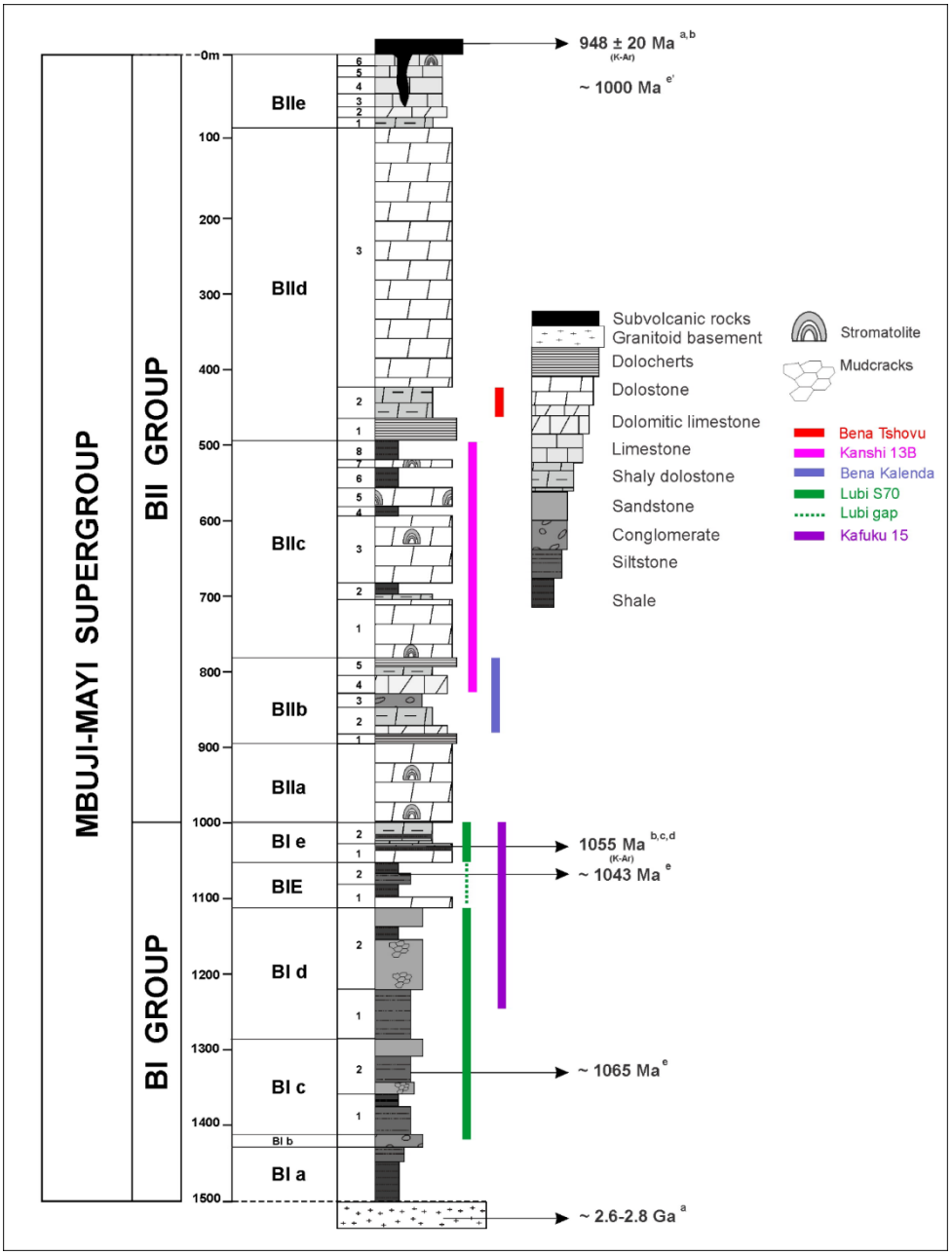

Fig. 2.4. Log stratigraphique général du Supergroupe de Mbuji-Mayi. Les âges d'après (a) *Cahen et al., 1984*, (b) *Cahen, 1974*, (c) *Cahen, 1954*, (d) *Holmes et Cahen*, 1955, (e) *François et al., 2017* (e') *François et al., in prep*. Modifié d'après *François et al., 2017*.

Groupe BI

Sous-groupe BIa : alternance de quartzites rouges et de shales avec un horizon de chert rose (~1500 m). Non représenté dans la région sous étude mais visible dans la province du Katanga, non loin des villages Makukulu et Kiankodi (*Cahen et Mortelmans, 1947 ; Cahen et Lepersonne, 1967*).

Sous-groupe BIb : alternance de grès à stratification oblique et de conglomérat, puis poudingue à gros blocs provenant du socle (17 m).

Sous-groupe BIc :

- Formation BIc1 : shales avec psammite rouge et des passées gréseuses (101 m) ;
- Formation BIc2 : psammite rouge argileux à intercalations gréseuses (180 m).

Sous-groupe BId :

- Formation BId1 : psammite rouge généralement argileuse, avec passées gréseuses (59 m) ;
- Formation BId2 : psammite gréseux rouge, parfois carbonaté ; et quartzite (33 m).

Sous-groupe BIE : visible localement dans la région de Kafuku.

- Formation BIE1 : dolomie argileuse grise et shales brun-rose (31.5 m) ;
- Formation BIE2 : succession de psammite argileuse, dolomie argileuse grise et shales rouge (28 m) ;

Sous-groupe BIe :

- Formation BIe1 : dolomie siliceuse foncée à galène (4m) passant à une dolomie argileuse rose, puis à une dolomie gréseuse rose et enfin à un psammite dolomitique et argileux rouge (25,5 m) ;
- Formation BIe2 : psammite quartzo-feldspathique gris et rose, avec dolomie argileuse et dolomie siliceuse foncée en alternance avec des shales (26,5 m).

Groupe BII

Sous-groupe BIIa : dolomie grise avec stromatolithe (~105 m).

Sous-groupe BIIb :

- Formation BIIb1 : dolomie siliceuse grise (9 m) ;

- Formation BIIb2 : dolomie calcareuse souvent bréchifiée et dolomie argileuse (39 m) ;

- Formation BIIb3 : conglomérats polygénétiques à galets de dolomies diverses et dolomies argileuses (19 m) ;
- Formation BIIb4 : calcaire dolomitique claire d'aspect crayeux, généralement argileux au sommet et silicifié à sa base (23 m) ;
- Formation BIIb5 : dolomie argileuse à la base et dolomie silicifiée foncée au sommet (25 m).

Sous-groupe BIIc :

- Formation BIIc1 : dolomie grise avec stromatolithes (89 m) ;
- Formation BIIc2 : shales noirs encadré de dolomies argileuses grises (21 m) ;
- Formation BIIc3 : dolomie grise avec stromatolithes (88 m) ;
- Formation BIIc4 : shales noirs encadrés des dolomies argileuses (12,5 m) ;
- Formation BIIc5 : dolomie grise avec stromatolithes (25 m) ;
- Formation BIIc6 : shales noirs et dolomies argileuses grises (27 m) ;
- Formation BIIc7 : dolomie grise avec stromatolithes (5 m) ;
- Formation BIIc8 : shales noirs à altération verte ou mauve, passant aux dolomies argileuses (24 m).

Sous-groupe BIId :

- Formation BIId1 : shales bigarrés à cherts (15 m) ;
- Formation BIId2 : succession des dolomies grises, dolomies argileuses et calcaires dolomitiques clairs (42 m) ;
- Formation BIId3 : dolomie grise à cherts divers avec des passées de dolomie argileuse rose et bancs isolés de brèches intraformationnelles (343 m) ;

Sous-groupe BIIe :

- Formation BIIe1 : dolomie argileuse passant à une dolomie calcareuse (13,5 m) ;
- Formation BIIe2 : calcaire gris avec passées et couches silicifiées ; puis calcaire magnésien ou dolomitique (15 m) ;
- Formation BIIe3 : calcaire magnésien à fond rose et gris (11 m) ;
- Formation BIIe4 : calcaire bréchifié gris (10 m) ;
- Formation BIIe5 : calcaire lité gris, parfois rose (24 m) ;

- Formation BIIe6 : calcaire plus ou moins siliceux, gris et/ou rose ; avec stromatolithes (~17,5 m).

Au sommet de la séquence, il y a des roches subvolcaniques (de composition basaltiques à trachy-andésitique souvent chloritisés, pouvant contenir du quartz, fréquemment amygdaloïdes) dont la mise en place commence dès la fin de la formation BIIe2.

2.4. Echantillonnages et méthodes analytiques

Les matériels étudiés ont été obtenus au cours de trois séries d'échantillonnages effectuées dans les collections du département « Géodynamiques et Ressources Minérales » du Musée Royal de l'Afrique Centrale (MRAC, Tervuren). Cinq sondages recoupant différentes formations du Supergroupe de Mbuji-Mayi ont été échantillonnés : (1) Bena Tshovu (33 échantillons), (2) Bena Kalenda (98 échantillons), (3) Kanshi 13B (244 échantillons), (4) Kafuku 15 (116 échantillons) et (5) Lubi S70 (aussi appelé Tshinyama, 308 échantillons). Au total 799 échantillons ont été étudiés. La liste des échantillons et leur description lithologique sont dans l'annexe A3.

2.4.1. Description des sondages étudiés

Ces sondages sont localisés dans la région de Sankuru – Mbuji-Mayi, sur un axe NO-SE (Fig. 2.3). Kanshi 13B, Bena Tshovu, Bena Kalenda recoupent le Groupe BII alors que Lubi S70 et de Kafuku 15 recoupent le Groupe BI (Figs. 2.4–2.5). Wazilewski (*1953*), Raucq (*1957 et 1970*) et Delpomdor (*2013*) ont décrit de manière détaillée ces différents sondages. Voici une présentation succincte de ces sondages, du Nord-Ouest vers le Sud-Est :

Bena Tshovu (60 m de long), ne recoupe que de manière discontinue le milieu du sous-groupe BIId (BId2 Formation) ; lequel montre une alternance des calcaires dolomitiques et argileux silicifiés par endroit. Des brèches (avec des éléments carbonatés et silicifiés) sont également identifiées.

Bena Kalenda (31 m de long) traverse le sous-groupe BIIb (de BIIb5 au BIIb2). On peut y observer des dolomies cherteuses évoluant des dolomies argileuses avec quelques passées de cherts (Formation BIIb5), ensuite des calcaires et dolomies argileuses (Formation BIIb4). Des conglomérats polygéniques associés aux dolomies argileuses et aux cherts composent la Formation BIIb3. La Formation BIIb2 est constituée de shales (renfermant des brèches) et de dolomies calcaires.

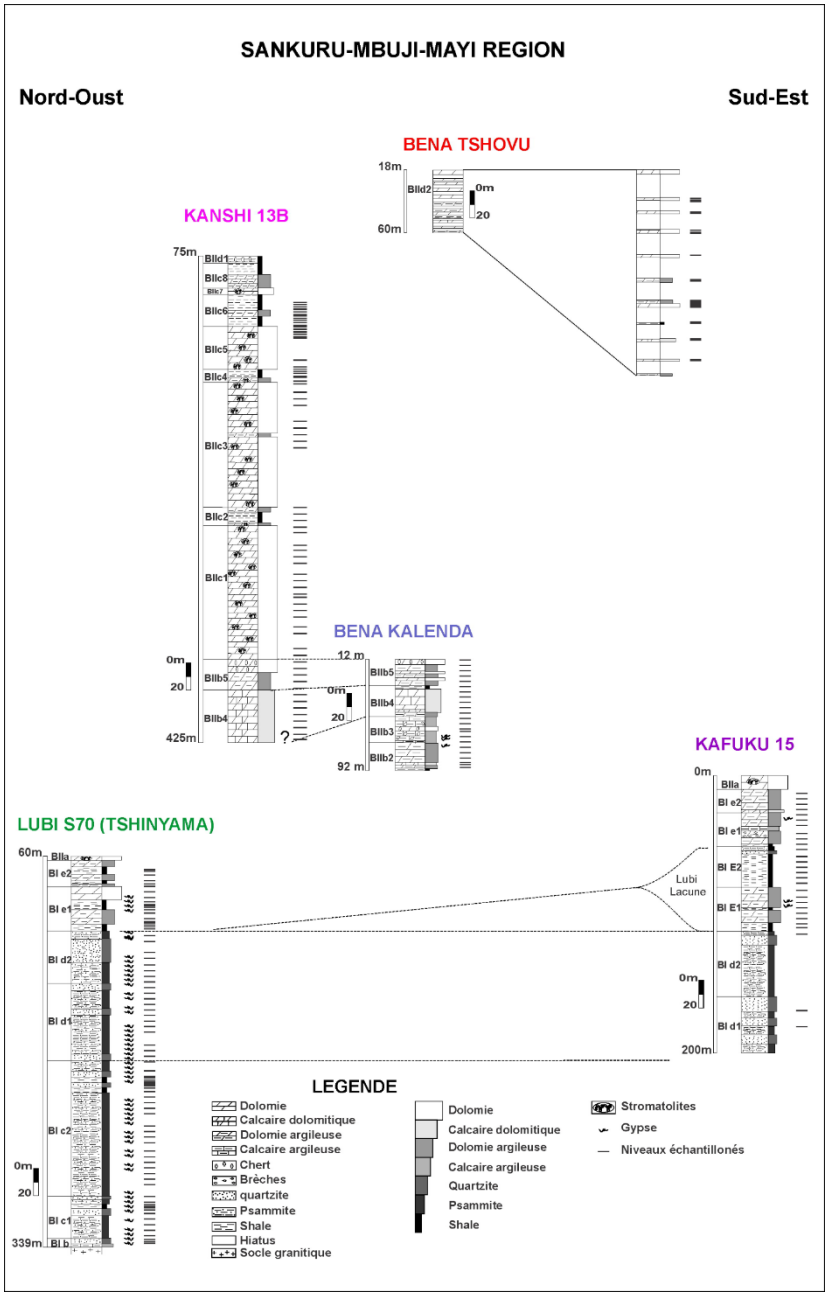

Fig. 2.5. Logs stratigraphiques des sondages étudiés. Les discontinuités sont exclusivement présentes dans le sondage de Bena Tshovu. Modifié d'après *Baludikay et al., 2016*.

Kanshi 13B (425 m de long) recoupe le Groupe BII depuis le sous-groupe BIId (à sa base) jusqu'au sommet du sous-groupe BIIb. Il s'agit d'une alternance de shales avec des dolomies argileuses et stromatolithiques.

Lubi S70, long de 349 m, atteint le socle granitique en traversant la base du sous-groupe BIIa jusqu'au sommet du sous-groupe BIb. Le sous-groupe BIe comprend en sa partie inférieure (la Formation BIe1) des dolomies siliceuses, des shales et des dolomies argileuses tandis que

sa partie supérieure (la Formation BIe2) est composée des dolomies cherteuses évoluant à des dolomies argileuses et des shales. Les sous-groupes BId et BIc sont constitués d'une alternance des psammites et des quartzites avec une intercalation des shales. Une alternance de quartzites conglomératiques et calcaires argileuses constitue le sous-groupe BIb. Excepté dans le niveau BIe2, l'anhydrite et/ou le gypse remplissent les veines et les fractures dans tout le reste des niveaux du sondage.

Kafuku 15 (200 m de long) recoupe la base du sous-groupe BIIa jusqu'au sous-groupe BIId. Des quartzites micacés et des dolomies siliceuses ou argileuses avec brèches intraformationnelles constituent la Formation BIe2. Des dolomies cherteuses passant aux calcaires dolomitiques et argileux associés aux brèches composent la Formation BIe1. La Formation BIE2 montre des shales évoluant aux quartzites micacés et aux psammites argileuses. La Formation BIE1 révèle une composition faite de dolomies argileuses alternant avec des shales. Les formations BId2 et BId1 sont constituées d'une alternance des psammites roses et vertes avec quartzites micacés roses.

2.4.2. Préparation des échantillons

Une fois les échantillons sélectionnés, la matière organique (kérogène) contenue dans les échantillons a été extraite par attaque acide selon le protocole appliqué au sein du laboratoire Early Life Traces and Evolution-Astrobiology (*Giraldo et al., 2018*). Ce protocole a été adapté du protocole proposé par Grey (*1999*).

Dans un premier temps, environ 25 g d'échantillon sont lavés et nettoyés de contamination superficielle éventuelle, broyés dans un mortier en agate pour éviter toute contamination, puis rincés à l'eau et séchés à l'étuve. Ils sont par la suite immergés dans 100 ml de HCl 35% pendant 7h afin d'éliminer la fraction carbonatée de la masse rocheuse. L'acide est ensuite neutralisé dans 1 L d'eau mQ. Au bout de 12h, l'échantillon est décanté et immergé dans 150 mL de HF 58-62 % pendant 5 jours afin d'éliminer la fraction silicatée. La solution est légèrement agitée à la main de temps en temps pour homogéneiser l'attaque acide. Par la suite, l'acide est décanté et neutralisé avec 1 L d'eau mQ matin et soir pendant 5 autres jours en prenant garde de ne pas éliminer le dépôt (macérat) qui renferme les microfossiles. Afin de supprimer les minéraux néoformés (fluorides) lors de la neutralisation, l'échantillon est traité avec 250 mL d'HCl 35% au bain-marie pendant 2h. L'HCl est ensuite décanté et neutralisé une dernière fois avec 1L d'eau mQ.

Le résidu est ensuite filtré d'abord avec un filtre à 25 µm puis avec un filtre à 10 µm. Le résidu est ensuite rincé avec de l'eau mQ et placé dans des flacons de stockage. Deux lames sont par la suite préparées avec la fraction supérieure à 25 µm et 1 lame avec la fraction entre 25 et 10 µm. Pour cela une goutte de la solution contenant les microfossiles est mélangée avec du polyvynile avant d'être étalée sur une lamelle de verre. La lamelle est ensuite placée à l'étuve pour 12h à 40°C. La lamelle est ensuite retournée sur une lame de verre propre et fixée avec de l'Eukit. Un total de 263 échantillons provenant des cinq sondages a été préparé soit 765 lames (Fig. 2.6).

Pour permettre l'observation de microfossiles *in situ* et analyses en microspectroscopie Raman, des lames pétrographiques ont également été confectionnées. Une mince tranche parallèle au plan de stratification a été découpée avec une scie en diamant. Cette tranche a été placée dans un four à 60 ° C pendant 1 jour. Après séchage, elle a été montée sur une lame de verre par liaison à froid avec une résine époxy (<60 ° C pour ne pas affecter le matériau carboné). L'épaisseur de l'échantillon a été réduite, par polissage, à 30 µm avec des grains abrasifs de plus en plus fins (9, 6, 1, ¼ µm), en diamant, pour obtenir un polissage miroir. Un total de 14 lames pétrographiques a été confectionné.

2.4.3 Microscopie et identification des microfossiles

La microscopie optique a été réalisée pour identifier les caractéristiques morphologiques des microfossiles telles que la taille, les types d'ornementation, les processus, les structures de désenkystement et la multicellularité. Elle a été également utile à la détermination de la diversité des assemblages et de l'abondance de chaque espèce, ainsi qu'à l'observation de leur état de préservation et à la caractérisation de palynofacies. Cette étude a été réalisée laboratoire Early Life Traces & Evolution-Astrobiology, Département de Géologie de l'Université de Liège, sur un microscope Zeiss Axio Imager A1m équipé d'une caméra digitale Zeiss Axiocam MRc5. Les observations ont été faites avec les objectifs x10, x20, x40 et les objectifs à immersion dans l'huile x63 et x100. L'identification des espèces a été effectuée en utilisant principalement les articles de référence de Butterfield et al. (*1994*), Hofmann et Jackson (*1994*) et Yankauskas et al. (*1989*). L'abondance de chaque espèce était estimée par comptage d'au moins 300 spécimens par lame. La mesure des dimensions (diamètre des microfossiles sphéroidaux, longueur et largeur des microfossiles ovoïdes ou filamenteux) a été réalisée avec le logiciel Axiovision 4.9 de Zeiss associé à la caméra Axiocam MRc5, qui a permis la microphotographie

digitale. La position de chaque spécimen a été repertoriée grâce à l'utilisation d'un England Finder standard.

2.4.4. Analyses géochimiques

a. Analyses géochimiques et isotopiques du fer et du molybdène

La spéciation du fer et les analyses de concentration et des isotopes du Fe et du Mo ont été réalisées, selon les méthodes développées respectivement par Poulton, Rouxel et Barling (*Barling and Anbar 2004; Barling et al., 2001; Poulton and Canfield, 2005; Poulton and Canfeld 2011; Rouxel et al., 2005*). Elles sont utiles dans la compréhension de la paléoécologie des assemblages récupérés, afin de tester le lien éventuel entre la diversité, l'abondance des assemblages et la présence de microfossiles eucaryotes avec les conditions redox des paléo-environnements. Pour la spéciation du fer, 63 échantillons sélectionnés parmi les échantillons de shale ont été analysés au laboratoire de la *School of Earth and Environment* de l'Université de Leeds (Yorkshire, Grande Bretagne) par C. François (Uliège), en collaboration avec R. Guilbaud et S. Poulton (Université de Leeds). Les échantillons de shale analysés étaient exclusivement prélevés dans les sondages de Kanshi 13B, Lubi S70 et Kafuku 15, Bena Kalenda et Bena Tshovu ne contenant que des facies carbonatés. De plus, la caractérisation des concentrations et du signal isotopique du fer et du molybdène ([Fe], [Mo], δ^{56}Fe et de δ^{98}Mo) a été réalisée pour 158 échantillons au sein du laboratoire G-TIME (*Géochimie : Traçage isotopique, minérale et élémentaire*) de l'Université libre de Bruxelles (Belgique) et au Laboratoire Cycles Géochimiques et ressources à Brest (France) par D. Asael (Uliège) en collaboration avec V. Debaille (ULB), et O. Rouxel (LCG–Ifremer). Les détails sur le traitement des échantillons sont repris dans le chapitre 5 et les données en annexes (A5).

b. Isotopes du carbone, de l'oxygène et du soufre

Les isotopes stables du carbone, de l'oxygène et du soufre ont été mesurés pour comprendre les changements à court terme du flux des nutriments, de la productivité ainsi que l'enfouissement du carbone organique, des sulfures sédimentaires mais aussi l'influence éventuelle d'altértion hydrothermale. Les valeurs obtenues ont permis également d'établir une corrélation avec d'autres sections contemporaines ailleurs dans le globe (Chimiostratigraphie). Ces analyses ont été effectuées en sous-traitance. Un total de 568 échantillons provenant des sondages de Kanshi 13B (n = 220), Kafuku 15 (n = 111) et Lubi S70 (n = 237) a été traité au laboratoire SIFIR (*Stable Isotopes For Innovative Research*) du Département des sciences

géologiques, Université du Manitoba (Canada) par A. Bekker. Tandis que 59 échantillons de Bena Kalenda (n = 41) et Bena Tshovu (n = 18) ont été analysés au laboratoire du Prof. Dr. M. Joakimski, GeoZentrum Nordbayern, Université de Erlangen-Nuremberg, Allemagne. Les détails sur le traitement des échantillons sont repris dans le chapitre 4 et les données en annexe A4.

c. Analyses géochimiques des majeurs, mineurs et traces

Les concentrations des éléments majeurs, mineurs et traces de 158 échantillons provenant des sondages de Kanshi 13B (n = 35), Lubi S70 (n = 86) et Kafuku 15 (n = 37) ont été obténues grâce au spectromètre quadripole ICP-MS (Inductively Coupled Plasma Mass Spectrometry) du laboratoire G-TIME, Université libre de Bruxelles. Cependant, seules les données sur le Fe, Al, Mn, Mo et U ont été exploitées. Ces données et celles des autres éléments non utilisées (Ti, Cr, Co, Cu, Zn, Ge, Pb, V, Ni, Ba, Ca, K, Mg, Na, P, S, Sr) sont en annexe A5.

2.4.5. Géothermométrie

a. Spectroscopie Raman

La spectroscopie Raman a été utilisée pour l'évaluation de la maturité thermique du kérogène contenu dans nos roches. Des spectres Raman obtenus des kérogènes extraits (microfossiles et matière organique amorphe ; 16 échantillons) et/ou en lame mince (4 échantillons) riches en matière organique, ont été traités. Les paramètres spectraux ainsi obtenus ont servi, à l'aide du géothermomètre défini par Kouketsu et ses collaborateurs (*Kouketsu et al., 2014*) et de la réflectance Raman (*Liu et al., 2013*), à estimer les températures atteintes par les kérogènes. L'acquisition et le traitement des données, repris dans le chapitre 6, ont été réalisés dans le laboratoire Early Life Traces & Evolution-Astrobiology, au Département de Géologie de l'Université de Liège (Belgique). Pour contraindre et valider les résultats obtenus au moyen de la géothermométrie Raman, le Kübler index (KI), la réflectance des bitumes solides et le TAI (Thermal Alteration Index) ont été mesurés en parallèle. Ce travail a donné lieu à une publication dans *International Journal of Coal Geology* (2018).

b. Kübler index (KI)

Le KI a été mesuré grâce aux analyses minéralogiques par diffraction des rayons-X (XRD) effectuées sur 5 échantillons, avec l'aide de N. Fagel, F. Fontaine et E. Pleuger au

laboratoire AGEs (*Argiles, Géochimie et Environnements sédimentaires*), UR Geology de l'Université de Liège (Belgique). Historiquement, les valeurs de KI sont utilisées pour déterminer les limites de la diagenèse, de l'anchizone et de l'épizone (*Kübler & Jaboyedoff, 2000*). Les valeurs obtenues (voir chapitre 6, pour les détails sur le mode d'acquisition des mesures) ont donc permis d'estimer les gammes de températures subies par les échantillons de roches étudiées.

C. Réflectance des bitumes solides

Pour des roches (pré-dévoniennes) dépourvues de vitrinite comme celles étudiées ici, les bitumes solides sont utilisées comme équivalents à la vitrinite (*Jacob, 1989; Landis & Castaño, 1995; Riediger, 1993*). Les analyses étaient réalisées sur 2 échantillons, au laboratoire d'EMR Group (*Energy and Mineral Resources*) du Département des Géosciences et Géographie de l'Université d'Aachen (Allemagne) en collaboration avec le professeur R. Littke. Les valeurs obtenues ont permis d'estimer les températures à l'aide du « VRG » (pour Vitrinite Réflectance Geothermometer) de Barker & Pawlewicz (*1994*). Le chapitre 6 reprend en détails la préparation des échantillons et l'acquisition des mesures.

d. TAI (Thermal Alteration Index)

La microscopie optique nous a permis d'évaluer la couleur dominante qui se dégageait dans les microfossiles contenus dans une lame palynologique. Celle-ci était évaluée à l'aide d'une nouvelle échelle des valeurs TAI (*Baludikay et al., 2018*). Le chapitre 6 reprend également tous les détails sur la nouvelle échelle TAI proposée.

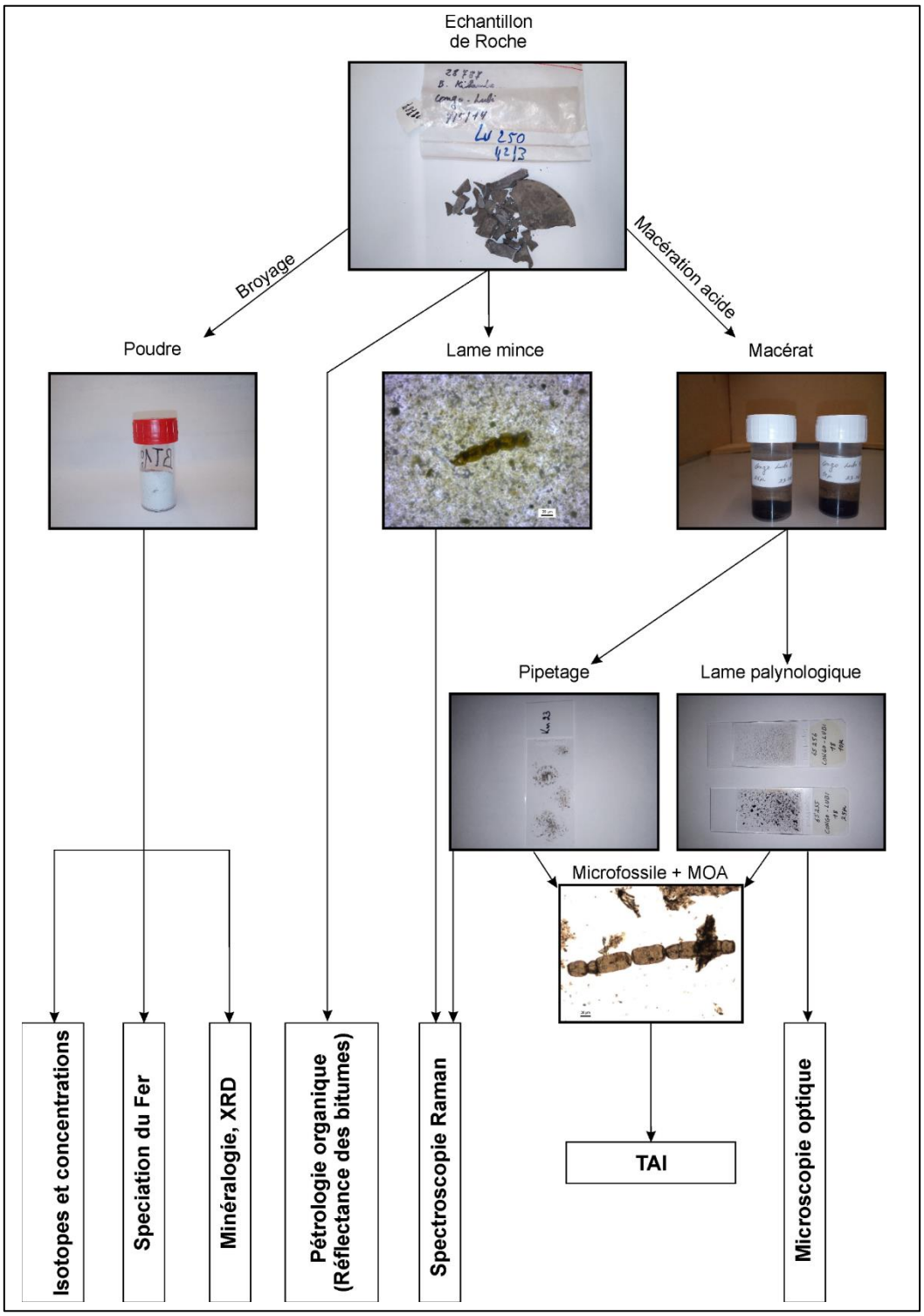

Fig. 2.6. Schéma représentant succinctement et sans aucune hiérarchisation les différentes approches méthodologiques réalisées. MOA : Matière Organique Amorphe ; TAI : Thermal Alteration Index (indice d'altération thermique).

Chapitre 3 : Diversité, Paléobiologie et implications sur la biostratigraphie

3.1. Introduction

Le contenu fossilifère du Supergroupe de Mbuji-Mayi avait fait l'objet de deux précédentes études, lesquelles avaient rapporté respectivement 34 et 41 espèces (*Baudet, 1987; Maithy, 1975*). Ces assemblages consistaient en deux types de palynomorphes (microfossiles à paroi organique) : les acritarches (microfossiles se présentant en vésicules de formes variées et dont l'affinité biologique est inconnue ; *Evitt, 1963*) et les formes filamenteuses. Cependant nombre de leurs espèces se sont avérées être des synonymes à la lumière des travaux récents (*Butterfield et al. 1994 ; Hofmann et Jackson, 1994*). Cette nouvelle investigation a donc permis une actualisation des anciennes données, mais aussi la découverte d'une nouvelle diversité grâce à un échantillonnage plus extensif et de nouvelles méthodes de préparation et d'analyses. L'objectif était d'améliorer notre compréhension de l'évolution de la biosphère au Mésoprotérozoïque et de proposer une biostratigraphie du Supergroupe de Mbuji-Mayi. Les stromatolites columnaires localisés dans le Groupe BII ont également fait l'objet d'une investigation par Bertrand-Sarfati (*1972*). Quatre groupes ont été identifiés par l'auteur : *Baicalia*, *Conophyton*, *Gymnosolen*, *Kasaia* et *Tungussia*.

Un total de 49 espèces a été identifié dont 22 décrites pour la première fois en Afrique Centrale, telle que l'espèce *Trachyhystrichosphaera aimika*, fossile index de la transition Mésoprotérozoïque – Néoprotérozoïque. Grâce à l'abondance du matériel recueilli, les trois espèces du genre Arctacellularia (A. *tetragonala, A. ellipsoida et A. Kelleri*), ont été regroupées et synonymisées en une seule espèce *Arctacellularia tetragonala* Maithy, 1975.

Maithy (*1975*) avait, uniquement sur base de la morphologie, interprété ces microfossiles comme restes d'algues, champignons, acritarches et Incertae sedis. Ces interprétations nous paraissent trop hasardeuses sans information sur la structure, l'ultrastructure et la chimie de la paroi de ces microfossiles ; informations rendues disponibles à l'aide de la microscopie électronique à balayage, microscopie en transmission et microscopie infrarouge et Raman (*Arouri et al., 2000; Javaux & Marshall 2006*). Cependant, les organismes

eucaryotes possèdent certains caractères morphologiques complexes, inconnus chez les bactéries et les archées, pouvant faciliter leur identification par microscopie optique sans les attribuer à des clades particulières (*Javaux et al., 2003*). Aussi avons-nous identifié 11 espèces interprétées sans ambiguïté comme eucaryotes.

Cette étude a fait l'objet d'une publication dans Precambrian Research (2016) : **« A diverse and exquisitely preserved organic-walled microfossil assemblage from the Meso–Neoproterozoic Mbuji-Mayi Supergroup (Democratic Republic of Congo) and implications for Proterozoic biostratigraphy »** qui constitue la sous-section §3.2 de ce chapitre. La sous-section §3.3 reprend la paléontologie systématique laquelle constituait les données supplémentaires de cette même publication.

3.2. Résumé de l'article

Un assemblage de microfossiles bien conservé et diversifié est reporté dans les roches sédimentaires du Supergroupe Méso-Néoprotérozoïque de Mbuji-Mayi dans la province du Kasaï orientale, partie centrale de la République Démocratique du Congo. 49 taxons appartenant à 27 genres ont été identifiés, dont 11 espèces d'eucaryotes non ambigus, 10 espèces d'eucaryotes ou de procaryotes possibles et 28 espèces de probables bactéries. Cet assemblage est plus diverse que ceux précédemment rapportés mais inclut des taxa aussi décrits dans les assemblages mondiaux contemporains. Cet assemblage est caractérisé par des sphéromorphes abondants, des agrégats coloniaux filamenteux et des formes filamenteuses, ainsi qu'une diversité relativement faible d'acanthomorphes incluant le fossile index du Mésoprotérozoïque tardif et du début Néoprotérozoïque – *Trachyhystrichosphaera aimika* – signalé pour la première fois en Afrique centrale. Cette espèce co-existe avec d'autres taxons également signalés pour la première fois en Afrique : *Trachyhystrichosphaera botula*, *Jacutianema solubila*, cf. *Tappania* sp., *Valeria elongata* et de nombreux autres taxons. La corrélation avec d'autres successions géochronologiquement contraintes qui contiennent *Trachyhystrichosphaera* confirme *T.aimika* comme fossile indice prometteur pour définir l'intervalle Mésoprotérozoïque tardif – début Néoprotérozoïque. Les données biostratigraphiques disponibles permettent de suggérer un âge fin Mésoprotérozoïque à Tonien pour le Supergroupe Mbuji-Mayi. Cet âge est compatible avec les nouvelles données géochronologiques publiées, datant le Supergroupe à 1065–1000. Ga (*François et al., 2017*). La comparaison avec les assemblages du Protérozoïque mondial permet de définir des

assemblages de microfossiles utiles pour la biostratigraphie. Cette étude améliore de manière significative notre compréhension de la diversité de la biosphère du Mésoprotérozoïque tardif et du Néoprotérozoïque inférieur, et en particulier la diversification des premiers eucaryotes, conservés dans les roches de la République Démocratique du Congo et plus largement en Afrique où les investigations micropaléontologiques sont rares.

Precambrian Research 281 (2016) 166–184

Contents lists available at ScienceDirect

Precambrian Research

journalhomepage:www.elsevier.com/locate/precamres

A diverse and exquisitely preserved organic-walled microfossil assemblage from the Meso–Neoproterozoic Mbuji-Mayi Supergroup (Democratic Republic of Congo) and implications for Proterozoic biostratigraphy

B.K. Baludikay [a,*], J.-Y. Storme [a], C. François [a], D. Baudet [b], E.J. Javaux [a,*]

[a] Palaeobiogeology, Palaeobotany, Palaeopalynology Lab, UR GEOLOGY, University of Liège, 4000 Liège, Belgium

[b] Geodynamics & Mineral Resources Service, Royal Museum for Central Africa, 3080 Tervuren, Belgium

article info

Article history:
Received 15 September 2015
Revised 29 February 2016
Accepted 22 May 2016 Available online 28 May 2016

Keywords:
DR Congo
Mbuji-Mayi Supergroup
Proterozoic
Microfossils
Biostratigraphy

abstract

A well preserved and diversified microfossil assemblage is reported from the Meso–Neoproterozoic Mbuji-Mayi Supergroup in the Kasai oriental Province, central part of Democratic Republic of Congo. A total of 49 taxa belonging to 27 genera were identified, including 11 species of unambiguous eukaryotes, 10 species of possible eukaryotes or prokaryotes and 28 species of probable bacteria. This assemblage is more diverse than previously reported but includes taxa reported in coeval worldwide assemblages. It is characterized by abundant sphaeromorphs, filamentous colonial aggregates and filamentous forms, as well as a relatively low diversity of acanthomorphs including the Late Mesoproterozoic and Early Neoproterozoic index fossil – Trachyhystrichosphaera aimika – reported for the first time in Central Africa. This species co-occurs with other taxa also reported for the first time in Africa: Trachyhystrichosphaera botula, Jacutianema solubila, cf. Tappania sp., Valeria elongata and numerous other taxa. Correlation with other geochronologically constrained successions that contain Trachyhystrichosphaera confirms T. aimika as promising index fossil to define the Late Mesoproterozoic–Early Neoproterozoic interval. The available biostratigraphic data enable to suggest a minimum Tonian age for the Mbuji-Mayi Supergroup. This age is consistent with the published and new geochronological data. Comparison with worldwide Proterozoic assemblages permits to define microfossil assemblages useful for biostratigraphy. This study significantly improves our understanding of the diversity of the Late Mesoproterozoic–Early Neoproterozoic biosphere, and in particular the diversification of early eukaryotes, preserved in the Democratic Republic of Congo rock record and more broadly in Africa where micropaleontological investigations are sparse.

1. Introduction

Proterozoic microfossils constitute a major source of paleontological information essential for understanding early life evolution. In particular, they document the evolution of biological innovations and patterns of diversification of early eukaryotes (e.g. Butterfield, 2015; Javaux, 2011; Javaux and Knoll, in review; Knoll, 2014) but are also helpful for biostratigraphic correlations and paleoenvironmental reconstruction of Proterozoic rocks (Butterfield and Chandler, 1992; Knoll, 2009; Knoll et al., 2006). To date, few paleontological investigations have been carried out in the Pre-Ediacaran Proterozoic of Africa. Prior to our new study presented here, two early studies investigated the micropaleontology of the Mbuji-Mayi (former Bushimay) Supergroup in Democratic Republic of Congo (DRC) (Baudet, 1987; Maithy, 1975). They reported respectively 34 and 41 taxa of organic-walled microfossils. However, our taxonomic revision, based on more recent work on Precambrian organic-walled microfossils (Butterfield et al., 1994; Hofmann and Jackson, 1994; Sergeev et al., 1997; Sergeev, 2009; Yankauskas et al., 1989) suggests that many of these were synonymous. Other studies report few acritarchs in the Late Mesoproterozoic Taoudeni Basin of Mauritania (Amard, 1984, 1986; Lottaroli et al., 2009), mostly species of Leiosphaeridia and Arctacellularia, although a new study evidences a higher diversity and the occurrence of acanthomorphs (Beghin et al., in review). Baudet (1988) reported 20 microfossil taxa, especially sphaeromorphs, in the Mesoproterozoic Kavumwe Group of Burundi (Deblond et al., 2001; Fernandez-Alonso et al.,

Corresponding authors.
E-mail addresses: bkbaludikay@ulg.ac.be (B.K. Baludikay), ej.javaux@ulg.ac.be (E.J. Javaux).

http://dx.doi.org/10.1016/j.precamres.2016.05.017
0301-9268/

2012). In the Neoproterozoic Kwahu Group of Ghana (>0.85 Ga Abetifi and Anyaboni formations), Couëffé and Vecoli (2011) reported 10 genera: Leiosphaeridia, Pterospermopsimorpha, Synsphaeridium, Coneosphaera, Arctacellularia, Navifusa, Satka, Valeria, Trachysphaeridium and putative Trachyhystrichosphaera (the latter is doubtful based on published illustration, where no processes are visible, cfr. their figure 6.8).

To improve our understanding of the Late Mesoproterozoic–Early Neoproterozoic biosphere evolution and especially the microfossil record of Central Africa, we studied the assemblage of organic-walled microfossils preserved in fine-grained siliciclastic rocks of the Meso–Neoproterozoic Mbuji-Mayi Supergroup, in the Sankuru-Mbuji-Mayi area, DRC (Figs. 1 and 2).

Our new study of a larger number of samples (263) from 5 drill cores, using a non-standard maceration protocol minimizing mechanical shocks, reveals an exceptionally diverse and well-preserved assemblage of 49 taxa of organic-walled microfossils. Among those, 22 taxa are reported for the first time in the assemblage but are known elsewhere. Comparison with coeval worldwide assemblages shows that the Mbuji-Mayi assemblage is more diverse but includes taxa known elsewhere except for one possible new taxon (unnamed acanthomorph), permitting to develop a worldwide biostratigraphy for the Late Mesoproterozoic–Early Neoproterozoic interval.

2. Geological setting, depositional environments and age of the Mbuji-Mayi Supergroup

The Mbuji-Mayi Supergroup is a sedimentary sequence unaffected by regional metamorphism (Raucq, 1957), deposited in the intracratonic failed-rift Sankuru-Mbuji-Mayi-Lomami-Lovoy Basin (SMLL; Delpomdor and Préat, 2013; Delpomdor et al., 2013a,b) which extends from SE to NW between North Katanga and Kasai provinces. In the South-eastern part of the SMLL Basin (i.e. Northwest Katanga Province), the Mbuji-Mayi Supergroup overlies the Mesoproterozoic Kibaran Belt while in the North-western part of SMLL Basin, where we focused our work (i.e. Oriental Kasai Pro-vince), it rests unconformably upon the Archean Kasai Block (Fig. 1; Cahen and Mortelmans, 1947; Raucq, 1957, 1970). Amygdaloidal basaltic lavas overlie the Mbuji-Mayi Supergroup, at the confluence of Mbuji-Mayi and Sankuru rivers (Cahen et al., 1984). Lithostratigraphically, the Mbuji-Mayi Supergroup consists of two distinct successions; a lower siliciclastic sequence (500 m thick) of the BI Group and an upper carbonate sequence (1000 m thick) with stromatolitic build-ups and black shales of the BII Group (Figs. 2 and 3; Raucq, 1957, 1970). The sediments which formed the BI Group came from the Kibaran Belt, the Bang-weulu and Kasai blocks. They indicate a detrital transport from the SE and/or E of SMLL Basin (Delpomdor et al., 2013a). The BI Group comprises six subgroups in ascending order: BIa, BIb, BIc, BId, BIE and BIe. The BIa is not represented in the Western part of the SMLL Basin (i.e. Sankuru-Mbuji-Mayi area), but has been observed in the South-eastern part, especially near Makululu and Kiandoki villages (Cahen and Mortelmans, 1947) and the BIE is only visible in the Kafuku Region. The BII Group, which comprises mostly transgressive carbonates, consists of five subgroups in ascending order: BIIa, BIIb, BIIc, BIId and BIIe. Detailed descriptions of these subgroups have been given in Raucq (1957, 1970) and updated (especially for the carbonates) in Delpomdor et al. (2013a, 2015).

A total of 11 microfacies are recognized from the BIe to BIIe subgroups showing that carbonates were deposited in a marine environment that evolved to evaporitic marine, lacustrine and

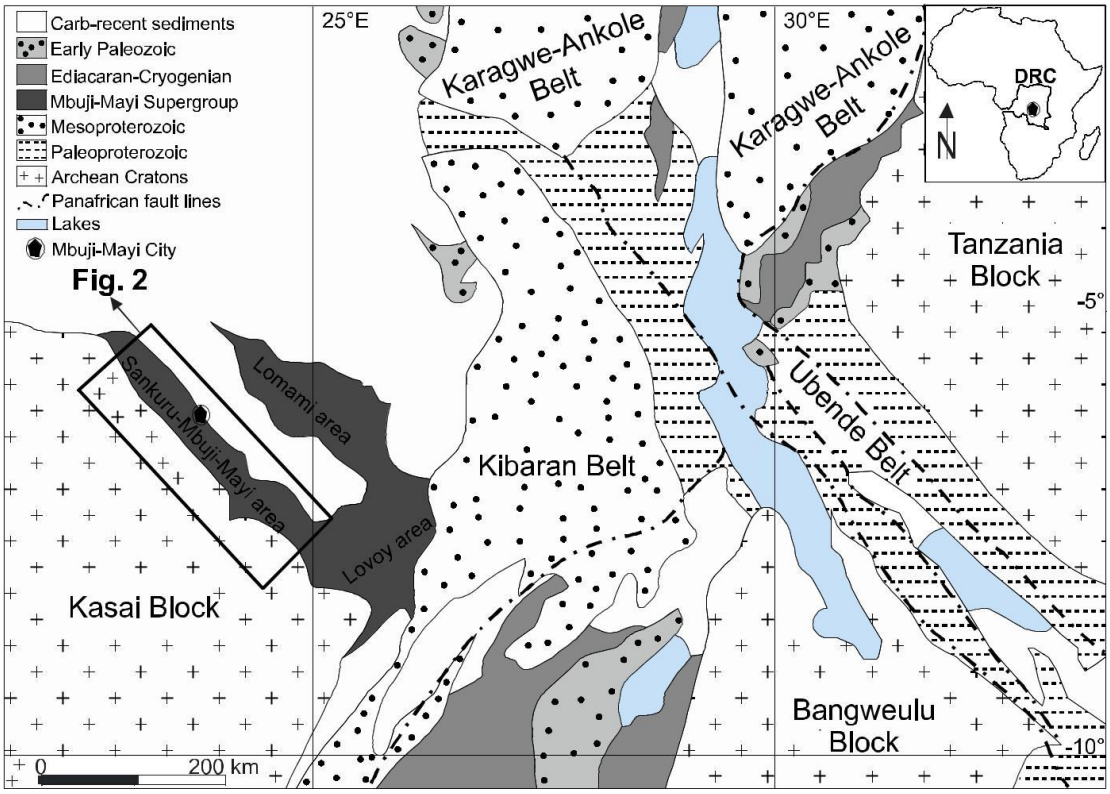

Fig. 1. Tectonic setting synthesis of some Paleoproterozoic–Neoproterozoic Basins in Central Africa (Modified after Kadima et al., 2011 and references therein).

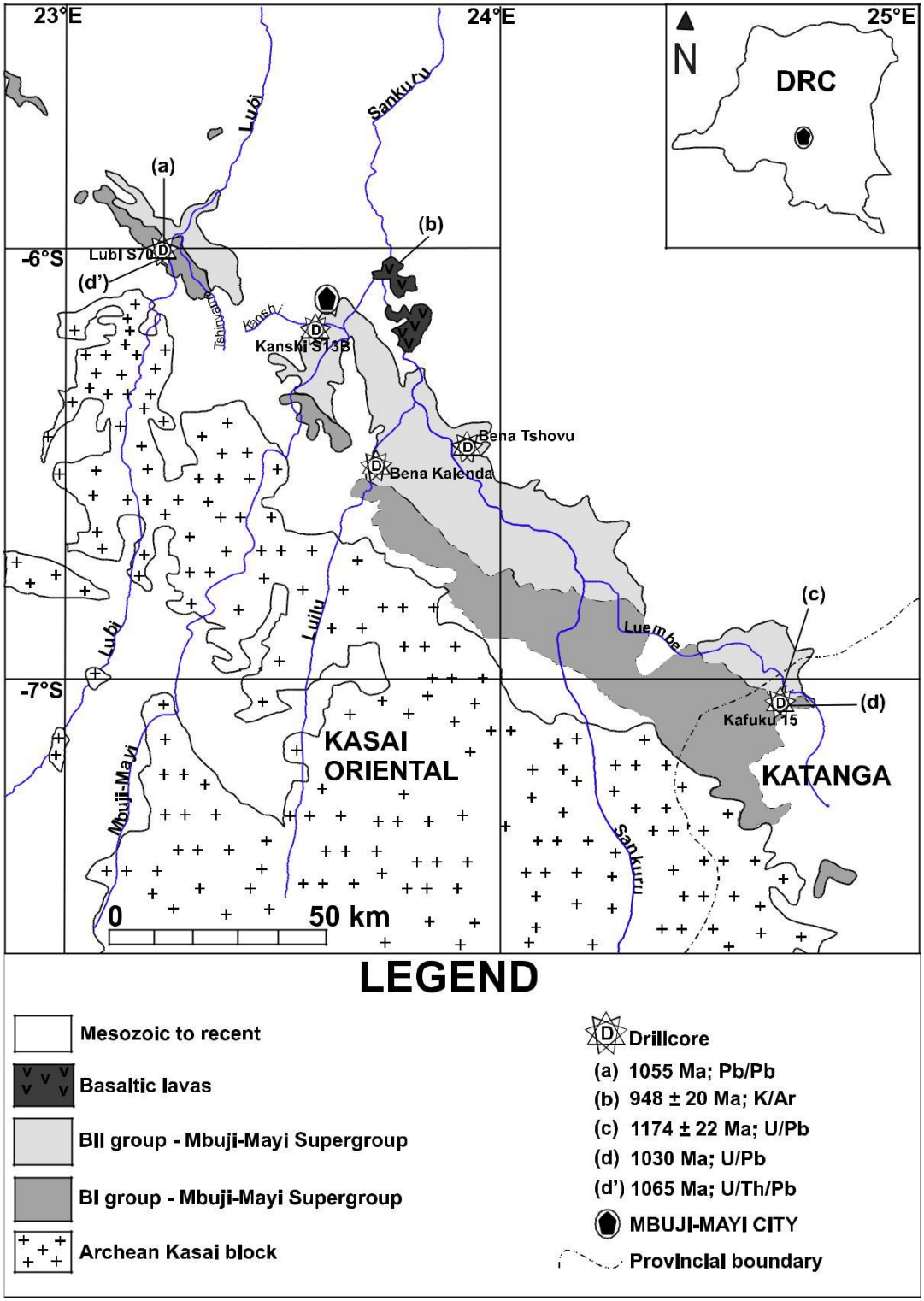

Fig. 2. Simplified geological map of the Mbuji-Mayi Supergroup in the Sankuru-Mbuji-Mayi region. Location of boreholes are indicated by white stars: Lubi S70; Kanshi S13B; Bena Kalenda; Bena Tshovu in eastern Kasai and Kafuku 15 in northwestern Katanga (Democratic Republic of Congo), modified from Delpomdor et al., 2013a. (See caption of Fig. 3 for references).

sabkha settings in the superficial parts of a ramp-system (Delpomdor et al., 2013b, 2015).

Syngenetic galena from three samples (two coming from BIe_1 Formation in Lubi and Senga-Senga valleys and the third from contact between BIIa and BIIb in Luembe Valley) gave a $^{207}Pb/^{206}Pb$ age of 1065, 1040 and 910 Ma respectively (Cahen, 1954; Holmes and Cahen, 1955; Raucq, 1957). The model age is about 1055 Ma (Cahen, 1974). Amygdaloidal basaltic lavas overlying the Mbuji-Mayi Supergroup at the Sankuru-Mbuji-Mayi confluence yielded an age of 948 ± 20 Ma (Cahen et al., 1984). Recently, Delpomdor et al. (2013a) reported a maximum age of 1174 ± 22 Ma, for the Mbuji-Mayi Supergroup deposit, established

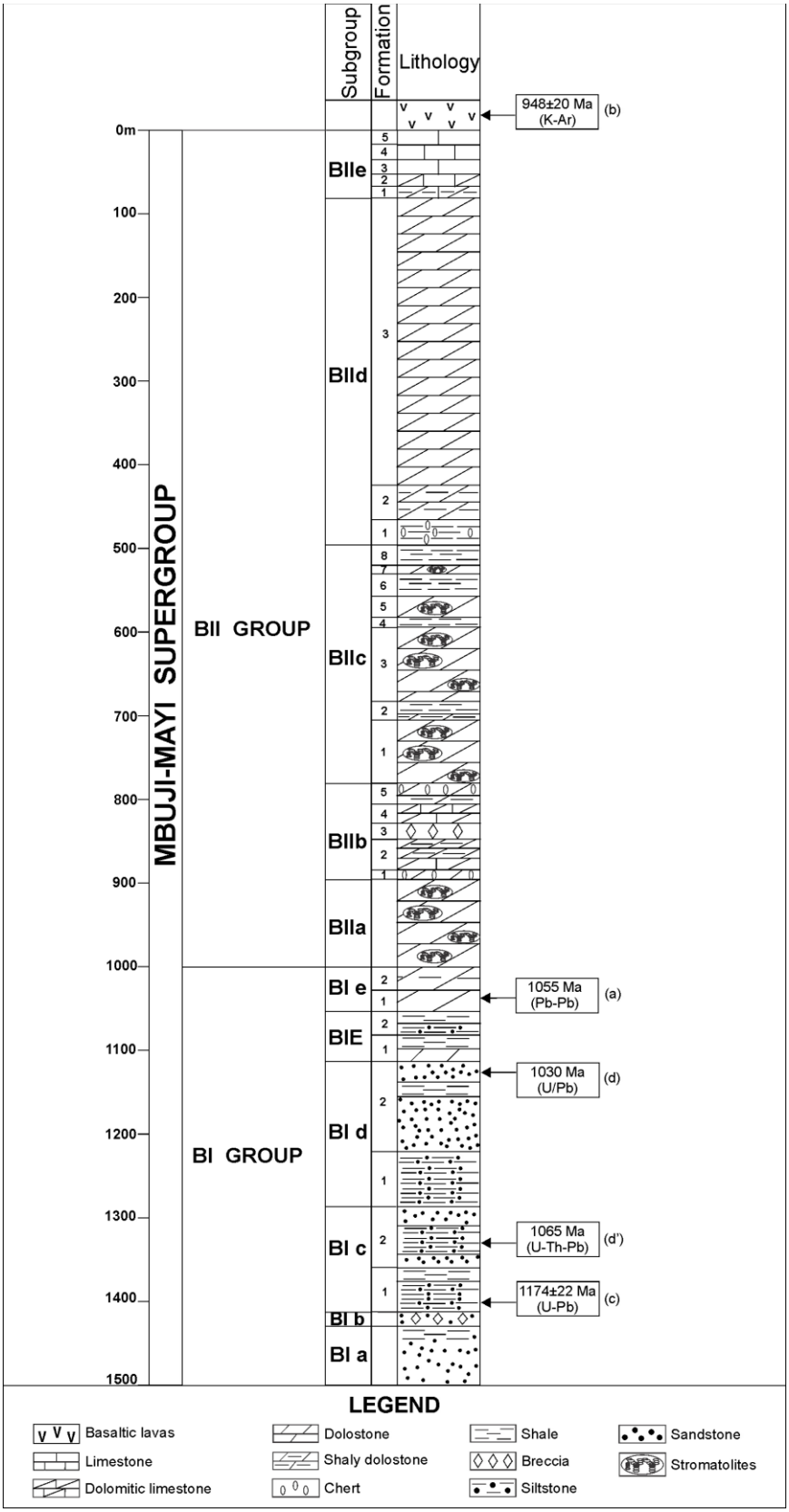

Fig. 3. Synthetic lithostratigraphy of Mbuji-Mayi Supergroup (modified from Raucq, 1957, 1970). Radiometric data from (a) Cahen (1974), (b) Cahen et al. (1984), Delpomdor et al. (2013a), (d) and (d') François et al. (2015 and *in preparation*)

by U-Pb methods on detrital zircon grains from the BId subgroup (in Kafuku 15 drill cores).

3. Materials and methods

3.1. Samples

In this study, five drill cores located within the Sankuru-Mbuji-Mayi area (western part of SMLL Basin) between Lubi and Luembe rivers (Fig. 2) were sampled. These drill cores were drilled in the 1950's and the cores are stored in the Department of Geology from the Royal Museum for Central Africa (RMCA) in Tervuren, Belgium. The studied drill cores were described by Wazilewski (1953) and Raucq (1957, 1970), from NW to SE (Fig. 4; with depths and number of treated samples in brackets). The drill core Lubi S70 (in Lubi Valley, 349 m depth and 96 samples) consists of the base of Mbuji-Mayi Supergroup, i.e. from the base of BIIa Subgroup up to the top of BIb Subgroup and reaches the contact with the granitic basement of the Kasai Block. The drill core Kanshi S13B (425 m depth, 66 samples) located at 11.5 km on the west of the Kanshi and Mbuji-Mayi rivers confluence, crosses the BII Group, more precisely from the base of the BIId Subgroup to the top of the BIIb Subgroup. The drill core Bena Tshovu (60 m depth, 6 samples) intersects the middle of the BIId Subgroup. The drill core Bena Kalenda (91 m depth, 28 samples) crosses the bottom of the BIIb Subgroup. Finally the drill core Kafuku 15 (200 m depth, 67 samples) cuts through the base of the BIIa Subgroup up to BId Subgroup. Thus, a total of 263 shale and siltstone samples have been investigated for micropaleontology in this study.

3.2. Sample preparation and microscopy

Organic-walled microfossils were extracted from thinly laminated siltstone and light to dark grey shale samples using slow acid maceration techniques (Grey, 1999), involving the dissolution of the mineral rock matrix by use of concentrated HCl and HF, followed by hot HCl to remove neo-formed fluorides, rinsing with dis-tilled water and decanting between each steps, with no centrifugation to minimize mechanical shocks. No oxidation was applied on organic residues. The macerates were filtered using 25 lm and 10 lm mesh-size filters for removal of fine-grained amorphous organic matter and facilitating taxonomic study of palynomorphs. For each sample, two slides of two size fractions (10–25 lm and >25 lm) were mounted permanently for optical microscopy study. Transmitted-light photomicrographs were acquired using an Axio Imager A1m microscope equipped with an AxioCam MRc5 digital camera (both Carl Zeiss, Germany). All specimens discussed here are deposited in the laboratory of Paleo biogeology-Paleopalynology-Paleobotany (PAL^3), Department of Geology, UR GEOLOGY, at the University of Liege. Specimens illustrated are provided with a slide number followed by an England Finder coordinates. Maithy's original slides (MRAC collection, Tervuren) were also examined.

4. Diversity of the Mbuji-Mayi assemblage

As noted above, the former studies carried out on Mbuji-Mayi assemblage (Baudet, 1987 and Maithy, 1975) reported several species of acritarchs and filamentous forms. Several of these species were synonymized to others species in later studies (Butterfield et al., 1994; Hofmann and Jackson, 1994; Sergeev et al., 1997; Sergeev, 2009; Yankauskas et al., 1989) or in the present study, as discussed in the systematic paleontology section (in supplementary data).

Our new investigation shows that organic-walled microfossils from the Mbuji-Mayi Supergroup are characterized by abundant sphaeromorph acritarchs, filamentous colonial aggregates and filamentous forms with a relatively low diversity of acanthomorphs (spine-bearing acritarchs).

A total of 49 taxa belonging to 27 genera are identified (Fig. 5), increasing the diversity relatively to previous reports, with some taxa reported for the first time in the Mbuji-Mayi Supergroup.

On the basis of morphological features, we categorize the Mbuji-Mayi assemblage into three groups:

(1) unambiguous eukaryotes, (2) possible eukaryotes or prokaryotes and (3) prokaryotes, probably bacteria.

(1) Unambiguous eukaryotes (11 species). – These include all acritarchs with processes that extend from vesicles walls (acanthomorphs): Germinosphaera bispinosa Mikhailova, 1986 (Fig. 6A–C); Trachyhystrichosphaera aimika Timofeev et al., 1976 (Fig. 6D–L); Trachyhystrichosphaera botula Tang et al., 2013 (Fig. 6M–O), and an unnamed form (Fig. 6P and Q); acritarch with neck-like expansions ?cf. Tappania sp. (Figs. 6R and 7A, B); acritarchs with ornamented walls: Lophosphaeridium granulatum Maithy, 1975 (Fig. 7C–E), Valeria elongata Nagovitsin, 2009 (Fig. 7F and G) and Valeria lophostriata Yankauskas, 1982 (Fig. 7H); disphaeromorphs (vesicle enclosing another vesicle): Pterospermopsimorpha insolita Timofeev, 1969 (Fig. 7I–L) and Pterospermopsimorpha pileiformis Timofeev, 1966 (Fig. 7M and N); and the multicellular Jacutianema solubila Timofeev and Hermann, 1979 (Fig. 7O–R) interpreted as the Gongrosira-phase of a vaucheriacean xanthophyte (Butterfield, 2004) or an undetermined eukaryote (Butterfield, 2015). All these microfossils show a level of morphological complexity, combining wall ornamentation or processes expanding from the wall surface, recalcitrant composition and large size, or large cell size and multicellularity, a combination unknown in prokaryotes to date (Javaux et al., 2003).

(2) Possible eukaryotes or prokaryotes (10 species). – Here, are included large smooth-walled vesicles that do not preserve enough characters to place them unambiguously among eukaryotes and could as well be prokaryotic. Sphaeromorphs with recalcitrant organic walls and occasional excystment structures by partial or medial split include several species of Leiosphaeridia (Fig. 8A–I). Older populations from the Mesoproterozoic Roper Group (Australia) have been shown to possess multilayered walls considered as a diagnostic criteria for eukaryotes when combined with large size, excystment structures, and recalcitrant composition (Javaux et al., 2004), however these observations cannot be expanded to all leiospheres without time-consuming ultrastructural analyzes, since Leiosphaeridia spp. are probably polyphyletic. The species reported here include: Leiosphaeridia crassa Naumova, 1949 (Fig. 8A–C); Leiosphaeridia jacutica Timofeev, 1966 (Fig. 8D); Leiosphaeridia minutissima Naumova, 1949 (Fig. 8E); Leiosphaeridia tenuissima Eisenack, 1958 (Fig. 8F); Leiosphaeridia ternata Timofeev, 1966 (Fig. 8G) and Leiosphaeridia sp. (Fig. 8H and I). Other species that could be eukaryotic or prokaryotic include relatively large single oval vesicles such as Navifusa actinomorpha Maithy, 1975 (Fig. 8J and K) and Navifusa majensis Pyatiletov, 1980 (Fig. 8L), large vesicles with smaller attached vesicles Coneosphaera sp. (Fig. 8M and N), vesicles forming multicellular chains Arctacellularia tetragonala Maithy, 1975 (Figs. 8O–R, 9A–J and 10) previously interpreted as putative fungi at different stages of their life cycle (Hermann and Podkovyrov, 2008).

(3) Prokaryotes, probably bacteria (28 species). – This category captures all remaining microfossils with simple organization and occurring in filamentous colonial aggregates, or filamentous and coccoidal forms: Chlorogloeaopsis kanshiensis Maithy, 1975 (Fig. 9K) and Chlorogloeaopsis zairensis Maithy, 1975 (Fig. 9L); Polysphaeroides filliformis Hermann in Timofeev et al., 1976 (Fig. 9M–R); Glomovertella miroedikhia Hermann in Hermann and Podkovyrov, 2008 (Fig. 11A and B); Obruchevella valdaica Shepeleva, 1974

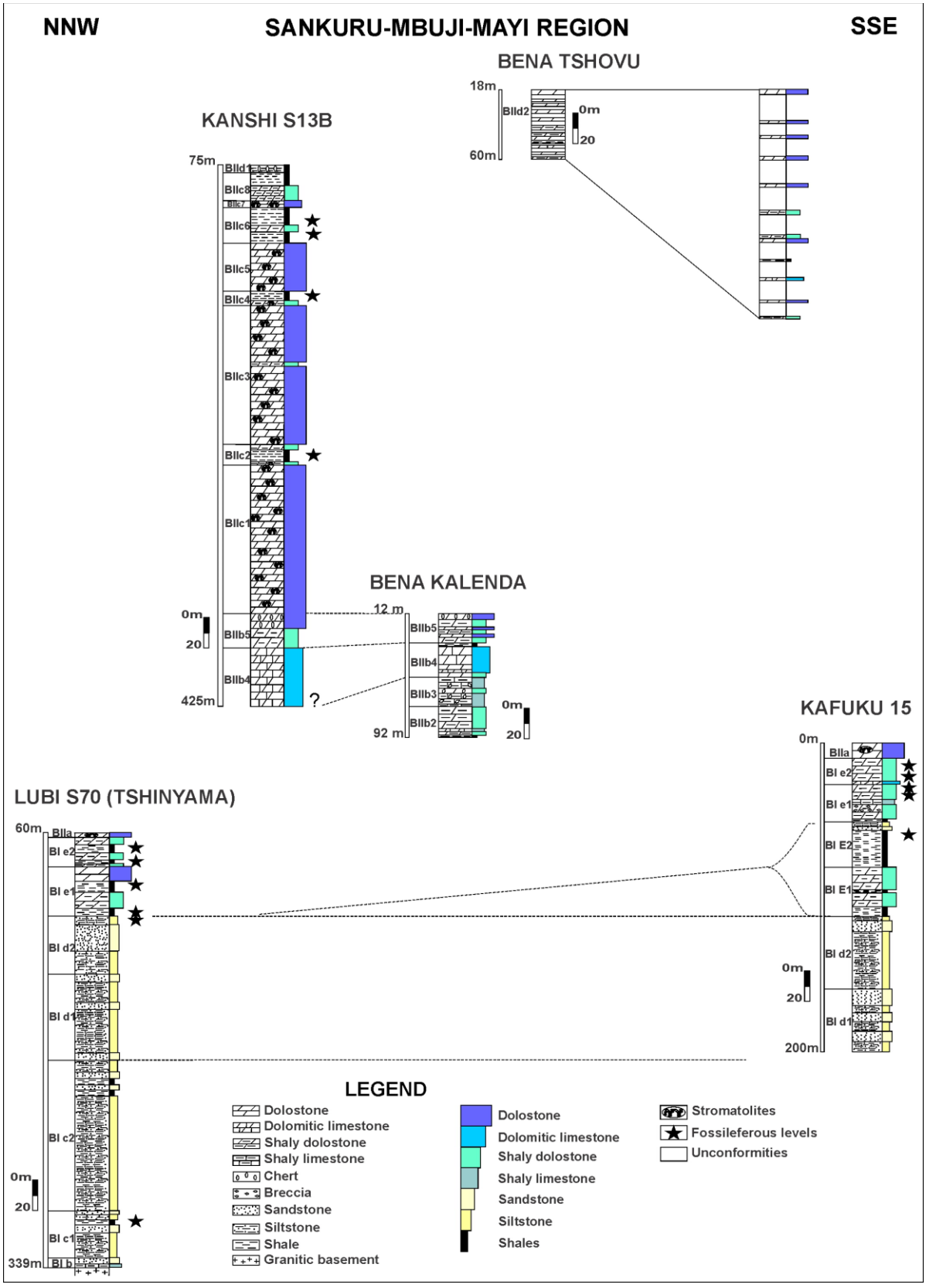

Fig. 4. Detailed lithology of studied drill cores with indication of fossiliferous levels. Unconformities are exclusively present in Bena Tshovu drill core. Modified from Delpomdor et al. (2013a) and Raucq (1970).

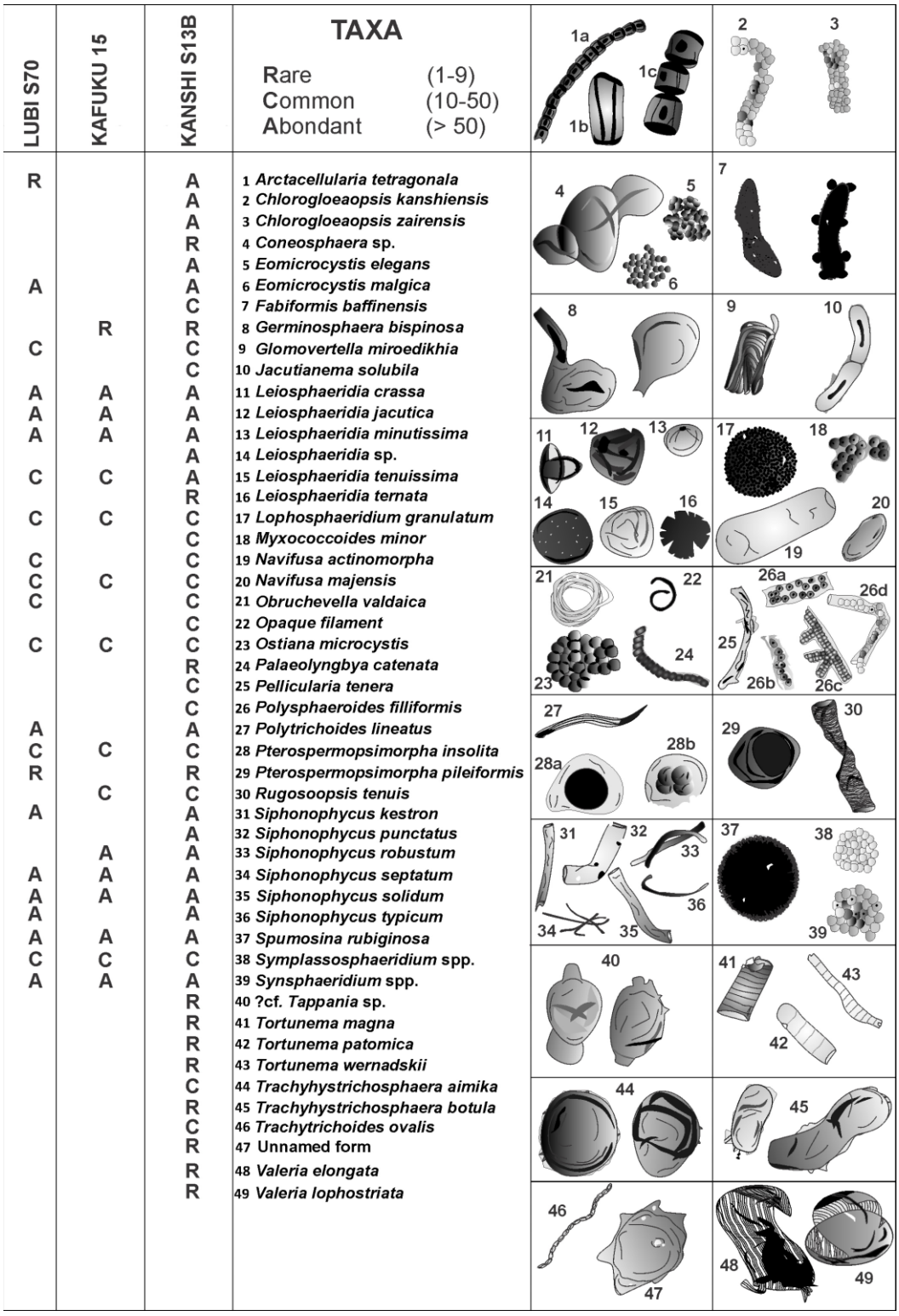

Fig. 5. The taxonomic composition of Mbuji-Mayi assemblage and their distribution relative to studied drill cores.

(Fig. 11C); Opaque filament (possibly pyritized Siphonophycus sp, but this remains to be evidenced, Fig. 11D); Palaeolyngbya catenata Hermann, 1974 (Fig. 11E and F); Pellicularia tenera Yankauskas,1980 (Fig. 11G); Polytrichoides lineatus Hermann, 1974 (Fig. 11H); Rugosoopsis tenuis Timofeev and Hermann, 1979 (Fig. 11I–K); Siphonophycus kestron Schopf, 1968 (Fig. 11L); Siphonophycus

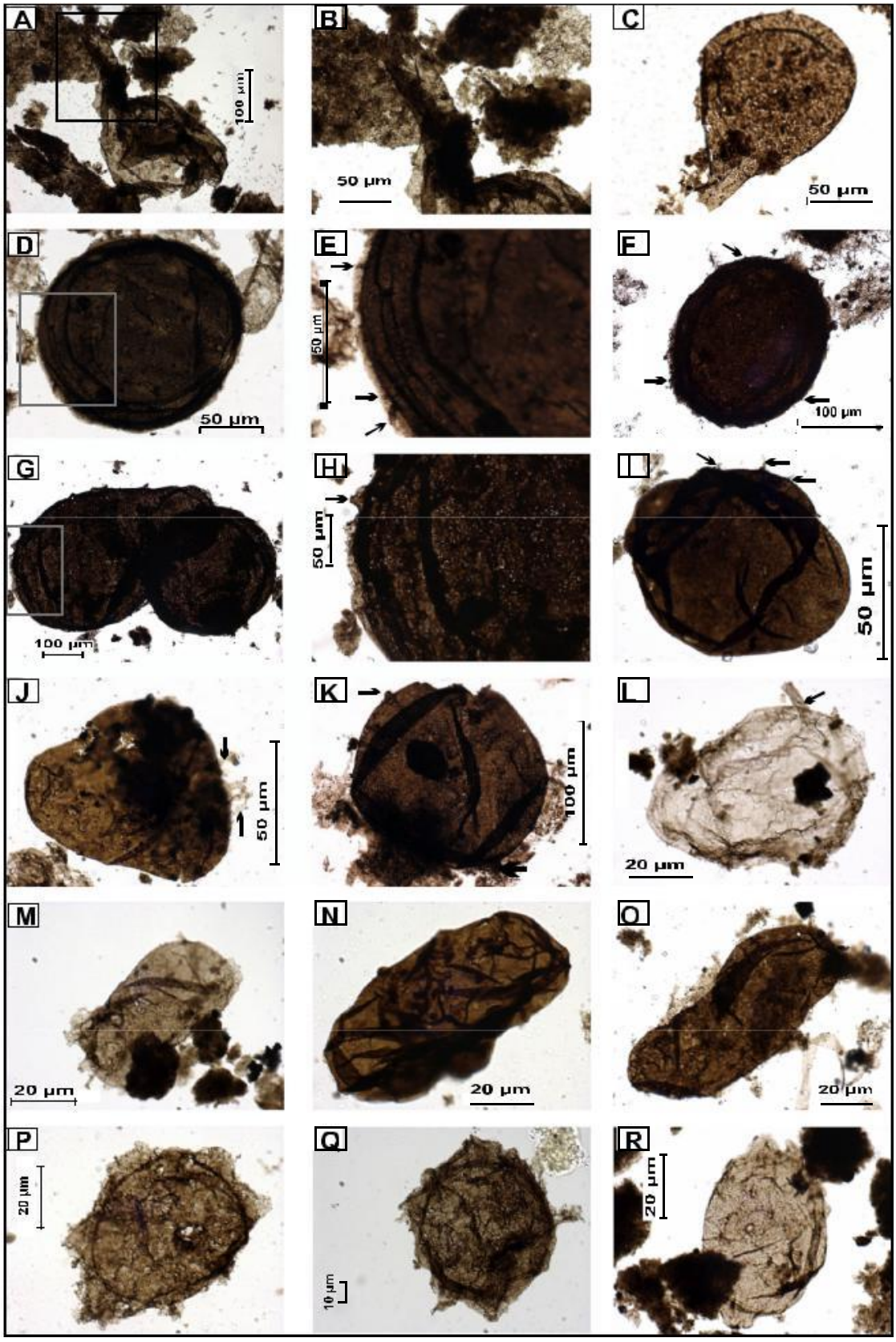

Fig. 6. (A–C) Germinosphaera bispinosa, (A) specimen 65066/W-44-1 and (B) magnification of box area in A; (C) Germinosphaera bispinosa, specimen 65066/Z-57-1. (D–L) Trachyhystrichosphaera aimika, with processes at the arrows (D) specimen 65078/G-44-1; (E) magnification of box area in D; (F) specimen 65084/S-56-4; (G) specimen 71270/ V-32-3; (H) magnification of box area in G; (I) specimen 65078/S-41-4; (J) specimen 65092/P-40-3; (K) specimen 65092/W-37-1; (L) specimen 65058/P-42-3. (M–O) Trachyhystrichosphaera botula, (M) specimen 65059/V-58-1; (N) specimen 65084/O-45-3; (O) specimen 65092/L-30-4. (P and Q) Unnamed form, specimens 65092/B-54-2 and 65096/C-56-2 respectively. (R) ?cf. Tappania sp., specimen 65061/Q-34-1; (R) specimen.

174

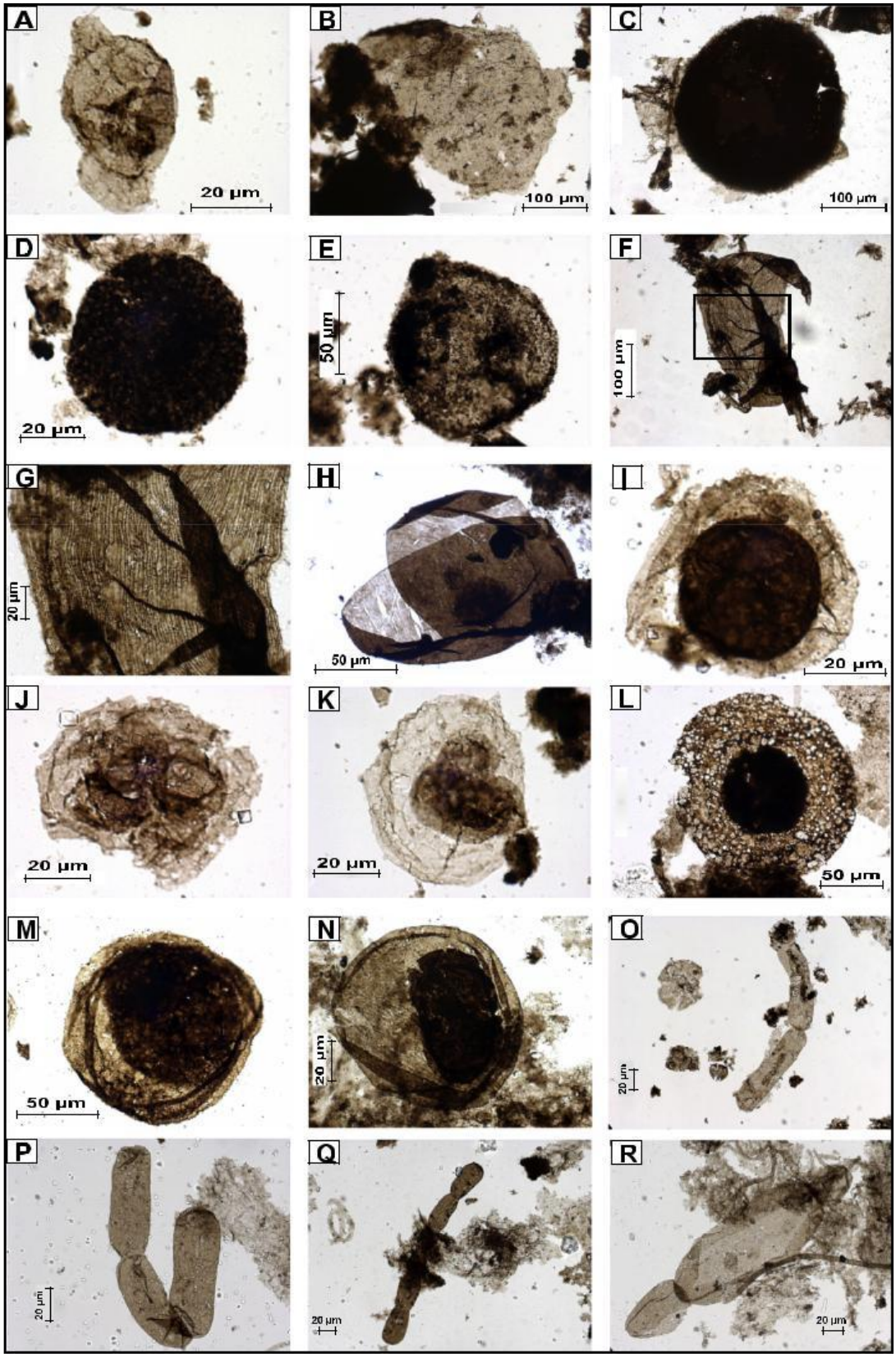

Fig. 7. (A and B)?cf. Tappania sp., specimens 65065/J-29-3 and 65066/J-40-4 respectively. (C–E) Lophosphaeridium granulatum, specimens 65078/P-29-2, 65255/R-48-2 and 65062/F-59-4 respectively. (F and G) Valeria elongata, (F) specimen 65066/T-39-1, with longitudinal striations and (G) magnification of box area in F. (H) Valeria lophostriata, specimen 71707/J-51-2, with concentric striations on inner side of the wall. (I–L) Pterospermopsimorpha insolita, (I) specimen 65092/F-38-4; (J) and (K) dividing specimens, 65078/ G-58-4; 65087/L-49-2 respectively; (L) specimen with perforations, probably caused by mineral dissolution during extraction process, 65086/J-34-3. (M and N) P. pileiformis specimens 65080/N-36-4 and 65080/S-32-1 respectively. (O–R) Jacutianema solubila, (O) and (P) botuliform cells in pair or triad, specimens 65083/U-60-4 and 65080/E-33-1 respectively; (Q) specimen 65078/O-28-2, linear chain showing incomplete division; (R) specimen 65080/Q-39-1, sausage-shaped cells with associated thin-walled vesicles.

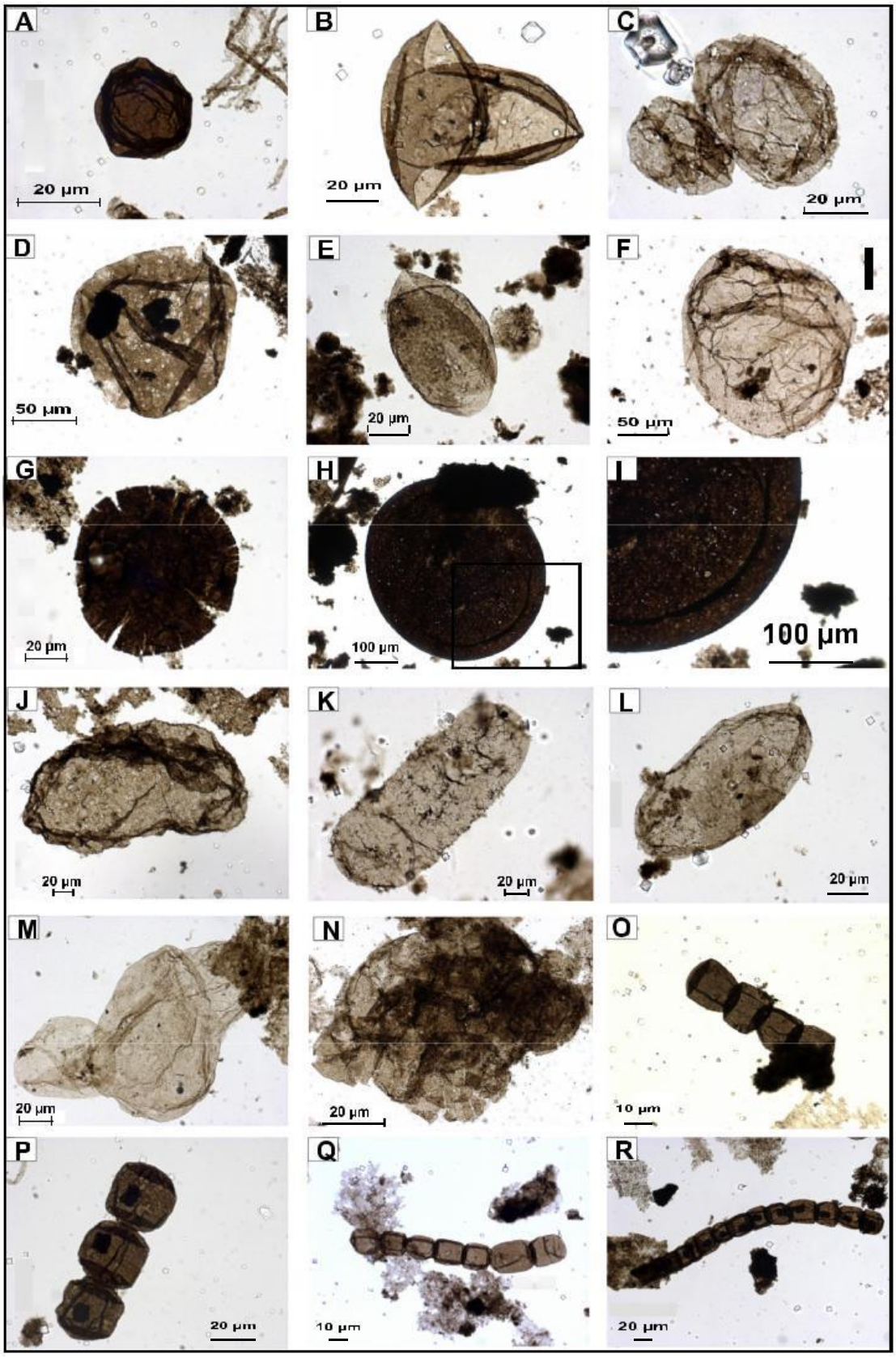

Fig. 8. (A–C) Leiosphaeridia crassa, (A) specimen 65078/R-59-2; (B) specimen 65078/F-55-1, with excystment structure by medial split and (C) two joined vesicles, specimens 65078/J-55-1; (D) L. jacutica, specimen 65058/O-43-2; (E) L. minutissima, specimen 65063/D-32-2; (F) L. tenuissima, specimen 65064/S-26-2; (G) L. ternata, specimen 65088/P-36-2; (H and I) Leiosphaeridia sp. with concentric peripheral folding and tiny pores on more opaque wall, (H) specimen 71270/H-32-3 and (I) magnification of box area in H. (J and K) Navifusa actinomorpha, (J) specimen 65078/R-49-2; (K) specimen 67082/B-36-3. (L) N. majensis, specimen 65078/F-54-1. (M and N) Coneosphaera sp., specimens 65084/E-48-3 showing a stage of cell-division and 65080/O-39-4. (O–R) Arctacellularia tetragonala, (O) specimen 65078/N-49-3 with ellipsoidal cells; (P) specimen 65078/M-53-3 showing a development of cells shape from ellipsoidal to barrel-shaped; (Q) specimen 65078/F-54-2; (R) specimen 65078/H-50-4.

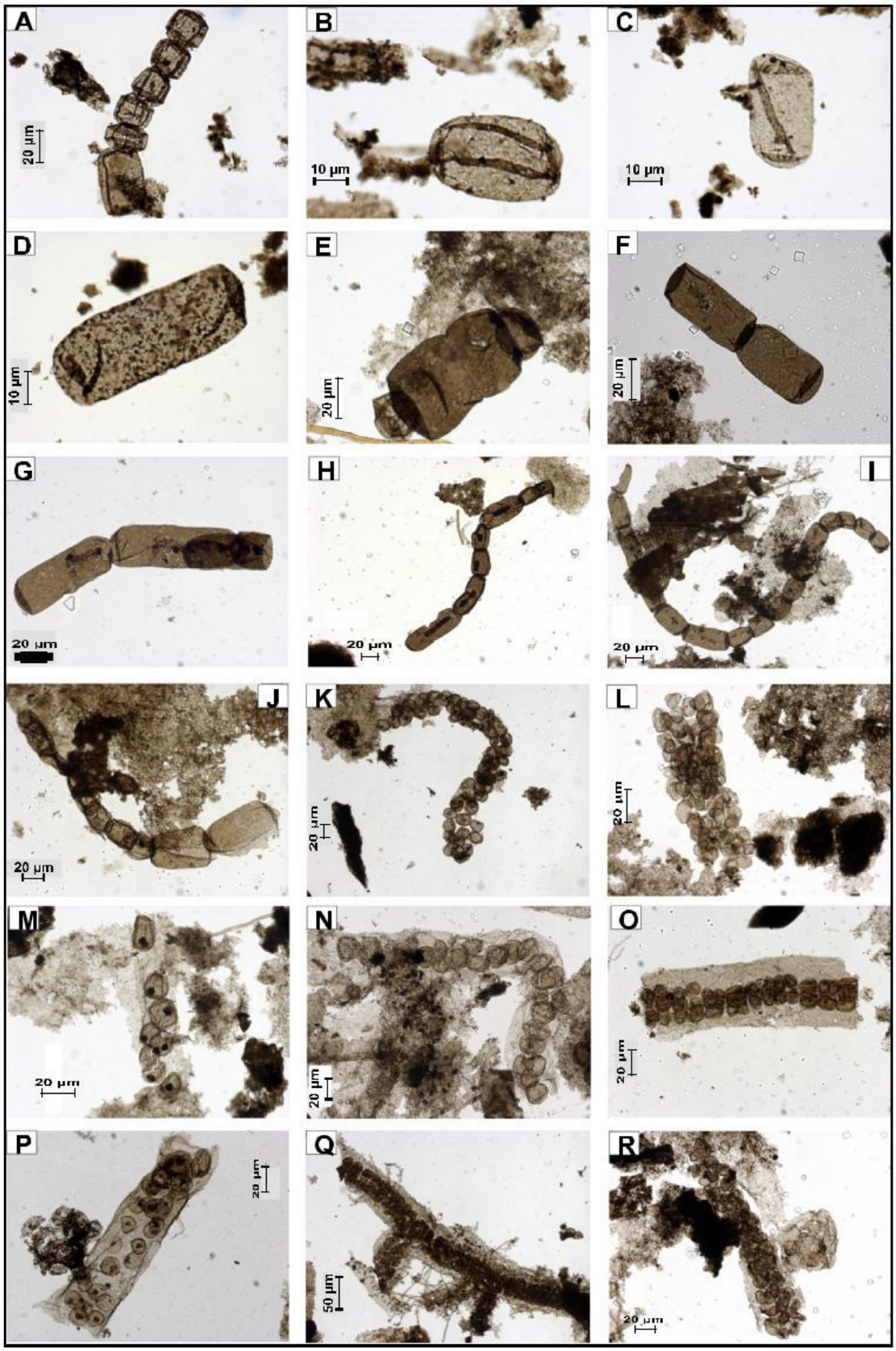

Fig. 9. (A–J) Arctacellularia tetragonala, (A) specimen 65091/X-58-4 with barrel-shaped cell in one of ends; (B–D) single vesicle, previously regarded as A. kelleri, specimens 65067/O-60-1, 65065/J-34-3 and 65067/H-39-3 respectively; (E) barrel-shaped vesicle with small vesicles in ends, specimen 65078/V-51-4; (F and G) dyads of cylindrical vesicles, specimens 65078/G-58-3 and 65078/Q-52-2 respectively; (H–J) chains of several barrel-shaped and ellipsoidal vesicles with or without dark inclusion, specimens 65078/N-53-4, 65078/H-47-1 and 65086/C-29-4 respectively. (K) Chlorogloeaopsis kanshiensis, specimen 65080/P-52-4. (L) Chlorogloeaopsis zairensis, specimen 65078/N-60-3. (M–R) Polysphaeroides filliformis, (M and N) cells in one row, specimens 65081/G-53-465080/X-31-3 respectively; (O) specimen 65080/N-48-3; (P) cells irregularly distributed in sheath, specimen 65080/E-53-3; (Q) branched specimen 65080/L-52-3 and (R) specimen 65078/P-57-3, with sheath more degraded and less conspicuous.

punctatus Maithy, 1975 (Fig. 11M); Siphonophycus robustum (Fig. 11N.r) and Siphonophycus septatum Schopf, 1968 (Fig. 11N. s); Siphonophycus solidum Golub, 1979 (Fig. 11O); Siphonophycus typicum Hermann, 1974 (Fig. 11N.t); Tortunema magna Tynni and Donner, 1980 (Fig. 11P); Tortunema patomica Kolosov, 1982 (Fig. 11Q); Tortunema wernadskii Shepeleva, 1960 (Figs. 11R, 12A); Trachytrichoides ovalis Hermann in Timofeev et al., 1976 (Fig. 12B and C); Eomicrocystis elegans Golovenok and Belova, 1984 (Fig. 12D and E); Eomicrocystis malgica Golovenok and Belova, 1985 (Fig. 12F); Fabiformis baffinensis Hofmann in Hofmann and Jackson, 1994 (Fig. 12G and H); Myxococcoides minor Schopf, 1968 (Fig. 12I); Ostiana microcystis Hermann in Timofeev et al., 1976 (Fig. 12J); Spumosina rubiginosa Andreeva, 1966 (Fig. 12K); Symplassosphaeridium spp. (Fig. 12L) and Synsphaeridium spp. (Fig. 12M). All these species are present in the Kanshi S13B drill core while both the Lubi S70 and Kafuku 15 cores contain respectively 22 and 16 taxa. No microfossils were recovered from the (mostly carbonate) Bena Kalenda and Bena Tshovu drill cores. The fossiliferous formations are, from bottom to top: BIc_1, BId_2 (clastic facies with interbedded shales); BIE_2, BIe_1, BIe_2 (essentially homogenous dolo-mudstones and dolo-laminites with interbedded shales); $BIIc_2$, $BIIc_4$ and $BIIc_6$ (dark grey/brown shales). The richest level, in terms of diversity and abundance, is located in the Kanshi S13B drill core ($BIIc_6$ Formation) between 111 and 122.9 m depth. The color of the microfossils and particulate organic matter in the investigated samples varies from light brown to dark brown, even to black for most samples from the Kafuku 15 drill core. Difference in diversity and abundance of recovered microfossils (Fig. 13) in these drill cores are probably more related to differences in facies and diagenetic alteration, the Lubi S70 and Kafuku 15 sedimentary rocks representing very shallow environments with signs of emersion (mudcraks, gypsum/anhydrite layers), that have been interpreted as lacustrine and sabkha environments in supratidal zone (Delpomdor et al., 2013b, 2015). However, new geochronology is ongoing to better constrain the age of the BI and BII groups (previously dated between 1174 and 948 Ma) and test if the difference in diversity and abundance could be related to stratigraphy rather than ecology and preservation (François et al., 2015). The highest diversity, abundance and better preservation of organic materials including microfossils, occur in subtidal to intertidal marine shales deposited between stromatolitic carbonates preserved in the Kanshi S13B drill core (Upper part of Mbuji-Mayi Supergroup).

5. Biostratigraphic implications

As seen above, the Mbuji-Mayi assemblage is exceptionally diversified (49 taxa) and well-preserved. All of these microfossils (except one taxon) are known from different coeval Late Mesoproterozoic and Early Neoproterozoic assemblages worldwide (Fig. 14), although not all species are reported in every assemblage. Similar assemblages occur in Eurasia: the possible Tonian Lower Vychegda Formation (Lower assemblage) in Russia (Vorob'eva et al., 2009a); the Tonian Chichkan Formation in Kazakhstan (Sergeev and Schopf, 2010); the Tonian Miroedikha Formation, the Latest Mesoproterozoic Suukhaya Tunguska Formation and Lakhanda Group in Siberia (Hermann, 1990; Hermann and Podkovyrov, 2007, 2008; Knoll et al., 1995; Petrov and Semikhatov, 1997; Semikhatov et al., 2000; Sergeev et al., 1997; Yankauskas et al., 1989); the Mesoproterozoic Dzhelindukon Formation, Yurubchen Formation (Nagovitsin, 2009; Nagovitsin et al., 2010 and references therein) and Kotuikan Formation in Siberia (Vorob'eva et al., 2015); the Mesoproterozoic Sarda Formation of the Bahraich Group, Ganga Basin, in India (Prasad and Asher, 2001); the Tonian Gouhou Formation (Tang et al., 2015), Liulaobei Formation and Dongjia Formation

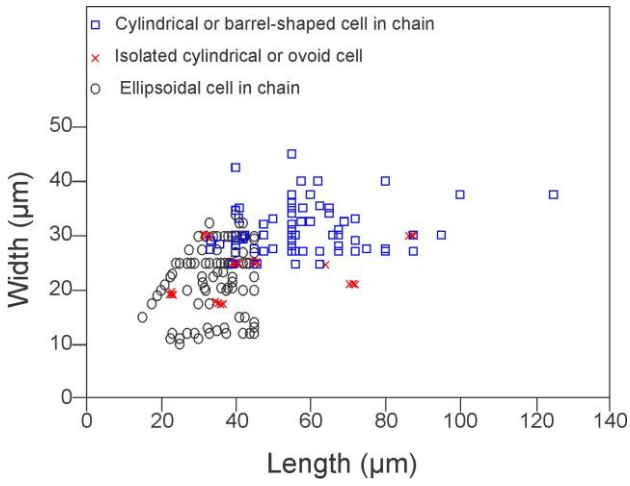

Fig. 10. Size distribution of Arctacellularia showing that ellipsoidal and barrel-shaped cells (that may occur within the same chain of cells) also overlap in diameter range, therefore suggesting they represent a single species (A. tetragonala) at different stage of development and displaying a variable cellular morphology.

in North China (Tang et al., 2013; Yin and Guan, 1999); the Tonian Svanbergfjellet Formation in Spitsbergen (Butterfield et al., 1994). In North America, taxa common with the Mbuji-Mayi assemblage occur in the Tonian Uinta Mountain Group and Chuar Group in USA (Nagy and Porter, 2005; Porter et al., 2003; Vidal and Ford, 1985); the Tonian Wynniatt Formation (Butterfield, 2005a,b; Butterfield and Rainbird, 1998); the Latest Mesoproterozoic Lone Land Formation (Samuelsson and Butterfield, 2001) and Bylot Supergroup (Hofmann and Jackson, 1994), all three in Canada. In Australia, some of the taxa are reported in the Tonian Kanpa Formation and Hussar Formation (Hill et al., 2000), the Alinya Formation (Zang, 1995) and Bitter Springs Formation (Schopf, 1968; Schopf and Blacic, 1971); and the Mesoproterozoic Roper Group (Javaux et al., 2001; Javaux and Knoll, in press). Similarities also occur with assemblages in the Mesoproterozoic Thule Supergroup, Greenland (Samuelsson et al., 1999) and Sao Francisco Craton, Brazil (Simonetti and Fairchild, 2000).

The Mbuji-Mayi assemblage is particular due to the association of taxa which are until now typical of Tonian of Asia (Trachyhystrichosphaera botula in the Liulaobei Formation) and the Mesoproterozoic–Early Neoproterozoic of East European Platform (G. miroedikhia, Polysphaeroides filliformis, V. elongata) with other ubiquist taxa (i.e. V. lophostriata, J. solubila, A. tetragonala, P. insolita, P. pileiformis, T. aimika ?cf. Tappania plana, G. bispinosa, S. rubiginosa, L. crassa, L. minutissima, L. jacutica, L. tenuissima, L. ternata, Tortunema spp., Siphonophycus spp. and others). J. solubila shows several morphotypes (Figs. 7P–R, 8A) similar to those only reported in the Tonian Svanbergfjellet Formation of Spitsbergen (Butterfield, 2004) and the El Mreiti Formation in Mauritania (Beghin et al., in review; this species is reported in several other locations but the variability is rarely reported) and A. tetragonala also displays a range of morphologies unreported elsewhere (Fig. 9D–H). There are also other differences between the Mbuji-Mayi and other contemporaneous assemblages: Kildinosphaera verrucata Vidal in Vidal and Knoll, 1983, Simia spp. and Satka spp. are absent in the Mbuji-Mayi assemblage, while an unnamed acanthomorph species has not been reported elsewhere so far.

All of the assemblages cited above range from the Late Mesoproterozoic to the Tonian, constraining the Mbuji-Mayi microfossil assemblage to this time range. This is consistent with geochronological data on the minimum age of the Mbuji-Mayi

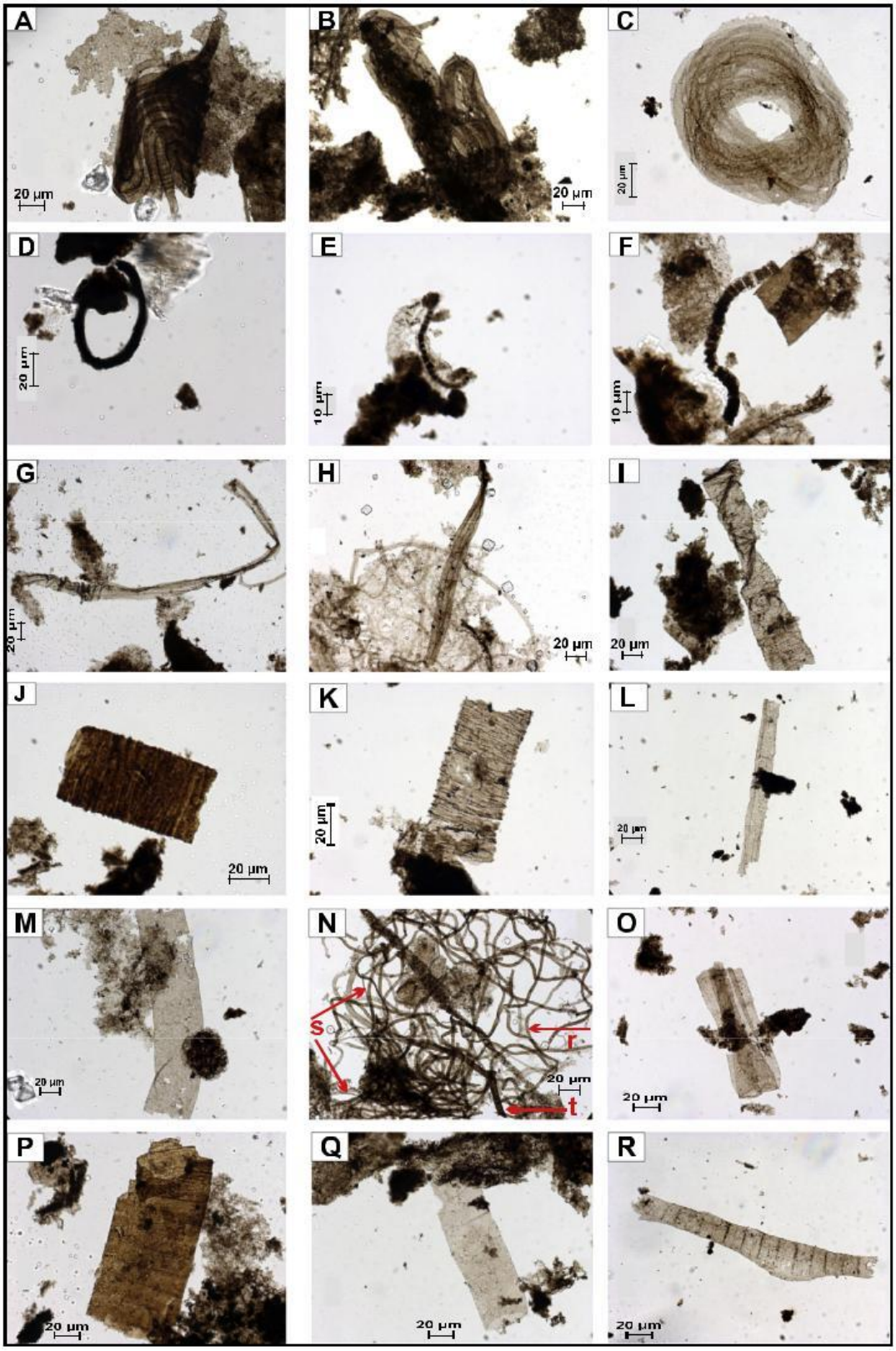

Fig. 11. (A and B) Glomovertella miroedikhia, specimens 65078/U-38-1 and 65092/J-50-1 respectively. (C) Obruchevella valdaica, specimen 65271/W-40-3. (D) Opaque filament, specimen 65058/V-46-2. (E and F) Palaeolyngbya catenata, specimens 65059/H-57-4 and 65081/Y-32-1 respectively. (G) Pellicularia tenera, specimen 65054/F-29-2. Polytrichoides lineatus, specimen 65078/V-60-3. (I–K) Rugosoopsis tenuis, (I) specimen 65064/P-35-1; (J) specimen 65064/N-30-3 with a thicker inner tubular sheath and specimen 65065/R-37-4. (L) Siphonophycus kestron, specimen 65065/V-40-4. (M) Siphonophycus punctatus, specimen 65078/U-48-3. (N) Microbial mat consisting of Siphonophycus robustum, denoted by arrow marked with ‘‘r” S. septatum denoted by arrow marked with ‘‘s” and S. typicum, denoted by arrow marked with ‘‘t”, specimen 65078/T-59-1. (O) Siphonophycus solidum, specimen 65067/Y-60-2. (P) Tortunema magna, specimen 65092/S-36-2. (Q) Tortunema patomica, specimen 65064/X-41-3. (R) Tortunema wernadskii, specimen 65065/X-59-4.

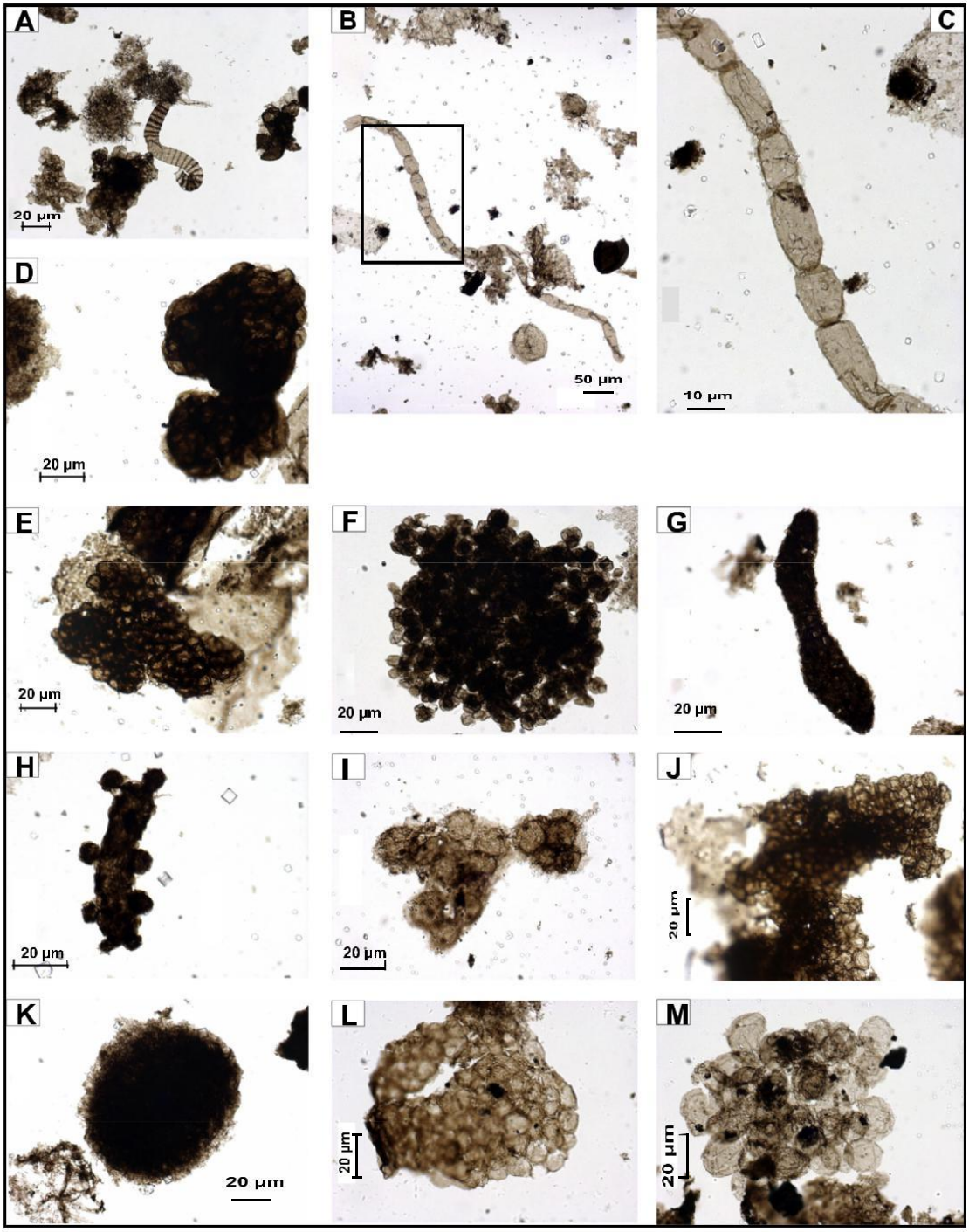

Fig. 12. (A) Tortunema wernadskii, specimen 65079/C-45-2. (B and C) Trachytrichoides ovalis, (B) specimen 65078/H-56-4; (C) magnification of box area in B. (D and E) Eomicrocystis elegans, specimens 65078/K-48-3, 65086/C-38-1 respectively. (F) Eomicrocystis malgica, specimen 65271/V-50-2. (G and H) Fabiformis baffinensis, specimens 65079/O-27-3 and 65078/K-49-2 respectively. (I) Myxococcoides minor, specimen 65080/F-46-4. (J) Ostiana microcystis, specimen 65086/W-26-1. (K) Spumosina rubiginosa, specimen 65078/T-50-1. (L) Symplassosphaeridium spp., specimen 65385/Q-51-4. (M) Synsphaeridium spp., specimen 65064/O-48-3.

1030 and 1065 Ma and obtained on diagenetic monazites and xenotimes coming from Lubi S70 and Kafuku 15 drill cores (François et al., in prep).

In addition, the Mbuji-Mayi assemblage includes a relatively low diversity of acanthomorphs that are distinct from the well-known Ediacaran Complex Acanthomorph Palynoflora or ECAP (Grey, 2005; Moczydłowska, 2005; Moczydłowska and Nagovitsin, 2012; Sergeev et al., 2011; Vorob'eva et al., 2009a). Nevertheless more than half (14 taxa) of the lowermost Vychegda assemblage including T. aimika (Vorob'eva et al., 2009a,b) also occurs in the Mbuji-Mayi assemblage (Fig. 14) but these are ubiquitous.

Most of the Mbuji-Mayi microfossils are stratigraphically extremely long-ranging and thus, they are of a limited biostratigraphic value. In particular, V. lophostriata and Leiosphaeridia spp. are known since the late Paleoproterozoic, the Changzhougou Formation, North China (Lamb et al., 2009; Peng et al., 2009) and the Mallapunyah Formation, Australia (Javaux et al., 2004). Simple leiospheres occur in even older rocks, such as the Archean Moodies Group, South Africa (Javaux et al., 2010) and the Paleoproterozoic

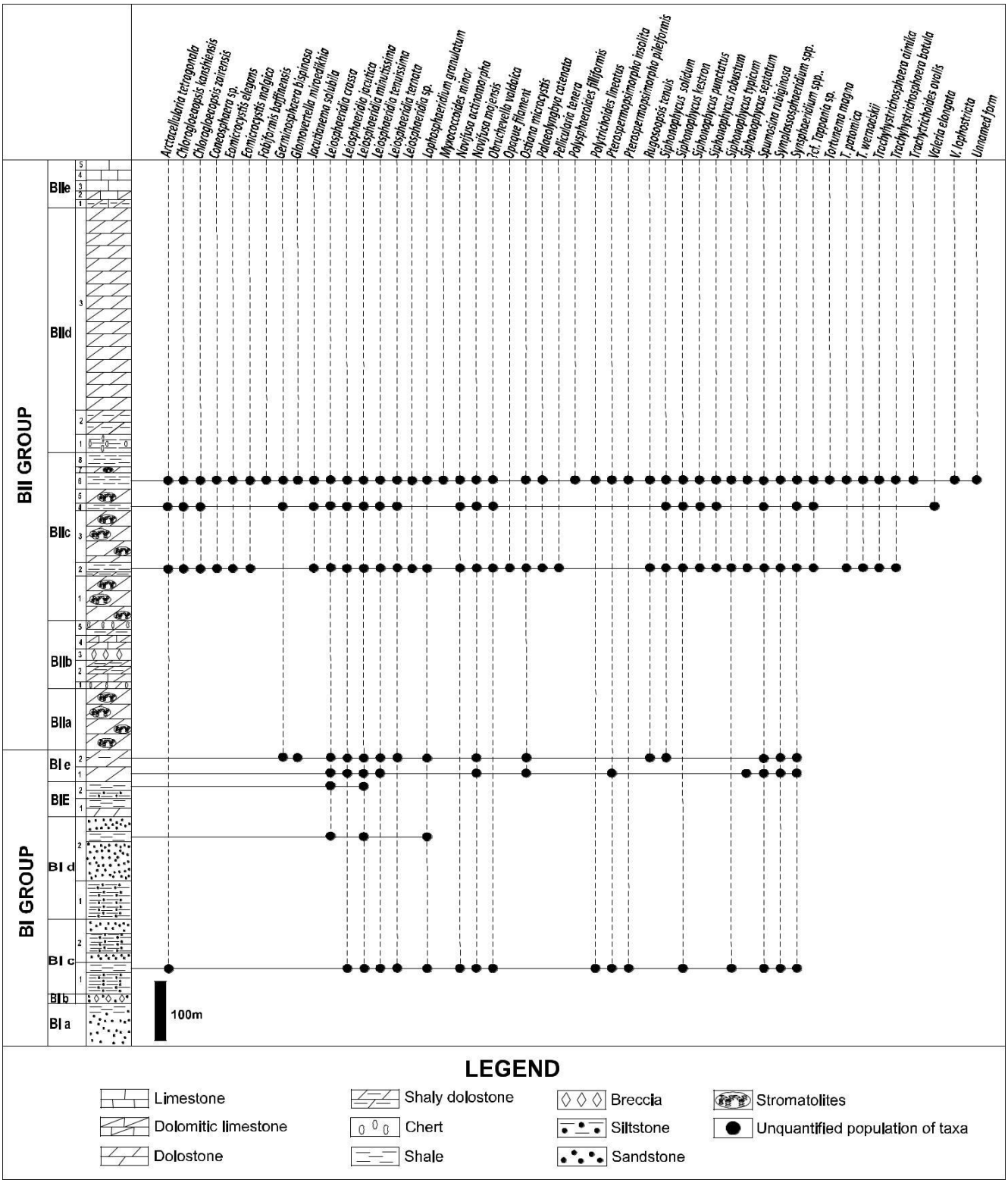

Fig. 13. Chart showing the distribution of microfossils within the Mbuji-Mayi Supergroup.

Kondopoga Formation, Karelia, Russia (Javaux et al., 2012). Only T. aimika may be a useful index fossil due to its relatively short stratigraphic extension (Moczydlowska, 2008; Sergeev, 2009). Indeed, T. aimika is reported from rocks ranging from the Late Mesoproterozoic: the Lakhanda Group, Siberia (Hermann, 1990; Semikhatov et al., 2000 and Yankauskas et al., 1989); the Lone Land Formation, Canada (Samuelsson and Butterfield, 2001) and the El Mreiti Formation, Mauritania (Beghin et al., in review), to pre-Sturtian successions: the Liulaobei Formation, China (Tang et al., 2013); the Wynniatt Formation, Canada (Butterfield, 2005a,b; Butterfield and Rainbird, 1998); the Sirbu shale Formation, India (Srivastava, 2009); the Svanbergfjellet Formation, Spitsbergen (Butterfield et al., 1994); the Alinya Formation, Australia (Zang, 1995); the Chichkan Formation, Kazakhstan (Sergeev and Schopf,

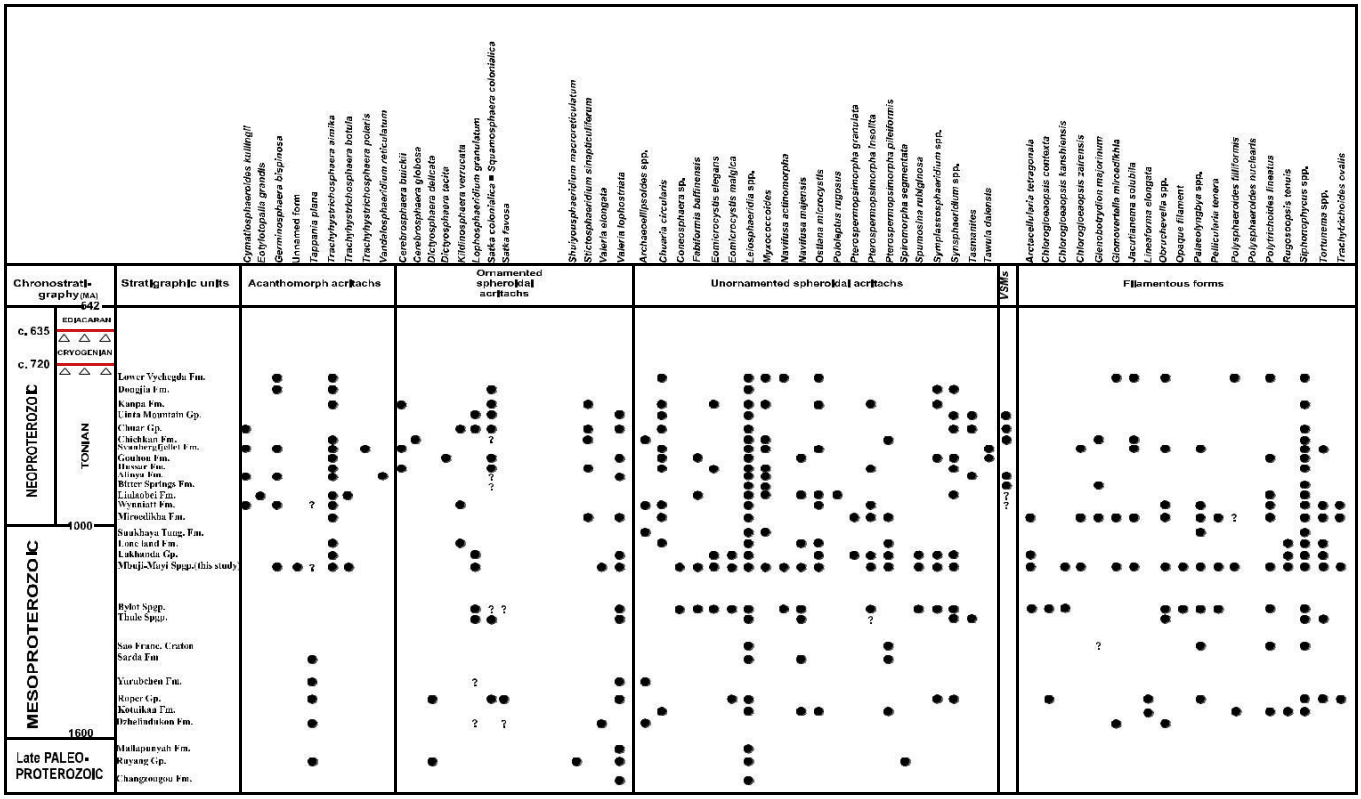

Fig. 14. Distribution of the main types of microfossils from the Late Paleoproterozoic through the Tonian, based on compilation data from some representative assemblages. The relative positions or orders are still uncertain and some of their possible ages may overlap. Therefore, species are listed alphabetically, and their order here has no indication on their relative position in each period (details on location, ages and various references, see in text), nor on biological affinities. Acanthomorph and ornamented spheroidal acritarchs are interpreted as eukaryotic (see text) while unornamented sphaeromorphs and filamentous forms include taxa that are eukaryotic (such as Jacutienema, Lineaforma, Pterospermopsimorpha, Tasmanites), others that could be prokaryotic or eukaryotic (Arctacellularia, Leiosphaeridia), and probable bacteria (Siphonophycus...). Cryogenian limits come from the new Precambrian chart (2015) of the International Commission on Stratigraphy (www.stratigraphy.org). The triangle symbol marks the chronostratigraphic level of the Sturtian and Marinoan glaciation intervals. Dark circles denote presence (unquantified abundance) of taxa. Question mark denotes form assumed similar to a putative species (e.g. Tappania? sp., in this study). Fm. – Formation; Gp. – Group; Spgp. – Supergroup; VSMs, vase-shaped microfossils.

2010) and the Lower Vychegda Formation, Russia (Vorob'eva et al., 2009a,b). Moreover, T. aimika co-occurs with T. botula previously reported in the Liulaobei Formation (Tang et al., 2013).

In summary, the Mbuji-Mayi assemblage has a transitional composition of Late Mesoproterozoic and Early Neoproterozoic (pre-Sturtian) assemblages known worldwide.

Comparison with worldwide marine assemblages (Figs. 14 and 15) permits to suggest assemblages useful for global pre-Sturtian Proterozoic biostratigraphy, although adjustments may be needed as new assemblages are discovered in the future:

– For the Late Paleoproterozoic – Early Mesoproterozoic: Archaeoellipsoides spp., Dictyosphaera delicata, L. granulatum, Satka favosa, Squamosphaera colonialica, T. plana, T. ovalis, V. lophostriata, are common, and Lineaforma elongata, Shuiyousphaeridium macroreticulatum, as well as V. elongata have more local distributions.

– For the Middle Mesoproterozoic – Early Neoproterozoic (Tonian): Archaeoellipsoides spp, A. tetragonala, G. bispinosa, J. solubila, L. granulatum, T. aimika, V. lophostriata are widespread;
K. verrucata and Simia annulare are common but not ubiquist; S. colonialica, and V. elongata has a more restricted distribution.

– Within the above time range, a few species have shorter strati-graphic range and are reported only in Tonian (pre-Sturtian) rocks so far: Cerebrosphaera buickii, Cymatiosphaeroides kullingii,
T. botula, Vandalosphaeridium reticulatum, and VSMs.

6. Conclusions

The exceptionally diverse and well-preserved organic-walled microfossil assemblage from the Mbuji-Mayi Supergroup is dominated by sphaeromorph acritarchs and filamentous forms, and a moderate diversity of eukaryotes. A total of 49 taxa belonging to 27 genera were identified, including 11 species of unambiguous eukaryotes, 10 species of possible eukaryotes or prokaryotes and 28 species of probable bacteria. This is one of the first detailed microfossil studies in the Mesoproterozoic–Neoproterozoic interval in Central Africa, revealing the occurrence of several taxa, including acanthomorphs, for the first time in Africa, but known elsewhere except for one unnamed, possibly new, species. Comparison with other microfossil assemblages shows that the Mbuji-Mayi assemblage is likely Late Mesoproterozoic–Early Neoproterozoic in age. This biostratigraphic constraint is consistent with avail-able geochronological data (Cahen et al., 1984; Delpomdor et al., 2013a; François et al., 2015, in prep.).

Although the Mbuji-Mayi eukaryotes do not display unique morphological characters permitting to relate them to modern protists and other eukaryotes, they could, based on molecular phylogenies (e.g. Eme et al., 2014), include stem group eukaryotes (before LECA, the last eukaryotic common ancestor), and stem and crown group members within crown groups (after LECA). Future micro-analyzes investigating the ultrastructure and chemistry of these microfossils may help refine their taxonomy (e.g. Javaux and Marshall, 2006). Regardless of taxonomy, these Meso

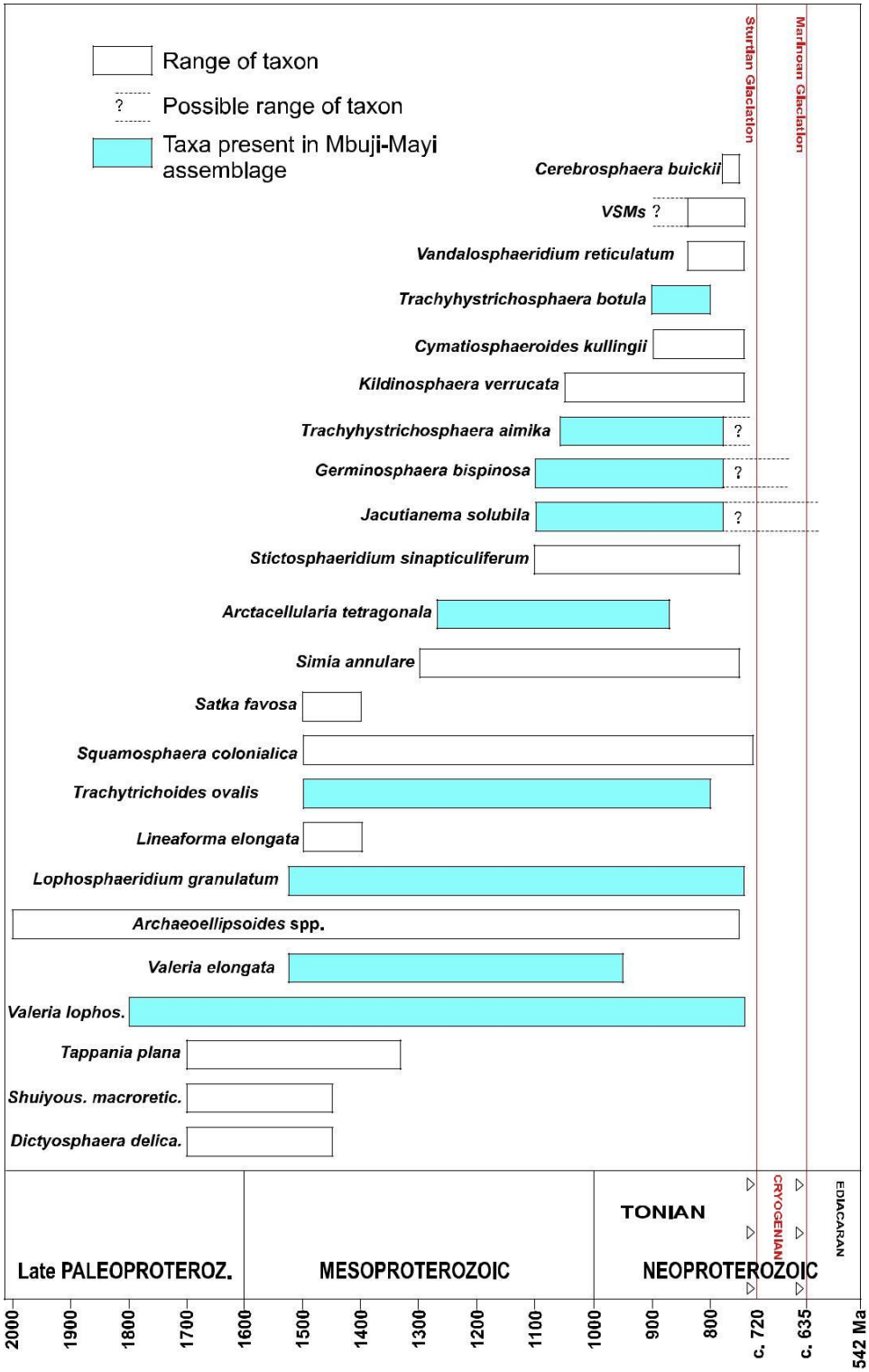

Fig. 15. Summary of microfossil assemblages useful for Proterozoic biostratigraphy (various references, see in text). Cryogenian limits come from the new Precambrian chart (2015) by International Commission on Stratigraphy (www.stratigraphy.org).

proterozoic–Neoproterozoic eukaryotes evidence the evolution of biological innovations such as a cytoskeleton and endomembrane system to control the plastic and complex morphology of process-bearing and ornamented acritarchs, life cycles with cyst and vegetative stages, and simple multicellularity. The diversity of eukaryotes observed here is broadly similar to worldwide contemporaneous marine successions. This confirms a general trend of moderate eukaryotic diversification, despite the early development of the eukaryotic cell toolkit in the late Paleoproterozoic, until about 1100–800 Ma when diversification of crown group eukaryotes occurs (Knoll et al., 2006; Javaux, 2011; Javaux and Knoll, in press). This eukaryotic diversification is possibly linked to changing redox conditions (Planavsky et al., 2011) and associated nutrient availability, and to increased ecological interactions

including protist or animal predation (Butterfield, 2015; Knoll, 2014; Porter, 2011).

Acknowledgments

Research funding came from the European Research Council Stg ELITE FP7/308074 and the BELSPO IAP PLANET TOPERS. We thank the Royal Museum for Central Africa (RMAC, Tervuren/Belgium) for access to the drill cores for sampling, M. Giraldo (ULg) for sample preparation and two anonymous reviewers for constructive comments on the submitted manuscript.

Appendix A. Supplementary data

Supplementary data associated with this article can be found, in the online version, at http://dx.doi.org/10.1016/j.precamres.2016. 05.017.

References

Amard, B., 1984. Nouveaux éléments de datation de la couverture protérozoïque du craton ouest-africain: un assemblage de microfossiles (Acritarches) caractéristique du Riphéen supérieur dans la formation d'Atar (Mauritanie). C. R. Acad. Sci. 299, 1405–1410.

Amard, B., 1986. Microfossiles (acritarches) du protérozoïque supérieur dans les shales de la formation d'Atar (Mauritanie). Precambrian Res. 31, 69–95.

Andreeva, E.M., 1966. Opisanie iskopaemyky spor predstaviteley Bryophyta, Lycopsida, Sphenopsida, Filicianae i rastitelnykh mikrofossily neyasnogo sistematicheskogo polozheniya, Rastitelnye mikrofossilii neyasnogo sistematicheskogo polozheniya. In: Pokorovskaya, I.M. (Ed.), Paleopalinologiya, vol. 1. VSEGEI, Trudy, pp. 114–135, Nedra, Leningrad.

Baudet, D., 1987. Implications of a palynological study in the Upper Precambrian from eastern Kasai and northwestern Shaba, Zaire. Geol. J. 22, 121–137.

Baudet, D., 1988. Etude palynologique dans le protérozoïque supérieur du Burundi. Newsletter 1, 1–5, IGCP nL255.

Beghin, J., Storme, J.Y., Houzay, J.P., Blanpied, C., Gueneli, N., Brocks, J.J., Poulton, S. W., Javaux, E.J. (in review). Microfossils from the Late Mesoproterozoic (1.1 Ga) Atar/El Mreïti Groups, Taoudeni Basin, Mauritania, Northwestern Africa. Precambrian Res.

Butterfield, N.J., 2004. A vaucheriacean alga from the middle Neoproterozoic of Spitsbergen: implications for the evolution of Proterozoic eukaryotes and the Cambrian explosion. Paleobiology 30, 231–252.

Butterfield, N.J., 2005a. Probable Proterozoic fungi. Paleobiology 31, 165–182.

Butterfield, N., 2005b. Reconstructing a complex early Neoproterozoic eukaryote, Wynniatt Formation, arctic Canada. Lethaia 38, 155–169.

Butterfield, N.J., 2015. Early evolution of the Eukaryota. Palaeontology 58, 5–17.

Butterfield, N.J., Chandler, F.W., 1992. Palaeoenvironmental distribution of Proterozoic microfossils, with an example from the Agu Bay Formation, Baffin Island. Palaeontology 35 (Part 4), 943–957.

Butterfield, N.J., Knoll, A., Swett, K., 1994. Paleobiology of the Neoproterozoic Svanbergfjellet formation, Spitsbergen. In: Foss. Strat. an Int. Monogr. Ser. Palaeontol. Stratigr., p. 84.

Butterfield, N.J., Rainbird, R.H., 1998. Diverse organic-walled fossils, including ''possible dinoflagellates", from the early Neoproterozoic of arctic Canada. Geology 26, 963–966.

Cahen, L., 1954. Extension et âge d'une minéralisation Cu, Pb, Zn, en Afrique centrale et australe. Bull. Soc. Belg. Géol. Paléontol. Hydrol. 63, 89–100.

Cahen, L., 1974. Geological background to the copper-bearing strata of southern Shaba, Zaïre. Gisements et provinces cuprifères. Centenaire Soc. Géol. Belg., 57– 77

Cahen, L., Mortelmans, G., 1947. Le système de la Bushimaie au Katanga. Bull. Soc. Belg. Géol. Paléontol. Hydrol. 56, 217–253.

Cahen, L., Snelling, N.J., Delhal, J., Vail, J.R., 1984. Geological and Evolution of Africa. Clarendon Press, Oxford.

Couëffé, R., Vecoli, M., 2011. New sedimentological and biostratigraphic data in the Kwahu Group (Meso- to Neo-Proterozoic), southern margin of the Volta Basin, Ghana: stratigraphic constraints and implications on regional lithostratigraphic correlations. Precambrian Res. 189, 155–175.

Deblond, A., Punzalan, L.E., Boven, A., Tack, L., 2001. The malagarazi supergroup of Southeast Burundi and its correlative bukoba supergroup of Northwest Tanzania: neo- and mesoproterozoic chronostratigraphic constraints from ar-ar ageson mafic intrusive rocks. J. African Earth Sci. 32, 435–449.

Delpomdor, F., Préat, A., 2013. Early and late Neoproterozoic C, O and Sr isotope chemostratigraphy in the carbonates of West Congo and Mbuji-Mayi supergroups: a preserved marine signature? Palaeogeogr. Palaeoclimatol. Palaeoecol. 389, 35–47.

Delpomdor, F., Linnemann, U., Boven, A., Gärtner, A., Travin, A., Blanpied, C., Virgone, A., Jelsma, H., Préat, A., 2013a. Depositional age, provenance, and tectonic and paleoclimatic settings of the late Mesoproterozoic middle Neoproterozoic Mbuji-Mayi Supergroup, Democratic Republic of Congo. Palaeogeogr. Palaeoclimatol. Palaeoecol. 389, 4–34.

Delpomdor, F., Blanpied, C., Virgone, A., Préat, A., 2013b. Paleoenvironments in Meso–Neoproterozoic carbonates of the Mbuji-Mayi Supergroup (Democratic Republic of Congo) – microfacies analysis combined with C-O-Sr isotopes, major-trace elements and REE + Y distributions. J. African Earth Sci. 88, 72–100.

Delpomdor, F., Blanpied, C., Virgone, A., Préat, A., 2015. Sedimentology and sequence stratigraphy of the late precambrian carbonates of the Mbuji-Mayi Supergroup in the Sankuru-Mbuji-Mayi-Lomami-Lovoy Basin (Democratic Republic of the Congo). In: de Wit, M.J., Guillocheau, F., de Wit, M.C.J. (Eds.), Geology and Resource Potential of the Congo Basin. Springer, Berlin Heidelberg, pp. 59–76.

Eisenack, A., 1958. Microfossilien aus dem Ordovizium des Baltikums. 1. Markasitschicht, Dictyonema-Scheifer, Glaukonitsand, Glaukonitkalk. Senckenbergian Lethaea 39, 389–404.

Eme, L., Sharpe, S.C., Brown, M.W., Roger, A.J., 2014. On the age of eukaryotes: evaluating evidence from fossils and molecular clocks. Cold Spring Harb. Perspect. Biol. 6.

Fernandez-Alonso, M., Cutten, H., De Waele, B., Tack, L., Tahon, A., Baudet, D., Barritt, S.D., 2012. The Mesoproterozoic Karagwe-Ankole Belt (formerly the NE Kibara Belt): the result of prolonged extensional intracratonic basin development punctuated by two short-lived far-field compressional events. Precambrian Res. 216–219, 63–86.

François, C., Baludikay, B.K., Storme, J.Y., Baudet, D., Javaux, E.J., 2015. Geochronological constraints on the diagenesis of the Mbuji-Mayi Supergroup, Democratic Republic of Congo (DRC). In: Goldschmidt Annual Meeting, Prague, 16–21 August 2015. Abstract 937.

Golovenok, V.K., Belova, M.Y., 1984. Rifeyskie mikrobioty v kembriyakh iz billyakhskoy serii Anabarskogo podnyatya [Riphean microbiota in cherts of Billyakh Group on Anabar Uplift]. Paleontol. Z. 4, 23–32 [English version: Paleontol. J. 1984, pp. 20–30.].

Golovenok, V.K., Belova, M. Yu., 1985. Riphean microbiotas in cherts of the Yeniseyskiy Kryazh (Ridge). Paleontol. Zh. 2, 94-103. English version.

Golub, I.N., 1979. Novaya gruppa problematichnykh mikroobrazovanij v vendskikh otlozheniyakh Orshanskoj vpadiny (Russkaya platforma), [A new group of problematic microstructures in Vendian deposits of the Orshanka Basin (Russian Platform)]. In: Sokolov, B.S. (Ed.), Paeontologiya Dokembriya i Rannego Kembriya. Nauka, Leningrad, pp. 147–155.

Grey, K., 1999. A modified palynological preparation technique for the extraction of large Neoproterozoic acanthomorph acritarchs and other acid-insoluble microfossils. Record 1999 (10), 23.

Grey, K., 2005. Ediacaran palynology of Australia. Mem. Assoc. Australas. Palaeontol. 31, 1–439.

Hermann, T.N., 1974. Finds of massive accumulations of trichomes in the Riphean. In: Timofeev, B.V. (Ed.), Microfossils of Proterozoic and early Paleozoic of the USSR. Nauka, Leningrad, pp. 6–10 (in Russian).

Hermann, T.N., 1990. Organic World Billion Year Ago. Academy of Sciences of the USSR, Instute of Precambrian Geology and Geochronology, Leningrad.

Hermann, T.N., Podkovyrov, V.N., 2007. Rugosoopsis: a new group of Upper Riphean animals. Geol. Soc. London Spec. Publ. 286, 429–431.

Hermann, T.N., Podkovyrov, V.N., 2008. On the nature of the Precambrian microfossils Arctacellularia and Glomovertella. Paleontol. J. 42, 655–664.

Hill, A.C., Cotter, K.L., Grey, K., 2000. Mid-Neoproterozoic biostratigraphy and isotope stratigraphy in Australia. Precambrian Res. 100, 281–298.

Hofmann, H.J., Jackson, G.D., 1994. Shale-Facies Microfossils from the Proterozoic Bylot Supergroup, Baffin Island, Canada. Mem. Paleontol. Soc. 37, 1–39.

Holmes, A., Cahen, L., 1955. African geochronology. Colon. Geol. Miner. Resour. 5, 3–38.

Javaux, E.J., 2011. Evolution of early eukaryotes in Precambrian oceans. In: Gargaud, M., Lopez-Garcia, P., Martin, H. (Eds.), Origins and Evolution of Life: An Astrobiology Perspective. Cambridge University Press, pp. 414–449.

Javaux, E.J., Knoll, A.H., Walter, M.R., 2001. Morphological and ecological complexity in early eukaryotic ecosystems. Nature 412, 66–69.

Javaux, E.J., Knoll, A.H., Walter, M.R., 2003. Recognizing and and interpreting the fossils of Early Eukaryotes. Origins Life Evol. Biosphere 33 (1), 75–94.

Javaux, E.J., Knoll, A.H., Walter, M.R., 2004. TEM evidence for eukaryotic diversity in mid-Proterozoic oceans. Geobiology 2, 121–132.

Javaux, E.J., Marshal, C.P., 2006. A new approach in deciphering early protist paleobiology and evolution: combined microscopy and microchemistry of single Proterozoic acritarchs. Rev. Palaeobot. Palynol. 139, 1–15.

Javaux, E.J., Marshall, C.P., Bekker, A., 2010. Organic-walled microfossils in 3.2-billion-year-old shallow-marine siliciclastic deposits. Nature 463, 934–938.

Javaux, E.J., Lepot, K., van Zuilen, M., Melezhik, V.A., Medvedev, P.V., 2012. Palaeoproterozoic microfossils. In: Melezhik, F., Kump, Lepland, Prave, Strauss (Eds.), Reading the Archive of Earth's Oxygenation. Springer, p. 490.

Javaux, E.J., Knoll, A.H., (in press) Micropaleontology of the lower Mesoproterozoic Roper Group, Australia and implications for early eukaryote evolution. J. Palaeontol.

Kadima, E., Delvaux, D., Sebangezi, S.N., Tack, L., Kabeya, S.M., 2011. Structure and geological history of the Congo Basin: an integrated interpretation of gravity, magnetic and reflection seismic data. Basin Res. 23, 499–527.

Kolosov, P.N., 1982. Verkhnedokembriyskie paleontologicheskie ostatki Sibirskoy platformy (Upper Precambrian Palaeontological Remains of the Siberian Plat-form). Nauka, Moscow, 96 pp. (in Russian).

Knoll, A.H., 2009. The coevolution of life and environments. Rend. Lincei 20, 301–306.
Knoll, A.H., 2014. Paleobiological perspectives on early eukaryotic evolution. Cold Spring Harb. Perspect. Biol. 6.
Knoll, A.H., Kaufman, A.J., Semikathov, M.A., 1995. The Carbon-Isotopic composition of proterozoic carbonates: Riphean successions from Northwestern Siberia (Anabar Massif, Turukhansk Uplift). Am. J. Sci. 295, 823–850.
Knoll, A.H., Javaux, E.J., Hewitt, D., Cohen, P., 2006. Eukaryotic organisms in Proterozoic oceans. Philos. Trans. R. Soc. Lond. B 361, 1023–1038.
Lamb, D.M., Awramik, S.M., Chapman, D.J., Zhu, S., 2009. Evidence for eukaryotic diversification in the similar to 1800 million-year-old Changzhougou Formation, North China. Precambrian Res. 173, 93–104.
Lottaroli, F., Craig, J., Thusu, B., 2009. Neoproterozoic-Early Cambrian (Infracambrian) hydrocarbon prospectivity of North Africa: a synthesis. Geol. Soc. Lond. Spec. Publ. 326, 137–156.
Maithy, P.K., 1975. Micro-organisms from the Bushimay system (Late Pre-cambrian) of Kanshi, Zaire. Palaeobotany 22, 133–149.
Mikhailova, N.S., 1986. New finds of the microfossils from the Upper Riphean deposits of the Krasnoyarsk region. In: Current Problems of Modern Paleoalgology. Nauka, Kiev, pp. 31–37 (in Russian).
Moczydłowska, M., 2005. Taxonomic review of some Ediacaran acritarchs from the Siberian Platform. Precambrian Res. 136, 283–307.
Moczydlowska, M., 2008. The Ediacaran microbiota and the survival of Snowball Earth conditions. Precambrian Res. 167, 1–15.
Moczydłowska, M., Nagovitsin, K.E., 2012. Ediacaran radiation of organic-walled microbiota recorded in the Ura Formation, Patom Uplift, East Siberia. Precambrian Res. 198–199, 1–24.
Nagovitsin, K., 2009. Tappania-bearing association of the Siberian platform: biodiversity, stratigraphic position and geochronological constraints. Precambrian Res. 173, 137–145.
Nagovitsin, K.E., Stanevich, A.M., Kornilova, T.A., 2010. Stratigraphic setting and age of the complex Tappania-bearing Proterozoic fossil biota of Siberia. Russ. Geol. Geophys. 51, 1192–1198.
Nagy, R.M., Porter, S.M., 2005. Paleontology of the Neoproterozoic Uinta Mountain Group. In: Dehler, C., Pederson, J.L., Sprinkel, D.A., Kowallis, B.J. (Eds.), Uinta Mountain Geology. Utah Geological Association Publication, pp. 49–62, 33.
Naumova, S.N., 1949. Spores of the Lower Cambrian. Izvestiya Akademiya Nauk SSSR, Seriya Geologicheskaya 4, 49–56 (in Russian).
Peng, Y., Bao, H., Yuan, X., 2009. New morphological observations for Paleoproterozoic acritarchs from the Chuanlinggou Formation,North China. Precambrian Res. 168, 223–232.
Petrov, P.Yu., Semikhatov, M.A., 1997. Structure and environmental conditions of a transgressive Upper Riphean Complex: Miroedikha Formation of the Turukhansk Uplift, Siberia. Lithol. Miner. Resour 1, 11–29.
Planavsky, N.J., McGoldrick, P., Scott, C.T., Li, C., Reinhard, C.T., Kelly, A.E., Chu, X., Bekker, A., Love, G.D., Lyons, T.W., 2011. Widespread iron-rich conditions in the mid-Proterozoic ocean. Nature 477, 448–451.
Porter, S.M., 2011. The rise of predators. Geology 39, 607–608.
Porter, S.M., Meisterfeld, R., Knoll, A.H., 2003. Vase-shaped microfossils from the Neoproterozoic Chuar Group, Grand Canyon: a classification guided by modern testate amoebae. J. Paleontol. 77, 409–429.
Prasad, B., Asher, R., 2001. Acritarch biostratigraphy and lithostratigraphic classification of Proterozoic and Lower Paleozoic sediments (Pre-unconformity sequence) of Ganga Basin, India. Paleontograph. Indica 5, 1–151.
Pyatiletov, V.G., 1980. The Yudomian assemblage of microfossils of South Yakutia.Geol. Geophys. 21 (7), 8–20 (in Russian).
Raucq, P., 1970. Nouvelles acquisitions sur le système de la Bushimay (No. Sciences géologiques nL 69), in-8. Tervuren (Belgique).
Raucq, P., 1957. Contribution à la connaissance du système de la Bushimay (Congo belge) (No. Sciences géologiques, Vol. 18), in-8. Tervuren (Belgique).
Samuelsson, J., Dawes, P.R., Vidal, G., 1999. Organic-walled microfossils from the Proterozoic Thule Supergroup, Northwest Greenland. Precambrian Res. 96, 1– 23.
Samuelsson, J., Butterfield, N.J., 2001. Neoproterozoic fossils from the Franklin Mountains, northwestern Canada: stratigraphic and palaeobiological implications. Precambrian Res. 107, 235–251.
Schopf, J.W., 1968. Microflora of Bitter Springs Formation, late Precambrian, central Australia. J. Paleontol. 42, 651–688.
Schopf, J.W., Blacic, J., 1971. Microorganisms from the Bitter Springs Formation (Late Precambrian) of the North-Central Amadeus Basin, Australia. J. Paleontol. 45, 925–960.
Semikhatov, M.A., Ovchinnikova, G.V., Gorokhov, I.M., Kuznetsov, A.B., Vasil'eva, I. M., Gorokhovskii, B.M., Podkovyrov, V.N., 2000. Isotopic age of the Middle-Upper Riphean boundary: Pb–Pb geochronology of the Lakhanda Group carbonates, Eastern Siberia. Trans. Russ. Acad. Sci. Earth Sci. 372, 216–221.
Sergeev, V.N., 2009. The distribution of microfossil assemblages in Proterozoic rocks. Precambrian Res. 173, 212–222.
Sergeev, V.N., Knoll, A.H., Petrov, P.Y., 1997. Paleobiology of the Mesoproterozoic Neoproterozoic transition: the Sukhaya Tunguska Formation, Turukhansk Uplift, Siberia Precambrian Res. 85, 201–239.
Sergeev, V.N., Schopf, J.W., 2010. Taxonomy, Paleoecology and Biostratigraphy of the Lat Neoproterozoic Chichkan microbiota of South Kazakhstan: the marine biosphere on the ev of metazoan radiation. J. Paleontol. 84, 363–401.
Sergeev, V.N., Knoll, A.H., Vorob'eva, N.G., 2011. Ediacaran microfossils from the Ur Formation, Baikal-Patom Uplift, Siberia: taxonomy and biostratigraphic significance. Paleontol. 85, 987–1011.
Shepeleva, E.D., 1960. Nakhodki sinezelenykh vodoroslej v nizhnekembrijskikh otlozheniyak Leningradskoj oblasti Finds of blue-green algae in Lower Cambrian deposits of the Leningra region. In: Problemy Neftyanoj Geologii i Voprosy Metodiki Laboratornykh Issledovani Nauka, Moscow, pp. 170–172.
Shepeleva, E.D. 1974. Stratigraficheskoe raschlenenie vendskikh otlozheniy tzentralnykh rayono Russkoy platformy po akritarkham, p. 13-23, In: Vozzhennikova, T.F., Timofeev, B.V Sheshegova, L.I. (Eds.), Mikrofossilii SSSR. [Microfossils USSR.] Transactions of th Institute of Geology and Geophysics, Issue 81, Nauka, Siberian Branch, Novosibirsk.
Simonetti, C., Fairchild, T.R., 2000. Proterozoic microfossils from subsurface siliciclastic rocks o the São Francisco Craton, south-central Brazil. Precambrian Res. 103, 1–29.
Srivastava, P., 2009. Trachyhystrichosphaera: an age-marker acanthomorph from the Bhande group, upper Vindhyan, Rajasthan. J. Earth Syst. Sci. 118 (5), 575– 582.
Tang, Q., Pang, K., Xiao, S., Yuan, X., Ou, Zh., Wan, B., 2013. Organic-walled microfossils fron the early Neoproterozoic Liulaobei Formation in the Huainan region of North China and thei biostratigraphic significance. Precambrian Res. 236, 157–181.
Tang, Q., Pang, K., Yuan, X., Wan, B., Xiao, S., 2015. Organic-walled microfossils from th Tonian Gouhou Formation, Huaibei region, North China Craton, and their biostratigraphi implications. Precambrian Res. 266, 296–318.
Timofeev, B.V., 1966. Micropaleontological Investigation of Ancient Formations. Nauka, Moscow (in Russian).
Timofeev, B.V., 1969. Proterozoic Sphaeromorphs. Nauka, Leningrad (in Russian).
Timofeev, B.V., Hermann, T.N., Mikhailova, N.S., 1976. Mikrofitofossilii dokembriya, kembriya i ordovika [Microphytofossils from the Precambrian, Cambrian and Ordovician]. Nauka, Leningrad (in Russian).
Timofeev, B.V., Hermann, T.N., 1979. The Precambrian microbiota of the Lakhanda Formation In: Sokolov, B.S. (Ed.), Paleontology of Precambrian and Early Cambrian. Nauka, Leningrad pp. 137–147 (in Russian).
Tynni, R., Donner, J., 1980. A microfossil and sedimentation study of the Late Precambria formation of Hailuoto, Finland. Geol. Surv. Finland Bull. 311, 27.
Vidal, G., Knoll, A.H., 1983. Proterozoic plankton. Geol. Soc. Am. Mem. 161, 265–277.
Vidal, G., Ford, T., 1985. Microbiotas from the late Proterozoic Chuar Group (Northern Arizona) and Uinta mountain Group (Utah) and their chronostratigraphic implications. Precambrian Res. 28, 349–389.
Vorob'eva, N.G., Sergeev, V.N., Knoll, A.H., 2009a. Neoproterozoic microfossils from th northeastern margin of the East European platform. J. Paleontol. 83, 161– 196.
Vorob'eva, N.G., Sergeev, V.N., Knoll, A.H., 2009b. Neoproterozoic microfossils from the margi of the East European Platform and the search for a biostratigraphic model of lower Ediacara rocks. Precambrian Res. 173, 163–169.
Vorob'eva, N.G., Sergeev, V.N., Petrov, P.Yu., 2015. Kotuikan Formation assemblage: a divers organic-walled microbiota in the Mesoproterozoic Anabar succession, northern Siberia Precambrian Res. 256, 201–222.
Wazilewski, I., 1953. Exploration en profondeur des formations du Système de la Bushima (Bakwanga, Kasai, Congo Belge). Université de Louvain.
Yankauskas, T.V., 1980. On the micropalaeontological characteristic of the Middle and Uppe Cambrian in the north-west of the East European Platform. Izvestiya Akademiya Nau Estonskoyi SSR. Geology 19 (4), 131–135 (in Russian).
Yankauskas, T.V., 1982. Microfossils of the Riphean in the southern Urals. In: Keller, B.M. (Ed. Stratotype of the Riphean. Palaeontology, Palaeomagnetism. Nauka, Moscow, pp. 84–120 (i Russian).
Yankauskas, T.V., Mikhailova, N.S., German, T.N., 1989. Precambrian Microfossils of the USSR Nauka, Leningrad, ed., (in Russian).
Yin, L.M., Guan, B., 1999. Organic-walled microfossils of Neoproterozoic Dongjia Formation Lushan County, Henan Province, North China. Precambrian Res. 94, 121–137.
Zang, W., 1995. Early Neoproterozoic sequence stratigraphy and acritarch biostratigraphy, easter Officer Basin, South Australia. Precambrian Res. 74, 119–175.

www.stratigraphy.org

International Commission on Stratigraphy (ICS). The latest version (v2015/01) of the International Chronostratigraphic Chart

3.3. Systematic Paleontology (Publié dans Precambrian Research, *Baludikay et al., 2016*, supplementary data).

Since the biological affinity of the organic-walled microfossils of the Mbuji-Mayi Supergroup is unknown, all morphotaxa are listed below in alphabetic order.

Genus *Arctacellularia* Hermann, 1976 *in* Timofeev et al., 1976, emend.
Hermann and Podkovyrov, 2008
Type species – *Arctacellularia tetragonala* (Maithy, 1975) n. comb. Hofmann and Jackson, 1994

Arctacellularia tetragonala (Maithy, 1975) n. comb. Hofmann and Jackson, 1994
(Figs. 8O–R, 9A–J and 10)
Gunflintia magna Maithy, 1975, p. 136, Pl. 1, Fig. 2.1;
Glenobotrydion tetragonalum Maithy, 1975, p. 139, Pl. 3, figs. 17, 18;
Arctacellularia ellipsoidea Hermann, 1976 *in* Yankauskas et al., 1989, p. 136, Pl. 38, figs. 1, 9, 14; Hermann, 1990, p. 26, Pl. 8, figs. 3–4; Hofmann and Jackson, 1994, p. 18, Pl. 12, figs. 16–18; Hermann and Podkovyrov, 2008, p. 661, Pl. 8, figs. 2, 5, 10, 17;
Arctacellularia doliiformis Hermann, 1976 *in* Yankauskas et al., 1989, p. 135, Pl. 38, figs. 2a, b;
Arctacellularia kelleri Hermann and Yankauskas *in* Yankauskas et al., 1989, p. 136, Pl. 38, figs. 3–5; Hermann and Podkovyrov, 2008, p. 661, Pl. 8, figs. 6, 8, 14, 16 and Pl. 9, figs. 13–16;
Arctacellularia varia Yankauskas and Hermann, 1989 *in* Yankauskas et al., 1989, p. 136, Pl.38, figs. 6–8, 10–13.
Arctacellularia tetragonala (n. comb.) Hofmann and Jackson, 1994, p.18, Pl. 12, figs. 19–20; Hermann and Podkovyrov, 2008, p. 660, Pl. 9, fig. 17–18; Couëffé and Vecoli, 2011, p. 169, Pl. 6, fig. 1.

Description. – Multicellular chains, unbranched, without external sheath covering, consisting of cells in close contact with each other. Cells brown to dark brown in color, are ellipsoidal and/or barrel-shaped. In the zone where the cells are in contact with each other, they have characteristic lenticular or ellipsoidal folds. Occasionally there are dark inclusions of variable size inside the cells. Single cells may detach from chains and also exhibit the typical terminal lenticular folds. Isolated cells are 17–30 µm wide ($\bar{x}$ = 22.34 ± 4.62 µm; N = 27) and 23–87 µm long ($\bar{x}$ = 47.52 ± 19.98 µm). Cylindrical or barrel-shaped cells have 27–45 µm wide ($\bar{x}$ = 31.8

± 4.69 µm; N = 93) and 30–125 µm long ($\bar{x}$ = 60.74 ± 15.47 µm), while ellipsoidal cells are 10–34 µm wide ($\bar{x}$ = 22.57 ± 6.41 µm; N=98; more than 189 specimens observed) and 15–45 µm long ($\bar{x}$ = 32.8 ± 8.1). Fragments of chains (2 to 16 cells) may reach up 350 µm in length.

Comments – Hofmann and Jackson (1994) revised the taxonomy of *Arctacellularia*, distinguishing two species: *A. ellipsoidea* Hermann, 1976 and *A. tetragonala* Maithy, 1975. They regarded *A. doliiformis* Hermann, 1976 and *A. sphaeria* Pyatiletov, 1980 as taphonomic variants of *A. ellipsoidea*. They also reassigned *Glenobotrydion tetragonalum* Maithy, 1975 to *Arctacellularia tetragonala* (Maithy, 1975) n. comb. Hofmann and Jackson, 1994. Indeed, the genus *Glenobotrydion* Schopf, 1968 refers to smaller (7 to 12 µm in diameter) spheroidal to ellipsoidal cells loosely associated in colonial ensheathed pseudofilamentous aggregates of up to few hundred cells. *Gunflintia magna* Maithy, 1975 (Pl. I, Fig. 2.1) erected with reference to the Paleoproterozoic genus *Gunflintia* (Barghoorn and Tyler, 1965) resembles in size range and morphology to *Arctacellularia* genus while his illustrated specimens in fig 3 and 4 resembles those of *Trachytrichoides ovalis*. *Arctacellularia varia* Yankauskas and Hermann (Yankauskas et al., 1989) is synonymized to *A. Tetragonala* (Hermann and Podkovyrov, 2008). A third species, *A. kelleri* Hermann and Jankauskas, 1989 refers to single barrel-shaped cells with characteristic lenticular terminal folds. Butterfield (2004) suggested a possible synonymy with *Jacutianema solubila* which however, does not have the lenticular folds in cells extremities. Hermann and Podkovyrov (2008) proposed an emended diagnosis of the genus *Arctacellularia* including an occasional association of chains with coiled filaments. Within the large population of specimens observed (N > 309) no association with coiled filaments has been observed in our material. Moreover, chains of cells show a large variability of morphology (ovoidal to barrel-shaped in the same specimen) and size range, but all exhibit the lenticular folds at cell extremities in contact or not with other cells. Because of size range and morphology overlap, we synonymize the three species to *A. tetragonala* (Maithy, 1975) n. comb. Hofmann and Jackson, 1994, and we consider *A. kelleri* as detached cell from chains. Hofmann and Jackson (1994) proposed that the cells of these species could be heterocysts or akinetes of modern cyanobacteria such as *Gloeotrichia anabaenopsis*. More recently, Hermann and Podkovyrov (2008) suggested that this genus may represent the polymorphism characteristic of fungal organisms (probably ascomycetes of filamentous structure) during different stages of their life cycle. However, these interpretations would require further chemical and ultrastructural analyzes to confirm their taxonomy.

Age and occurrence. – Mesoproterozoic and Neoproterozoic: Bylot Supergroup, Canada; Kwahu Group, Ghana; Mbuji-Mayi Supergroup, DRC; Miroedikha Formation, Siberia; Zilmerdak and Uk Formations, Southern Urals.

Genus *Chlorogloeaopsis* Maithy, 1975, emend. Hofmann and Jackson, 1994

Type species – *Chlorogloeaopsis zairensis* Maithy, 1975

Comments. – The spelling of the genus has been corrected by Hofmann and Jackson (1994, p. 18–19). Three species of *Chlorogloeaopsis*, unsheathed filamentous colonies of packed spheroidal cells, are recognized by these authors: *C. contexta* Hermann, 1976 n. comb. Hofmann and Jackson, 1994, has indistinct rows of cells and cell diameter ranging from 1 to 5 µm, *C. zairensis* Maithy, 1975 with cells 8 to 10 µm in diameter, 2–4 in row , while C. *kanshiensis* has 2 or 3 distinct rows of cells, 10–15 µm in diameter. The Mbuji-Mayi material includes the two following species.

Chlorogloeaopsis kanshiensis Maithy, 1975, n. comb. Hofmann and Jackson, 1994

(Fig. 9K)

Glenobotrydion kanshiensis Maithy, 1975, p. 139, Pl. 3, fig. 19;

Chlorogloeaopsis kanshiensis Maithy, 1975 *in* Hofmann et al., 1994, p. 20, Pl. 12, figs. 23–24.

Description. – Elongated filamentous colonial aggregate, composed of deformed spheroidal cells. Cells do not have a uniform size and all do not have an internal dark inclusion. Cells (13–35 µm in diameter) are arranged in two or three rows, well distinct, 26–62 µm wide and up to 450 µm long (N =150). Enveloping sheath absent.

Comments. – Maithy (1975) reported this species under *Glenobotrydion kanshiensis*, subsequently transferred to *C. kanshiensis* (new combination, Hofmann and Jackson, 1994). Cells of *C. kanshiensis*, larger than *C. zairensis* cells, are arranged in two or three rows clearly distinct and some cells also have an internal dark inclusion, although this later feature might not be diagnostic but probably only taphonomic. In our material, cells dimensions are larger than those from Bylot Supergroup, (12–19 µm, Hofmann and Jackson, 1994).

Age and occurrence. – Mesoproterozoic and Neoproterozoic: Bylot Supergroup, Canada; BII Group from Mbuji-Mayi Supergroup, DRC and Svanbergfjellet Formation, Norway.

Chlorogloeaopsis zairensis Maithy, 1975

(Fig. 9L)

Chlorogloeaopsis zairensis Maithy, 1975, p. 139, Pl. 3, figs. 21–23; Butterfield et al., 1994, p. 73, Pl. 20, fig. I.

Description. – Elongated filamentous colonial aggregate, composed of spheroidal cells, without envelope; arranged in two or several indistinctly defined rows of 22–42 µm wide and up to 135 µm long (N = 104). Cells diameter 7–12 µm.

Comments. – *C. zairensis* differs from *C. kanshiensis* by the fact that rows of cells often are indistinct and by the smaller cell diameter.

Age and occurrence. – Neoproterozoic: Zilmerdak Formation, Siberia and BII Group from Mbuji-Mayi Supergroup, DRC.

Genus *Coneosphaera* Luo, 1991

Type species – *Coneosphaera inaequalalis* Luo, 1991

***Coneosphaera* sp.**

(Fig. 8M–N)

Description. – Thin-walled microfossils consisting of a larger spheroid with two or five smaller spheroids of more or less uniform size closely or loosely attached. Diameter ranges from 27 µm to 177 µm for the large spheroids and 15 µm to 59 µm for the small spheroids, the ratio of large to small cells being of the order of 2:1 to 4:1 (N = 4).

Comments. – The genus *Coneosphaera* describes loosely aggregated colonies of small spheroids surrounding a single, larger spheroid (Luo, 1991; Hofmann and Jackson, 1994). Our specimens are larger than *C. inaequalalis* from the Changlongshan Formation in China. They also are different to *C. artica* from Society Cliffs Formation into Bylot Group (Canada) which has a larger number of small spheroids surrounding the large spheroid. On the other hand, some specimens resemble cells under germination (budding, Fig. 8M) illustrating that *Coneosphaera* may represent a variant in the life-cycle of the probably polyphyletic genus *Leiosphaeridia*, although this genus occurs usually as single cells, or as cyst with excystment structure, or as colonies of similar diameter cells (*Synsphaeridium* and *Symplassosphaeridium*), or sometimes as vegetative cells dividing by binary division. Nonetheless, given the limited material available, we leave this taxon in open nomenclature.

Genus *Eomicrocystis* Golovenock and Belova, 1984

Eomicrocystis elegans Golovenok and Belova, 1984

(Fig. 12D–E)

Symplassosphaeridium bushimayensis Maithy, 1975, p. 141 Pl. 4, fig. 32;

Eomicrocystis elegans Golovenok and Belova, 1984 *in* Yankauskas et al., 1989, p. 91, Pl. 19, fig. 9; Hofmann et al., 1994, p. 25, Pl. 18, fig. 1;

Description. – Colonies composed of several compressed globular clusters of almost uniform size (about 35 µm), dark brown to dark in color. Each cluster consists of tens cells closely packed 3–5 µm in diameter (N = 13). No envelope around the colonies.

Comments. – Due to the small cell diameter (± 1 µm) of *Symplassosphaeridium bushimayensis* (Maithy, 1975), this species is referred here to *E. elegans*. The isolated globular clusters assigned to S*ymplassosphaeridium* spp in our material differs from *E. elegans* in the larger cell size (8–14 µm). Regarded as analogue to modern cyanobacteria "*Microcystis*" (Hofmann and Jackson, 1994), the genus *Eomicrocystis* differs from genus *Myxococcoides* by lacking an organic matrix or distinct envelope enclosing the clusters.

Age and occurrence. – Widely distributed in Proterozoic successions

Eomicrocystis malgica Golovenock and Belova, 1986

(Fig. 12F)

Eomicrocystis malgica Golovenok and Belova, 1986 *in* Yankauskas et al., 1989, p. 91, Pl. 19, fig. 7; Hofmann et al., 1994, p. 25, Pl. 18, figs. 2–4;

Description. – Irregular colonies of many cells, dark brown in color. The colonies are loosely packed and without an enclosing matrix or sheath. Cells diameter range from 5 to 7 µm whereas the size the colonies varies from 30 to 120 µm (N = 53).

Comments. – After examination of Maithy's original slide, it appears that the forms reported as *Sphaerophycus densus* (Maithy, 1975, p. 137, Pl. 1, figs. 6–7) are actually pyrite grains. In our material, the individual cells are larger than those reported (3–4.5µm) from Bylot Supergroup (Hofmann and Jackson, 1994) and they are distinguishable from colonies here assigned to *Synsphaeridium* spp. by the loose clumps and the small size of vesicles.

Age and occurrence. – Widely distributed in Proterozoic successions.

Genus *Fabiformis* Pyatiletov, 1988

Type species – *Fabiformis porosus* Pyatiletov, 1988

Fabiformis baffinensis Hofmann, 1994

(Fig. 12G–H)

Fabiformis baffinensis Hofmann, 1994, *in* Hofmann and Jackson, 1994, p. 31, Pl. 19, figs. 9–12.

Description. – Aggregates of small granules (about 1–2 µm in diameter), generally irregular, dense, elongate and slightly curved. Dark in color with ends rounded, these aggregates of spongy appearance have dimensions ranging from 69–110 µm length to 12–24 µm width (N = 7).

Comments. – The aggregates appear to be composed of the same kind of micrometric granule that built spheroidal aggregates described under *Spumosina rubiginosa*. Both genera might represent two different habits of a single species, assumed be bacterial (Hofmann and Jackson, 1994). One specimen is composed of eight distinguishable small aggregates (6–8 µm in diameter) of spheroidal cells attached on the periphery of the elongate body (Fig. 11H). This specimen is similar to specimen from Bylot Supergroup (Hofmann and Jackson, 1994, p. 29, Pl. 19, fig. 7), which has only one aggregate. The forms tentatively assigned to *F. baffinensis* in Tang et al., 2013 (p. 161, figs. 5A, B) differ from *F. baffinensis* by their larger size, their lack of spongy appearance and the presence of an outer translucent membrane (even if this is not clearly distinct in the fig. 5A). Forms also assigned to *F. baffinensis* in Tang et al. (2015) have larger cells (7 µm in diameter). Hence, we do not consider these forms as belonging to this species.

Age and occurrence. – Late Mesoproterozoic and Neoproterozoic: Bylot Supergroup, Canada; Mbuji-Mayi Supergroup, DRC.

Genus *Germinosphaera* Mikhailova, 1986, emend. Butterfield, 1994

Type species – *Germinosphaera bispinosa* Mikhailova, 1986

Germinosphaera bispinosa Mikhailova, 1986, emend. Butterfield, 1994

(Fig. 6A–C)

Germinosphaera unispinosa Mikhailova, 1986 *in* Yankauskas et al., 1989, p. 142, Pl. 47, fig. 1; Yin and Guan 1999, p. 128, figs. 5 (2, 4, 6, 9);

Germinosphaera bispinosa Mikhailova, 1986 *in* Butterfield et al., 1994, p. 38, figs. 16d–e.

Description. – Spheroidal vesicle, thin-walled, light brown in color. Here with a single long tubular process, normally up to 178 µm long and 10–55 µm basal width, communicating freely with vesicle cavity. Sometimes vesicle surface psilate and folded. Vesicle width 100–220 µm (N = 3).

Comments. – Both *G. unispinosa* and *G. bispinosa* have been brought together under *G. bispinosa* (Butterfield et al., 1994) as a species of *Germinosphaera* bearing one or multiple tubular and filamentous processes unobstructed and communicating freely with vesicle interior. Putative cylindrical process separated by septa from vesicle cavity of *G. unispinosa* from

Dongjia Formation is probably taphonomic based on available illustrations (Yin and Guan, 1999 p. 128, fig. 5 parts 2, 4, 6 and 9).

Age and occurrence. – Latest Mesoproterozoic and Early Neoproterozoic: Mbuji-Mayi Supergroup, DRC; Yenisey Formation, Russia; Dongjia Formation, China and Svanbergfjellet Formation, Norway.

Genus *Glomovertella* Reitlinger, 1948

Type species – *Glomovertella firma* Reitlinger, 1948

Glomovertella miroedikhia Hermann, 2008

(Fig. 11A–B)

Glomovertella eniseica Hermann *in* Yankauskas et al. 1989, p. 108, Pl. 21, fig. 12 and Pl. 29, figs. 5, 7, 8;

Glomovertella miroedikhia Hermann *in* Hermann and Podkovyrov, 2008, p. 662, Pl. 8, figs. 9, 13, 15 and Pl. 9, figs. 4, 6, 11.

Description. – Individual aseptate filaments, unbranched, showing a coiling into loop-shaped pattern or linear clumps, closely spaced and arranged parallel to each other. Clumps of filaments range from 40–70 µm in width and 100–220 µm length whereas filaments 5–10 µm wide and remain constant in width throughout of each specimen (N = 21). Only one specimen (Fig. 10A) shows pseudoseptate folding on one end.

Comments. – The same species was reported previously as *G. eniseica* (Yankauskas et al., 1989). In a recent publication (Hermann and Podkovyrov, 2008), the emended diagnosis allowed the establishment of the new species *G. miroedikhia* which differs from the former in the parallel arrangement of filaments in the coils instead of a tangle of filaments. It is possible that all spiraling filaments attributed to *Glomovertella* and *Obruchevella* are related as suggested by Hofmann and Jackson (1994). However, in our material *Obruchevella valdaica* (Fig. 10C) differs from *G. miroedikhia* (Fig. 10A–B) in its translucent appearance and always concentric coils. In addition, our material does not show a morphological gradation between the two. The smooth coiled tubular structures of *Glomovertella* have been interpreted either as characteristic of microsclerotia of fungi (Hermann and Podkovyrov, 2008) or as the sheaths of oscillatorian cyanobacteria (Vorob'eva et al., 2009a). However, coiled filaments also occur in several other types of Bacteria and eukaryotic algae.

Age and occurrence. – Mesoproterozoic and Neoproterozoic: Mbuji-Mayi Supergroup, DRC and Mirojedikha Formation, Siberia.

Genus *Jacutianema* Hermann and Timofeev, 1979, emend. Butterfield, 2004

Type species – *Jacutianema solubila* Hermann and Timofeev, 1979

Jacutianema solubila Hermann and Timofeev, 1979, emend. Butterfield, 2004

(Fig. 7O–R)

? *Brevitrichoides bashkiricus* Yankauskas, 1980 *in* Yankauskas et al., 1989, p. 102, Pl. 21, Fig. 2.1;

Jacutianema solubila Hermann and Timofeev, 1979 *in* Yankauskas et al., 1989, p. 110, Pl. 29, fig. 1; Butterfield, 2004, p. 250, figs. 3a, 4a–m and 5d–f.; Vorob'eva et al., 2009a, p. 187, Pl. 15, fig. 7.

Description. – Spheroidal, ellipsoidal or cylindrical cells occurring in pairs, triads or chains tenuously attached. No branching observed, translucent and light brown to brown in color. Presence of a thin and conspicuously more degraded tubular envelope covering some cells. Diameter of spheroids or width of cylindrical cells 20–70 µm, length of cylindrical cells 39 to 190 µm (N = 17). Cylindrical cells occasionally contain darker axial structures 30–40% the diameter and 39–60% the length of the outer wall which are best interpreted as remains of degraded cytoplasm (Butterfield, 2004 and references therein).

Comments. – *J. solubila* differs from the genus *Arctacellularia* by the lack of characteristic thickened intercellular septa of lenticular form, and by the loose contact of adjacent cells; lack of thick folds on cells walls but also by the presence of a thin tubular envelope covering some cells (Fig. 7O). The former was first interpreted as the *Gongrosira*-phase akinetes (essentially, resting cells with subsequent germination) of *vaucheriacean* algae (Butterfield, 2004) and more recently as an eukaryotic "multicellular problematicum" (Butterfield, 2015) whereas *Arctacellularia* has been compared to fungi (Hermann and Podkovyrov, 2008 and reference therein, see discussion above).

Age and occurrence. – Mesoproterozoic and Neoproterozoic: Nureyen Formation, Siberia; Mbuji-Mayi Supergroup, DRC; Svanbergfjellet Formation, Spitsbergen; Vychegda Formation, East European Platform.

Genus *Leiosphaeridia* Eisenack, 1958

Type species – *Leiosphaeridia baltica* Eisenack, 1958

Comments. – Yankauskas et al., (1989) listed 20 genera they reassigned to *Leiosphaeridia* genus; some of which were previously used in Maithy (1975) and Baudet (1987) studies: *kildinella* Shepeleva and Timofeev, 1963; *Kildinosphaera* Vidal, 1983; *Nucellosphaeridium* Timofeev, 1966; *Orygmatosphaerdium* Timofeev, 1959; *Protoleiosphaeridium* Timofeev,

1959; *Trachysphaeridium* Timofeev, 1959; *Trematosphaeridium* Timofeev, 1959 and *Zonosphaeridium* Timofeev, 1959. Here, we follow Yankauskas's emendations to recognize the taxa belonging to *Leiosphaeridia* genus. Some taxa reported in the previous studies belong to this genus while others are reassign to other genera. In all, five species of *Leiosphaeridia* were recognized in the Mbuji-Mayi Supergroup: *L. crassa* – thick-walled, < 70 µm; *L. jacutica* – thick-walled, 70–800 µm; *L. minutissima* – thin-walled, < 70 µm; *L. tenuissima* – thin-walled, 70–200 µm and *L. ternata* – thicker-walled, with radial fractures, 3–70 µm.

Leiosphaeridia crassa Naumova, 1949 emend.
Yankauskas *in* Yankauskas et al., 1989
(Fig. 8A–C)

Leiosphaeridia crassa Naumova, 1949 *in* Yankauskas et al., 1989, p. 75–76, Pl. 9, figs. 5–10 (see for further synonymy);
Protoleiosphaeridium densum Maithy, 1975, p. 140, Pl. 4, figs. 29–30;
Protoleiosphaeridium laevigatum Maithy, 1975, p. 141, Pl. 4, fig. 31;
Trematosphaeridium zairiensis Maithy, 1975, p. 141, Pl. 4, fig. 33;
Kildinosphaera chagrinata Vidal, 1983 *in* Baudet, 1987, p. 134, Pl. 1, figs1, 2.

Description. – Spheroidal vesicle, thick-walled, with smooth surface and rectilinear or curvilinear folds. Dark brown to light brown in color. Diameter ranges from 22 to 67 µm (N > 1148). Some specimens with a longitudinal rupture or medial split, interpreted as an excystment structure (Fig. 8B).

Comments. – This is a common constituent in all formations analyzed. As noted above, *Protoleiosphaeridium* and *Trematosphaeridium* genus have already been reassigned to *Leiosphaeridia*. With respect to *Trematosphaeridium zairiensis* (Maithy, 1975, p. 141, Pl. 4, fig. 33), it was said to contain small circular perforations but this is not visible from the illustrated specimen. By contrast, no description goes along with the illustrations of *Kildinosphaera chagrinata* (*in* Baudet, 1987, p. 134, Pl. 1, figs1, 2), however it had been transferred to *L. crassa* (Yankauskas et al., 1989, p. 75) and illustrated specimens match with *L. crassa* diagnosis.

Age and occurrence. – Widely distributed in Proterozoic successions.

Leiosphaeridia jacutica Timofeev, 1966, emend.
Mikhailova and Yankauskas *in* Yankauskas et al., 1989
(Fig. 8D)

Chuaria circularis, Walcott, 1899 *in* Baudet, 1987, p. 136, Pl. 3, fig. 1;

Kildinella hyperborica Timofeev, 1966 *in* Baudet, 1987, p. 134, Pl. 1, figs. 8,9;
Leiosphaeridia jacutica Timofeev, 1966 *in* Yankauskas et al., 1989, p. 77–78, Pl. 12, figs. 3a, 3b, 7, 9 (see for further synonymy);
Kildinella timofeevii Maithy, 1975, p. 143, Pl. 6, fig. 47;
Orygmatosphaeridium vulgarum Maithy, 1975, p. 143, Pl. 6, fig. 45;
Vavosphaeridium densum Maithy, 1975, p. 142, Pl. 5, fig. 39.

Description. – Spheroidal vesicle, sometimes compressed, thick-walled with smooth surface, and rectilinear or curvilinear folds. Dark brown to brown in color and diameter ranging from 70 to 550 µm (N =202).

Comments. – Maithy (1975) reported this species under three different names (cfr. above in synonymy) while they have the same major characters (thick-walled, thick-folds, smooth surface and diameter > 70 µm). Minor characters are probably induced by taphonomic factors. However specimen (Pl. 4, fig. 36) illustrated as *Vavosphaeridium densum* should be rather reassign to *Spumosina rubiginosa* due to his spongy appearance (cfr. below).

Age and occurrence. – Widely distributed in Proterozoic successions

Leiosphaeridia minutissima Naumova, 1949, emend.
Yankauskas *in* Yankauskas et al., 1989
(Fig. 8E)
Leiosphaeridia minutissima Naumova, 1949 *in* Yankauskas et al., 1989, p. 79–80, Pl. 9, figs. 1–4, 11 (see for further synonymy);
Orygmatosphaeridium trizonatum Maithy, 1975, p. 143, Pl.6, fig. 46.

Description. – Spheroidal vesicle, thin-walled with smooth surface, and commonly different types of folds (rectilinear or curvilinear). Light brown in color; 12–62 µm in diameter (N > 1171).

Comments. – With *L. crassa*, this species is the most abundant constituent within this assemblage (occurs in all fossiliferous samples). Except for the diameter range of 60–80 µm, *Orygmatosphaeridium trizonatum* Maithy (1975) is similar to *L. minutissima*. Hence, specimens with diameter > 70 µm would be considered as *L. tenuissima*.

Age and occurrence. – Widely distributed in Proterozoic successions.

***Leiosphaeridia* sp.**
(Fig. 8H–I)
Tasmanites sp. Maithy, 1975, p. 145, Pl. 6, fig. 53.

Description. – Thick-walled, entirely opaque smooth-walled vesicle with concentric peripheral folding and pierced by tiny pores, irregular in shape and distribution on the surface, and probably taphonomic. Neither transverse canals nor outer sheath have been observed. Vesicle 260–470 µm in diameter (N =6).

Comments – Pores closely arranged and transverse canals are major characters of *Tasmanites* genus. However our material and *Tasmanites* sp Maithy (1975) lack transverse canals. Moreover, unlike the other species of *Leiosphaeridia* recovered (see above), this species is only present in Kanshi S13B drill cores (upper part of Mbuji-Mayi Supergroup, exclusively in $BIIc_2$ and $BIIc_6$ Formations) where it co-occurs with others species of *Leiosphaeridia*. This may be *T. aimika* resembling *Leiosphaeridia* through erosion of its processes and outer sheath. Because of these distinctive features and its limited occurrence, we consider it with reservations as *Leiosphaeridia* sp.

Leiosphaeridia tenuissima Eisenack, 1958

(Fig. 8F)

Leiosphaeridia tenuissima Eisenack, 1958 *in* Yankauskas et al., 1989, p. 81, Pl. 9, figs. 12, 13 (see for further synonymy);

Kildinella timanica Timofeev, 1969 *in* Baudet, 1987, p. 135, Pl. 2, figs. 8,9;

Archaeofavosina sinuta Maithy, 1975, p. 142, Pl. 5, figs. 41–42;

Archaeofavosina naumovae Maithy, 1975, p. 142, Pl. 5, fig. 40.

Description. – Simple spheroidal vesicle, thin-walled with smooth surface, and irregular folds. Brown to light brown in color; diameter ranging between 75 and 500 µm (N = 107); and some specimens with internal small, round, organic body.

Comments. – The size and the thin-walled of both *Archaeofavosina sinuta* and *A. naumovae* (Maithy, 1975) suggest they are synonymous with *L. tenuissima*. The small circular or irregular pitted structure on the wall is only a secondary character.

Age and occurrence. – Widely distributed in Proterozoic successions.

Leiosphaeridia ternata Timofeev, 1966, emend.

Mikhailova and Yankauskas *in* Yankauskas et al., 1989

(Fig. 8G)

Leiosphaeridia ternata Timofeev, 1966 *in* Yankauskas et al., 1989, p. 81, Pls. 11–12, figs. 2–4 and Pl. 12, figs. 4, 5, 8 (see for further synonymy); Hofmann and Jackson, 1994, p. 22, Pl. 17, figs. 5–7; Simonetti et al., 2000, p. 21, fig. 8f;

Leiosphaeridia sp Samuelsson and Butterfield 2001, p. 243, figs. 5c, 5e.

Description. – Spheroidal vesicle, compressed, with thicker-walled, opaque to nearly opaque; commonly ruptured by radial fractures at the margin of the vesicle, suggesting a rigid wall. The diameter ranges from 15 to 220 µm (N = 97).

Age and occurrence. – Mesoproterozoic and Early Neoproterozoic: Roper Group, Australia; Bylot Supergroup, Canada; São Francisco Craton, Brazil; Lakhanda Group, Siberia; Mbuji-Mayi Supergroup, DRC; Miroedikha Formation, Siberia; Lone land Formation, Franklin Mountains, Canada and Kanpa Formation, Australia.

Genus *Lophosphaeridium* Timofeev 1959

Type species – *Lophosphaeridium rarum* Timofeev, 1959

Lophosphaeridium granulatum Maithy, 1975

(Fig. 7C–E)

? Trachysphaeridium laminaritum Timofeev, 1966 *in* Baudet (1987), p. 137, Pl. 4, figs. 4–5; *in* Vidal et al., 1985, p. 373, fig. 8, A–C;

Lophosphaeridium granulatum Maithy, 1975, p.143, Pl. 4, fig. 38; Hofmann and Jackson, 1994, p. 22, Pl. 17, figs. 8–9;

? Trachysphaeridium laufeldi Vidal, 1976 *in* Vidal et al., 1985, p. 375, fig. 7, A–B;

? Lophosphaeridium sp Nagovitsin, 2009, p. 141, figs. 3a–d;

Description. – Spheroidal vesicle, dark brown, ornamented by thick granules (0.88 and 3.38 µm). Vesicle diameter ranging from 60 to 260 µm, (N = 19).

Comments – Vesicles densely covered with closely arranged micrometric granula (Fig. 7C–E) but density and opacity vary between specimens.

Age and occurrence. – Mesoproterozoic and Early Neoproterozoic: Bylot Supergroup, Canada; Dzhelindukon, Verdreshe and Yurubchen Formations, Siberia and Mbuji-Mayi Supergroup, DRC.

Genus *Myxococcoides* Schopf, 1968

Type species – *Myxococcoides minor* Schopf, 1968

Myxococcoides minor Schopf, 1968

(Fig. 12I)

? *Myxococcoides inornata* Schopf, 1968 *in* Sergeev and Schopf, 2010, p. 393, figs. 12.1, 12.1a; *Myxococcoides minor* Schopf, 1968, p. 676, Pl. 81, fig. 1 and Pl. 83, fig. 10; Butterfield et al., 1994, p. 73, Fig. 2.10c; Sergeev and Schopf, 2010, p. 393, figs. 12.3, 12.4;

*Myxococcoides congoen*sis Maithy, 1975, p. 138, Pl. 2, fig. 10.

Description. – Spheroidal cells, dark brown, occurring in loose clusters of several cells (~ 16); all embedded in a thin organic matrix. Cells 14–21 µm in diameter and some contain an opaque inclusion (~ 1µm) attached to their inner wall. Fourteen colonies observed.

Age and occurrence. – Mesoproterozoic and Neoproterozoic: Sukhaya Tunguska Formation, Siberia; Mbuji-Mayi Supergroup, DRC; Bitter Spring Formation, Australia; Chichkan Formation, Kazakhstan and Svanbergfjellet Formation, Spitsbergen, Norway.

Genus *Navifusa* Combaz, Lange and Pansart, 1967

Type species – *Navifusa bacilla* Deunff, 1955

Navifusa actinomorpha Maithy, 1975, emend. Hofmann and Jackson, 1994

(Fig. 8J–K)

Leiofusa actinomorpha Maithy, 1975, p. 144, Pl. 5, fig. 43;

Navifusa actinomorpha Hofmann and Jackson (n. comb.), 1994, p. 20, Pl. 15, figs. 5–8;

Navifusa sp Vorob'eva et al., 2009a, p. 186, Pl. 14, figs. 10, 12.

Description. – Smooth-walled ellipsoidal vesicle, with rounded or pointed ends. Sometimes small opaque internal residue; translucent, brown to light brown in color; 56–147 µm wide and 108–312 µm long, (N = 26).

Comments. – Although larger (150–300 µm wide and 300–800 µm long), *Navifusa* sp (Vorob'eva et al., 2009a, p. 186, Pl. 14, figs. 10, 12) overlaps slightly the size of our material and is similar in morphology by its description and its illustration. Hence we suggest these new dimensions have to be extended to *Navifusa actinomorpha*.

Age and occurrence. – Late Mesoproterozoic and Neoproterozoic: Bylot Supergroup, Canada; Mbuji-Mayi Supergroup, DRC and Vychegda Formation, East European Platform.

Navifusa majensis Pyatiletov, 1980

(Fig. 8L)

Leosphaeridia kanshiensis Maithy, 1975, p. 142, Pl. 6, fig. 44;

Navifusa majensis Pyatiletov, 1980 *in* Hofmann and Jackson, 1994, p. 20, Pl. 15, figs. 1–4 (see for further synonymy); Samuelsson et al., 1999, p. 8, fig. 5a; Couëffé et al., 2011, p. 169, Pl. 6, fig. 7; Tang et al., 2013, p. 166, fig. 5h;

Description. – Egg-shaped vesicle, solitary, thin-walled with rounded ends (no septa observed); brown to dark brown in color. Some specimens are wrinkled, others folded; the vesicle width ranges from 25 to 49 µm and length between 64–116 µm, (N = 53).

Comments. – *N. majensis* differ from *N. actinomorpha* by smaller size and ovoid shape.

Age and occurrence. – Late Mesoproterozoic and Early Neoproterozoic: Bylot Supergroup, Canada; Thule Supergroup, Greenland; Kwahu Group, Ghana; Mbuji-Mayi Supergroup, DRC and Liulaobei Formation, China.

Genus *Obruchevella* Reitlinger, 1948

Type species – *Obruchevella delicata* Reitlinger, 1948

Obruchevella valdaica Shepeleva, 1974, emend. Yankauskas et al., 1989

(Fig. 11C)

? Glomovertella glomerata Reitlinger, 1948 *in* Yankauskas et al., 1989, p. 108, Pl 31, figs. 8–10;

Obruchevella valdaica Shepeleva, 1974 *in* Hofmann et al., 1994, p. 13, Pl. 11, figs. 18, 20–21 (see for further synonymy); Samuelsson et al., 1999, p. 16, figs. 5c–d;

? *Glomovertella eniseica* Hermann, 1976 *in* Hermann and Podkovyrov, 2008, p. 662, Pl. 9, figs. 1–3;

? Leiotrichoides in Hermann, 1990, p. 26, Pl. 8, fig.1;

? *Obruchevella cylindrica* Tynni and Donner, 1980 *in* Yankauskas et al., 1989, p. 113, Pl. 26, fig. 15.

Description. – Compressed aseptate tubular filaments of translucent appearance with subcircular outline, and arranged into coils more or less concentric; central portion commonly missing. Filaments of uniform width range between 2–10 µm with length difficult to evaluate due to coiling. Coils diameter 60–140 µm (N = 37).

Comments. – Here, we follow reassignments given by Hofmann and Jackson (1994) and maintain *O. valdaica* as a distinct species of uncalcified, axially compressed, coiled tubes. In our material *O. valdaica* (Fig. 10B) differs from the *G. miroedikhia* (Fig. 10A) in the translucent appearance and always concentric coils. In addition, filaments always are not in parallel arrangement in the skein. Filaments assigned to this genus, are generally interpreted as remains of *Spirulina*-like cyanobacteria (Vorob'eva et al., 2009a) although other bacteria and some eukaryotic algae show similar morphology.

Age and occurrence. – Widely distributed in Mesoproterozoic and Neoproterozoic successions.

Opaque filaments

(Fig. 11D)

Description. – Filaments unbranched, straight, curved, sinuous, some looped, opaque and mostly fragmentary up to least 100 µm long, 7.3–7.5 µm wide. Internal structure not visible (N = 15).

Comments. – Although surface or internal morphological details are not visible, this filamentous form is similar in size and morphology to co-occurring *Siphonophycus* filaments, possibly pyritized. Similar forms are reported from Artic Bay and Society Cliffs Formations (Hofmann and Jackson, 1994, p. 15, Pl. 12, figs. 1–5).

Genus *Ostiana* Hermann, 1976 *in* Timofeev et al., 1976

Ostiana microcystis Hermann, 1976

(Fig. 12J)

Ostiana microcystis Hermann, 1976 *in* Yankauskas et al., 1989, p. 83, Pl. 14, figs. 1–2, 6; Hermann, 1990, p. 14, Pl. 2, Fig. 2.1 and Pl. 3 figs. 1–2; Butterfield et al., 1994, p. 74, figs. 5f–I; Samuelsson et al., 2001, p. 243, fig. 5j;, p. 373, Pl. 4, fig. 12; Vorob'eva et al., 2009a, p. 185, Pl. 14, fig. 11; Tang et al., 2013, p. 163, fig. 5e.

Description. – Spheroidal and ellipsoidal cells arranged into irregular planar colonies, light brown to dark brown. Within colonies, cells connected to one another on two or more sides, seem to overlap when in bi-layered sheets (Fig. 11J), and compressed along junctions. Diameter cells 8–15 µm; colony size up to 1700µm wide. Tens of colonies observed.

Age and occurrence. – Latest Mesoproterozoic and Neoproterozoic: Lakhanda Group and Burovaya Formation, Siberia; Mbuji-Mayi Supergroup, DRC; Mirojedikha and Nureyen Formations, Siberia; Liulaobei Formation, China; Svanbergfjellet Formation, Spitsbergen, Norway; Lone Land Formation, Franklin Mountains, Canada and Vychegda Formation, East European Platform.

Genus *Palaeolyngbya* Schopf, 1968, emend. Butterfield et al., 1994

Type species – *Palaeolyngbya barghoorniana* Schopf, 1968

Palaeolyngbya catenata Hermann, 1974

(Fig. 11E–F)

Palaeolyngbya catenata Hermann, 1974 *in* Butterfield et al., 1994, p. 61, Fig. 2.15F–G;

?*Palaeolyngbya* sp. in Hofmann and Jackson, 1994, p. 17, Pl. 12, Fig. 2.11–22.

Description – Dark trichome narrow, multicellular, uniseriate, unbranched surrounded by lighter colored, amorphous filamentous sheath; cells diameter 3–13µm and sheaths ranging from 9 to 31 µm wide (N = 3).

Comments. – This fossil is scarce, one specimen from $BIIc_2$ and two from $BIIc_6$ Formations.

Genus *Pellicularia* Yankauskas, 1980

Pellicularia tenera Yankauskas, 1980

(Fig. 11G)

Pellicularia tenera Yankauskas, 1980 *in* Yankauskas et al., 1989, p. 139, Pl. 42, figs. 3–5; Hofmann and Jackson, 1994, p. 12, Pl. 11, figs. 11–12.

Description. – Filamentous sheaths, light brown, crumpled, slightly tapering, with longitudinal and somewhat curved thin folds; some specimens with pyrite grains around. Fragments with ends broken off ranging up to 420 µm long and 12-49 µm wide (N = 10).

Age and occurrence. – Mesoproterozoic and Neoproterozoic: Bylot Supergroup, Canada; Mbuji-Mayi Supergroup, DRC and Shtandin Formation, Siberia.

Genus *Polysphaeroides* Hermann *in* Timofeev et al., 1976

Type species – *Polysphaeroides filiformis* Hermann, 1976

Polysphaeroides filiformis Hermann, 1976

(Fig. 9M–R)

Entosphaeroides bilinearis Maithy, 1975, p. 138, Pl. 2, figs. 13–14;

Entosphaeroides irregularis Maithy, 1975, p. 138, Pls. 2–3, figs. 15, 16;

Palaeomicrocystis schopfii Maithy, 1975, p. 138, Pl. 2, figs. 11–12;

Polysphaeroides filliformis Hermann *in* Yankauskas et al., 1989, p. 119, Pl. 27, figs. 8–9; Vorob'eva et al., 2009a, p. 188, Pl. 15, figs. 8, 9, 16; Vorob'eva et al., 2015, p. 207, fig. 9.13.

Description. – Spheroidal cells arranged more or less closely into filamentous aggregates, straight or curved, surrounded by a common sheath with ends broken off. Cells are arranged into three different ways in the sheath: 1 or 3 rows of cells; multiples colonies of tiny cells as well as cells overlapping each other with a randomly distribution. Some specimens are branched; cells diameter 5–25 µm and sometimes internal inclusions (3–6 µm); filamentous aggregates ca. 16–40 µm in diameter. Sheaths surrounding filamentous aggregates are translucent, with 40–65 µm width and maximum length up to 800 µm (N = 38).

Comments. – *Entosphaeroides bilinearis*, *Entosphaeroides irregularis* and *Palaeomicrocystis schopfii* Maithy (1975) are similar to *P. filliformis*. The first has cells arrangement into two rows; the second has cells in colonies and the latest shows an irregular distribution with overlapping cells, all three are enclosed by a tubular sheath. In addition, the *Polysphaeroides* genus (Hermann *in* Timofeev et al., 1976) was erected without reference to

Maithy species. Although some of our specimens (N = 21) contain dark inclusions in cells, this is not a good diagnostic feature for identification of organic-walled microfossils as it depends on preservation. So, for the above reasons, we reassign these three species to *P. filliformis*. In our material, tubular sheaths are not closed at both ends as in *P. filliformis* from Vychegda Formation (Vorob'eva et al., 2009a). Occasionally sheaths are degraded (Fig. 9R, top part of the colony has lost the outer sheath) and less conspicuous, and might be confused with *Chlorogloeaopsis kanshiensis*. Filaments of *Polypshaeroides* have been compared to modern *stignonematalean* cyanobacteria (Hermann, 1990).

Age and occurrence. – Late Mesoproterozoic and Neoproterozoic: Nureyen and Kotuikan Formations, Siberia; Upper Mbuji-Mayi Supergroup, DRC; Burovaya and Miroedikha Formations, Siberia; Vychegda Formation, East European Platform.

Genus *Polythricoides* Hermann, 1974, emend. Timofeev et al., 1976

Type species – *Polythricoides lineatus* Hermann, 1974

Polythricoides lineatus Hermann, 1974, emend. Timofeev, Hermann and Mikhailova, 1976 (Fig. 11H)

Polytrichoides lineatus Hermann, 1974, *in* Yankauskas et al., 1989, p. 119, Pl. 30 figs. 5–7; Hermann, 1990, p. 28, Pl. 9, figs. 8–9; Hofmann and Jackson, 1994, p. 12, Pl. 11, figs. 13–14; Vorob'eva et al., 2009a, p. 188, fig. 15.13–14; Tang et al., 2013, p. 173, Fig. 14a–f; Vorob'eva et al., 2015, p. 207, fig. 9.5, 7–11;

Description. – Bundles of 3–13 filaments, presenting a longitudinally striated aspect due to parallel orientation of filaments; widths of filaments in individual bundles uniform, between 3–6 µm; bundles of filaments without sheath, up to 384 µm long and 18–37 µm wide (N = > 87).

Comments. – Unsheathed filaments bundles have been observed in our material unlike those from Vychegda and Koitukan Formations (Vorob'eva et al., 2009a; 2015). This form is interpreted as *Microcoleus*-like cyanobacteria (Hofmann and Jackson, 1994 and Vorob'eva et al., 2015).

Age and occurrence. – Widely distributed in Proterozoic successions.

Genus *Pterospermopsimorpha* Timofeev, 1966, emend.

Yankauskas and Mikhailova *in* Yankauskas et al., 1989

Type species – *Pterospermopsimorpha pileiformis* Timofeev, 1966

Pterospermopsimorpha insolita Timofeev, 1969, emend.
Mikhailova *in* Yankauskas et al., 1989
(Fig. 7I–L)

? *Pterospermopsimorpha pileiformis* Timofeev, 1966 *in* Simonetti et al., 2000, p. 25, figs. 8q–r;

Pterospermopsmorpha insolita Timofeev, 1969 *in* Yankauskas et al., 1989, p. 49, Pl. 3, figs. 5, 6; Hofmann and Jackson, 1994, p. 24, Pl. 17, figs. 10–12;

Nucellosphaeridium magnum Maithy, 1975, p. 144, Pl. 7, fig. 55;

? *Pterospermopsimorpha saccata* Yin, 1978 *in* Yin and Guan, 1999, p. 134, figs. 3.11 and 6.1;

? *Archaeodiscina* sp Baudet, 1987, p. 135, Pl. 2, figs. 3–4.

Description. – Thin-walled spheroidal vesicle, smooth and transparent surface with or without folds, enveloping one or more dark brown vesicles (18–69 µm in width). The inner vesicle occupying at least the half of outer vesicle (38–200 µm in diameter, N = 14).

Comments. – Without any comparison to genus *Pterospermospimorpha* Timofeev, 1966, Maithy (1975) reported three disphaeromorph acritarchs under genus *Nucellosphaeridium* Timofeev, 1969 (*N. magnum*, *N. triangulatum* and *N. zonatum*) solely on the basis of size and texture of the internal vesicle. However, *Nucellosphaeridium* genus has been reassigned to *Leiosphaeridia* genus (Yankauskas et al., 1989). These authors emended the *Pterospermopsimorpha* diagnosis, without reference or comparison to Maithy species, using mainly the texture and the thickness of the outer envelope for distinguishing three different taxa belonging to this genus (*P. granulata*, *P. insolita* and *P. pileiformis*). According to this diagnosis, *Nucellosphaeridium magnum* (Maithy, 1975, Pl. 7, fig. 55) which has a thin-walled outer vesicle and a smooth surface, is regarded as synonym to *P. insolita*. The reticulate structure mentioned on surface of its outer vesicle is probably caused by mineral imprints. Some specimens in our material (Fig. 7L) present this character.

Age and occurrence. – Mesoproterozoic and Early Neoproterozoic: Bylot Supergroup, Canada; Sao Francisco Craton, Brazil; Lakhanda Group, Siberia; Kwahu Group, Ghana; Mbuji-Mayi Supergroup, DRC; Dongjia Formation, China and Kanpar Formation, Australia.

Pterospermopsimorpha pileiformis Timofeev, 1966, emend.
Mikhailova *in* Yankauskas et al., 1989
(Fig. 7M–N)

Pterospermopsimorpha pileiformis Timofeev, 1966 *in* Yankauskas et al., 1989, p. 49, Pl. 3, figs 7, 8; Hermann, 1990, p. 12, Pl. 1, figs. 15, 18; Butterfield et al., 1994, p. 44, fig. 14h;

Samuelsson et al., 2001, p. 243, fig. 5b; Sergeev and Schopf, 2010, p. 338, Pl. 15, figs. 1–2, 4–5; Vorob'eva et al., 2015, p. 206, fig. 8.10.

Nucellosphaeridium zonatum Maithy, 1975, p. 144, Pl. 6, fig. 48;

Nucellosphaeridium triangulatum Maithy, 1975, p. 143–144, Pls. 6–7, figs. 50 and 54;

Description. – Inner vesicle compressed well distinct, dark brown, spheroidal and occasionally fragmented with a diameter ranging 42–92 µm; enveloped by a slightly wrinkled thick-walled spheroidal vesicle with thick folds, 65–150 µm in diameter (N = 8). The inner vesicle occupying at least the two-thirds of outer vesicle.

Comments. – As previously noted, we use only texture and thickness of outer vesicle to distinguish the species in our material. Hence, *Nucellosphaeridium zonatum* and *N. triangulatum* Maithy (1975) are considered synonyms to *P. pileiformis* due to the thicker-walled their outer vesicle relative to forms here referred as *P. insolita*.

Age and occurrence. – Mesoproterozoic and Early Neoproterozoic: Zigazino-Komarovsk Formation, Siberia; Mbuji-Mayi Supergroup, DRC; Miroedikha Formation, Siberia; Svanbergfjellet Formation, Norway and Lone Land Formation, Franklin Mountains, Canada.

Genus *Rugosoopsis* Timofeev and Hermann 1979, emend. Butterfield, 1994

Type species – *Rugosoopsis tenuis* Timofeev and Hermann, 1979

Rugosoopsis tenuis Timofeev and Hermann, 1979, emend. Butterfield, 1994

(Figs. 11I–K)

Rugosoopsis tenuis Timofeev and Hermann, 1979 *in* Yankauskas et al., 1989, p. 139, Pl. 29, figs. 3; Butterfield et al., 1994, p.61–62, Fig. 2.15b (see for further synonymy); Samuelsson et al., 2001, p. 241, figs. 3a, b, d; Hermann and Podkovyrov, 2007, p. 430, Fig. 1.3–1.5;

? *Plicatidium latum* Yankauskas, 1980 *in* Yankauskas et al., 1989,139, Pl. 41, figs. 3–4;

? *Rugosoopsis* sp. Yankauskas et al., 1989, Pl. 40, figs. 7;

? *Rectia costata* Yankauskas, 1989 *in* Yankauskas et al., 1989, p. 121, Pl. 41, figs. 1, 5 and 8;

? *Karamia* sp. *in* Hofmann and Jackson, 1994, p. 15, Pl. 11, Fig. 2.13.

Description. – Tubular sheath wrinkled with transverse markings not always regularly spaced, 40–42 µm in width and 69 up to 462 µm in length; dark brown in color (N = 12).

Comments. – In our material, the inner filament is not preserved but identification is based on the presence of the pronounced transverse fabric of the sheath. Most of them, yellow brown in color, have a thicker tubular sheath (fig. 1OJ) and are very similar to *rectia costata* (Yankauskas et al., 1989, p. 121, Pl. 41, fig. 5). Interpreted either as a kind of extracellular sheaths of oscillatoriacean cyanobacteria (Butterfield et al., 1994) or as the oldest microscopic

vermiform organism (Hermann and Podkovyrov, 2007), its biological affinity remains to be established.

Age and occurrence. – Mesoproterozoic and Neoproterozoic: Lakhanda Group, Siberia; Mbuji-Mayi Supergroup, DRC; Svanbergfjellet Formation, Norway and Lone Land Formation, Canada.

Genus *Siphonophycus* Schopf, 1968, emend. Knoll et al., 1991

Type species – *Siphonophycus kestron* Schopf, 1968

Comments – *Siphonophycus* species are common in Proterozoic fossiliferous successions, and Mbuji-Mayi Supergroup is no exception, they are occurring in all formations. All species previously assigned to genus *Eomycetopsis* in Maithy (1975) are here placed in synonymy with *Siphonophycus*; under this genus are grouped all unbranched, smooth-walled, tubular sheaths without septae; solitary or in groups. They likely represent detritus derived from benthic microbial mats and include a disparate range of organisms of possibly: bacterial, cyanobacterial, protistan and fungal origin (Butterfield et al., 1994; Hofmann and Jackson, 1994; Sergeev and Schopf, 2010). There are some overlap between sizes of different species reported by these authors. Size overlap is influenced by sample lithology where species are recovered, either in maceration residues (shale facies) or compressed specimens in thin section (cherty facies). To differentiate *Siphonophycus* species recognized in Mbuji-Mayi assemblage, we follow, here, the classification introduced by Butterfield et al. (1994) while extending the range size of some species comparatively to those from Bylot Supergroup (Hofmann and Jackson, 1994).

Siphonophycus kestron Schopf, 1968

(Fig. 11L)

Siphonophycus kestron (Schopf) *in* Butterfield et al., 1994, p. 67, Fig. 2.11D; Hofmann and Jackson, 1994, p. 12, fig. 11.8–11.9; Sergeev and Schopf, 2010, p. 385, fig. 8.5.

Comments. – Tubular filamentous sheaths with diameters in the range of 14–17 µm; twenty six specimens recovered from Kanshi drill cores.

Siphonophycus punctatus Maithy, 1975

(Fig. 11M)

Siphonophycus punctatus Maithy, 1975, p. 137, Pl. 1, fig. 5; Tang et al., 2013, p. 166, fig. 13H and 13L.

Comments. – Five specimens with chagrinate texture of tubular filamentous sheath, 40–65 µm in diameter. Reported from Liulaibei Formation (Tang et al., 2013) but misspelt *S. punctatum* (32–64 µm) in the text.

Siphonophycus robustum (Schopf, 1968) emend. Knoll et al., 1991
(Fig. 11N)
Siphonophycus robustum (Schopf) *in* Butterfield et al., 1994, p. 64–66, Fig. 2.16A (see for further synonymy); Hofmann and Jackson, 1994, p. 10, fig. 11.5; Sergeev and Schopf, 2010, p. 387, fig. 6.4.

Comments. – Most common *Siphonophycus* species from Mbuji-Mayi assemblage, with a size ranging between 2 and 4 µm. Those reported from the Bylot Supergroup (Hofmann and Jackson, 1994) is given as 2.3–6.5 µm whereas those from Svanbergfjellet (Butterfield et al., 1994) range between 2–3 µm.

Siphonophycus septatum (Schopf, 1968) emend. Knoll et al., 1991
(Fig. 11N)
Siphonophycus septatum (Schopf) *in* Butterfield et al., 1994, p. 64, figs. 22G–H (see for further synonymy); Hofmann and Jackson, 1994, p. 10, figs. 11.1–11.4.

Comments. – Unbranched tubular sheath, smooth-walled, solitary or in groups, 1–2 µm in diameter. Several mat populations and isolated specimens recovered.

Siphonophycus solidum (Golub, 1979) n. comb. Butterfield, 1994 (*in* Butterfield et al., 1994)
(Fig. 11O)
Siphonophycus capitaneum (Nyberg and Schopf, 1984) *in* Hofmann and Jackson, 1994 (24-37 µm);
Siphonophycus solidum Butterfield et al., 1994, p. 67, Fig. 2.15H–I, 27D (see for further synonymy); Sergeev and Schopf, 2010, p. 387, figs. 7.6–7.8, 8.1–8.2.

Comments. – Diameter of tubular filamentous sheath ranges from 24 to 37 µm (N = 66).

Siphonophycus typicum (Hermann, 1974), n. comb.
Butterfield, 1994 *in* Butterfield et al., 1994
(Fig. 11N)
Eomycetopsis cylindrical Maithy, 1975, p. 140, Pl. 4, figs. 27–28;
Eomycetopsis rugosa Maithy, 1975, p. 140, Pl. 4, figs. 25–26;
Eomycetopsis septata Maithy, 1975, p. 140, Pl. 3, Fig. 2.13;

Siphonophycus rugosum (n. comb.) Hofmann and Jackson, 1994, p. 10, figs. 11.6–11.7;
Siphonophycus typicum Butterfield et al., 1994, p. 66, figs. 23B – 23D, 26B (see for further synonymy).

Comments. – With *S. robustum*, *S. typicum* represents the most abundant species of *Siphonophycus* (several hundred specimens) from the Mbuji-Mayi assemblage, 4–12 µm in diameter. *S. rugosum* recovered from maceration residues (Hofmann and Jackson, 1994, Bylot Supergroup) reported with 6.5–13.5 µm.

Genus *Spumosina* Naumova, 1968, emend. Yankauskas and Medvedeva, 1989 (*in* Yankasuskas et al., 1989)

Spumosina rubiginosa, Andreeva, 1966, emend. Yankauskas and Medvedeva, 1989
(Fig. 12K)

Spumosina rubiginosa, Andreeva, 1966 *in* Yankauskas et al., 1989, p. 84, Pl. 11, figs. 5–6; Hofmann et al., 1994, p. 30, Pl. 19, figs. 5–8 (see for further synonymy);
Vavosphaeridium bharadwajii Salujha, Rawat and Rehman, 1971 (*in* Maithy, 1975, p. 142, Pl. 4, fig. 35);
Vavosphaeridium densum Maithy, 1975, p.142, Pl. 4, fig. 36;
Granomarginata minuta Maithy, 1975, p. 141, Pl. 4, fig. 34;
Trematosphaeridium sp Baudet, 1987, p.136, Pl. 3, figs. 2, 3.

Description. – Spheroidal aggregates of smaller granules (about 1–2 µm in diameter) with spongy appearance; dark brown to dark in color. The aggregates (20–280 µm in diameter) present a peripheral part slightly more transparent than central part (N = 102).

Comments. – *Granomarginata minuta* and *Vavosphaeridium bharadwajii* all in Maithy (1975) match to *S. rubiginosa* in their description and their illustration. Specimens illustrated as *Vavosphaeridium densum* (Maithy, 1975, Pl. 4, fig. 36) and *Trematosphaeridium* sp (Baudet, 1987, p.136, Pl. 3, figs. 2, 3) match also to *Spumosina* genus. It is preferable to transfer them to *S. rubiginosa.* As seen above (discussion on *Fabiformis baffinensis*), both genera might represent two different habits of a single species.

Age and occurrence. – Late Mesoproterozoic and Neoproterozoic: Bylot Supergroup, Canada; Lakhanda Group, Siberia; Mbuji-Mayi Supergroup, DRC and Ust-Pinega Formation, East European Platform.

Genus *Symplassosphaeridium* Timofeev, 1959

***Symplassosphaeridium* spp.**
(Fig. 12L)

Symplassosphaeridium sp Yankauskas et al., 1989, p. 85, Pl. 15, figs. 6–8;

Symplassosphaeridium spp Hofmann et al., 1994, p. 25, Pl. 18, figs. 5–7.

Description. – Compact globular aggregates of small spheroidal vesicles, light brown to dark brown; diameter of compressed aggregates 43–95 µm and individual vesicles 8–14 µm (N = 41).

Comments. – Numerous authors consider both genus *Symplassosphaeridium* and *Synsphaeridium* to be synonymous (e.g., Samuelsson et al., 1999). Here we follow Yankauskas et al. (1989) and Hofmann et al. (1994) and treat both as distinct taxa. *Symplassosphaeridium* occurs in compact round clusters whereas *Synsphaeridium* has cells that are commonly larger and packaged in more irregular clusters.

Age and occurrence. – Widely distributed in Proterozoic rocks.

Genus *Synsphaeridium* Eisenack, 1965

***Synsphaeridium* spp.**

(Fig. 12M)

Myxococcoides verrucosa Maithy, 1975, p. 137, Pl. 1, fig. 9;

Palaeoanacystis psilata Maithy, 1975, p. 137, Pl. 1, fig. 8;

Synsphaeridium sp Yankauskas et al., 1989, p. 85, Pl. 15, figs. 9–12; Tang et al., 2013, p. 162, figs. 4h–j;

Synsphaeridium spp Hofmann and Jackson., 1994, p. 25, Pl. 18, figs. 8–13; Samuelsson et al., 1999, p. 9, fig. 4f;

Description. – Irregular, nonlinear aggregates composed of a few or many flattened, contiguous spheroidal cells, with smooth walls; light brown to dark brown. Some specimens with internal opaque inclusions; diameter vesicles ranging from 10 to 35 µm, generally uniform within each aggregate that may up 100 µm (N = 203).

Comments. – *Palaeoanacystis psilata* (Maithy, 1975) is similar to *Synsphaeridium* in habit and size. *Myxococcoides verrucosa* (Maithy, 1975, p. 137, Pl. 1, fig. 9), has cells which are not enclosed by organic sheaths and the reported micro-verrucose texture of cells surface appear to represent degradational variants. Hence, we consider them as synonyms to *Synsphaeridium* sp.

Age and occurrence. – Widely distributed in Proterozoic rocks.

Genus *Tappania* Yin Leiming, 1997

Type species – *Tappania plana* Yin Leiming, 1997

?cf. *Tappania* sp.

(Figs. 6R–, 7A–B)

Description. – Smooth-walled vesicles, spheroidal to sub-spheroidal, with broad tubular and neck-like extensions. Vesicle 32–263 µm in diameter with expansions ranging from 10 to 39 µm width (N = 7).

Comments. – Our specimens resemble some of the *Tappania plana* specimens reported in the Roper Group, Australia (Javaux et al., 2001; Javaux and Knoll, in prep) which do not possess tubular processes but bear trapezoidal neck-like expansions. They differ from *Gemmuloides doncookii* Samuelsson and Butterfield, 2001 or *Gangasphaera bulbousus* Prasad and Asher, 2001, which have spheroidal or hemispheroidal protrusions. However, populations of *Tappania* described eslewhere includes a wide range of morphotypes, including many specimens with processes unobserved so far in our material. Moreover, to date, *T. plana* has been reported only in older Mesoproterozoic and late Paleoproterozoic successions. Therefore the taxonomy of our specimens is ambiguous and are tentatively placed as cf. *Tappania* sp..

Genus *Tortunema* Hermann, 1976 emend. Butterfield et al., 1994

Type species – *Tortunema wernadskii* Schepeleva, 1960

Tortunema magna Tynni and Donner, 1980, n. comb. Butterfield et al., 1994

(Fig. 11P)

Tortunema magna Tynni and Donner, 1980 *in* Samuelsson et al., 2001, p. 242, fig. 4g.

Description. – Unbranched filamentous sheath, fragmentary, with thin annular lines giving a pseudoseptate appearance to the sheath. Yellow brown in color; intervals between thin lines are more or less regular but less than sheath diameter (70 µm). The outline of pseudo-cells appears rectangular in the compressed state. Only three fragments recovered.

Comments. – Butterfield et al. (1994) emended the diagnosis while proposing new combinations to classify three species of *Tortunema* on the basis of sheath diameter: *T. werdnaskii* Schepeleva, 1960 (10–23 µm), *T. patomica* Kolosov, 1982 (25–60 µm) and *T. magna* Tynni and Donner, 1980 (60–100 µm). In our material, *T. magna* also differs from *T. patomica* and *T. wernadskii* not only by its diameter, but also by its thickness and darker coloration suggesting original differences in composition and/or thickness since they co-occur with the 2 other species in the same sample, thus they have been subjected to the similar taphonomic conditions.

Age and occurrence. – Neoproterozoic: Upper Mbuji-Mayi Supergroup, DRC; Hailuoto Formation, Finland and Lone Land Formation, Franklin Mountains, Canada.

Tortunema patomica Kolosov, 1982, n. comb. Butterfield et al., 1994

(Fig. 11Q)

? *Tortunema sp*. Samuelsson et al., 1999, p. 17, figs 5e, f.

Description. – Unbranched filamentous sheath, fragmentary, 30 and 46 µm wide with thin annular lines giving a pseudoseptate aspect; translucent sheath light gray in color. Intervals between thin lines are more or less regular. The outline of pseudo-cells appears rectangular in the compressed state (N =2).

Age and occurrence. – Mesoproterozoic and Neoproterozoic: Thule Supergroup, Greenland; Lakhanda Group, Siberia; Upper Mbuji-Mayi Supergroup, DRC; Miroedikha Formation, Siberia.

Tortunema wernadskii Shepeleva, 1960, emend. Butterfield et al., 1994

(Figs. 11R, 12A)

Tortunema werdnaskii Shepeleva, 1960 *in* Butterfield et al., 1994, p. 67–69, figs. 24H, 27A–C (see for further synonymy);

? *Tortunema hermanii* Yankauskas et al., 1989, p. 123, Pl. 40, figs. 1–6;

? *Oscillatoriopsis* spp Hofmann et al., 1994, p. 15, Pl. 12, figs. 6–10;

Description. – Unbranched filamentous sheath, fragmentary, with thin annular lines (pseudoseptate); light gray and light brown in color. Intervals between thin lines are more or less regular. Sheath diameter range from 10 to 23 µm wide, the largest fragment ranging up to 222 µm long (N =5)

Comments. – Some of our material (Fig. 10R) are similar to forms reported as *Oscillatoriopsis* spp (Hofmann and Jackson, 1994, p. 15, Pl. 12, figs. 6–10). However such species reported by Hofmann have been transferred to *Tortunema* spp (Samuelsson et al., 1999).

Age and occurrence. – Mesoproterozoic and Neoproterozoic: Lakhanda Group, Siberia; Upper Mbuji-Mayi Supergroup; Svanbergfjellet Formation, Norway; Miroedikha Formation, Siberia.

Genus *Trachyhystrichosphaera* Timofeev and Hermann, 1976, emend.

Hermann and Yankauskas *in* Yankauskas et al., 1989; Butterfield et al., 1994 and Tang et al., 2013

Type species – *Trachyhystrichosphaera aimika* Hermann, 1976 (*in* Timofeev et al., 1976)

Comments – The diagnosis of this genus has been in several times emended since Yankauskas et al. (1989). Butterfield et al. (1994, see for further synonyms) discussed extensively this genus and emended its diagnosis recognizing only two species, *T. aimika* and

T. polaris. Other published *Trachyhystrichosphaera* species were either synonymized with *T. aimika* or excluded from *Trachyhystrichosphaera* because they did not have the characteristic features of this genus. Recently, Tang et al. (2013, see for new synonyms) emended the diagnosis to accommodate *T. botula* which has tomaculate vesicles. Here, we follow the recent diagnosis given by Tang et al. (2013). – Large spheroidal, ovoidal, or tomaculate vesicles with a variable number of highly heteromorphic, hollow, basally separate and randomly distributed processes. Processes communicate freely with vesicle cavity. Presence or not of an outer sheath surrounding the processes; and sometimes an inner body in the vesicle. This genus displays a remarkably highly variable morphology in the vesicle shape, wall texture and colour, and processes heteromorphy, suggesting it represents vegetative cells (Butterfield et al., 1994).

Trachyhystrichosphaera aimika Hermann, 1976, emend. Hermann and Yankauskas *in* Yankauskas et al., 1989; Butterfield et al., 1994 and Tang et al., 2013

(Fig. 6D–L)

Trachyhystrichosphaera aimika Hermann, 1976 *in* Yankauskas et al., 1989, p. 46, Pl. 1 figs. 6, 8; Butterfield et al., 1994, p. 45, figs. 18a–f; Tang et al,. 2013, p. 174, figs. 8a–f (see for further synonymy); Vorob'eva et al., 2009a, p. 183, Pl. 8, fig. 11;

Prolatoforma aculeata Mikhailova, 1992 *in* Vorob'eva et al., 2009a, p. 180, Pl. 8, figs. 10, 12.

Description. – Broadly spheroidal vesicles with hollow processes communicating freely with the vesicle cavity, light brown to dark brown. 1 to 9 tubular and conical processes per vesicle. An outer membrane and an irregularly shaped internal body may be present. Some vesicles occur in dyads. Vesicles 55–350 µm in diameter (N = 21). Processes 1.25–11.5 µm in length and 2.12–3.43 µm in basal width.

Comments. – This species is reported here for the first time in Central Africa. The specimen observed in BIIc2 Formation (Fig. 6L) has a thin-walled and transparent wall with a long processus while those from BIIc6 Formation (Fig. 6D–K) have a thick wall with several short processes.

Age and Occurrence. – Latest Mesoproterozoic and Neoproterozoic (pre-Cryogenian): Karatau and Lakhanda Groups, Siberia; Mbuji-Mayi Supergroup, DRC; Miroedikha Formation, Siberia; Luilaobei Formation, China; Wynniatt Formation, Fifteenmile Group and Lone Land Formation, Canada; Svanbergfjellet Formation, Spitsbergen, Hunnberg Formation and Ryssö Formation, Norway; Sirbu Shale Formation, India and Lower Vychegda Formation, East European Platform.

Trachyhystrichosphaera botula Tang et al., 2013

(Fig. 6M–O)

Trachyhystrichosphaera botula Tang, in Tang et al., 2013, p. 175, figs. 11a-h, 12a.

Description. – Elliptical vesicles, flattened with thick folds and rounded ends. Vesicles 60–170 µm in length, 30–70 µm in width (N = 3). Processes tubular, 1.25 µm in width and up to 5.06 µm in length. A degraded outer membrane may be present.

Comments. – This species also is reported for the first time in Central Africa. Our material are smaller than those described in Tang et al., (2013) nonetheless the length/width ratio ranges from 2 to 2.5.

Age and occurrence. – Early Neoproterozoic: BII Group from Mbuji-Mayi Supergroup, DRC, Liulaobei Formation, China.

Genus *Trachytricoides* Hermann, 1976 *in* Timofeev et al., 1976

Trachytricoides ovalis Hermann, 1976

(Fig. 12B–C)

Trachytricoides ovalis, (Hermann) *in* Yankauskas et al., 1989, p. 124, Pl. 33, figs. 10–11; Hermann, 1990, p. 26, Pl. 8, Fig. 2.1;

Gunflintia barghoornii Maithy 1975, p. 136, Pl. 2, figs. 3–4.

Description. – Multicellular filament, unbranched, straight, curved or sinuous with distinct septa. Smooth and thin-walled oval cells, without folds; light brown in color, and no inclusions inside. Cells are different size within an individual filament with length > width, 11–21 µm in width and 27–60 µm in length. Length of filament ranging up to 675 µm (N = 12).

Comments. – *T. ovalis* co-occurs with others species showing similar morphotype (*Arctacellularia ellipsoidea* and *A. tetragonala*). However, it differs from these species in its thinner smooth wall and especially by the lack of characteristic thickened intercellular septa of lenticular form.

Age and occurrence. – Mesoproterozoic and Neoproterozoic: Roper Group, Australia; Upper Mbuji-Mayi Supergroup, DRC; Miroedikha Formation, Siberia.

Genus *Valeria* Yankauskas, 1982, emend. Nagovitsin, 2009

Type species – *Valeria lophostriata* Yankauskas, 1982

Diagnosis. – Spheroidal or elongated vesicles with striated surface ornamentation.

Valeria elongata Nagovitsin, 2009

(Fig. 7F–G)

Valeria elongata Nagovitsin, 2009, p. 139, fig. 4f.

Description – Flattened, elongate vesicle, thick-walled, and distinct folds with longitudinal striations. Dark brown in color and translucent, 147 µm in diameter (one, incomplete specimen observed).

Comments. – *V. elongata* differs from *V. lophostriata* by the very elongate shape of vesicle and its longitudinal striation as opposed to latitudinal striation. Reported for the first time in Mbuji-Mayi Supergroup, our specimen does not contain occasional equidistant ring zones with the wall, which are perpendicular to striation like those described by Nagovitsin (2009).

Age and occurrence. – Mesoproterozoic and Early Neoproterozoic: Dzhelindukon Formation, Siberian Platform and Upper Mbuji-Mayi Supergroup, DRC.

Valeria lophostriata Yankauskas, 1982

(Fig. 7H)

Kildinosphaera lophostriata Vidal and Siedlecka, 1983, p. 59, fig. 6A–G and *in* Vidal and Ford, 1985, p. 361, fig. 4C, E–F;

Valeria lophostriata in Yankauskas et al., 1989, p. 86, Pl. 16, figs. 1–5 (and synonyms therein); Hofmann and Jackson, 1994, p. 24, Pl. 17, figs. 14–15 and Pl. 19, fig. 4;, p. 201, fig. 3e; Samuelsson et al., 1999, p. 15, fig. 8e; Navigotsin, 2009, p. 139, fig. 4e.

Description – Spheroidal vesicle, thick-walled with medial split and latitudinal concentric striations, ± 78 µm in diameter (one specimen recovered).

Age and occurrence. – late Paleoproterozoic to Neoproterozoic: Ruyang Group and Changzougou Formation, China; Roper Group, Australia; Bylot Supergroup, Canada; Dzhelindukon and Yurubchen Formations, Siberian Platform; Thule Supergroup, Greenland; Upper Mbuji-Mayi Supergroup, DRC and Chuar Group, USA.

Unnamed form

(Fig. 6P–Q)

Description. – Spheroidal vesicles with broad conical processes and surrounded an outer mucilaginous layer; thick-walled with compression folds around the vesicle periphery. Diameter vesicle 47–73 µm; process length 8–10 µm, width 5–10 µm (near base), (N = 2).

Comments. – Unnamed form differs from *Timanisphaera* genus (Vorob'eva et al., 2009a) by its much smaller size and the presence of an outer mucilaginous layer surrounding vesicle. We observe only 2 specimens, preventing the creation of a new species.

Chapitre 4 : Chimiostratigraphie

4.1. Introduction

La chimiostratigraphie ou « stratigraphie géochimique » consiste à étudier les variations de la composition chimique des sédiments le long de séquences stratigraphiques ou temps géologique. Les proxies utilisés en chimostratigraphie sont généralement des indicateurs de la chimie de l'eau de mer ou des conditions environnementales au moment du dépôt des sédiments ou peu après, ou des indicateurs de provenance (*Ramkumar, 2015*). Bien que les isotopes stables de carbone, oxygène, soufre, strontium, molybdène et autres soient des proxies les plus couramment utilisés en chimiostratigraphique pour les roches de tous les âges (*Anbar 2004; Anbar and Knoll, 2002; Bartley and Kah 2004; Bartley et al., 2001, 2007; Bekker et al., 2003, 2006; Delpomdor et al. 2017; Frank et al., 2003; Gilleaudeau and Kah 2013, 2015; Halverson et al. 2005, 2007, 2010; Kah et al., 2001, 2012; Knauth and Kennedy 2009; Knauth et al., 2003; Shen et al., 2003*), la speciation du fer (*Canfield et al., 2007, 2008*; *Shen et al., 2008*) est également classée parmi les proxies de la chimiostratigraphie (*Ramkumar, 2015 ; Halverson et al., 2010*). La chimiostratigraphie a à son actif diverses applications, telles que la reconstruction de paléoenvironnements, la détermination du cadre tectonique des bassins sédimentaires, la chronostratigraphie indirecte (par corrélation avec des sections de référence bien contraintes radiométriquement et/ou biostratigraphiquement) et l'établissement de corrélations locales (intra-bassin), régionales ou globales (interbassins). Les carbonates du Supergroupe Mésoprotérozoîque de Mbuji-Mayi (*François et al., 2017 ; François et al., in prep*) ont récemment fait l'objet d'une investigation chimiostratigraphique, à l'aide des isotopes stables de carbone, oxygène et de strontium (*Delpomdor and Préat 2013; Delpomdor et al. 2013*). Ces auteurs ont reporté des excursions positives et négatives dans la composition isotopique du carbone ($\delta^{13}C_{carb}$). Ils ont corrélé l'excursion négative enregistrée dans la séquence supérieure (Groupe BII) à la première grande excursion de $\delta^{13}C_{carb}$ du Néoprotérozoïque, mieux connue sous le nom de « Bitter Springs Anomaly, BSA ou Bitter Springs Stage, BSS » (*Halverson et al., 2007; Hill and Walter 2000*). Cette correlation étendait l'âge minimum du Supergroupe de Mbuji-Mayi entre ~ 811 et ~ 788 Ma, intervalle temporel pour le BSS (*Swanson-Hysell et al. 2015*). Nous établissons, ici, une chimiostratigraphie sur base des compositions isotopiques du carbone et de l'oxygène, dans un nouveau cadre géochronologique (entre 1065 et 100 Ma ;

François et al., 2017 ; in prep) et biostratigraphique (*Baludikay et al,. 2016*) donnant un âge Mésoprotérozoïque au Supergroupe de Mbuji-Mayi.

4.2. Matériel et procédés d'analyses

Comme signalé dans le chapitre 2 (§ 2.4.4), un total de 627 échantillons provenant de sondages de Bena Tshovu, Bena Kalenda, Kanshi 13B, Kafuku 15 et Lubi S70 ont été analysés dans deux laboratoires différents. Au laboratoire SIFIR (*Stable Isotopes For Innovative Research*) de l'Université du Manitoba (Canada), les teneurs du carbone organique total (TOC) et du soufre total (TS) ainsi que les isotopes du carbone (inorganique $\delta^{13}C_{carb.}$ et organique $\delta^{13}C_{org.}$), d'oxygène ($\delta^{18}O_{carb}$) et du soufre ($\delta^{34}S$) ont été mésurés. Les détails des données récueillies, pour chaque échantillon analysé, sont en annexes (A4).

Des sections polies de chaque échantillon de carbonate ont été évaluées par pétrographie optique afin d'identifier les parties moins altérées (c-à-d, sans veines, sans silicification et décoloration). Des échantillons en poudre (~ 2 mg) de phases carbonatées individuelles ont été obtenus par perforation des sections polies, à l'aide d'une perceuse en diamant de 1,0 mm de diametre, afin d'obtenir des sous-échantillons homogènes du point de vue pétrographique. La détermination des teneurs en carbone organique total (TOC) et en soufre total (TS) a été réalisée à l'aide d'un analyseur Eltra IR C/S. Des coupelles en étain ont été utilisées comme catalyseur pour une combustion en flux continu. Les analyses isoptopiques du carbone et de l'oxygène ont été réalisées à l'aide d'un analyseur d'éléments Costech 4010 et d'un dispositif à carbonate GasBenchII, les deux couplés à un spectromètre de masse à rapport isotopique « Thermo Finnigan Delta V Plus ». Les poudres ont été mises en réaction à 70°C avec de l'acide phosphorique anhydre, et ont été acheminées sous un flux de He de haute pureté dans le spectromètre. La normalisation des échantillons a été réalisée en utilisant l'étalonnage à deux points décrits dans *Coplen et al.,* (*2006*). Les standards internationaux (USGS40 et USGS41) ont été analysés au début, au milieu et à la fin de chaque série. Tous les rapports d'isotopes de carbone sont rapportés en notation delta relativement aux normes standards internationales sur l'échelle V–PDB (Vienna–Pee Dee Belemnite). Pour surveiller la qualité de la préparation des échantillons et les performances de l'analyse, la norme internationale USGS Green River SGR-1b ($\delta^{13}C_{org}$ = -29,3 ± 0,1‰ V–PDB) a été traitée et analysée comme une inconnue. Des analyses répétées du standard SGR-1b ont donné la valeur $\delta^{13}C_{org}$ de -29,5 ± 0,1‰ (n = 24).

Pour les isotopes de soufre, environ 0,2–0,4 mg de poudre des sulfates (gypse et anhydrite, Fig. 4.1) ont été analysés à l'aide d'un analyseur d'éléments Costech 4010, couplé à un spectromètre de masse à rapport

isotopique « Thermo Finnigan Delta V Plus ». Les rapports d'isotopes de soufre sont rapportés en notation delta par rapport aux normes internationales sur l'échelle V–CDT (Vienna– Canyon Diablo Troilite). Trois normes internationales (IAEA-SO-5, IAEA-SO-6 et NBS127) ont été analysées au début, au milieu et à la fin de chaque série. La courbe d'étalonnage a été calculée pour chaque analyse par régression linéaire par la méthode des moindres carrés à l'aide des rapports isotopiques connus et mesurés d'étalons. Pour contrôler la qualité des performances d'analyse, trois normes internes BaSO4 (FE-1; + 11,7 ± 0,4 VCDT (n = 20), BN-2; + 4,2 ± 0,5 VCDT (n = 20) et Aldrich BaSO4; + 5,1 ± 0,7 ‰ VCDT (n = 22)) ont été analysés avec des échantillons inconnus, avec les résultats de $\delta^{34}S$ = + 11,5 ± 0,3 ‰ (n = 8), FE-1; + 4,2 ± 0,6 ‰ (n = 10), BN-2; et 5,1 ± 0,8 ‰ (n = 9), Aldrich BaSO4.

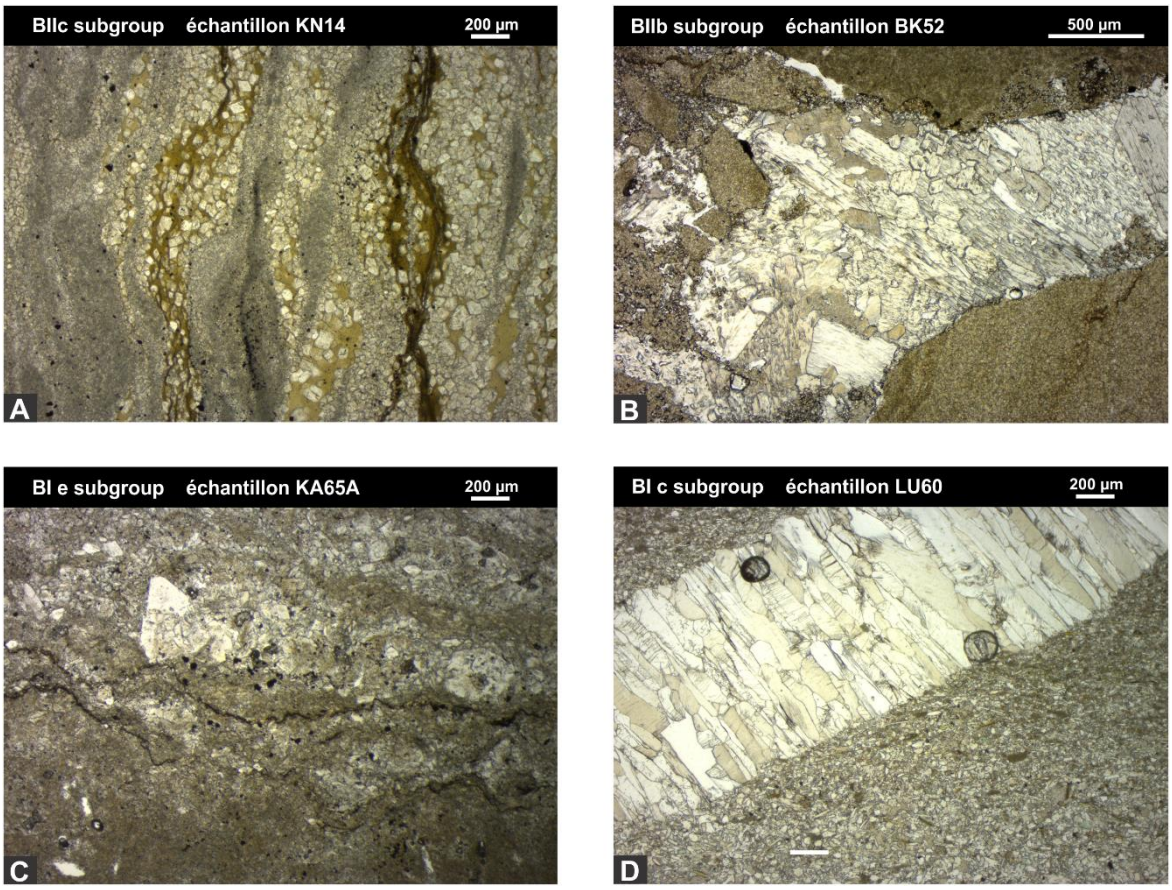

Fig.4.1. Lames pétrographiques de (A) dolomie argileuse avec feldspath et matière organique, sondage de Kanshi 13B ; (B) brêche dolomitique présentant de larges fractures remplies d'anhydrite et de gypse, sondage de Bena Kalenda ; (C) dolomie argileuse avec feldspath, quartz et oxyde, sondage de Kafuku 15 et (D) psammite composé de quartz, feldspath, mica blanc, biotite et chlorite avec de grandes fractures de gypse, anhydrite et célestite, sondage de Lubi S70.

Au laboratoire du Prof. Dr. M. Joakimski, GeoZentrum Nordbayern, Université de Erlangen-Nuremberg, Allemagne, seuls les $\delta^{13}C_{carb}$ et $\delta^{18}O_{carb}$ ont été mésurées. A l'exception du standard international (NBS19) utilisé, le procédé et l'appareillage sont identiques au précédent. Toutes les valeurs sont également rapportées en notation sur l'échelle V–PDB, en attribuant respectivement une valeur $\delta^{13}C$ et $\delta^{18}O$ de +1,95‰ et de -2,20‰, conformement au standard international NBS19. La reproductibilité a été vérifiée par une analyse répétée des normes de laboratoire et est meilleur que ± 0,03 et ± 0,05 respectivement. Les valeurs isotopiques de l'oxygène ont été corrigées en utilisant les facteurs de fractionnement proposés par *Kim et al.,* (*2007*) et *Rosenbaum and Sheppard* (*1986*).

4.3. Resultats et perspectives

Globalement, les isotopes de carbone inorganique ($\delta^{13}C_{carb}$), dans les niveaux étudiés, affichent des valeurs allant de -9,3 à +5,4‰ ; ceux de l'oxygène ($\delta^{18}O_{carb}$) varient -16,9 à +4,2‰. Les valeurs des isotopes de carbone organique ($\delta^{13}C_{org}$) varient de -33,2 à -17,8‰. Les isotopes de soufre ($\delta^{34}S$) affichent des valeurs positives allant de 7,9 à 27,7‰. La table 4.1 reprend les valeurs minimales et maximales ainsi que le nombre d'échantillons analysés pour chaque sondage

Sondage	**$\delta^{13}C_{carb}$ (‰)**			**$\delta^{18}O_{carb}$ (‰)**			**$\delta^{13}C_{org}$ (‰)**			**$\delta^{34}S$ (‰)**		
	Min	Max	N	Min	Max	N	Min	Max	N	Min	Max	N
Bena Tshovu	-3,9	+3,1	18	-15,9	+0,5	18	/	/	/	/	/	/
Bena Kalenda	-3,4	+ 3,3	40	-9,8	-0,4	40	/	/	/	/	/	/
Kanshi 13B	-1,7	-5,4	181	-5,8	+4,2	181	−32,6	−21,1	132	/	/	/
Kafuku 15	-6,7	+1,1	58	-9,0	-2,2	58	−29,0	−17,8	72	+21,5	+23,2	7
Lubi S70	-9,3	+3,5	35	-16,9	-1,9	35	−33,2	−24,2	116	+7,9	+27,7	108

Table 4.1. Valeurs récapitulatives des mesures isotopiques de chaque sondage. Min = valeur minimale, Max = valeur maximale et N = nombre d'échantillons analysés.

4.3.1. Isotopes de carbone et d'oxygène

La chimiostratigraphie des carbonates requiert l'évaluation des effets potentiels de la diagenèse sur la préservation de la signature marine primaire dans les valeurs d'isotopes de carbone enregistrées. Pour la composition isotopique de carbone cette évaluation est opérée à l'aide des tendances des éléments traces et des isotopes de $\delta^{18}O_{carb}$ (*Franck et al., 2003; Frimmel, 2010 ; Guo et al. 2013*). La valeur de $\delta^{13}C_{carb}$ pour un échantillon est jugée non altérée si Mn/Sr < 2, Fe/Sr < 50 et $\delta^{18}O$ > 10‰ sur l'échelle V–PDB (*Frimmel, 2010*). Cependant, les analyses des éléments traces sur ces carbonates n'étaient pas effectuées.

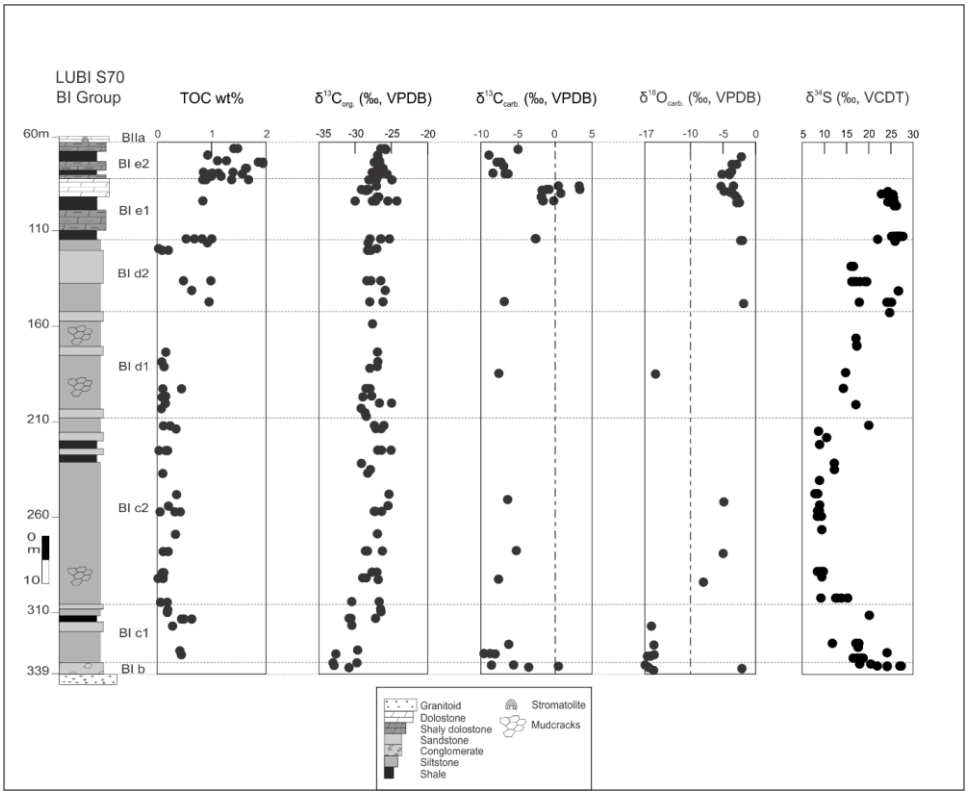

Fig. 4.2. Colonne lithostratigraphique du sondage de Lubi S70 : variations stratigraphiques du carbone organique total (TOC), de la composition isotopique du carbone inorganique ($\delta^{13}C_{carb}$), carbone organique ($\delta^{13}C_{org}$), oxygène ($\delta^{18}O_{carb}$) et soufre ($\delta^{34}S$).

La validité des mesures de la composition isotopique $\delta^{13}C_{carb}$ de nos carbonates a donc été évaluée uniquement avec les tendances isotopiques du $\delta^{18}O_{carb}$. Les carbonates des successions marines de la fin du Mésoprotérozoïque à travers le monde enregistrent un shift moyen variant de 0 à + 3,5‰ (*Bartely et al., 2007; Frank et al., 2003; Guo et al., 2013; Gilleaudeau and Kah 2013; Kah et al., 2012*) . La majorité (n = 320) des valeurs de $\delta^{13}C_{carb}$ des carbonates du

Supergroupe de Mbuji-Mayi tombe dans cette gamme. Cependant, les valeurs plus basses que -5‰, non communes dans le Mésoprotérozoïque à moins qu'elles ne soient altérées, sont observées dans les sous-groupes BIb, BIc, BId et dans la formation BIe2 (Figs. 4.2–4.3).

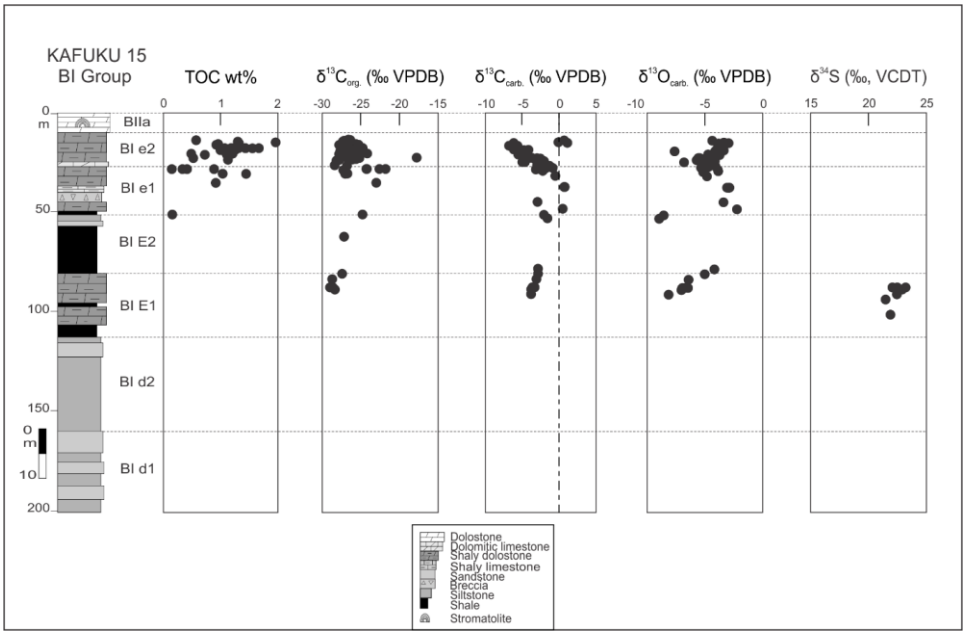

Fig. 4.3. Colonne lithostratigraphique du sondage de Kafuku 15 : variations stratigraphiques du carbone organique total (TOC), de la composition isotopique du carbone inorganique ($\delta^{13}C_{carb}$), carbone organique ($\delta^{13}C_{org}$), oxygène ($\delta^{18}O_{carb}$) et soufre ($\delta^{34}S$).

Les valeurs de $\delta^{18}O < 10$ ‰ sont observées dans les sous-groupes BIb, BIc, BId et BIId (Figs. 4.2, 4.5). Le graphique croisé de $\delta^{18}O$ vs $\delta^{13}C$ a été utilisé pour caractériser l'altération diagénétique des carbonates de Supergroupe de Mbuji-Mayi (Fig. 4.6). Ce graphique permet d'identifier au total 9 échantillons de Lubi S70 (n = 8) et de Bena Tshovu (n = 1) qui affichent un appauvrissement substantiel à la fois en $\delta^{13}C$ et en $\delta^{18}O$, suggérant la préservation d'une signature isotopique largement altérée (*Knauth and Kennedy, 2009*). Cependant, la majorité (n = 320) des carbonates se retrouve en dehors du domaine marin (Fig. 4.6) suggérant que la signature primaire marine n'a pas été aussi préservée. Celle-ci ayant été modifiée durant les processus de stabilisation durant la diagenèse précoce ou tardive (*Knauth and Kennedy 2009; Gilleaudeau and Kah, 2013*). Les variations séculaires de $\delta^{13}C_{org}$ sont dues soit à productivité biologique accrue dans les eaux de surface entraînant un plus grand enfouissement $\delta^{13}C_{org}$, soit à une conservation améliorée de la matière organique dans des conditions anoxiques, soit encore un taux de sédimentation élevé (*Kah et al., 2012 ; Guo et al., 2013*).

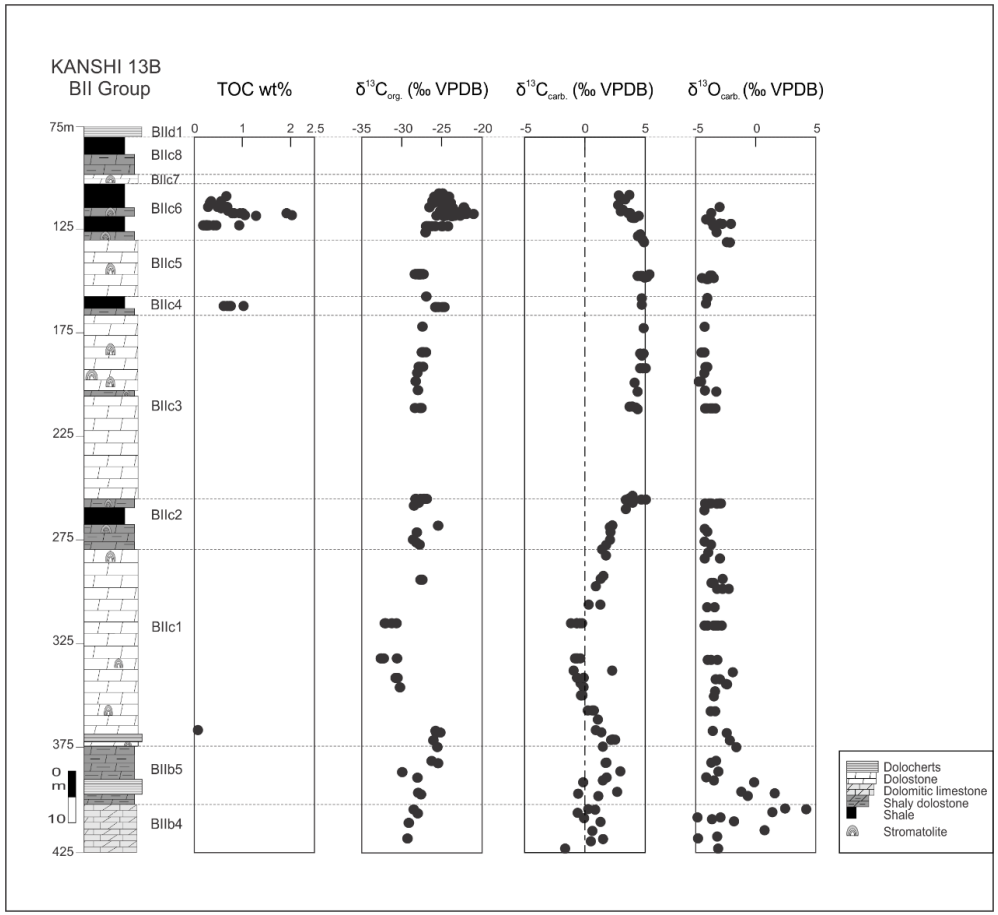

Fig. 4.4. Colonne lithostratigraphique du sondage de Kanshi 13B : variations stratigraphiques du carbone organique total (TOC), de la composition isotopique du carbone inorganique ($\delta^{13}C_{carb}$), carbone organique ($\delta^{13}C_{org}$) et oxygène ($\delta^{18}O_{carb}$).

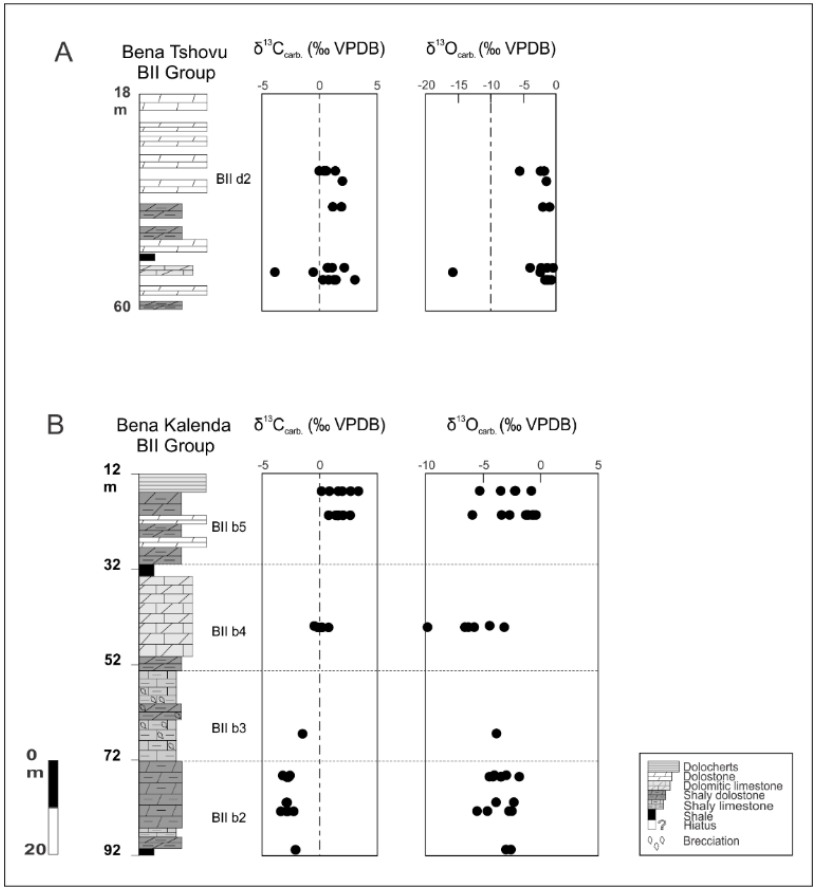

Fig. 4.5. Colonne lithostratigraphique du (A) sondage de Bena Tshovu et (B) Bena Kalenda : variations stratigraphiques de la composition isotopique du carbone inorganique ($\delta^{13}C_{carb}$) et carbone organique ($\delta^{13}C_{org}$).

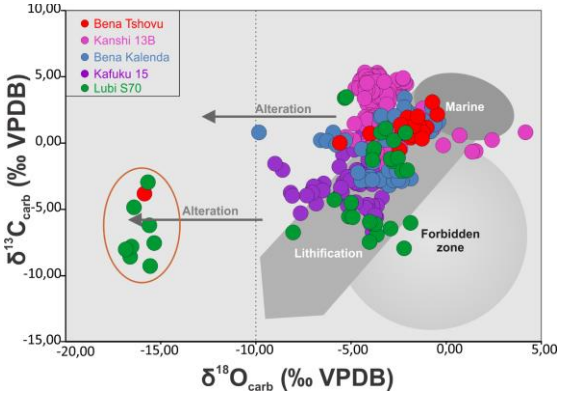

Fig. 4.6. Diagramme $\delta^{13}C_{carb}$ vs $\delta^{13}C_{org}$. Les échantillons encerclés à gauche ont enregistré un signal largement altéré. Modifié d'après *Knauth and Kennedy, 2009*.

La covariation entre $\delta^{13}C_{org}$ et $\delta^{13}C_{carb}$ observée dans le profil stratigraphique composé de ces sondages (Fig. 4.7) laisse suggérer qu'un seul et même événement serait responsable de toutes ces variations. Cependant, ceci est une hypothèse à tester à l'aide de futures analyses des éléments traces et majeures sur ces carbonates, pour mieux contraindre les causes de ces variations isotopiques et les comparer aux variations mondiales contemporaines.

4.3.2. Isotopes de soufre

Les valeurs de $\delta^{34}S$ obtenus dans les sondages de Lubi S70 et Kafuku 15 obtenues sur des sulfates reflètent toutes un shift positif ($8 > \delta^{34}S < 26$ ‰) suggérant la présence des bactéries réductrices de sulfate (*Mcfadden and Kelly 2011*). Tout comme pour les carbonates, les valeurs de $\delta^{34}S$ tombent également dans la gamme des valeurs de la fin du Mésoprotérozoïque (*Guilleaudeau and Kah, 2015 ; Kah et al., 2004*). Des mesures ultérieures sur des sulfures associées à la matière organique (Fig. 4.8) s'avèrent nécessaires pour des plus amples inf[illegible]

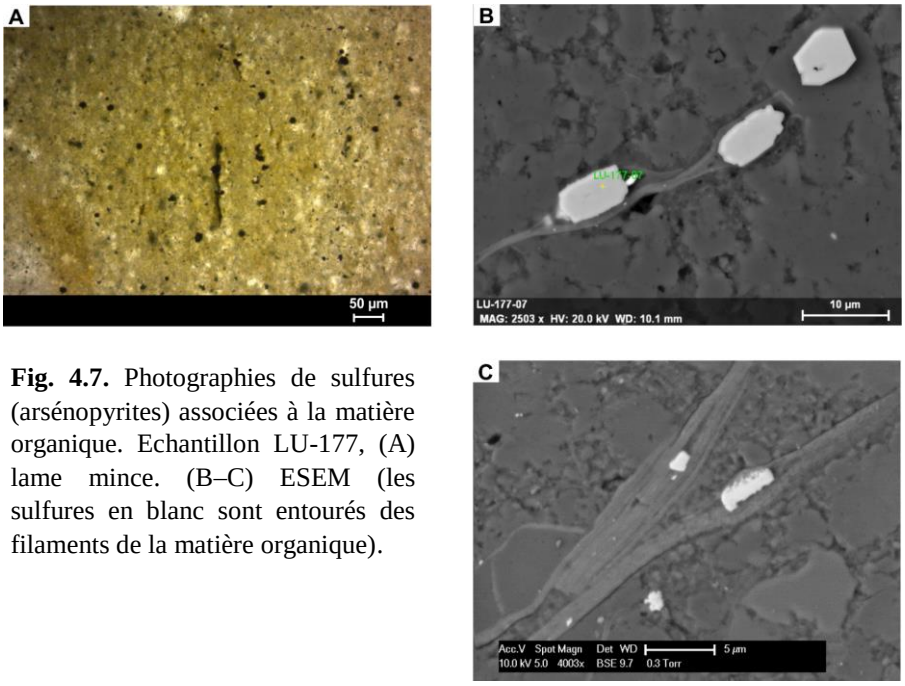

Fig. 4.7. Photographies de sulfures (arsénopyrites) associées à la matière organique. Echantillon LU-177, (A) lame mince. (B–C) ESEM (les sulfures en blanc sont entourés des filaments de la matière organique).

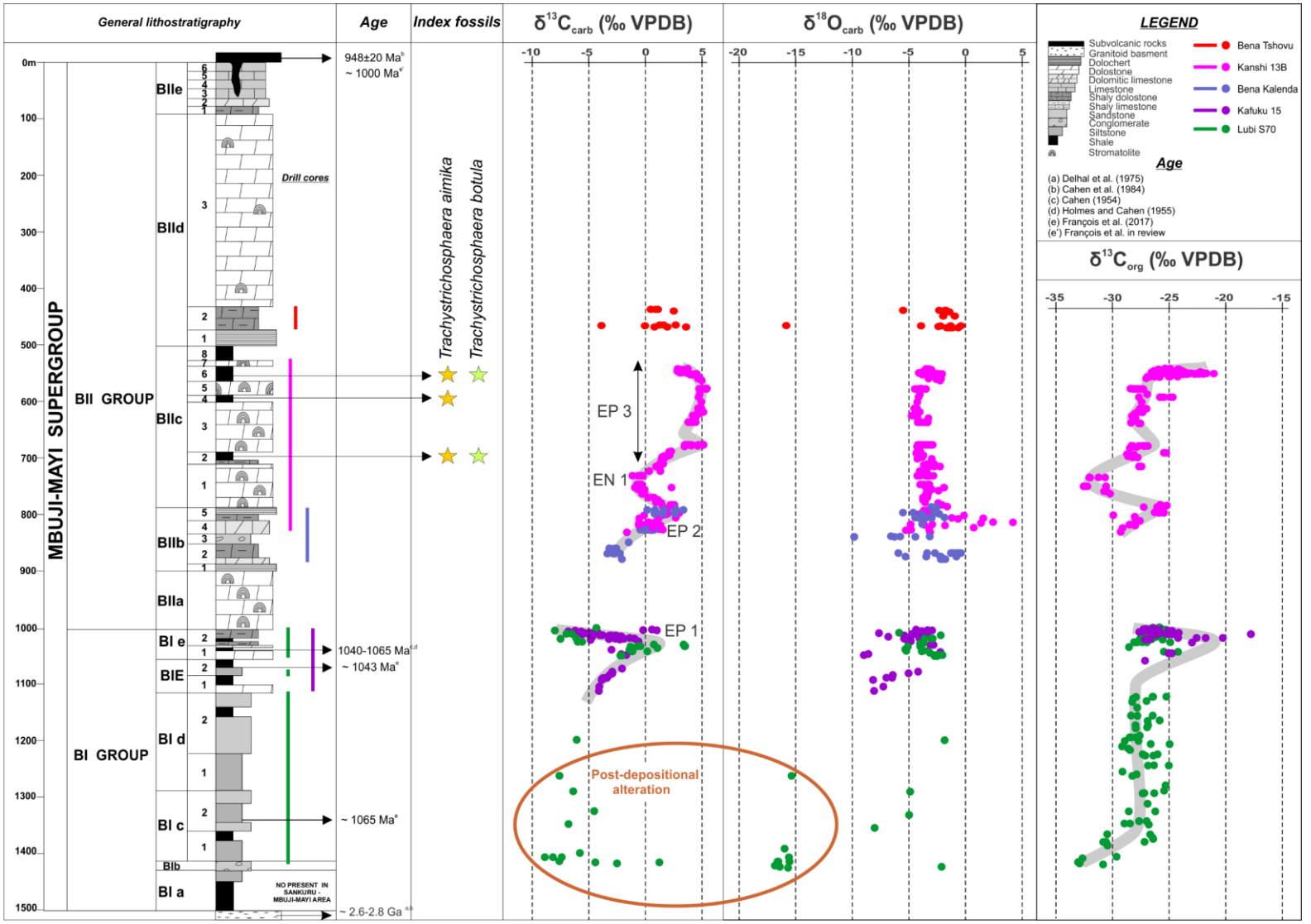

Fig. 4.7. Profil chimiostratigraphique de $\delta^{13}C_{carb}$ $\delta^{18}O_{carb}$ et $\delta^{13}C_{org}$ associé aux données radiométriques et biostratigraphiques (fossile index de la transition fin Mésoprotérozoïque – début Néoprotérozoïque). EP : excursion positive ; EN : excursion négative.

Chapitre 5 : Paléoécologie des assemblages

5.1. Introduction

Ce chapitre présente la distribution des assemblages de microfossiles en rapport avec les conditions paléoenvironmentales. L'objectif poursuivi consistait à déterminer la paléoécologie de premiers eucaryotes contenus dans les roches du Supergroupe de Mbuji-Mayi, et examiner les liens entre la chimie océanique et l'évolution de la biosphère eucaryote. Pour atteindre cet obejectif, nous avons combiné de nouvelles analyses de la distribution environnementale d'assemblages de microfossiles décrits précédemment (Chapitre 3 ou *Baludikay et al., 2016*) et des analyses géochimiques sur des échantillons de shales du Supergroupe de Mbuji-Mayi. Nous avons utilisé en particulier la spéciation du fer, les concentrations de métaux majeurs et en traces (Mn, Mo et U) ainsi que la composition isotopique du fer et du molybdène ; qui sont des proxies couramment utilisés pour délimiter les conditions d'oxydoréduction dans les eaux de fond, à la fois dans des contextes anciens et modernes. Toutes ces données rédox, ainsi que les données sur la diversité des microfossiles et leur abondance relative, sont utilisées pour détecter les tendances possibles en matière de diversité et de prédominance de taxons dans des conditions anoxiques, dysoxiques et oxiques. Les échantillons étudiés provennaient exclusivement des sondages de Kanshi 13B, Kafuku 15 et Lubi S70 qui sont les seuls à renfermer des niveaux fossilifères. Les résultats qui découlent de cette étude sont présentés dans la sous-section §5.3 sous forme de draft de l'article : « **Palaeoecology of Mesoproterozoic organic-walled microfossil assemblages from the Mbuji-Mayi Supergroup, DRC** » en préparation pour Precambrian Research. Les données suplémentaires de ce chapitre sont reprises dans les annexes A5 et A6.

5.2. Résumé de l'article

On pense souvent que des conditions essentiellement anoxiques de l'ère Mésoprotérozoïque (1600–1000 Ma) auraient limité la diversification initiale des eucaryotes (*Anbar and Knoll, 2002; Knoll and Nowak, 2017*), car les eucaryotes ne vivaient que dans des habitats oxygénés. Cependant, des études récentes ont mis en évidence des cas montrant une diversité florissante des premiers eucaryotes dans des environnements dysoxiques et anoxiques, affirmant que de nombreux fossiles de premiers eucaryotes représenteraient des organismes adaptés à ou préservés dans des habitats à faible teneur en oxygène (*Porter et al., 2018 and*

references therein). Pour comprendre le rôle éventuel de l'anoxie dans la diversification de premiers eucaryotes, une étude détaillée associant micropaléontologie et proxies rédox à haute résolution est cruciale. Nous combinons ici les analyses de la distribution environnementale des assemblages de microfossiles et les analyses géochimiques des shales du Supergroupe de Mbuji-Mayi (~1065 à ~1000 Ma) en République démocratique du Congo, afin de déterminer la paléoécologie des premiers eucaryotes et d'examiner les liens entre la chimie océanique et l'évolution de la biosphère. La spéciation du fer, les concentrations en métaux majeurs et en traces (Mn, Mo et U) ainsi que les isotopes du fer et du molybdène sont utilisés. Les eucaryotes des assemblages de microfossiles du Supergroupe de Mbuji-Mayi sont plus diversifiés et abondants dans les environnements marginaux anoxiques et ferrugineux, ce qui révèle une préférence écologique et/ou une meilleure préservation. Cependant, il n'est pas possible pour le moment de mettre en évidence leurs exigences écologiques en termes de disponibilité en oxygène et/ou en éléments nutritifs, car leur habitat et leur métabolisme benthiques ou planctoniques sont inconnus.

5.3. Palaeoecology of Mesoproterozoic organic-walled microfossil assemblages from the Mbuji-Mayi Supergroup, DRC.

B.K. Baludikay[1*], C. François[1] , D. Asael[2], R. Guilbaud[3], S. Poulton[3,] , O. Rouxel[4], D. Baudet[5] V. Debaille[6], N. Mattielli[6] & E.J. Javaux[1*]

[1] Early Life Traces & Evolution Lab – UR Astrobiology, Geology Department, University of Liege, Belgium
[2] Department of geology and geophysics, Yale University, New Haven, USA
[3] School of Earth and Environment, University of Leeds, Leeds LS2 9JT, United Kingdom
[4] IFREMER, Centre de Brest, 29280 Plouzané, France
[5] Geodynamics & Mineral Resources Service, Royal Museum for Central Africa, Tervuren, Belgium
[6] Laboratoire G-TIME, Université Libre de Bruxelles, Brussels, Belgium.

Keywords: Palaeoecology–palaeoredox conditions–early eukaryotes.

*Corresponding authors: bkbaludikay@uliege.be; ej.javaux@uliege.be.

Abstract:

It is often thought that dominantly anoxic conditions from Mesoproterozoic era (1600–1000 Ma) would have limited early eukaryote diversification because eukaryotes lived only in oxygenated habitats. However, recent studies evidenced cases showing a flourishing diversity of early eukaryotes in dysoxic and anoxic environments, arguing that many early eukaryote fossils would represent organisms adapted to low oxygen habitats. To understand the role, if any, that anoxia played in eukaryotic diversification, detailed study combining micropaleontology and redox proxies at high-resolution is crucial. Here, we combine analyses of the environmental distribution of microfossil assemblages and geochemical analyses of hosting shale from the ~ 1065 to ~ 1000 Ma Mbuji-Mayi Supergroup in Democratic Republic of the Congo, in order to determine the palaeoecology of early eukaryotes, and to examine links between oceanic chemistry and the evolution of eukaryotic biosphere. Iron speciation, major and trace metal concentrations (Mn, Mo and U) as well as iron and molybdenum isotopes are used. Eukaryotic taxa from Mbuji-Mayi Supergroup microfossil assemblages reveal ecological preference to and/or better preservation in anoxic and ferruginous marginal environments. However, it is not possible at this time to evidence their ecological requirements both in terms of oxygen and/or nutrients availability, since their benthic or planktonic habitat and metabolism are unknown.

1. Introduction

Throughout the Proterozoic, paleontological evidences indicate that eukaryotes appeared at ca. 1650 Ma and diversified from 1100 Ma (*Javaux, 2011;Loron et al., 2018)* to 800 Ma (*Butterfield, 2001; Butterfield, 2015; Javaux and Knoll, 2016; Knoll, 2014; Knoll et al., 2006; Knoll and Nowak, 2017;Riedman and Sadler, 2017; Xiao and Tang, 2018*) with the highest diversity restricted to coastal environments near microbial mats or river inputs (*Javaux et al., 2001; Beghin et al., 2017)*, and only rare taxa in anoxic basins (*Javaux and Knoll, 2016*). It has often been argued anoxic and sulfidic conditions, commonly widespread in Mesoproterozoic oceans (*Planavsky et al., 2011; Poulton and Canfield, 2011; Reinhard et al., 2013*), would have restricted eukaryotic diversification and abundance either directly or indirectly through nutrient limitation (*Anbar and Knoll, 2002; Cohen and Macdonald, 2015; Kah and Bartley, 2011; Reinhard et al., 2016*). Accordingly, the increase of eukaryotes ca. 800 Ma would reflect their diversification within expanded oxygenated habitats in the global ocean. However, in a recent study, this view that eukaryotic diversification would be restricted to oxygenated environments has been called into question (*Javaux and Knoll, 2016; Porter et al., 2018*). These authors pinned up cases supporting a flourishing diversity of eukaryotic communities in anoxic and sulfidic environments at the time when early eukaryotes evolved. Detailed studies combining micropaleontology and redox proxies at high-resolution are rare (*Beghin et al., 2017; Guilbaud et al., 2018; Javaux and Knoll, 2016)* but necessary to understand the role, if any, that anoxia played in eukaryotic diversification. Here, we combine new analyses of the environmental distribution of previously described microfossil assemblages (*Baludikay et al., 2016*) and geochemical analyses of hosting shales from the ~ 1065 to ~ 1000 Ma Mbuji-Mayi Supergroup (*François et al., 2017; François et al. in prep*) in order to determine the palaeoecology of early eukaryotes, and to examine links between oceanic chemistry and the evolution of eukaryotic biosphere. In particular, we use iron speciation, major and trace metal concentrations (Mn, Mo and U) as well as iron and molybdenum isotopic systematics; which are commonly used proxies to delineate bottom water redox conditions, in both modern and ancient settings (*Algeo and Tribovillard, 2009; Algeo and Lyons, 2006; Algeo and Rowe, 2012; Anbar, 2004; Anbar and Rouxel, 2007; Arnold et al., 2004; Asael et al., 2013; Diamond et al., 2018; Doyle et al., 2018; Lyons et al., 2009; McManus et al., 2002; Planavsky et al., 2018; Poulton and Canfield, 2011; Tribovillard et al., 2012*). All these redox data, together with microfossil diversity data and their relative abundance are used to detect possible trends in diversity and taxon dominance in anoxic, dysoxic and oxic conditions.

2. Geological context of the Congo Basin

Localised in Central Africa, the Congo Basin (Fig. 1) is an intraCratonic basin covering an area of about 1.8 million km^2 (*Kadima et al., 2011a*). It is centred on the Democratic Republic of the Congo (DRC), and extends to the West into Angola, Republic of the Congo and Gabon, and on the North into the Central African Republic. It contains up to 9 km of sedimentary rocks ranging from Late Mesoproterozoic to recent and had a complex geological and tectonic evolution (*Delvaux and Fernandez-Alonso, 2015; Kadima et al., 2011a, 2011b*). In its southeastern margin, in DRC, the Mbuji-Mayi Supergroup and the Kibaran belt (Fig. 2) constitute the basal series of the Congo Basin. This sedimentary sequence is buried in the deepest part of the Congo Basin and outcropping in the Mbuji-Mayi area due to denudation and rock uplift at the margin of the basin (*Delvaux and Fernandez-Alonso, 2015*).

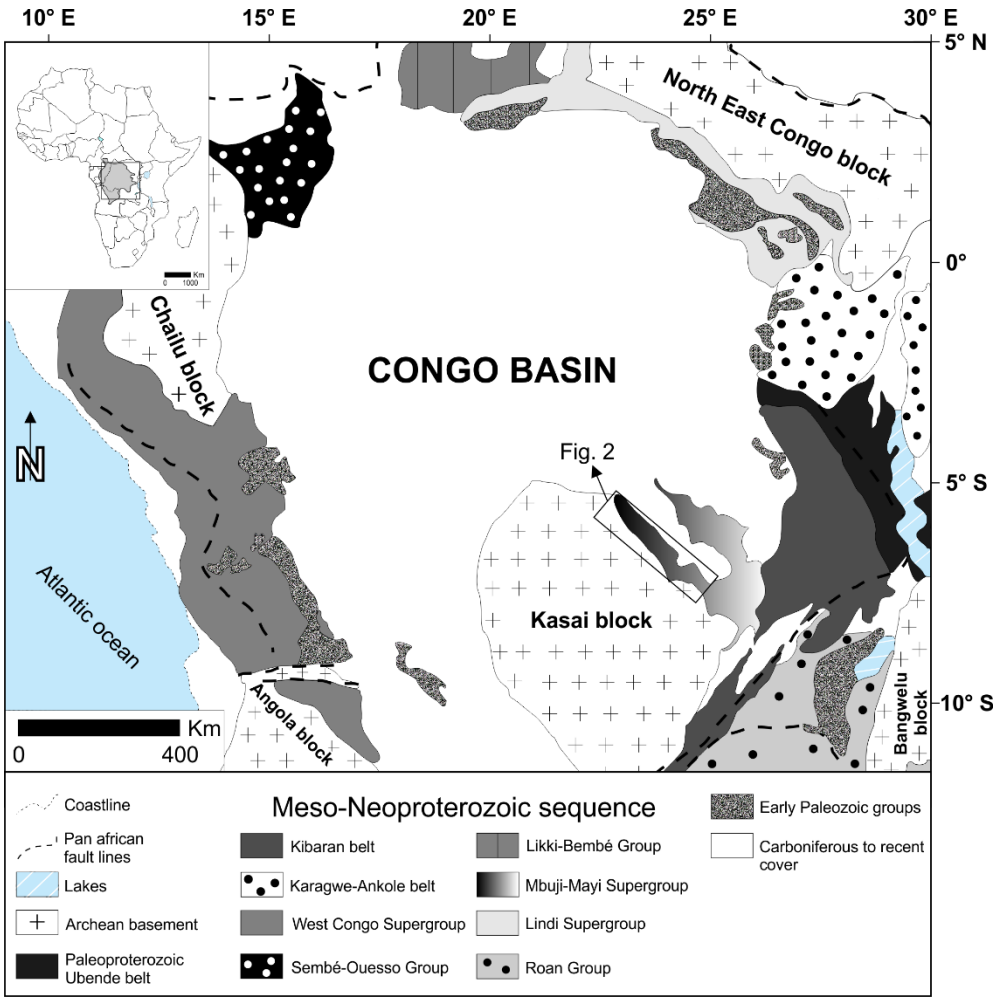

Fig.1. Simplified geological map of Congo Basin. Modified from *Kadima et al., 2011a*.

The Mbuji-Mayi Supergroup rests unconformably upon the Archean Kasai block in its southern and western parts while a number of Proterozoic mobile belts in its eastern part (*Cahen and*

Mortelmans, 1947; Raucq, 1957, 1970; Tack et al., 2010) surrounds it. Repeated deformation along the margins of the Kasai block have uplifted these Proterozoic mobile belts, causing them to become important provenance sources for sediments in the Mbuji-Mayi Supergroup (*Delpomdor et al., 2013a; François et al., 2017; Milesi et al., 2006*). Two distinct lithostratigraphic sequences are identified for this Supergroup, from the oldest to the youngest: BI Group and BII Group (Figs. 2 and 3)

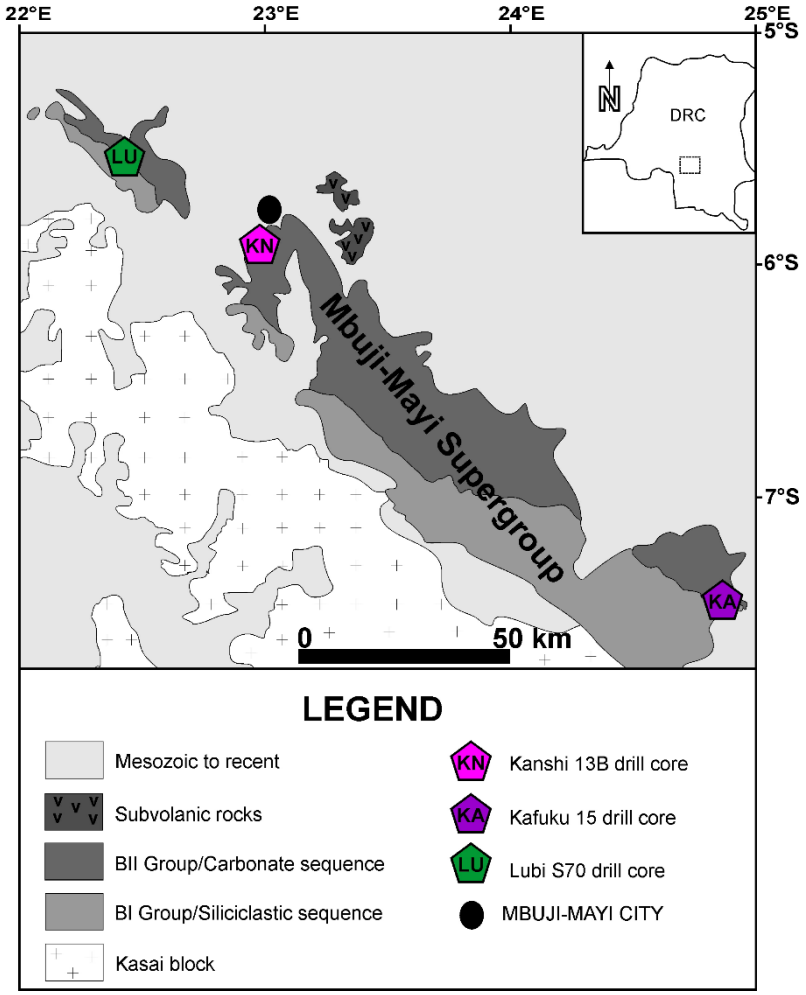

Fig. 2. Simplified geological map of the Mbuji-Mayi Supergroup in the Sankuru–Mbuji-Mayi region. Locations of drill cores are indicated by white polygons: LU = Lubi S70; KN = Kanshi 13B and KA = Kafuku 15. Modified from *Baludikay et al., 2016*.

The BI Group (~ 500 m thick) is a siliciclastic sequence composed of quartzite, shale, siltstone and some carbonate horizons in its upper part. The BII Group (~ 1000 m thick) is a stromatolitic carbonated sequence intercalated with thin organic-rich shales and chert horizons (*Bertrand-Sarfati, 1972; Delpomdor et al., 2013a; Raucq, 1957, 1970*). BI and BII Groups are both subdivided into six (BIa, BIb, BIc, BId, BIE and BIe) and five (BIIa, BIIb, BIIc, BIId and BIIe) subgroups respectively. Detailed descriptions of these subgroups have been given in

Raucq (*1957, 1970*) and updated (especially for the carbonates) in Delpomdor et al. (*2013a, 2017*).

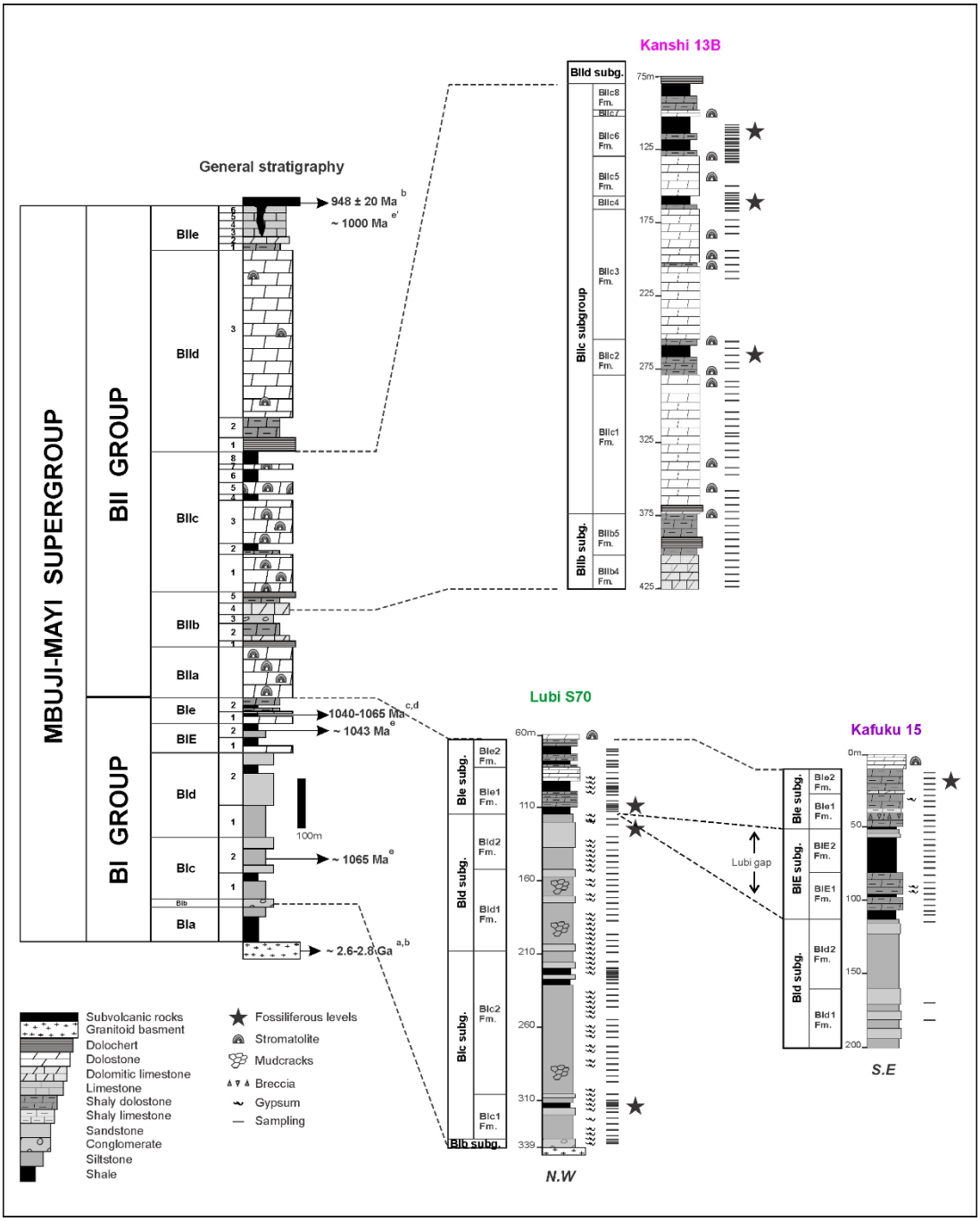

Fig. 3. Stratigraphy of Mbuji-Mayi Supergroup and lithostratigraphic columns of studied drill cores. Ages from (a) *Delhal et al., 1975*; (b) *Cahen et al., 1984*; (c) *Cahen, 1954*; (d) *Holmes and Cahen, 1955*; (e) *François et al., 2017* and (e') *François et al. in prep*. Modified from *Baludikay et al., 2016* and *François et al., 2017*.

Microfacies analyses suggest a shallow marine environment, associated to a ramp-system, which evolved to evaporitic and lacustrine environments (*Delpomdor et al., 2013b and 2015*). Radiometric data yielded a K/Ar age of 948 ± 20 Ma (*Cahen et al., 1984*) from basaltic

lavas topping the BII Group and a conventional $^{207}Pb/^{206}Pb$ age around 1055 Ma for the top of BI Group (Cahen 1974). Recently, new U-Th-Pb dating on diagenetic minerals such as xenotimes and monazites from BI Group reveal ages between 1030 and 1065 Ma (François et al. 2017). A new Ar/Ar dating from basaltic lavas provide minimum age from 1006 to 1009 Ma for the top of the Supergroup (*François et al., in prep*). This late Mesoproterozoic age is also consistent with the microfossil assemblage (*Baludikay et al., 2016*).

3. Description of studied drill cores

For this study, we sampled three drill cores stored in the Royal Museum of Central Africa (RMCA) (Figs. 2 and 3). Each sample has a serial number (RG number) allowing its identification in the collection. The lithological descriptions refer to those of Raucq (*1950 and 1970*) and updates from Delpomdor et al. (*2013a*) and François et al. (*2017*):

3.1. **Lubi S70** drill core (former Tshinyama S70, 339 m-long; samples RG57625–57825) crosses the BI Group (Figs. 3 and 4A) At the base of drill core, the BIb Formation (339–336.55 m) consists of an alternation of dark, grey or pink siltstones often brecciated and dark cherty sandstones with conglomerates and some gypsum nodules. The overlying BIc1 Formation (336.55–308.5 m) mainly consists of grey green siltstones alternating with sandstones and organic-rich dark shales; with some occurrences of gypsum nodules. The BIc2 Formation (308.5–209.4 m) consists of laminated argillaceous siltstones interbedded with sandstones and grey shales; abundant pyrite and some red mudstones (sometimes with carbonate). Gypsum is frequent and mudcraks are observed. The BId1 Formation (209.4–155.5 m) is characterized by grey carbonated argillaceous siltstones alternating with pink sandstones. Gypsum is irregularly distributed; mudcracks and cross-bedding are common. The BId2 Formation (155.5–116 m) mainly consists of finely laminated grey to greenish siltstones interbedded with dark shales in the upper part; sandstones as well as abundant gypsum veins are also observed. The BIe1 Formation (116–86.2 m) consists of grey dolostones and shaly dolostones alternating with dark shales and occurrence of gypsum-thick veins. The BIe2 Formation (86.2–66.6 m) consists of grey cherty dolostones evolving to grey shaly dolostones and shales. Finally, at the top the drill core, thelower part of BIIa Subgroup (66.6–60 m) shows mainly grey dolostones with stromatolites.

3.2. **Kafuku 15** drill core (200 m-long; samples RG41361–41384) which also cut through the BI Group (Figs. 3 and 4B) reveals, from bottom to top, the following succession: the BId1 Formation (200–159 m) with carbonated siltstones and pink argillaceous sandstones. The BId2 Formation (159–109.5 m) consists of feldspar-rich pink siltstones alternating with

micaceous sandstones. The BIE1 Formation (109.5–78.8 m) consists of shaly dolostones and shales with some gypsum veins. The BIE2 Formation (78.5–53.25 m) consists of dark shales evolving into argillaceous sandstones and siltstones. The BIe1 Formation (53.25–26.4 m) shows grey sandy dolostones with shales and polygenic intraformational breccia; with pink shaly limestones passing to cherty dolostones. The BIe2 Formation (26.4–9.9 m) exhibits shaly dolostones with argillaceous sandstones and dolomitic limestones, and occurrence of sulphides (pyrite and marcasite). The bottom of BIIa Subgroup (9.9 m to the top) is characterized by grey stromatolitic dolostones and siliceous dolostones.

3.3. **Kanshi 13B** drill core (425 m-long; samples RG32201 to 32463) crosses the BII Group (Figs. 3 and 4C) and includes, from bottom to top, the following succession: the BIIb4 Formation (425–399 m) is mainly constituted of massive to finely dark grey dolomitic limestones. The BIIb5 Formation (399–375 m) consists of grey shaly dolostones alternating with cherty dolostones. The BIIc1 Formation (375–281.99 m) shows mainly dark grey stromatolitic dolostones. The BIIc2 Formation (281.99 – 254.88 m) exhibits dark pyritic shales interbedded with dark grey stromatolitic shaly dolostones. The BIIc3 Formation (254.88–171.49m) consists of grey greenish shaly dolostones interbedded with grey dolostones and includes some stromatolites. The BIIc4 Formation (171.49–157 m) shows dark grey shaly dolostones with dark pyritic shales. The BIIc5 Formation (157 – 129.79 m) mainly consists of pink grey stromatolitic dolostones. The BIIc6 Formation (129.79–107 m) contains grey stromatolitic shaly dolostones (with wavy laminations), alternating with dark pyritic shales. The BIIc7 Formation (107–102.6 m) is characterized by grey stromatolitic dolostones. The BIIc8 Formation (102.6–80 m) exhibits dark grey shaly dolostones with dark shales containing pyrite. The bottom of BIId1 Formation (80–75 m) shows green and grey shales with abundant chert.

4. Materials and methods

4.1. Sampling

A total of 234 samples was collected. Sampling locations are shown in Figs. 2 and 3. Among these, 77 samples were processed for microfossil analyses (Kanshi 13B, n = 26; Kafuku 15, n = 17; Lubi S70, n = 34), while geochemical analyses were performed on 157 samples (Kanshi 13B, n = 34; Kafuku 15, n = 37; Lubi S70, n = 86). Shales and siltstones globally dominated samples lithologies.

4.2. Microfossil quantitative analyses

Organic-walled microfossils were extracted from shales using acid maceration following palynological processing techniques modified to minimize mechanical shock (K. Grey 1999). A total of 101 palynological slides (2 sizes fractions per sample, from 10 to 25µm and > 25µm) were mounted and examined with an Axio Imager A1m (Carl Zeiss) transmitted-light microscope. The extracted kerogen includes amorphous organic matter (AOM) and structured organic matter (also called "palynomorphs") such as organic-walled microfossils and mat-forming filaments. A minimum of 300 microfossils was counted per sample, and chosen as statistical threshold, as other studies suggested previously (Tyson 1995). The counting was ended once the plateau of taxonomic richness was reached (i.e. the number of species did not increase anymore with the number of specimens counted). However, 12 samples on 27 did not achieve this threshold (≥ 300) despite mounting several slides per sample: 4 samples from BIe2 Formation (Kafuku 15 drill core); 1 for BId2 and BIe1 formations, both in Lubi drill core; 2 for BIIc2; 1 for BIIc4 and 3 for BIIc2 formations, all in Kanshi 13B drill core (Table S1). This could be due either to absence or low preservation of palynomorphs related to paleoenvironmental conditions or diagenesis (see below). The total number of species observed in a sample constitutes the sample richness (S). The relative abundance of a particular species (%) in a sample is estimated as: $\% = \frac{n}{N} \times 100$ (1); where n and N respectively represent the total number of specimens counted for this species, and the total number specimens of all species counted in this sample. The Simpson's index of Diversity measures the diversity of species and take into account the number of species and abundance of each species. It represents the probability that two specimens randomly selected in a sample will belong to different species and is calculated as: Simpson's index of Diversity = (1 − D) (2); where $D = \sum(n/N)^2$ (3), refers to the Simpson's index, with n and N as defined above. Simpson's index of Diversity (1 − D) varying from 0 to 1, values close to 1 indicate more diversity in the sample (Simpson 1949).

4.3. Palynofacies analysis

Tyson's criteria (*Tyson, 1995*, Table 20.6; p. 352) were used to characterize the palynofacies, and to describe several types of AOM. Six palynofacies were identified (Table 1) in order to identify their possible relationship with physico-chemical conditions specific to different depositional environments. The palynofacies were defined by using the association of three categories of elements present in a macerated sample: AOM, organic-walled microfossils,

Table 1. The main criteria used to describe palynofacies (based on the description of amorphous organic matter "AOM", modified after (*Tyson, 1995*), as well as the presence of microfossils and sulphides).

Property	Lustre			Color				Heterogeneity				Cohesiveness		**Sulphide inclusions			Typical association		
Characteristic	1	2	3	4	5	6	6bis*	7	8	9	10	21	22	27	28	29	30	31	32
Description	Hyaline	Glossy	Matt	Yellow-orange-red	Orange-brown	Grey to grey brown	Dark-brown to black*	Homogenous	With small opaque speckles	Clotted lumpy structure	With obvious organic inclusions	Forms coherent particles	Tends to disintegrate and finely dispersed	Inclusions absent	Inclusions rare	Inclusions common to abundant	Organic-walled microfossils dominate kerogen assemblage	Kerogen assemblage mixed (AOM + microfossils)	'AOM' dominates kerogen assemblage
Palynofacies																			
1			X			X		O	±	O		X			O		±		
2			X			X		O		O	±		X		O			±	
3			X				X	X		O		X				X			±
4			X				X	X				X	±			X			X
5			X		X		±	X		O		X				X			X
6			O				O	O				O			O				X

Characteristics 11 to 20 were not used here as they require fluorescence microscopy, which has not been used in this study.
X: abundant; ±: common; O: rare

*: a color characteristic non-present in original Tyson's table (*1995*, Table 20.6)

** **Pyrite content** in original Tyson's table

fragments of filamentous microbial mat and sulphide contents. Microscopic observation was carried out to assess the diversity of AOM differing by their lustre, color, heterogeneity, and cohesiveness of organic particles (Table 1). However, we added a new color characteristic ("dark-brown to black"), absent in the original Tyson's table. Given fluorescence microscopy was not used in this study, only criteria obtained by transmitted light microscopy are considered here. We used qualitative visual recognition and semi-quantitative (abundant, common and rare) both on kerogen assemblage and sulphide contents.

4.4. Geochemistry

Redox conditions are important in deciphering the palaeoecology and preservation of microfossil assemblages. They can be characterized by detailed understanding of the environmental behavior of important redox-sensitive species such as Fe, Mo, U and also Mn which is a special minor element influencing the behavior of trace metals (*Doyle et al., 2018; Peacock et al., 2007; Tribovillard et al., 2006, 2012*). To reconstruct palaeoredox conditions in our sedimentary sequence, we combined data from Fe speciation, major, minor and trace metals (Al, Fe, Mn, Mo, and U) but also Fe and Mo isotope composition.

4.4.1. Iron speciation

Samples (n= 64) were crushed (< 63 µm) at the Geology Department of the University of Liege. Then they were processed at School of Earth and Environment (Leeds University, Yorkshire, England) to extract sequentially highly reactive iron (Fe_{HR}) which includes carbonate-associated iron (Fe_{carb}), ferric (hydroxyl)oxides (Fe_{ox}), magnetite (Fe_{mag}) and iron sulphide (Fe_{py}). Highly reactive iron was quantified against total iron (Fe_T). Fe_{carb}, Fe_{ox} and Fe_{mag} were obtained with Na-acetate, Na-dithionite, and ammonium oxalate, respectively. By contrast, Fe_{py} was released by precipitation of Ag-sulphide using chromous chloride and Ag-nitrate (*Canfield et al., 1986*). Total iron (Fe_T) extractions were carried out on ashed samples (8 h at 450 °C) using a HNO_3-HF-$HClO_4$ mixed-acid digestion. The detailed procedure was describe in *Poulton and Canfield, 2005*. Iron concentrations were measured by Atomic Absorption Spectrometer and replicate extractions gave a RSD of 8.97% (Fe_{carb}), 3.28% (Fe_{ox}), 6.68% (Fe_{mag}), 4.58% (Fe_{py}), and 3.44% (Fe_T). Prior to the calculation of highly reactive on total (Fe_{HR}/Fe_T) and pyrite on highly reactive (Fe_{py}/Fe_{HR}) iron ratios, the samples were screened to ensure sufficient total Fe, since low Fe_T carbonate-rich samples with Fe_T < 0.5 wt% are not suitable for reconstructing redox conditions and can give erroneous results (*Clarkson et al., 2014*).

The identification of water column anoxia via Fe_{HR}/Fe_T ratios is based on extensive calibration in modern (*Canfield et al., 1986; Poulton and Raiswell, 2002; Raiswell and Canfield, 1998*) and ancient *(Poulton and Raiswell, 2002; Raiswell et al., 2001*) marine settings. Sediments deposited under anoxic water columns are typically enriched in Fe_{HR}, resulting in $Fe_{HR}/Fe_T \geq 0.38$ (*Poulton and Canfeld, 2011*). By contrast, sediments deposited under oxic water column conditions are depleted in those minerals, resulting in $Fe_{HR}/Fe_T \leq 0.22$ (*Poulton and Canfield, 2011*). Values between these values are considered equivocal (*Poulton and Canfield, 2011*), and may represent anoxic deposition where the water column enrichment of Fe_{HR} has been masked by rapid sedimentation, or where some unsulfidized Fe_{HR} has been converted to Fe-rich sheet silicates during early diagenesis (*Cumming et al., 2013; Poulton and Raiswell, 2002; Poulton et al., 2010*). For samples that were clearly deposited from anoxic bottom waters, the extent of pyritization of the highly reactive Fe pool can be used to distinguish euxinic ($Fe_{py}/Fe_{HR} > 0.7$) from ferruginous ($Fe_{py}/Fe_{HR} < 0.7$) water column conditions (*März et al., 2008; Poulton and Canfield, 2011*). These ratios are used to reconstruct the average chemical composition of bottom waters, over the time interval represented by a sample, from the sediment-water interface up to the bottom of the chemocline, which may vary in depth.

4.4.2. *Major (Al, Mn) and trace (Mo, U) metals.*

Powdered samples were ashed in quartz beakers at 600 °C for at least 24 h and loss of weight during ignition (LOI) was determined. About 200 mg of each sample was dissolved in two steps using mixtures of HNO_3 + HF and HNO_3 + HCl acids. Solutions were then taken up with 20 mL of 7 mol/L HCl. Splits from each sample were taken, evaporated, and brought up in 5 percent HNO_3 for elemental analysis. Mo and U concentrations were measured using a Nu Plasma MC-ICP-MS, while Al and Mn concentrations were measured using a Quadrupole ICP-MS at the G-TIME Lab (ULB), Belgium. Calibration of the instruments was performed by running a multi-element solution at different concentrations and blank solutions, while standardization was done via measurements of reference materials (SDO-1, Nod A-1, and Nod P-1). Enrichment factors (EF) were used to compare the respective enrichments of authigenic fraction of Mo, U and Mn. EF for a given element (X) is calculated as: $X_{EF} = \left[\left(\frac{X}{Al}\right) sample \Big/ \left(\frac{X}{Al}\right) AS \right]$ (4); where *X* and *Al* represent the concentrations of element (X) and Aluminum, respectively. Samples were normalized using the average shale (AS) compositions of Wedepohl (*1971*). Although Al normalization has some potential pitfalls (*Tribovillard et al.,*

2006), enrichment factors are useful for rapid assessment of the authigenic fraction of Mo, U and Mn in large numbers of samples. In practice, a value above 1 represents an enrichment and a value less than 1 denotes a depletion, relative to average shale.

4.4.3. Mo isotope analysis

We used a ^{97}Mo– ^{100}Mo double spike solution prepared gravimetrically from Oak Ridge Laboratory metal powders. Optimization of the double spike isotope composition relative to the SPEX standard gave ^{95}Mo/^{98}Mo, ^{97}Mo/^{98}Mo and ^{100}Mo/^{98}Mo isotopic ratios of 0.278, 16.663 and 15.704, respectively. Data reduction was done according to (*Siebert et al., 2001*), where iterations were repeated until the difference in the δ^{98}Mo value between two consecutive iterations was smaller than 0.001‰. The typical number of iterations was ≤ 4. Molybdenum concentrations during isotopic measurements varied from 100 to 500 ppb, depending on the Mo content of the sample powders. Within a given session, standards and samples were measured at a constant concentration. However, the external precision of the measurement was not affected within this range—yielding 2SD = ±0.06‰, where the typical standard error of a single measurement (2SE) was 0.05‰. The MC-ICP-MS machine was operated at low resolution with an ESI Apex Q introduction system measuring all Mo isotopes masses together with ^{91}Zr and ^{99}Ru in order to monitor isobaric interferences. During each session of Mo isotope analysis, we performed frequent measurements of our in-house laboratory Mo standard (Mo SPEX lot 11-177Mo), the NIST-3137 standard and the Johnson Matthey Specpure® Mo plasma standard (Lot #802309E; RochMo2) used in previous studies (*Barling and Anbar, 2004 and others*). We have also preformed frequent measurements of georeferenced materials including SDO-1, Nod A-1 and Nod P-1. Mo isotope compositions are reported using the δ notation, where

$\delta^{98}\text{Mo}\ (‰) = 1000 \cdot [(^{98}\text{Mo}/^{95}\text{Mo})_{\text{sample}}/(^{98}\text{Mo}/^{95}\text{Mo})_{\text{SPEX}} - 1]$ (5), calculated relative to our in-lab Mo SPEX standard (Lot 11-177Mo). A calibration of the SPEX standard relative to NIST-3137 (lot 891307) and Rochester (Lot 802309E) gave:

$\delta^{98/95}\text{Mo}_{\text{SPEX}} = \delta^{98/95}\text{Mo}_{\text{NIST3137}} - 0.35 \pm 0.12‰$ (6);

$\delta^{98/95}\text{Mo}_{\text{SPEX}} = \delta^{98/95}\text{Mo}_{\text{roch}} - 0.05 \pm 0.06‰$ (7).

We choose to report our results relative to the SPEX standard since it is, within error (1SD), identical to the Rochester standard which is the most common standard in the recent Mo isotope literature.

4.4.4. Fe isotope analysis

For the determination of Fe isotope ratios we followed the methods of Rouxel et al. (*2005*, *2008a*, *2008b*), providing us with high precision measurements without argon interferences on the Neptune instrument. Samples were processed at the Domaines Océaniques (UMR 6538), UBO, France; by operating the MC-ICP-MS in either medium or high-resolution mode, and we used Ni as an internal standard for mass bias correction. The "sample-standard bracketing" technique was also used to correct for instrumental mass discrimination by normalizing the isotope ratios to the average measured composition of the standard that was run before and after the sample. Fe isotope values are reported relative to the standard IRMM-14 using the following conventional delta notations:

$$\delta^{56}Fe = 1000 \cdot [(^{56}Fe/^{54}Fe)_{sample}/(^{56}Fe/^{54}Fe)_{IRMN-14} - 1] \quad (8),$$

Based on a complete duplicated procedure (i.e., powder ashing, acid attack, chemical purification and isotope analysis), the long-term external reproducibility is 0.07‰ for $\delta^{56}Fe$ values (2 standard deviations). We also measured the following georeference materials: BHVO-2 ($\delta^{56}Fe = 0.09 \pm 0.07$‰) and Nod-P1 ($\delta^{56}Fe = -0.49 \pm 0.08$‰).

4.4.5. Carbon (TOC, TC and TIC)

Total organic carbon (TOC) and total carbon (TC) were measured on an Eltra IR C/S analyzer in the SIFIR Laboratory at the University of Manitoba (commercial subcontracting). The carbonate fraction was removed prior to TOC analysis via two sequential dissolutions with 20% (vol/vol) HCl for 24h. Samples were then washed with Milli-Q water until all the remaining acid had been removed and subsequently dried at 70°C. Total inorganic (TIC) was calculated as the difference between total carbon (TC) and total organic carbon (TOC).

5. Results

5.1. Microfossil quantitative analysis

Abundance of each species of organic-walled microfossils (countings) are provided in Table S1 (Supplementary). Among the 77 selected samples, only 27 samples contain microfossils. A total of 49 species were identified in the Mbuji-Mayi Supergroup, and subdivided out into three groups (Fig. S1): unambiguous eukaryotes (11 species), possible eukaryotes or prokaryotes (10 species) and probable bacteria (28 species) (see *Baludikay et al., 2016* for more details). There is an increasing trend in total species richness (S), upward in

stratigraphy, from the older samples (S = 23, in the BIc1 Formation) to the top (S = 43, in the BIIc6 Formation). However, we note a decrease in species richness in the BId2, BIe1 and BeI2 formations where S = 6; 2 and 14 respectively (Figs. 4A–4C).

The drill core Lubi S70 revealed three fossiliferous levels (Fig. 4A). From bottom to top (Table S1): (1) in green shales at 312.2–308.5 m depth (BIc1 Formation); where three unambiguous eukaryote species (5%, *Lophosphaeridium granulatum*, *Pterospermopsimorpha insolita* and *P. pileiformis*), eight possible eukaryotes or prokaryotes (86%) and twelve probable bacteria (9%) were recorded, (2) in grey shales at 141 m and 119 m depth (BId2 Formation) and (3) in dolostones-containing grey shales at 114 m depth (BIe1 Formation), where the microfossil diversity decreased and was essentially dominated by leiospheres (99%; possible eukaryotes or prokaryotes). Species identified as probable bacteria are not present into these two last formations while one unambiguous eukaryote species (*L. granulatum*; 1%) is present in the BId2 Formation. The BIe1 Formation recorded the lower species richness from all formations. In addition, the total number of counted specimens (N) did not exceed 65 (Table S1).

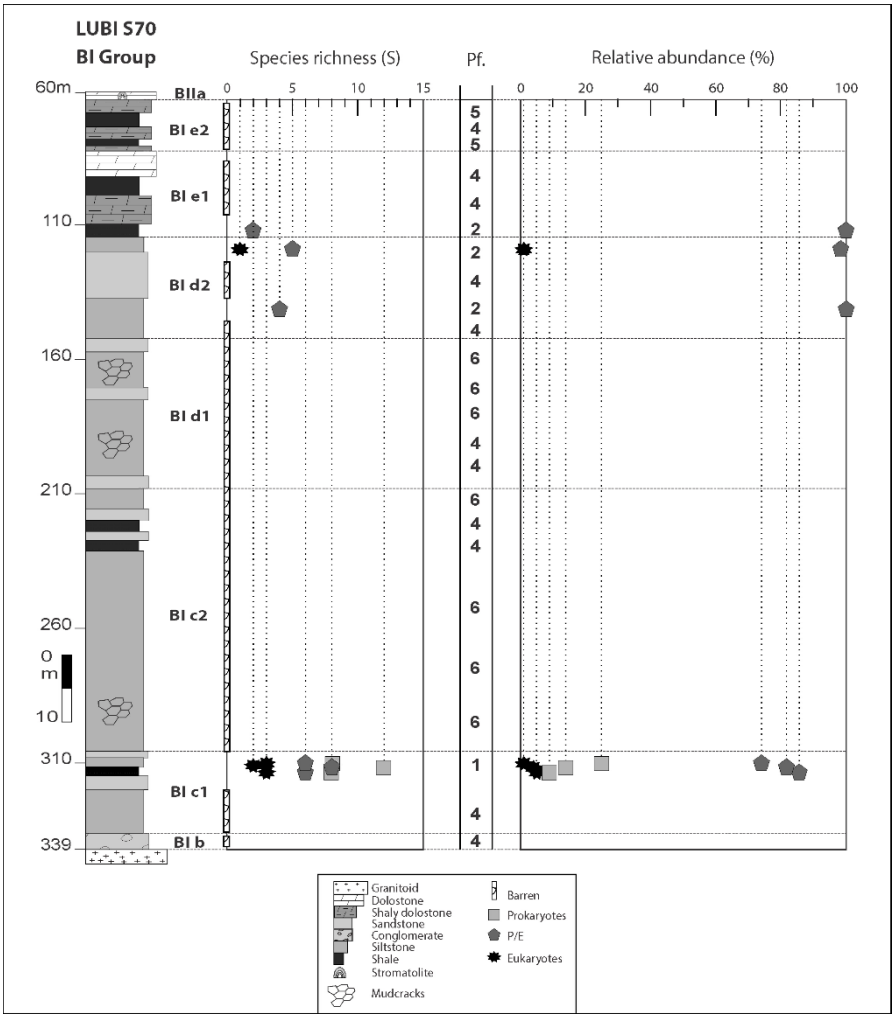

Fig. 4A. Lithostratigraphic column of Lubi S70 core – BI Group. Quantitative microfossil analysis: species richness (S =) and relative abundance (%) of unambiguous eukaryotes (E), possible eukaryotes or prokaryotes (P/E) and probable bacteria (P). (For further details, see Supplementary Table S1 and Fig. S1).

In contrast, in the Kafuku 15 drill core (Fig. 4B), only BIe2 Formation revealed microfossils assemblage. The total species richness (S) was 5 (with N ≤ 42), at the bottom of the BIe2 Formation (at 23.6 m and 19.6 m depth, dolostones-containing dark shales and dark shales respectively), and increased to 14 species (with N ≤ 116) at the top (15.6 m to 14 m depth, dark shales).

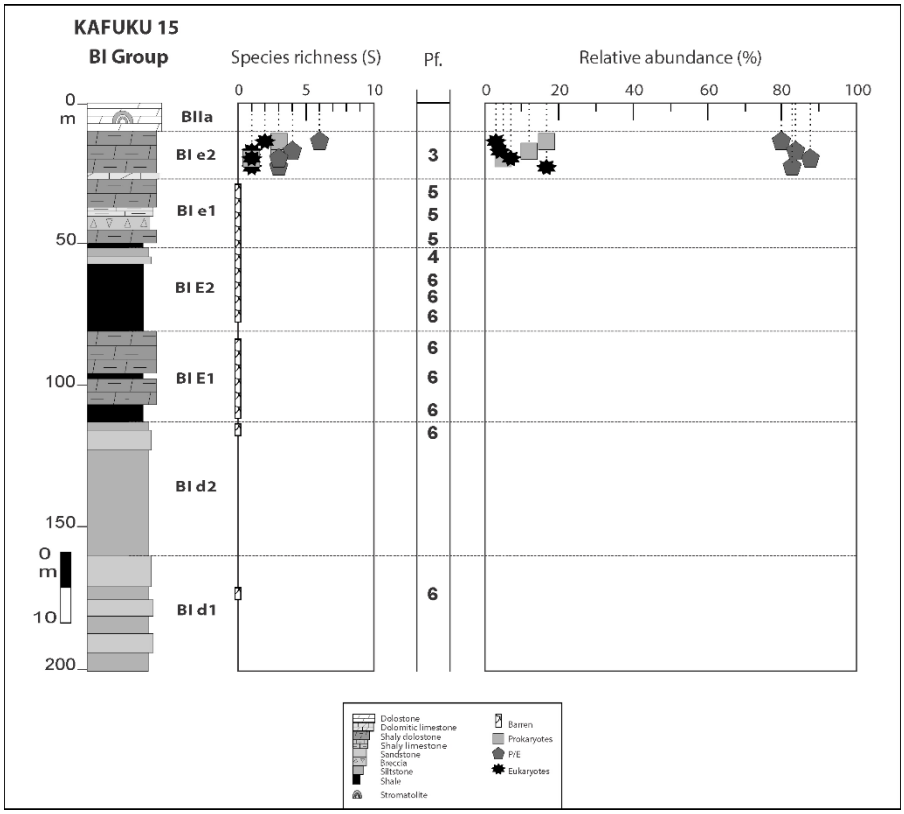

Fig. 4B. Lithostratigraphic column of Kafuku 15 core – BI Group. Quantitative microfossils analysis: species richness (S =) and relative abundance (%) of unambiguous eukaryotes (E), possible eukaryotes or prokaryotes (P/E) and probable bacteria (P). (For further details, see Supplementary Table S1 and Fig. S1).

The BIe2 Fm. microfossil assemblage included three unambiguous eukaryote species (4%; *Germinosphaera bispinosa*, *L. granulatum* and *P. insolita*), six possible eukaryotes or prokaryotes (84%) and five probable bacteria (12%; see Table S1).The total species richness (S) equal to 5 (with N ≤ 42), at the bottom of BIe2 Formation (at 23.6 m and 19.6 m depth, dolostones-containing dark shales and dark shales respectively), and increases to 14 species (with N ≤ 116) at the top (15.6 m to 14 m depth, dark shales). The BIe2 microfossil assemblage includes three unambiguous eukaryote species (4%, *Germinosphaera bispinosa*, *L. granulatum* and *P. insolita*), six possible eukaryotes or prokaryotes (84%) and five probable bacteria (12%; see Table S1).

The Kanshi 13B drill core preserved the most diverse microfossil assemblages, in the three formations where shales were sampled (Fig. 4C). The BIIc2 Formation recorded a new increase of species with S = 33 species (at 267.84–254.88 m depth, grey-greenish shale).

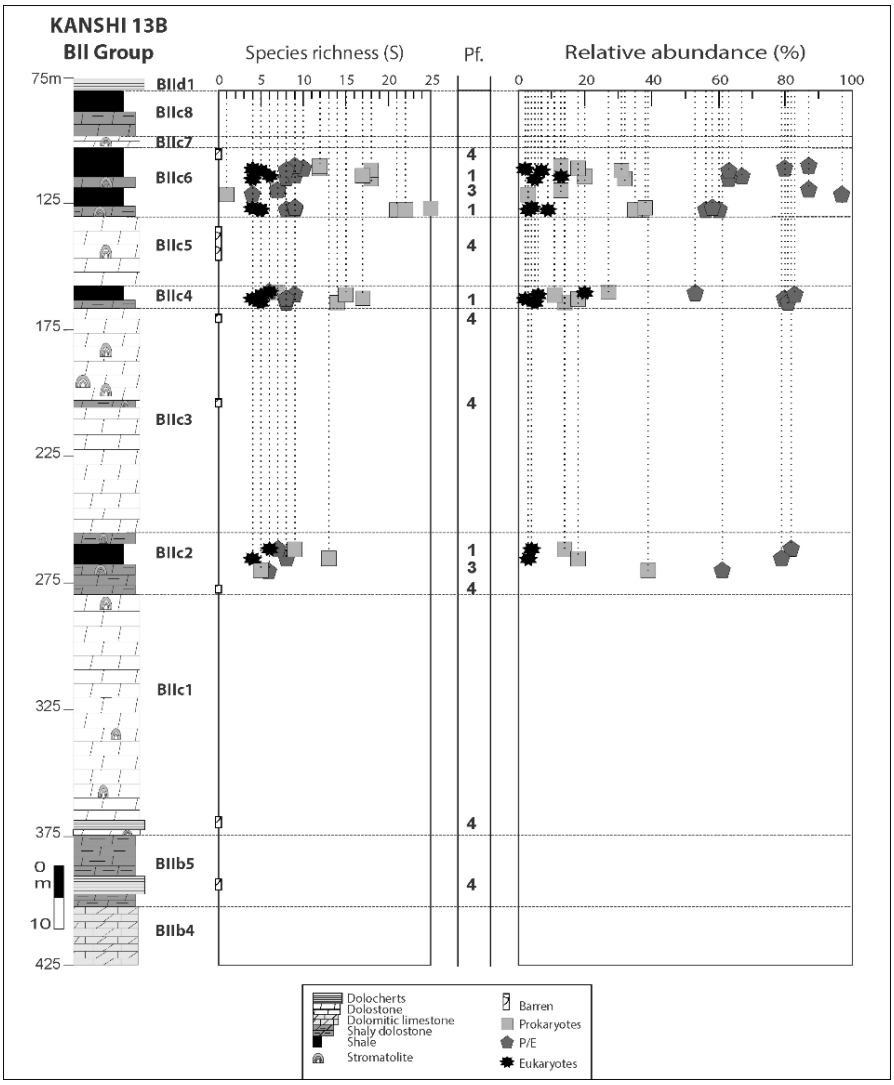

Fig. 4C. Lithostratigraphic column of Kanshi 13B core – BII Group. Quantitative microfossils analysis: species richness (S =) and relative abundance (%) of unambiguous eukaryotes (E), possible eukaryotes or prokaryotes (P/E) and probable bacteria (P). (For further details, see Supplementary Table S1 and Fig. S1).

This microfossil assemblage is composed of seven unambiguous eukaryote species (4%), where the first occurrence of genus *Trachyhystrichosphaera* (the Late Mesoproterozoic and Early Neoproterozoic index fossil – *Trachyhystrichosphaera aimika*, 1.5% – and *T. botula*) is observed as well as one acanthomorph species assigned to *cf. Tappania* sp.; eight possible eukaryotes or prokaryotes (82%) and eighteen probable bacteria (14%, see Table S1). The BIIc4 Formation recorded 42 species (at 162–158 m depth, dark shale). Eight unambiguous eukaryote species (6%) includes two new species (*Jacutianema solubila* and *Valeria elongata*) not

observed into underlying levels; while nine species are possible eukaryotes (83%) and twenty-five probable bacteria (11%). A moderate increase of *Trachyhystrichosphaera aimika* making up to 4.44% of the assemblage was observed. The BIIc6 Formation recorded the highest total species richness (S = 43), including eight unambiguous eukaryotes (13%; *Jacutianema solubila, Lophosphaeridium granulatum, Pterospermopsimorpha insolita, P. pileiformis, Trachyhystrichosphaera aimika, T. botula, Valeria lophostriata* and an unnamed form with conical-like expansions), ten possible eukaryotes or prokaryotes (67%) and twenty-five probable bacteria (20%). The species richness varied through the formation: at 122.9–120 m depth, green shales, included 38 species; at 118–115.72 m depth, dolostones-containing shales, had 5–14 species, where no unambiguous eukaryotes was observed; and at 113.86–111 m depth, grey dark shales included 21–32 species. The shales of the BIIc8 Fm. were not accessible for sampling.

5.2. Palynofacies analysis

Microscopic observations of AOM, microfossils, fragments of filamentous microbial mats and sulphide contents permitted to characterized six palynofacies (Pf1, Pf2, Pf3, Pf4, Pf5 and Pf6, Fig.5):

- Palynofacies 1 (Pf1) represents 23% of all studied samples. It is composed of microfossils with a high taxonomic richness (i.e. $S \geq 14$) and abundant AOM. AOM, grey to grey-brown in color, are coherent and heterogeneous with opaque organic inclusions, occurring in thin layers with fragments of filamentous microbial mats (Figs. 5A, B). Sulphide inclusions are rare. It occurs in Kanshi 13B drill core, exclusively in BIIc2, BIIc4, BIIc6 formations (Fig. 4C and Table S1) as well as in Lubi S70 drill core, especially in BIc1 Formation (Fig. 4A and Table S1).

- Palynofacies 2 (Pf2) occurs in 4% of studied samples (Figs. 5C, D). It is characterized by a low taxonomic richness of microfossils (i.e. $S \leq 6$) and any less AOM. Grey to grey-brown in color, AOM are heterogeneous with opaque inner zone and show a spongy appearance which are finely dispersed. In addition, sulphide inclusions are scarce. It occurs in BId2 and BIe1 formations (Lubi S70).

- Palynofacies 3 (Pf3) represents 8% of studied samples (Figs. 5E, F). It is defined by presence of microfossils with a moderate to low taxonomic richness (i.e. $S \leq 11$) and opaque AOM, dark black in color, exhibiting homogenous and coherent particles. It contains abundant sulphide

inclusions. It occurs in BIIc2 and BIIc6 formations (Kanshi 13B) as well as in BIIe2 Formation (Kafuku 15).

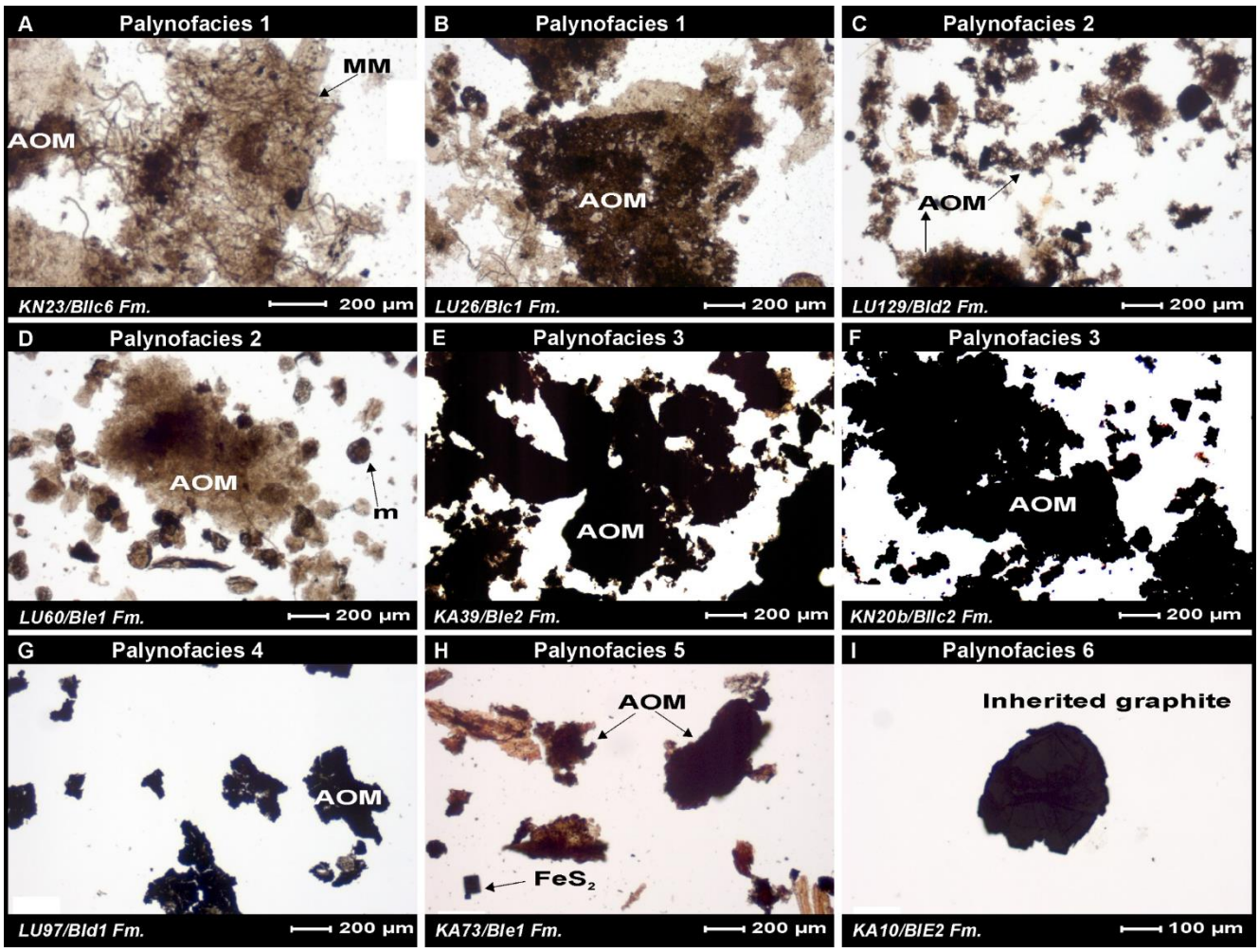

Fig. 5. (A, B) Palynofacies 1(Pf1): Abundant organic-walled microfossils with grey-brown AOM and rare sulphide inclusions; MM = Microbial Mat. (C, D) Palynofacies 2 (Pf2): grey-brown AOM dominant. (E, F) Palynofacies 3 (Pf3): Equal abundance of dark AOM and palynomorphs, with sulphide inclusions. (Pf G) Palynofacies 4 (Pf4): Absence of palynomorphs with relatively low abundance of dark-grey AOM. (H) Palynofacies 5 (Pf5): Absence of palynomorphs with orange-brown AOM and abundant sulphide inclusions. (Fig. I). Palynofacies 6 (Pf6): Palynomorphs absent with graphitized AOM. (See details in text).

- Palynofacies 4 (Pf4) Occurring in 30% of studied samples, is defined by absence of microfossils, an opaque and homogenous AOM, a dark-grey color, and common to abundant sulphide inclusions (Fig. 5G). With the exception of BIIc4 Formation (Kanshi 13B) as well as BIE1, BIe1 and BIe2 formations (Kafuku 15), Pf4 occurs in all others investigated formations (Table S1).

- Palynofacies 5 (Pf5) represents 8% of studied samples. Microfossils are absent; AOM are orange-brown to black in color, and presents homogenous and coherent forms. Sulphide inclusions are common to abundant (Fig. 5H). This palynofacies occurs exclusively in BIe2 Formation (Lubi S70) and BIe1 Formation (Kafuku 15).

- Palynofacies 6 (Pf6) represents 27% of studied samples. Microfossils are absent; AOM and sulphide are scarce. However, AOM or carbonaceous material is graphitized (Fig. 5I). It occurs in Kafuku 15 (BIe1, BIE2, BIE1, BId2 and BId1 fms.) and in Lubi S70 (BId1 and BIc2 fms.).

5. 3. Geochemical results

5.3.1. Fe speciation

All geochemical data are reported in supplementary Table S2 as well as Figs. 6 (A–C). Fe speciation data only concern samples with Fe_T contents greater than 0.5%. In the Lubi S70 drill core (Fig. 6A), Fe_{HR}/Fe_T ratios are low, with an average value of 0.10 ± 0.08 (n = 29) for the BIc1 to BIe1 formations. In the BIe2 Formation, excepted for one sample with Fe_{HR}/Fe_T = 0.13, other samples reveal moderately high Fe_{HR}/Fe_T ratios, with an average of 0.40 ± 0.13 (n = 9). However, the Fe_{py}/Fe_{HR} ratios are well below 0.7 (average of 0.53 ± 0.15). In the Kafuku 15 drill core (Fig. 6B), except for three samples exhibiting Fe_{HR}/Fe_T ratios low (average of 0.14 ± 0.09) all other samples reveal higher Fe_{HR}/Fe_T ratios, with an average of 0.56 ± 0.24 (n = 14). Only six samples are pyritized, with an average Fe_{py}/Fe_{HR} of 0.80 ± 0.06. In the Kanshi 13B drill core (Fig. 6C), Fe_{HR}/Fe_T is low (0.12; one sample) for the BIIc1 Formation. The BIIc4 and BIIc6 formations show higher Fe_{HR}/Fe_T ratios, with an average of 0.49 ± 0.25 (n = 2 and 7 respectively). However, Fe_{py}/Fe_{HR} ratios are below 0.7.

5.3.2. Major, minor and trace metals

Concentrations of redox-sensitive trace elements in the examined samples, from the three drill cores, show wide variations. In the Lubi S70 drill core, molybdenum varies from 0.11 to 42.15 ppm (average of 3.7 ± 7.4 ppm); while uranium ranges from 0.48 to 46.77 ppm (average of 3.8 ± 4.9 ppm); and manganese shows values ranging from 148.63 to 3725.55 ppm (average of 782.6 ± 508.5 ppm). In the Kafuku 15 drill core, molybdenum concentrations are 0.13 to 69.76 ppm (average of 5.3 ± 11.3 ppm); uranium displays moderate range, from 0.17 to 13.16 ppm (average of 4.8 ± 3.5 ppm); and manganese contents are 40.34 to 681.43 ppm (average of 331.4 ± 133.7 ppm). Samples from the Kanshi 13B drill core, exhibit lower contents relative to first-two above. Indeed, molybdenum concentrations range from 0.04 to 2.19 ppm (average of 0.8 ± 0.4 ppm); uranium contents are 0.52 to 4.72 ppm (average of 3.4 ± 0.9 ppm); whereas manganese does not display large variation with values ranging from 131.57 to 436.45 ppm (average of 222.7 ± 72.04 ppm).

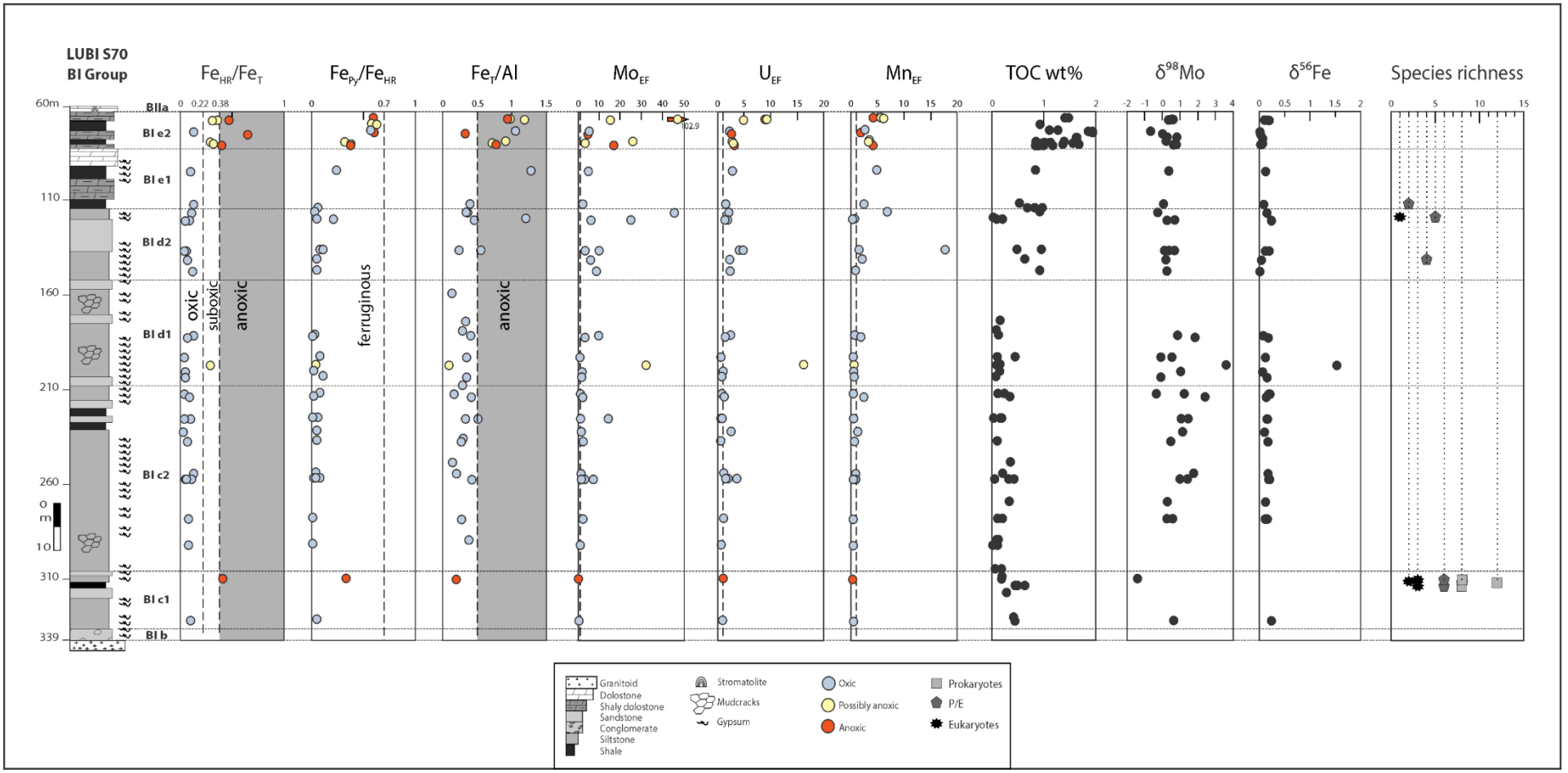

Fig. 6A. Lithostratigraphic column of Lubi S70 drill cores– BI Group. From left to right: Fe_{HR}/Fe_T and Fe_{Py}/Fe_{HR} ratios (iron speciation data); FeT/Al ratio; enrichment factor of molybdenum; enrichment factor of uranium; (F) Enrichment factor of manganese; total organic carbon (TOC); molybdenum isotopic composition; iron isotopic composition and taxonomic richness.

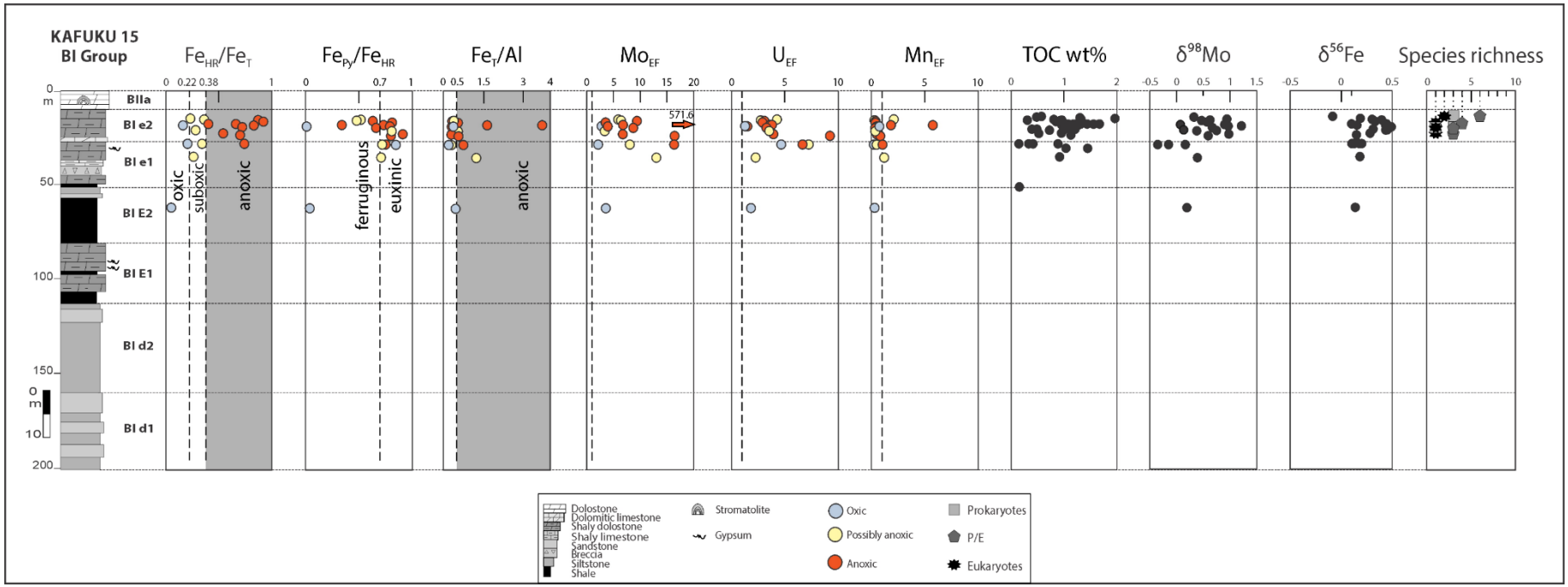

Fig. 6B. Lithostratigraphic column of Kafuku 15 drill core – BI Group. From left to right: Fe_{HR}/Fe_T and Fe_{Py}/Fe_{HR} ratios (iron speciation data); FeT/Al ratio; enrichment factor of molybdenum; enrichment factor of uranium; (F) Enrichment factor of manganese; total organic carbon (TOC); molybdenum isotopic composition; iron isotopic composition and taxonomic richness.

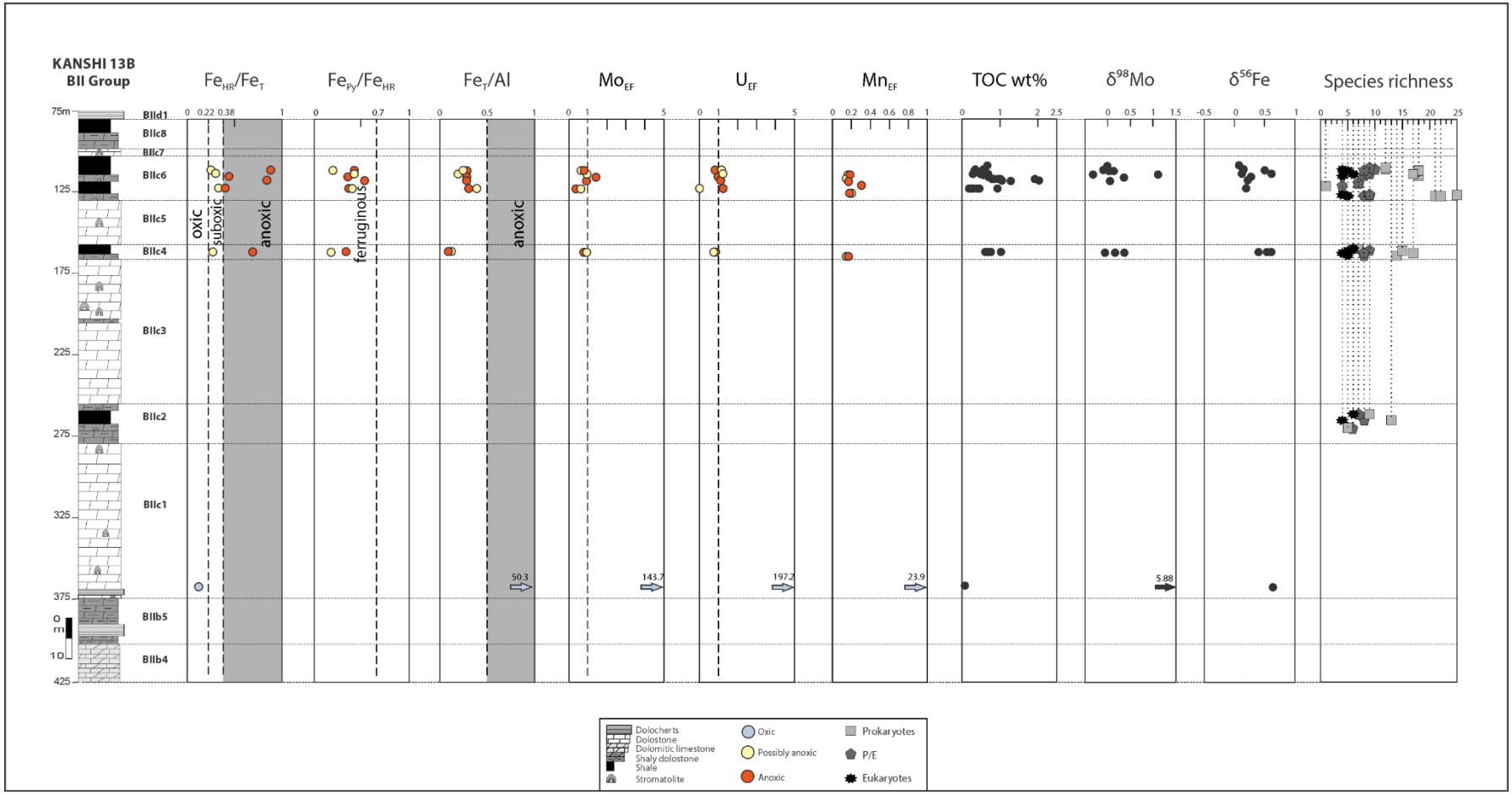

Fig. 6C. Lithostratigraphic column of Kanshi 13B drill core – BII Group. From left to right: Fe_{HR}/Fe_T and Fe_{Py}/Fe_{HR} ratios (iron speciation data); FeT/Al ratio; enrichment factor of molybdenum; enrichment factor of uranium; (F) Enrichment factor of manganese; total organic carbon (TOC); molybdenum isotopic composition; iron isotopic composition and taxonomic richness.

5.3.3. Molybdenum and iron isotopes

Molybdenum isotopes were measured in 76 samples of shale from the drill cores Lubi S70 (n = 44), Kafuku 15 (n = 20) and Kanshi 13B (n = 12). In the Lubi S70 drill core (Fig. 6A), where Fe speciation reveals dominantly oxic conditions (i.e. BIc1 to BIe1 formations), δ^{98}Mo values show a large range of -1.42‰ to +3.60‰ (average of +0.69 ± 0.91‰; n = 32). At the opposite, the δ^{98}Mo values from the top of Lubi S70 (i.e. BIe2 Formation) are -0.68‰ to +0.81‰ (average of +0.39 ± 0.42‰; n = 12). However, in the Kafuku 15 (Fig. 6B), the δ^{98}Mo values range from -0.35‰ to 1.21‰ (average of +0.49 ± 0.41‰; n = 20). Six samples, one from BIe1 and five from BIe2 formations, registering euxinic conditions, yield an average δ^{98}Mo of +0.70 ± 0.32‰. In the Kanshi 13B drill core (Fig. 6C), the δ^{98}Mo values range -0.33‰ to 1.1‰ (average of 0.15 ± 0.37‰, n = 11), except for one anomalous data +5.88‰ in the BIIc1 Formation.

The δ^{56}Fe values measured in the Lubi S70 drill core are all positive, and except for one sample with heavier composition (+1.53‰) from the BId1 Formation, all others range from +0.01‰ to +0.24‰ (average of +0.13 ± 0.07‰, n = 41). In the Kafuku 15 drill core, δ^{56}Fe values ranging from -0.08 to +0.49‰ (average of +0.25 ± 0.15‰; n = 21). In the Kanshi 13B drill core, δ^{56}Fe values are all positive and range from +0.07‰ to +0.64‰ (average of +0.34 ± 0.21‰; n = 13).

5.3.4. TOC composition

Organic carbon is low throughout the succession, with values ranging from 0.02 to 1.94 wt% (average of 0.62 ± 0.55 wt%, n = 74); 0.15 to 1.95 wt% (average of 0.44 ± 1.02 wt%, n = 30) and 0.08 to 2.03 wt% (average of 0.71 ± 0.50 wt%; n = 33) for Lubi S70, Kafuku 15 and Kanshi 13B drill cores respectively.

6. Discussion

6.1. Depositional environments

The predominance of dolostones in the upper part of the Mbuji-Mayi Supergroup, likely reflects an environment where the hydrologic regime enabled easy and sustained access to meteoric fluids and/or brines required for widespread dolomitization of $CaCO_3$ precursors (*Delpomdor et al., 2015*). Such settings are more typical of marginal marine to continental

environments than of deeper water environments (*Veizer et al., 1992*). The Mbuji-Mayi Supergroup is interpreted as a shallow-water sedimentary sequence deposited from marine to nearshore settings in a ramp-system (*Delpomdor et al., 2013b, 2015*). The outer (seaward) ramp includes the lower subtidal zone, while mid- and inner ramps correspond to upper subtidal zone and marine tidal-flat zone, respectively. Hence, the BIb, BIc and BId subgroups dominated by near-shore facies indicate a deposition in a marine tidal-flat subjected to small but frequent fluctuation, and evolving towards evaporative lacustrine ponds and sabkha (supported by the presence of gypsum and mudcracks). The BIE subgroup comprises sediments deposited in an upper subtidal zone. The BIe subgroup shows sediments deposited below the storm wave base in a lower subtidal zone on the outer ramp (*Delpomdor et al., 2017*). The BIIc Subgroup with characteristic stromatolites *Baicalia* and *Tungussia*-forms (Bertrand-Sarfati 1972) represents a shallow-subtidal environment. Absence of shallow-water structures (cross-laminations, mudcracks) and other indicators of shallow-water flows (ripples or trough-cross bedding), in the BIIc2, BIIc4 and BIIc6 formations, suggest deposition in relatively deeper water (but not beyond the photic zone) during a marine highstand (*Delpomdor et al., 2015*) with little detrital particles influx. At various time, possibly linked to slight sea-level fluctuations, reducing conditions appear with deposition of shales and interruption of stromatolitic activity.

6.2. Local redox proxies

Recently, new reviews have underlined the caution to take in interpreting palaeoredox data (*Hardisty et al., 2018; Raiswell et al., 2018*). Moreover, redox proxies and microfossil assemblages represent average estimates over a broad range of time, bottom and water column redox conditions and taphonomic biases, therefore not necessary representative of the living conditions of all preserved microorganisms. Data from iron enrichment (e.g., $Fe_T/Al > 0.5$) suggest deposition under anoxic conditions only for the BIe2 Formation in both Lubi S70 and Kafuku 15 drill cores (Figs. 6A–B; *Hardisty et al., 2018; Lyons and Severmann, 2006; Lyons et al., 2003; Raiswell and Canfield, 1998; Raiswell et al., 2018*). In contrast, Fe_{HR}/Fe_T ratios reveal anoxic conditions not only for BIe2 Formation but also for BIe1 (from Kafuku 15) as well as BIIc4 and BIIc6 formations, both from Kanshi 13B drill core.

6.2.1. Lubi S70 drill core

The BIc1 to BIe1 formations (Fig. 6A), with low Fe_{HR}/Fe_T and Fe_T/Al (an average of 0.10 and 0.38, respectively; Table S2), indicate oxic depositional conditions. This is consistent

with low total organic carbon content (TOC ≤ 1 wt. %). This low TOC as well as presence of mudcracks indicative of emersion (Fig. 6A) indicate exposition to possible atmospheric oxidizing conditions, responsible for the altered Mo signal as evidenced by the large range Mo isotope composition (–1.42 to +3.60‰) in an oxic setting. This oxic setting shows also substantial authigenic Mo enrichment (mean Mo_{EF} 6.96). Such enrichment into oxic setting is generally attributed either to sulfidic porewaters (*Hardisty et al., 2018; Owens et al., 2012*) or to Mn and Fe oxyhydroxides shutle, which can initiate Mo scavenging from seawater to sediments, with limited effect on aqueous U (*Bertine and Turekian, 1973; Algeo and Tribovillard, 2009; Doyle et al, 2018; Lyons and Severmann, 2006; Tribovillard et al., 2012*). However here, especially from BId2 to BIe1 formations, we rather observe Fe and Mn enrichment whithout evidence of sulfidic porewaters. Within BIe2 Formation, data from Fe_T/Al (mean of 0.77) and Fe_{HR}/Fe_T (mean of 0.40) but also Fe_{Py}/Fe_{HR} (mean of 0.53) identify ferruginous conditions (*Hardisty et al., 2018; Poulton and Canfield, 2005; 2011; Raiswell et al., 2018*). This marked Fe_T/Al enrichment co-occurs with Mn and Mo enrichments similar to those into BId2 and BIe1.

The δ^{56}Fe values, with the exception of one proximal sample from BId1 Fm. (1.53‰), shows that Fe isotope compositions are relatively invariant and near 0‰, regardless of the degree of Fe enrichment. This absence of Fe isotopic variability throughout the drill core, but also the lack of correlation between δ^{56}Fe and Fe/Al (Fig. 7) suggest hydrothermal source of Fe (*Owens et al., 2012; Planavsky et al., 2018; Severmann et al., 2004*). The hydrothermal inputs would have swamped Fe and Mn shuttle signal due to lack of negative shift in δ^{56} Fe (*Owens et al., 2012*).

6.2.2. Kafuku 15 drill core

BIe1 and BIe2 formations exhibits predominantly anoxic conditions with six samples displaying an euxinic fingerprint (Fig. 6B) according to Fe_{HR}/Fe_T (mean 0.69) and Fe_{py}/Fe_{HR} (mean 0.80) ratios. Fe_T/Al ratios show high values but with considerable variability from < 0.5 up to 3.70 (average 0.77). However, some samples display Fe_{HR}/Fe_T values < 0.38, Fe_{py}/Fe_{HR} ratio > 0.7 (up to 0.85) and Fe_T/Al < 0.5, which are commonly indicators of sulfidic porewaters accumulation (*Hardisty et al., 2018; Raiswell et al., 2018*). Mo concentrations from euxinic samples are below 25 ppm (Table S2), and suggest rather an intermittent euxinia where dissolved sulphide was present but only in the porewaters (*März et al., 2008; Raiswell et al., 2018*). δ^{98}Mo data from euxinic samples give a mean of 0.7‰. This is a very low value, which

probably does not represent the contemporaneous seawater value, confirming euxinia was not stable. Iron isotope composition values also show a variability (–0 08 to 0.49‰). The variability in both δ^{56} Fe and Fe_T/Al is consistent with an extensive early diagenetic remobilization within the sediments (*Owens et al., 2012*).

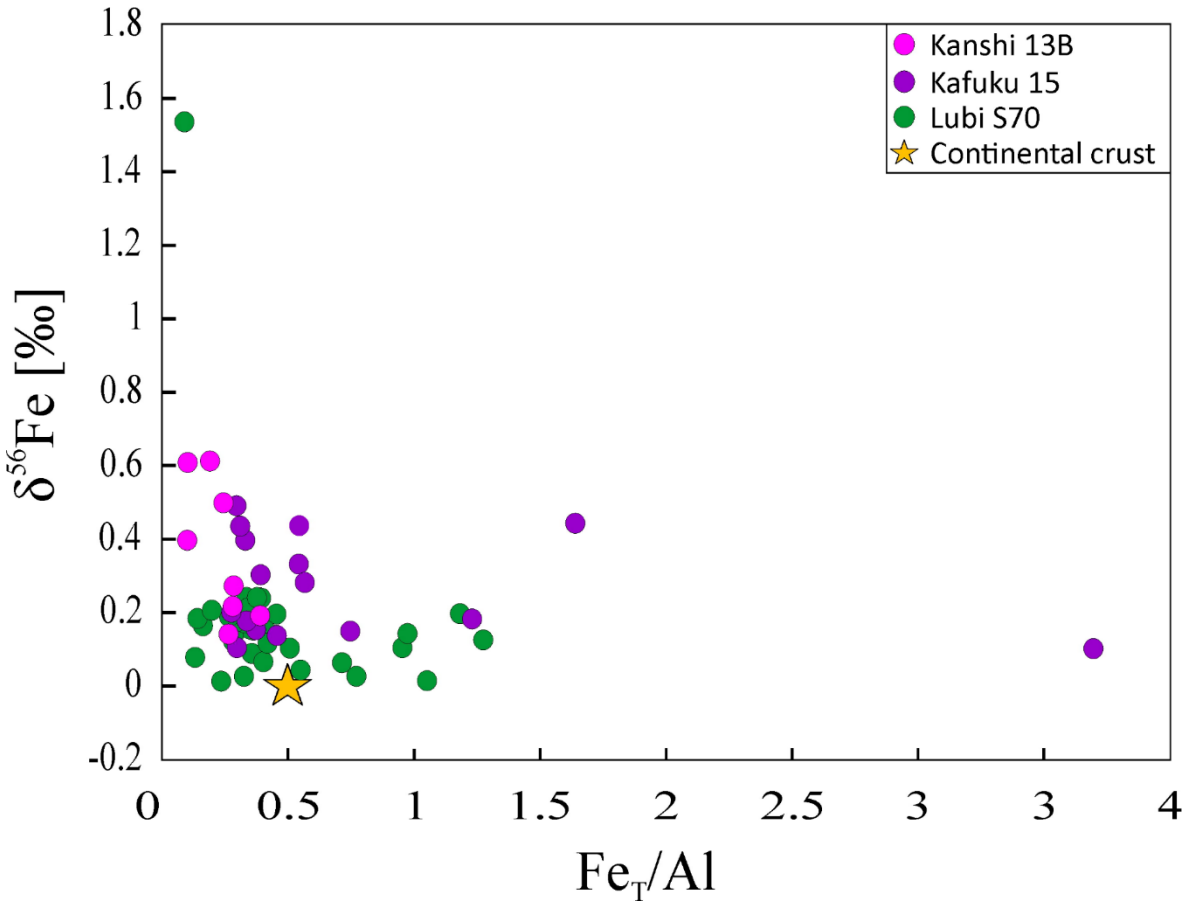

Fig. 7. δ^{56}Fe vs. Fe/Al ratios, star represents the continental crust value of Fe/Al = 0.5 and δ^{56}Fe = 0.09% (*Beard et al., 2003a; 2003b*).

6.2.3. Kanshi 13B drill core

Samples from BIIc4 and BIIc6 formations (Fig. 6C), with $Fe_{HR}/Fe_T > 0.22$ and $Fe_{py}/Fe_{HR} < 0.7$, shows predominantly ferruginous conditions. In contrast, Fe_T/Al ratios with the exception of an outlier point in BIIc1 Formation, are below 0.5 (the continental crustal average) that suggests no iron enrichment in these levels and consequently depositional conditions that may have been dominantly oxic (*Owens et al., 2012; Raiswell et al., 2018*). The lack of Mo enrichment (excepted one sample with 2.19 ppm) associated to minor U enrichments also imply largely oxic conditions (*Algeo and Tribovillard, 2009; Tribovillard et al., 2012*). However, the limited number of samples does prevent any meaningful interpretation of these data.

6.3. Paleoecology and Taphonomy

Mbuji-Mayi organic-walled microfossils exclusively occur in fine-grained siliciclastic (shale) facies. They occur in different assemblages relative to the depositional environments encountered (Figs. 8 and 9). The near-shore assemblage recorded in both intertidal and photic shallow-subtidal zones is preserved in sediments deposited under oxic (BIc1 Formation) and anoxic ferruginous (BIIc2, BIIc4, BIIc6 formations) conditions. It is characterized by both greatest taxonomic richness and abundance with an important presence of filamentous microbial mats (*Siphonophycus* spp. up to 20%; Table S1) indicating extensive benthic microbial mats living in the photic oxic zone, and thus probably cyanobacteria. The supratidal zone rich in mudcracks and gypsum, does not preserve microfossils, nor the dolostones, probably linked to diagenesis and exposure to oxidizing atmospheric conditions. However, stromatolites indicate photosynthetic activity in the shallow subtidal zone. The second assemblage is preserved in sediments below dysoxic-anoxic ferruginous and sulfidic conditions of the lower subtidal zone (BIe1 and BIe2 formations). Here, both abundance and taxonomic richness decrease, and benthic mats are absent. The third assemblage, preserved in upper subtidal (BId2 Formation), contains dominantly leiospheres, and species identified as probable bacteria are absent.

6.3.1. Lubi S70 drill core

The bottom section, from BIc1 to BId2, is consistent with near-shore or marginal marine setting, probably from supratidal to upper subtidal zone. However, the prevalence of oxic conditions in this bottom section (Fig. 6A), did not prevent an exquisitely preservation of organic material in the BIc1 Formation. The organic-walled microfossils abundance and moderate diversity (S=23) as well as abundant AOM are characteristic of palynofacies 1, Pf1 (Figs. 5A–5B). *Delpomdor et al.* (*2015*) reported a rapid sedimentation during deposition of this level. This would have led to a rapid burial of organic matter and prevented its degradation; hence the excellent preservation state of organic-walled microfossils in such oxic nearshore setting. The BIc2 and BId1 formations, with evidence of emersion, suggest supratidal deposition (Fig. 8). The absence of organic-walled microfossils probably reflects diagenesis and a near-complete oxidation of organic matter, consistent with the exclusive presence of palynofacies 4 and 6, Pf4 and Pf6 (Figs. 5G and 5I). On the other hand, oxic BId2 and BIe1 formations, deposited into upper subtidal and lower subtidal zones, respectively (*Delpomdor et al., 2015*), record a drastic decrease of species of microfossils (S = 6 and 2, respectively) and a

total absence of forms identified as probable bacteria (Fig. 4A and Table S1), but do preserve acritarch such as the eukaryotic *Lophosphaeridium granulatum* (1%) and smooth-walled sphaeromophs (leiospheres, 99%), probably indicating their ecological preference rather than a preservational bias (palynofaies 4). However, it is possible that the low number of samples recovered from BId2 and BIe1 could bias the real diversity of these oxic formations. Anoxic and ferruginous deposition of BIe2 Formation seems suitable to a better preservation of organic matter as indicated by palynofacies 5, Pf 5 (Fig. 5H). Nevertheless, no microfossil has been recovered from BIe2 in this study. This lack of microfossils is probably related to a sampling bias, because *Baudet* (*1987*) reported four species at 83 m depth in Lubi S70 (depth corresponding to BIe2 Formation). Unfortunately, only two species (*Leiosphaeridia crassa* and *L. ternata*) were formerly identified and illustrated.

6.3.2. Kafuku 15 drill core

Unlike in the Lubi S70 drill core, the anoxic BIe2 Formation from Kafuku 15 drill core (located approximately 190 km to SE from Lubi S70), preserves organic-walled microfossils (Fig. 4B and Table S1). The underlying formations do not record microfossils, an absence possibly caused by sampling bias. The dark appearance of microfossils and AOM from BIe2, as evidenced the palynofacies 3, Pf3 (Fig. 5E), is consistent with thermal diagenetic overprinting such as reported by *Delpomdor et al.* (*2017*). Despite this particular taphonomic effect, not observed in correlative levels from Lubi S70, the recovered assemblage although with modest diversity and low abundance, includes all three groups of microfossils (see section 5.1 above). However, benthic mats are absent, probably due to paleoenvironmental conditions, i.e. further from shore and in moderate depth but still in the photic zone. The three eukaryotic species recovered (*G. bispinosa*, *L. granulatum* and *P. insolita*) suggest that they may have been adapted to or preserved in anoxic and H_2S-rich conditions. Nevertheless, their low number may also reflect preservation bias, or low nutrient availability, as euxinia affects primary productivity, and thus may impact autotrophs and heterotrophs feeding on them, by limiting availability of biologically important trace metals such as Fe and Mo in seawater column *(Anbar and Knoll, 2002; Canfield, 1998; Canfield et al., 2006*).

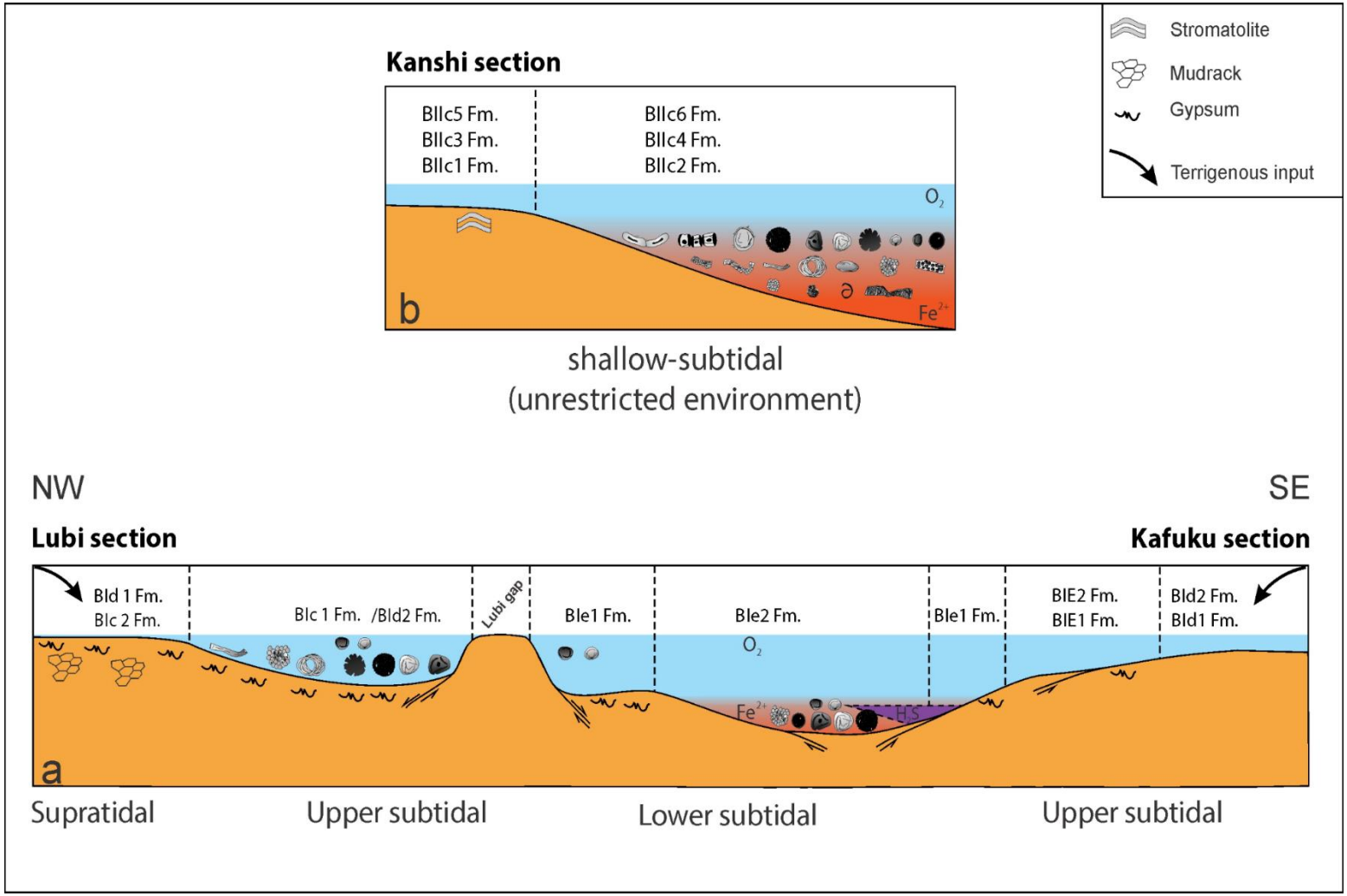

Fig. 8. Temporal and spatial paleoecological model for the Mbuji-Mayi Supergroup. Dominant species and notable features in their depositional environments. Only species with relative abundance ≥ 3% are represented. (a) BI Group between ca 1065 and 1043 Ma and (b) BII Group between 1043 and 1000 Ma. For the signification of the schematic drawing of the microfossils see Supplementary Table 1 and Supplementary Fig. S1.

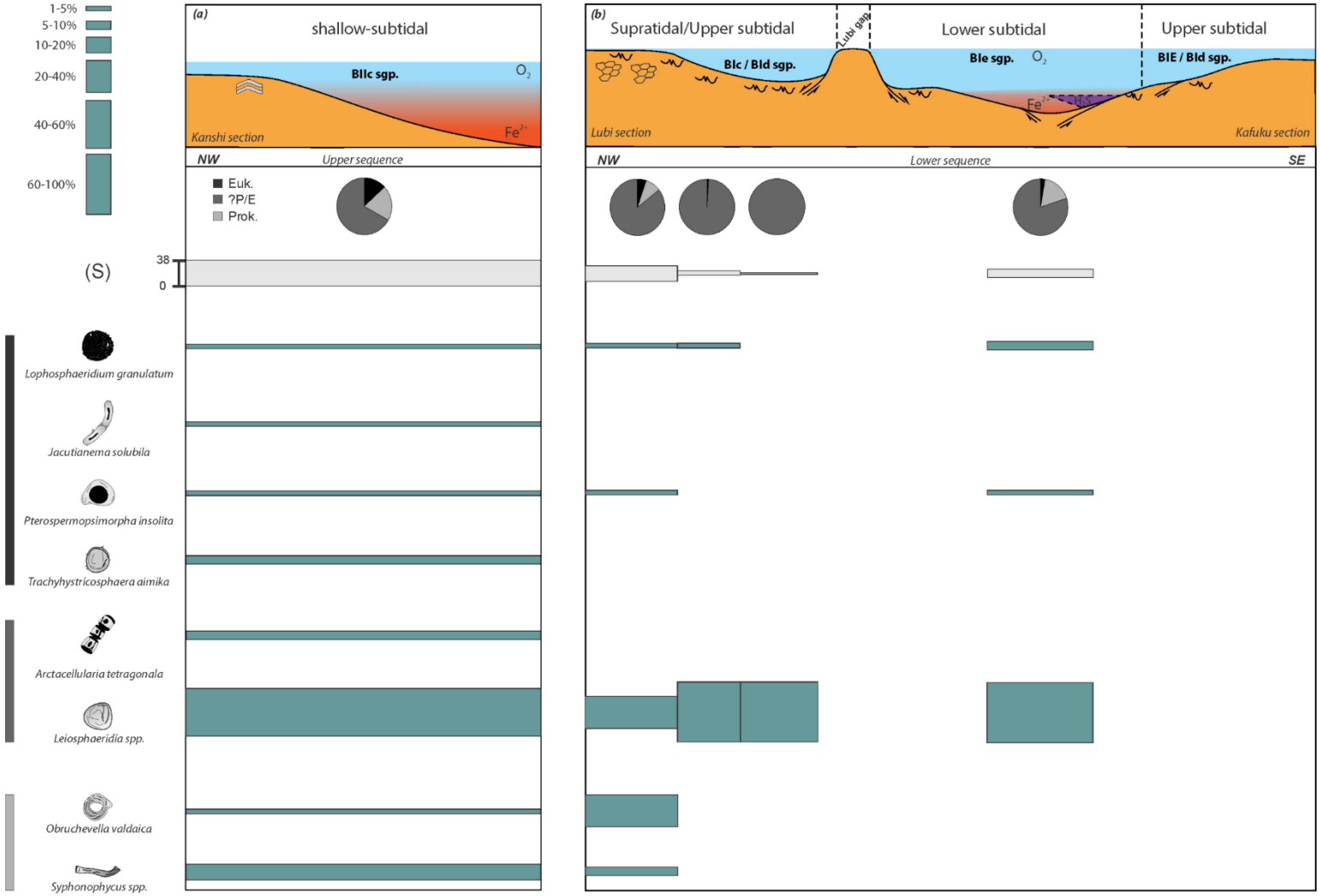

Fig. 9. Paleoecological distribution of the Mbuji-Mayi Supergroup. (a) BII Group and (b) BI Group. Representative species of eukaryotes (E, black line), possible eukaryotes or prokaryotes (P/E, gray-dark line) and probable bacteria (P, gray-light line). (S) = species richness. Green line width is proportional to the species relative abundance (%) calculated for a defined paleoenvironment (dashed black line). *Leiosphaeridia* spp. and *Siphonophycus* spp. means all species of the genus *Leiosphaeridia* and *Syphonophycus*. (For other legends see Figure 8).

6.3.3. Kanshi 13B drill core

The high diversity and abundance of organic-walled microfossils in BIIc2, BIIc4 and BIIc6 formations (Fig. 4C and Table S1) would have led to development of dysoxic and anoxic conditions, as oxidation of abundant organic matter depletes concentrations of dissolved oxygen in seawater (*Diaz and Rosenberg, 2008; Nagy et al., 2009*). These anoxic habitats host a higher diversity of eukaryotes, with seven taxa exclusively recovered from Kanshi 13 B (i.e. upper BII Group). Some of them are known since the Paleoproterozoic era (*Tappania* sp.?, *Valeria elongata* and *V. lophostriata; Javaux and Knoll, 2017; Nagovitsin, 2009; Nagovitsin et al., 2010*) while others are constrained from late Mesoproterozoic to early Neoproterozoic (*Jacutianema solubila, Trachyshytrichosphaera aimika, T. botula; Baludikay et al., 2016; Beghin et al., 2017; Butterfield et al., 1994; Tang et al., 2013; 2015; 2017*). The Mbuji-Mayi Supergroup depositional age being constrained to the late Mesoproterozoic at ca. 1065–1000 Ma (*François et al., 2017 and François et al., in prep*), their absence in the BI Group (i.e. Lubi S70 and Kafuku 15 drill cores) would be caused either by different depositional environment and/or by preservation bias. The eukaryotic acanthomorph acritarch *Trachyshytrichosphaera aimika,* an important index taxon for the late Mesoproterozoic-early Neoproterozoic, occurs as abundant and well-preserved monospecific assemblage especially in fluvio-deltaic sediments of the contemporaneous El Mreiti Group, Mauritania (*Beghin et al, 2017*).

6.3.4. Eukaryotic palaeoecology

Eleven eukaryotic taxa – *Germinosphaera bispinosa, Jacutianema solubila, Lophosphaeridium granulatum, Pterospermopsimorpha insolita, P. pileiformis, cf. Tappania plana, Trachyhytrichosphaera aimika, T. botula, Valeria elongata, V. lophostriata* and an unnamed acanthomorph – are preserved in the Mbuji-Mayi Supergroup (Baludikay et al., 2016; Fig. S1 and Table S1). This diversity is similar to other Mesoproterozoic successions where eukaryotic diversity does not exceed 15 taxa (Agić et al., 2017; Baludikay et al., 2016; Beghin et al., 2017; Cohen and Macdonald, 2015; Javaux and Knoll, 2016; Tang et al., 2017; Vorob'eva et al., 2015), except in the lower Shaler Supergroup where an exceptional diversity of 25 eukaryotes is recorded (Loron et al., 2018). The Mbuji-Mayi organic-walled microfossil assemblages show a dominance of prokaryotes and undetermined microfossils over eukaryotes whatever the depositional environment; but eukaryotic taxa reveal an ecological preference to marginal marine environments (i.e. intertidal and shallow subtidal zones) with a high diversity and abundance possibly linked to nutrient availability (Fig. 9). Except *Lophosphaeridium*

granulatum, *Pterospermopsimorpha insolita* and *P. pileiformis* that are preserved in both oxic (with maximum relative abundance of 2.9%, 1.3% and 1%, respectively) and anoxic (maximum relative abundance of 3.7%, 2% and 1.7%, respectively) sediments, all others are only preserved in anoxic conditions. The exclusive presence of *Jacutianema solubila* (4.8%), cf. *Tappania plana* (0.3%), *Trachyhytrichosphaera aimika* (6.7%), *T. botula* (1.5%), *Valeria elongata* (0.1%), *V. lophostriata* (0.3%) and an unnamed acanthomorph (0.3%), in anoxic and ferruginous shallow-subtidal zone (i.e. in the BIIc2, BIIc4 and BIIc6 formations) perhaps reflects preservation conditions and/or favored habitats. However, it is not possible at this time to evidence their ecological requirements both in terms of oxygen and/or nutrient availability, since their benthic or planktonic habitat and metabolism are still unknown. Indeed, planktonic organisms might live in the upper oxic zone of the water column and then sediment and get preserved in anoxic bottom sediments. Anaerobic or aerobic metabolisms can be proposed only if microfossil taxa occur exclusively in anoxic or oxic environments. For example, *Blastanophaera kokkoda*, a budding protist of the Mesoproterozoic Roper Group, Australia (Javaux and Knoll, 2016), occurs only in anoxic deep basinal facies and not in redox stratified shallower facies. If it was living in the upper oxic waters, it would be preserved in other facies as well. The Mbuji-Mayi sedimentary sequence in DRC, as the contemporaneous El Mreiti Group in Mauritania (*Beghin et al., 2017*), are mostly shallow-water and do not preserve deep facies to investigate their possible microfossil assemblages.

Nevertheless, a paleoenvironmental distribution of decreasing diversity and abundance, from near-shore environment seaward, is observed in the Mbuji-Mayi Supergroup. A similar trend is largely reported in other paleoecological studies of Proterozoic organic-walled microfossils (*Beghin et al., 2017; Butterfield and Chandler, 1992; Butterfield et al., 1994; Hofmann and Jackson, 1994; Javaux and Knoll, 2016; Javaux et al., 2001; Porter and Riedman, 2016; Tang et al., 2017; Timofeev et al., 1976 and others*). However, several parameters, namely sampling, preservation, water depth, productivity, redox conditions, nutrient availability and proximity to river influx may affect both diversity and relative abundance. Moreover, geochemical analyzes were not performed on all these successions to investigate possible causes of microfossil distribution.

More studies combining micropaleontology and geochemistry at high-resolution along environmental gradients, and micro-analyzes of single microfossils, are needed to decipher the palaeoecology, paleobiology, and causes of diversification of early eukaryotes.

7. Conclusions

The organic-walled microfossils occurrence and distribution from the late Mesoproterozoic shallow-water Mbuji-Mayi sedimentary sequence can be categorized into three environmental zones:

(1) An unrestricted inner ramp, intertidal to shallow-subtidal environment with maximum diversity and high relative abundance (BIc1, BIIc2, BIIc4 and BIIc6 formations);

(2) A restricted mid-ramp, in the upper subtidal zone, with low diversity (BId2 Formation);

(3) An outer ramp with moderate depth in the lower subtidal zone, displaying low to moderate diversity (BIe1 and BIe2 formations).

Palaeoredox proxies indicate redox stratified conditions during the Mbuji-Mayi Supergroup shallow-water deposition, with oxic conditions prevailing in supratidal, intertidal, subtidal environments in contact with the atmosphere, above anoxic ferruginous conditions of subtidal environments. Euxinic habitats were spatially and temporally limited in this shallow basin. With the exception of BIe2 from Kafuku 15, where sulfidic porewaters are reported, anoxic ferruginous sediments appear to record both maximum diversity, high relative abundance and best preservation of organic-walled microfossils, including eukaryotes, in shallow-water.

Acknowledgements

Research support came from European Research Council Stg ELITE FP7/308074, the BELSPO IAP PLANET TOPERS, the FRS-FNSR-FWO EOS ET-HOME, and the Francqui Foundation. We thank the Royal Museum for Central Africa (RMAC, Tervuren/Belgium) for access to drill cores for sampling, and M.Giraldo, J-Y. Storme as well as J. Beghin (Uliège) for sample preparation.

Chapitre 6 : Géothermométrie

6.1. Introduction

Cette étude a permis d'évaluer l'évolution thermique du bassin sédimentaire du Congo au cours du dépôt du Supergroupe de Mbuji-Mayi, mais aussi la maturité thermique de la matière organique et en particulier des microfossiles ainsi que la potentielle preservation de biomarqueurs caractéristiques de certaines espèces du vivant (algues, cyanobactéries).

Pour atteindre cet objectif, un total de 16 échantillons provenant des sondages de Kanshi 13B (n = 5), Kafuku 15 (n = 3) et Lubi S70 (n = 8) ont été analysés à la microspectroscopie Raman. En effet, l'utilisation de la microspectroscopie Raman comme indicateur indirect de la maturité thermique des roches revêt quelques avantages : elle permet une analyse rapide, ne requiert pas la présence de macéraux organiques spécifiques, nécessite très peu d'échantillon et est potentiellement non destructive (*Baludikay et al., 2018; Jubb et al,. 2018; Sauerer et al. 2017; Schito et al. 2017; Schmidt et al.,2017*). Les spectres Raman ont été obtenus sur des microfossiles et de la matière organique amorphe (MOA), pour amoprhous organic matter), à la fois dans du Kérogène isolé et *in situ* dans des lames minces. L'extraction des paramètres spectraux (Fig.6.1) a permis l'estimation des températures grâce : (1) au géothermomètre du métamorphisme de bas-degré (*Kouketsu et al. 2014*) et (2) au géothermomètre associé à la réflectance de la vitrinite (*Barker and Pawlewicz 1994*), dans laquelle la réflectance de la vitrinite a été remplacée par la réflectance Raman qui lui est équivalent (*Liu et al. 2013*).

Il convient de signaler que cette méthode consistant à appliquer la géothermométrie Raman directement sur des microfossiles du Protérozoïque en vue d'évaluer quantitativement la maturité thermique des roches hôtes, ne benéficiait d'aucune référence appropriée dans la littérature. Pour vérifier et contraindre les resultats obtenus avec la géothermomètrie Raman, des mesures de la réflectance du bitume solide, de l'indice d'altération thermique (TAI, pour thermale alteration index) et de l'indice de Kübler (KI, pour Kübler-index) ont également été effectuées dans un premier temps sur un nombre reduit d'échantillons (n = 2). Les mêmes analyses ont également été effectuées sur deux autres séquences du Protérozoïque notamment, le Groupe Atar/El Mreïti (bassin de Taoudeni, Mauritanie, n = 3) et la formation de Kanpa (Officer bassin, Australie, n = 3). Les résultats de ces analyses ayant validé cette méthode ont fait l'objet d'une publication dans *Journal of Coal Geology (2018)* : « **Raman**

microspectroscopy, bitumen réflectance and illite crystallinity scale : comparison of different geothermometry methods on fossiliferous Proterozoic sedimentary basins (DR Congo, Mauritania and Australia) ». Cet article est repris dans la sous-section §6.2 du présent chapitre. La sous-section §6.3 discutent des implications de toutes les données (n = 17) du Supergroupe de Mbuji-Mayi sur l'évolution thermique du Bassin du Congo.

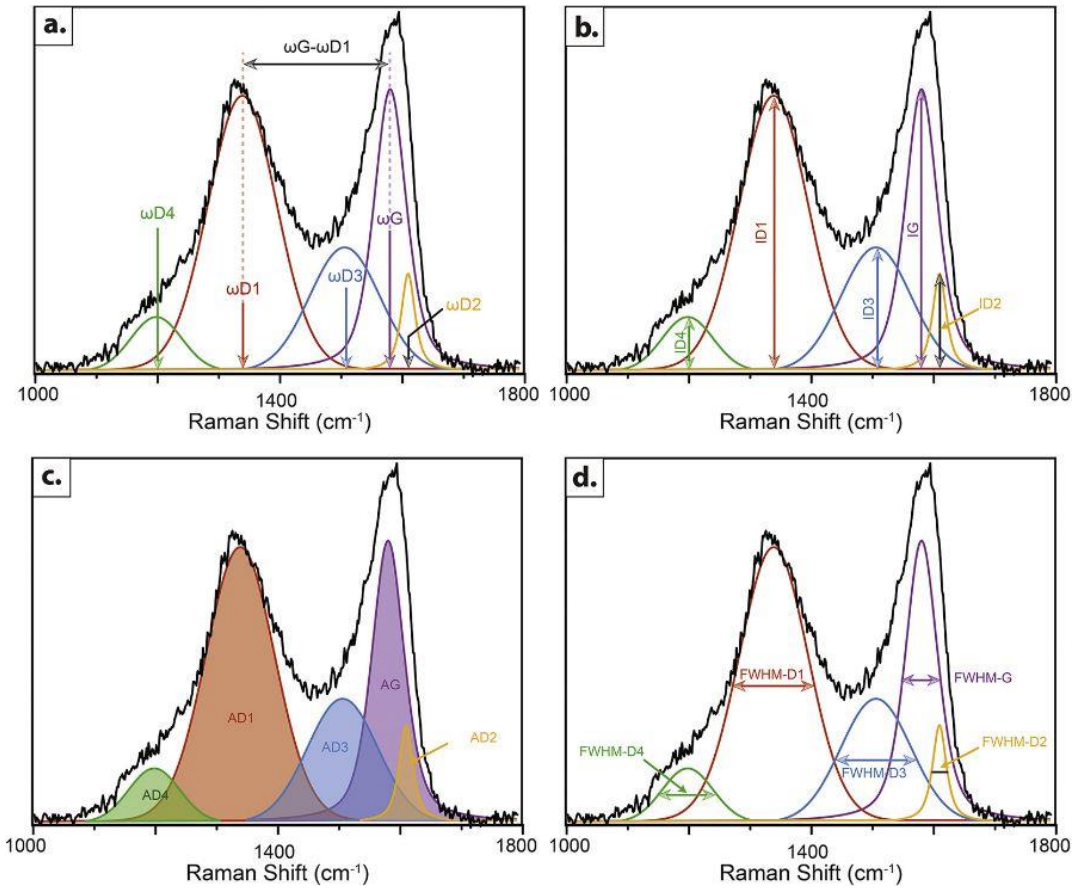

Fig. 6.1. Illustration des paramètres spectraux Raman à partir d'un spectre déconvolué. a, b, c et d représentent respectivement : la position du pic, l'intensité, la surface et la largeur à mi-hauteur des bandes D1 – D4 et G. D'après *Baludikay et al., 2018*.

6.2. Résumé de l'article

Les roches sédimentaires contenant des microfossiles sont des archives cruciales pour reconstituer l'évolution de la vie au début de la vie sur Terre. Cependant, la préservation des microfossiles dans les roches dépend de plusieurs facteurs physico-chimiques. Parmi ces facteurs, l'évolution thermique des roches hôtes peut être déterminante. Nous avons étudié ici des échantillons de shales carbonés contenant des assemblages de microfossiles à parois organiques conservés de manière exceptionnelle provenant de trois séquences sédimentaires

marines peu profondes du Protérozoïque: le Supergroupe de Mbuji-Mayi (République démocratique du Congo, bassin du Congo), le Groupe Atar/El Mreïti (Mauritanie, bassin de Taoudeni) et la formation de Kanpa (Australie, basin Officer). La maturité thermique de ces échantillons de roche est évaluée par la géothermométrie Raman, la réflectance Raman, la réflectance du bitume solide, la cristallinité de l'illite et l'indice d'altération thermique. La comparaison des résultats issus de ces différentes techniques permet de valider l'utilisation de la réflectance Raman sur les matériaux carbonés du Protérozoïque et en particulier pour les matériaux carbonés mal ordonnés. Nous montrons que le kérogène extrait (microfossiles et matière organique amorphe) est plus précis pour estimer la maturité thermique de séquences Protérozoïques à basse température que le kérogène en lame mince. Toutes les techniques fournissent une gamme de températures cohérente, à l'exception de la géothermométrie Raman, donnant des estimations légèrement plus élevées. La réflectance Raman apparaît comme un outil rapide, robuste et non destructif pour évaluer la maturité thermique de matériaux carbonés mal organisés provenant de roches du Protérozoïque

International Journal of Coal Geology 191 (2018) 80–94

Contents lists available ScienceDirect

International Journal of Coal Geology

journal homepage: www.elsevier.com/locate/coal

Raman microspectroscopy, bitumen reflectance and illite crystallinity scale: comparison of different geothermometry methods on fossiliferous Proterozoic sedimentary basins (DR Congo, Mauritania and Australia)

Blaise K. Baludikay[a,*], Camille François[a,*], Marie Catherine Sforna[a], Jérémie Beghin[a], Yohan Cornet[a], Jean-Yves Storme[a], Nathalie Fagel[b], François Fontaine[b], Ralph Littke[c], Daniel Baudet[d], Damien Delvaux[d], Emmanuelle J. Javaux[a]

[a] PPP Lab, GEOLOGY UR & Department, University of Liege, Belgium

[b] AGEs Lab, GEOLOGY UR & Department, University of Liege, Belgium [c] EMR Group, RWTH Aachen University, Germany

[d] Geodynamics & Mineral Resources Service, Royal Museum for Central Africa, Belgium

ARTICLEINFO

Keywords:
Raman microspectroscopy
Proterozoic organic-walled microfossils
Thermal history
Raman and bitumen reflectances
Illite crystallinity

ABSTRACT

Sedimentary rocks containing microfossils are crucial archives to reconstitute early life evolution on Earth. However, the preservation of microfossils within rocks depends on several physico-chemical factors. Among these factors, the thermal evolution of the host rocks can be decisive. Here, we investigated carbonaceous shale samples containing exquisitely preserved organic-walled microfossils assemblages from three Proterozoic shallow marine sedimentary sequences: the Mbuji-Mayi Supergroup (Democratic Republic of Congo, Congo Basin), the Atar/El Mreïti Group (Mauritania, Taoudeni Basin) and the Kanpa Formation (Australia, Officer Basin). Thermal maturity of these rock samples is evaluated with Raman geothermometry, Raman reflectance, solid bitumen reflectance, illite crystallinity and Thermal Alteration Index. The comparison of results coming from these different techniques validates the use of Raman reflectance on Proterozoic carbonaceous material and especially for poorly-ordered carbonaceous material. We show that extracted kerogen (microfossils and amorphous organic material) is more accurate to estimate the thermal maturity of low-grade temperature Proterozoic sequences than kerogen in thin section. All techniques provide consistent range of temperatures except for Raman geothermometry, giving slightly higher estimates. Raman reflectance appears to be a fast, robust and non-destructive tool to evaluate the thermal maturity of poorly-organized carbonaceous material from Proterozoic rocks.

1. Introduction

Using the microfossil record to reconstruct early life evolution requires the characterization of the physico-chemical conditions of preservation, and the determination of the thermal history of the sedimentary basin in which they were preserved. Initial and postdepositional taphonomic processes during and after fossilization such as burial, biogeochemical degradation, diagenesis, hydrothermal fluid circulation, metamorphism and late contamination may alter or erase the microfossil original properties, challenging the interpretation of the morphology, ultrastructure and geochemistry of the fossil remains, and thus of their biological affinity (Schiffbauer et al., 2012).

In post-Silurian rocks, the thermal maturity of carbonaceous material (CM) and by extension the thermal history of the basins, is usually estimated through the use of the vitrinite reflectance parameter (vR_0%; Littke et al., 2012; Taylor et al., 1998). In pre-Devonian or in marine Paleozoic sedimentary rocks where vitrinite is absent or rare, reflectance data of graptolites (GR_r %), chitinozoans (CR_r %) and scolecodonts (SR_r %) are more often used as a substitute to vitrinite (Bertrand, 1990; Bertrand and Héroux, 1987); However, the application of vitrinite and zooclast (those cited above) reflectance is restricted for Proterozoic sedimentary rocks. This limitation is due to the lack of higher land plants (vitrinite woody precursors) and of these zooclasts among CM encountered in rocks older than the Cambrian (Bertrand and Héroux, 1987; Du et al., 2014; Taylor et al., 1998). As a consequence, solid bitumen reflectance (bR_0%; Albert-Villanueva et al., 2016; Jacob,

* Corresponding authors at: Laboratoire de Paléobiogéologie-Paléobotanique-Paléopalynologie (PPP Lab) Quartier AGORA, Bâtiment B18, Allée du 6 Aout, 14, 4000 Liège (SartTilman), Belgium.
E-mail addresses: bkbaludikay@uliege.be (B.K. Baludikay), francois@uliege.be (C. François).

https://doi.org/10.1016/j.coal.2018.03.007
Received 7 December 2017; Received in revised form 19 March 2018; Accepted 22 March 2018
Available online 27 March 2018

1989; Landis and Castaño, 1995; Riediger, 1993; Schoenherr et al., 2007), the reflectance of non-fluorescent lamalginite (Ghori in Stevens and Apak, 1999) as well as the hydrocarbon-based methylphenanthrene index (Radke and Welte, 1983) can be used to estimate an equivalent to vR_0%. Rock-Eval pyrolysis (Espitalié et al., 1977) also allows estimating CM maturity by giving the temperature at which the maximum amount of hydrocarbons is generated from kerogen decomposition (T_{max}). However, Rock-Eval analysis T_{max} depends both on the maturity of a CM and its composition; thus it does not give the maximum temperature reached within a sedimentary basin. Furthermore, it is not useful for rocks which have reached temperatures exceeding 160–200 °C (Peters, 1986; Peters and Cassa, 1994). In fossiliferous rocks, the Thermal Alteration Index (TAI) scale and fluorescence color have been intensively applied (Staplin, 1969). However, the TAI scale is based on palynomorphs wall color that can be affected by the extraction method as well as by the wall thickness, the wall ultrastructure and the wall chemical (Peters and Cassa, 1994; Staplin, 1977). Further details regarding all maturity parameters of CM known in literature as well as different correlations between them have been compiled and discussed in Hartkopf-Fröder et al. (2015). Interested readers could refer to this recent review. In addition to these techniques based on the characterization of CM, the study of the chemical and structural changes in the series smectite/illite-smectite/illite/dioctahedral white mica has been widely used to assess the extent of burial diagenesis and the metamorphic grade of sedimentary successions (Kübler, 1964; Weaver, 1960). Clay minerals are routinely used to determine transition from diagenesis to metamorphism (e.g. Dunoyer de Segonzac, 1969), but the syngenicity of CM preserved in these rocks still need to be evidenced by Raman spectroscopy.

Raman spectroscopy is a fast and non-destructive technique, commonly applied on Precambrian rocks to discriminate CM associated to putative microfossils from void filling, fluid inclusions, migrating CM around minerals, and opaque minerals, but also to determine the thermal maturity of this CM and to evidence its syngenicity (Javaux et al., 2010; Liu et al., 2013; Marshall et al., 2005; Pasteris and Wopenka, 2003). Several geothermometers, from different geological settings of varying thermal and burial histories, based on CM Raman spectral parameters, have been developed to assess peak metamorphic temperatures experienced by host rocks in meteorites or metapelites (Beyssac et al., 2002; Kouketsu et al., 2014; Lahfid et al., 2010; Rahl et al., 2005).

Regional geology and mineral petrology permit to assess qualitatively the degree and type of metamorphism and thermal history of a basin. However, quantitative estimation of thermal maturity of the rocks and CM content is more challenging. Raman geothermometry has never been applied to unambiguous Proterozoic microfossils in order to reconstruct quantitatively the thermal evolution of their host rock, once their syngenicity is evidenced. Raman geothermometry has been calibrated for CM from coal series within metapelites (Beyssac et al., 2003, 2002; Kouketsu et al., 2014; Lahfid et al., 2010) and its use on Proterozoic microfossils need to be validated by independent techniques. Here, after an overlook on several methods, we present the temperature estimates obtained through Raman geothermometry based on spectral parameters (Kouketsu et al., 2014) and on Raman reflectance (Liu et al., 2013) for three Proterozoic sedimentary sequences: the Mbuji-Mayi Supergroup (Congo Basin, Democratic Republic of Congo (DRC)), the Atar/El Mreïti Group (Taoudeni Basin, Mauritania) and the Kanpa Formation (Officer Basin, Australia). We compared measurements obtained on microfossils and amorphous organic matter (AOM), extracted and in situ in thin sections, for these three different sequences. These temperatures were cross-validated with temperature estimates through TAI, solid bitumen reflectance, and 'illite crystallinity Kübler index'.

Geological context and samples

Congo Basin

Localized in Central Africa and covering four countries (Angola, DRC, Central African Republic, and Republic of the Congo), the Congo Basin (Fig. 1a) is an intracratonic basin extending about 1,200,000 km^2. It contains up to 9000 m of sedimentary rocks ranging from late Mesoproterozoic to Neogene and had a complex geological and tectonic evolution (Kadima et al., 2011a, 2011b; Delvaux and Fernandez, 2015). The sedimentary Mbuji-Mayi Supergroup (in the south part of Congo Basin, DRC) was deposited in shallow marine to evaporitic marine and lacustrine environments (Delpomdor et al., 2015). It is considered as equivalent to the basal series of the Congo Basin, buried in the deepest part of the basin and outcropping in the Mbuji-Mayi area due to denudation and rock uplift at the margin of the basin (Delvaux and Fernandez, 2015). This succession is weakly or not at all affected by regional metamorphism (Raucq, 1970) and rests unconformably on the Archean-Paleoproterozoic Congo-Kasai Craton in its southern and western parts, and on the Mesoproterozoic Kibaran Belt in its eastern part (Raucq, 1970). Two distinct lithostratigraphic successions were identified, from the oldest to the youngest: BI Group and BII Group. The BI Group (~500 m thick) is a siliciclastic sequence composed of quartzite, shale, siltstone and some carbonate horizons in its upper part. The BII Group (~1000 m thick) is a carbonate sequence intercalated with thin organic-rich shales and cherts horizons (Delpomdor et al., 2015; Raucq, 1970). Radiometric data constrain the Mbuji-Mayi Supergroup between 1065 and 1030 Ma for the diagenesis of the BI Group to 948 Ma for basaltic lavas which overlie the BII Group, i.e. in the late Mesoproterozoic to early Neoproterozoic (Cahen et al., 1984; François et al., 2017). Several drill cores were performed on the Mbuji-Mayi sedimentary sequence in the 1950's (preserved in the Royal Museum for Central Africa) but only two of them, Kanshi SB13 (425 m-long, Fig. 1a) and Lubi S70 (former Tshinyama S70, 339 m-long, Fig. 1a) cross horizons containing a large diversity of organic-walled microfossils. These drill cores preserve assemblages of organic-walled prokaryotic and eukaryotic microfossils, evidencing the evolution of complex life (early eukaryotes) for the first time in the Meso-Neoproterozoic record of Central Africa (Baludikay et al., 2016). The color of the microfossils and amorphous organic matter in the investigated samples varies from grey brown to dark brown in each sample. We selected one sample per drill core to investigate the thermal maturity of CM. Sample from Kanshi S13B (KN23–123, depth: 123 m) and Lubi S70 (LU18–312, depth: 312 m) drill cores come from the BIIc6 and BIc1 formations, respectively. In sample KN23–123, nine microfossil species and one OAM particle from extracted kerogen were analyzed, as well as two microfossil species and four AOM particles from thin section. In sample LU18–312, two microfossil species and one AOM particle from extracted kerogen were analyzed and in thin section, five microfossil species and one AOM particle (Table 1). The thermal maturity of the Congo Basin is not well-known, especially for the Proterozoic series. Unpublished vitrinite and bitumen reflectance are reported by Lucazeau et al. (2015) for the Mbandaka-1 well in the center of the basin, with a reflectance of 2.56% and modeled temperatures of 160–180° for the deeper part of the well (Neoproterozoic sediments). Vitrinite reflectance have been measured for the Cretaceous – Permian section of the basin (Sachse et al., 2012), with modeled temperatures of 100–120 °C. Recently, Raman microspectroscopy on the asphaltite inclusions within three carbonate samples from upper part of Mbuji-Mayi Supergroup, revealed palaeo-temperatures ranging from 150 to 260 °C (Delpomdor et al., 2018). Thus, the Congo Basin had a long history of sediment accumulation, tectonic inversion, and erosion since the Neoproterozoic (Kadima et al., 2011a; Delvaux and Fernandez, 2015) and is still tectonically active (Delvaux and Barth, 2010), leading to a record of highly disturbed thermal history.

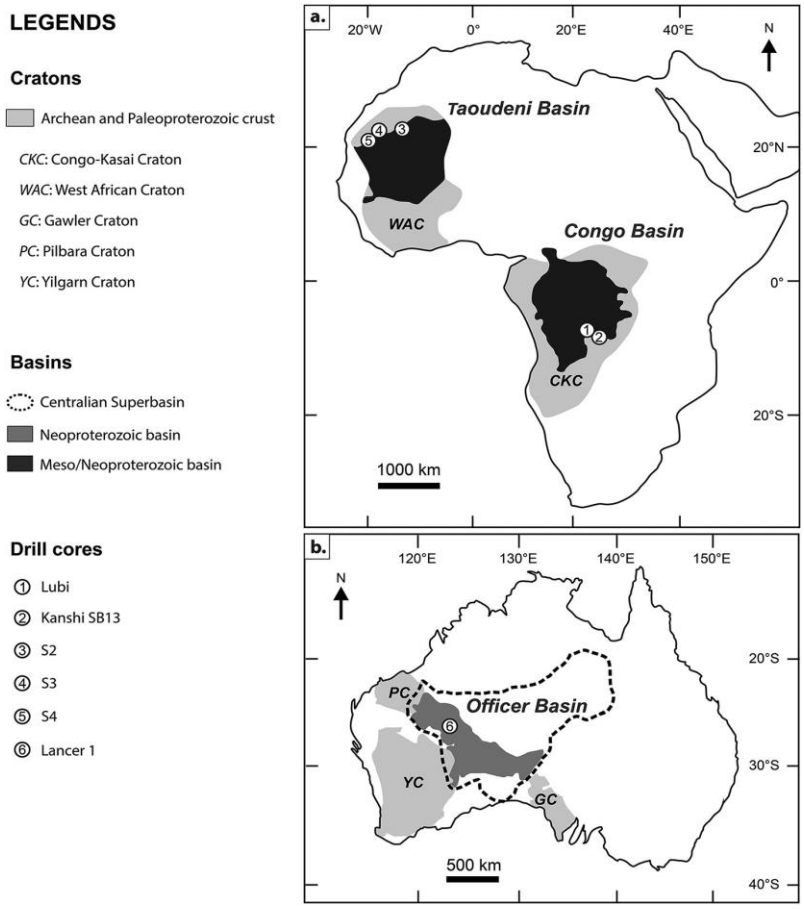

Fig. 1. Simplified geological map of (a) Congo Basin and Taoudeni Basin, and (b) Officer Basin with location of drill cores. Modified after Begg et al. (2009), Camacho et al. (2015) and Kadima et al. (2011a).

Taoudeni Basin

The Taoudeni Basin (> 1,750,000 km^2; Fig. 1a) is situated in northwestern Africa and extends from Mauritania to northern Mali and western Algeria. This basin is mainly of Proterozoic and Palaeozoic age and contains kilometer-thick (~1500–4000 m) mostly undeformed and unmetamorphosed sedimentary deposits overlying an Archean-Paleoproterozoic basement, the West African Craton (WAC) (Lahondère et al., 2003). The Atar/El Mreïti Group (Mauritania) is a shallow marine deposit of interbedded siliciclastic and carbonate sediments. ReeOs geochronology on organic-rich black shales suggests deposition ages of 1107 ± 12 Ma and 1109 ± 22 Ma (Rooney et al., 2010). These ages are supported by the microfossil assemblage composition suggesting a late Mesoproterozoic–early Neoproterozoic age and evidencing the diversification of early eukaryotes in Western Africa (Beghin et al., 2017). Four cores were drilled at the northern margin of the Taoudeni Basin by Total S. A. in 2004 (Rooney et al., 2010). They were named from the East to the West, S1, S2, S3 and S4 (Fig. 1a). S1 was not studied here because it is locally affected by a contact metamorphism resulting from dolerite intrusions. S2 is also not studied, because Raman spectra were unusable due to an intense fluorescence and low signal noise ratio (Fig. A1). A preliminary palynofacies analysis on extracted kerogen from the S2, S3, and S4 cores revealed a wide range of palynomorph colors. In the S2 drill core, the organic matter is translucent light yellow to black opaque via orange and brown in color. This suggests a low maturity of the carbonaceous material. In the S3 and S4 drill cores, organic walls of microfossils and amorphous organic matter are brown and light grey in color, respectively. Rock-Eval analyses on S2 drill core suggest that shales are immature and marginally in the oil-generative window of type II kerogen (Rooney et al., 2010). In contrast, vitrinite equivalent reflectance, vR_0eq % (obtained from bitumen reflectance data, bR_0%) from altered organic-rich shales of the S1 core show a maximum temperature peak of ~288 °C (Rooney et al., 2010). Albert-Villanueva et al. (2016) converted bitumen and pyrobitumen reflectance to vitrinite reflectance equivalent (vR_0eq %) from the R well, which is close to the S4 drill core studied. They obtained vR_0eq % between 0.40 and 1.28% (temperature of 63–87 °C) for bitumen while pyrobitumen gives vR_0eq % range from 1.15 to 3.49% (temperature of 164–312 °C). MartínMonge et al. (2017) calculated vitrinite reflectance equivalent from the hydrocarbon-based methylphenanthrene index and obtained values between 1.4 and 2% (main gas-generation window) for R1 and R2–R4 wells (corresponding respectively to S3 and S4 drill cores). These authors recognized three episodes of uplift and erosion (Panafrican, Hercynian and Alpine), which created large anticline fault-related structures and subsidence of the Taoudeni Basin. Moreover, ovoid structures related to Mesozoic magmatic intrusions were also recorded. All these events affected the thermal history of the basin. Here, two samples (grey shales) from the S3 and S4 drill cores were selected based

Table1

numberofconservedspectraafterinitialassessment.

AveragevaluesofcharacteristicRamanparameters,Ramanre fl ectanceandRamantemperatures.(N)=numberacquiredspectra;(N ,

SampleLocationGeologicalsequenceFormationDrillcoreDepth(m)RocktypeComment				SamplepreparationNN ,	ω_{D1}		ω_{G}		$\omega_{G-}\omega_{D1}$	
					Mean1	σ	Mean1	σ	Mean1	σ
KN23-123CongoBasinMbuji-Mayi	BIIc6KanshiS13B123	Darkgrey	AOM	extractedkerogen1091348.32.21594.72.7246.43.8						
Supergroup		shale	AOM1	Thinsection30131350.94.11597.52.9246.65.6						
			AOM2	Thinsection30171348.92.71596.91.7248.02.4						
			AOM3	Thinsection30101350.42.11596.82.9246.44.8						
			AOM4)=	Thinsection30231347.42.71597.41.8250.03.2						
			Arctacellulariatetragonala	extractedkerogen12121350.41.61593.32.9242.92.4						

th(m)RocktypeComment			SamplepreparationNN	’	ω_{D1}		ω_G		ω_{G}- ω_{D1}	
					Mean1	σ	Mean1	σ	Mean1	σ
r1680	Greyshale	Cerebrosphaerabuickii1	extractedkerogen20171351.73.41581.31.8229.62.7							
		Cerebrosphaerabuickii2	extractedkerogen20191349.42.01581.01.5231.62.5							
		Cerebrosphaerabuickii3	extractedkerogen20171349.63.31581.11.2231.54.2							
		Cerebrosphaerabuickii4	extractedkerogen20191354.52.01580.40.8225.92.4							
		Cerebrosphaerabuickii1	Thinsection871359.60.81589.53.3230.03.7							
		Cerebrosphaerabuickii2	Thinsection20161359.70.61589.33.9229.64.3							
		Cerebrosphaerabuickii3	Thinsection20141359.41.21589.03.5229.63.3							
r1955	Greyshale	Cerebrosphaerabuickii1	extractedkerogen20171354.43.21582.12.4227.73.4							

Table1 (continued)

Sample	FWHM-D1		FWHM-G		FWHM-D1/FWHM-GID1			IG		ID1/IG		RmcR$_0$ %		T(FWHM-D1)(°C)T(		RmcR$_0$%)(°C)	
	Mean1	σ	Mean1	σ	Mean1	σ	Mean1	σ	σ	Mean1	σ	Mean1	σ	Mean1	σ	Mean1	σ
S4-162	113.14.753.83.42.110.13745.8301.91312.7576.50.580.061.920.1123510885																
	104.32.240.12.22.610.195035.11231.29290.62254.80.540.052.370.0925452053																
	106.33.845.41.92.340.082090.21103.73970.21817.60.520.042.410.0825082073																
	105.35.545.27.12.360.242232.51816.74265.33603.30.530.042.340.282521220312																
	112.28.149.66.22.280.212020.6909.13741.51844.50.560.072.030.1523717936																
L1-472	135.54.684.32.31.610.071181.6118.91526.0144.20.780.060.850.171871012115																
	144.23.787.61.91.650.021387.0102.81822.1154.60.760.030.680.09168810410																
L1-680	137.39.179.63.41.730.15727.7161.71022.9210.80.710.071.120.151832014410																
	141.211.477.91.91.810.131265.8231.11631.7272.00.780.071.230.14174241519																
	147.210.877.62.21.900.121244.2177.21610.3203.20.770.061.220.231612315016																
	129.23.278.12.61.660.05870.6430.41194.3538.60.720.030.920.13200712810																
	133.36.680.73.01.650.034473.51125.36096.61857.70.750.071.140.201911414514																
	136.511.281.64.81.670.064170.41650.65831.32627.70.730.061.120.231842414316																
	135.56.580.03.91.700.085520.41577.36962.82621.70.820.091.120.181871414412																
L1-955	133.66.378.54.01.700.111073.5315.51273.4339.20.840.081.020.181911313614																
	138.17.389.06.01.550.09574.2122.6756.0155.60.760.091.010.171811613514																
	139.45.486.13.71.620.082462 1.53363.334098.14483.30.720.071.570.271781217015																
	142.610.381.23.91.760.0723307.13731.224592.75970.00.960.091.320.331722215620																

on an assemblage including fossil eukaryotes (Beghin et al., 2017). Sample from the S3 drill core comes from the Aguelt el Mabha Formation (S3–123, depth: 123 m) and sample from the S4 core comes from the Unit I-3 (S4–162, depth: 162 m). In sample S3–123, two microfossil species both from extracted kerogen and from thin section were analyzed, in addition to two AOM particles from extracted kerogen. In sample S4–162, one microfossil species and one AOM particle from extracted kerogen; and three AOM particles from thin section were analyzed (Table 1). Although Raman spectra from S2 drill core were unusable as mentioned above, one sample (green grey shale) from the Khatt Formation (S2–216, depth: 216 m) was characterized by XRD analyses and Thermal Alteration index (Table 2).

Officer Basin

The Officer Basin (Fig. 1b) is a part of the Centralian Superbasin, located in Western and Central Australia, an intracratonic basin of ~2,000,000 km^2 formed during the breaking-up of the Supercontinent Rodinia (Walter et al., 1995). The Centralian Superbasin is divided into 7 sub-basins, one of which is the Officer Basin. It is situated between the Yilgarn and Pilbara Craton in the West, the Gawler Craton in the Southeast and the Musgrave Orogenic Block in the North (Stevens and Apak, 1999) and recorded a quite long geological period with 1500 to 4000 m of sedimentary deposits. Ages range from the Tonian (1000–720 Ma) to the mid-Carboniferous (deduced from the palynological content) in most part of the basin (Grey et al., 2011). In addition, some areas also contain Cretaceous deposits (Mory and Haines, 2005; Stevens and Apak, 1999). The Centralian Superbasin is divided into four successive Supersequences (1 to 4). The Supersequence 2 is not recorded in the Officer Basin. The Supersequence 1 is principally composed of sandstone, dark mudstone and dolomite with small patches of siltstone and evaporites. It records shallow marine up to coastal and sabkha conditions and is composed, from bottom to top, of the Lefroy, Browne, Hussar and Kanpa formations. The basement of Centralian Superbasin, as the whole basin, is poorly dated with a KeAr age of 1058 ± 13 Ma (Mory and Haines, 2005). We focused on the Lancer 1 drill core in the west (Fig. 1b), which intercepts the whole Supersequence 1 and shows a wide microfossil diversity in the shaly horizons of the Hussar (494.1 m-thick) and Kanpa (241 m-thick) formations (Mory and Haines, 2005). Both contain the acritarch Cerebrosphaera (Cotter, 1997), an index microfossil of the Tonian period (Grey et al., 2011; Mory and Haines, 2005). Within the three rock samples of the Kanpa Formation that were investigated, we analyzed two specimen of Cerebrosphaera from extracted kerogen of sample L1–472 (depth: 472 m); four specimen from extracted kerogen and three specimen in thin section from sample L1–680 (depth: 680 m) as well as two specimen from extracted kerogen and two specimen in thin section from sample L1–955 (depth: 955 m). Interestingly, all studied Cerebrosphaera specimens show a variety of organic wall color ranging from a very light-brown to a mid-brown up to a dark brown color. A variable opacity can also be observed on the specimen, with some specimens showing a high transparency while others are entirely opaque. No temperature estimate has been attempted for the Lancer 1 in previous studies. However, analyses have been carried out for Empress 1A, a drill core situated 200 km north-west of the Lancer 1 drill core and crossing the Supersequence 1 and especially the Kanpa Formation. Temperatures comprised between ~120 °C and ~140 °C at minimum were obtained through the reflectance of non-fluorescent lamalginite converted to vitrinite equivalent reflectance (0.52 and 1%; Ghori inStevens and Apak, 1999). The Keene basalt intrusion inside the Kanpa Formation, in the Lancer 1 drill core at a depth of 527.3 to 576.2 m (Pirajno inMory and Haines, 2005), most probably influenced the temperature recorded into the sediments.

Table 2
Compilation of mean temperatures calculated from Raman spectral parameters, solid bitumen reflectance together with TAI scale and XI for all samples (extracted kerogen and thin section).

Sample	Sample preparation	Data from Raman parameters						Data from solid bitumen				Calculated temperatures						Data from XRD			
		FWHM-D1		ωG-ωD1		R_{Ramb} %		BR_0 %		R_0 eq %		T_{peak} from vR_0 eq (°C)		T_{peak} from R_{Ramb} % (°C)		T° from FWHM-D1 (°C)		TOC (wt %)	TAI scale	Kübler index (Δ°2θ)	XI domain
		Mean	1σ	Mean	1σ	Mean	1σ	Mean	1σ	Mean	1σ	Mean	1σ	Mean	1σ	Mean	1σ				
XN23-123	Extracted kerogen	108.6	4.4	243.7	2.9	1.87	0.15	2.28	0.15	2.46	0.15	208	5	186	7	244	9	0.4	3/3-	0.82	Diagenesis
	Thin section	109.3	6.1	248.4	3.9	2.13	0.21							196	8	243	13				
1U18-312	Extracted kerogen	112.7	3.3	239.4	2.7	1.64	0.13	2.22	0.15	2.41	0.14	206	5	175	7	236	7	0.5	3+/4-	0.57	Diagenesis
	Thin section	120.1	6.4	248.4	3.4	1.97	0.18							190	8	220	14				
82-216	–	–	–	–	–	–	–	–	–	–	–	–	–	–	–	–	–	–	2+/2	1.48	Diagenesis
	–	–	–	–	–	–	–														
83-123	Extracted kerogen	121.6	4.6	232.5	2.4	1.27	0.13	–	–	–	–	–	–	155	8	217	10	–	3	0.98	Diagenesis
	Thin section	125.1	5.3	234.8	3.8	1.40	0.21							162	12	209	11				
84-162	Extracted kerogen	112.7	6.2	245.4	2.6	1.97	0.14	–	–	–	–	–	–	190	6	236	13	–	3	0.48	Diagenesis
	Thin section	105.4	4.1	253.0	3.3	2.38	0.18							205	7	251	9				
11-472	Extracted kerogen	140.1	6.1	222.9	2.9	0.76	0.13	–	–	–	–	–	–	112	13	177	13	–	3-/3	1.23	Diagenesis
11-680	Extracted kerogen	138.5	11.1	229.6	3.8	1.12	0.20	–	–	–	–	–	–	143	13	180	24	–	3	0.87	Diagenesis
	Thin section	135.5	8.7	229.7	3.8	1.12	0.20							144	14	187	19				
11-955	Extracted kerogen	135.6	7.1	227.7	3.2	1.01	3.23	–	–	–	–	–	–	136	14	186	15	–	3-/3	–	–
	Thin section	141.0	8.3	235.7	6.01	1.44	0.32							163	19	175	18				

Proxies for temperature and maturity of CM estimates

Note that the use of the term "maturity" differs from one proxy to another. In Raman spectroscopy, the increase of CM maturity corresponds to the increase of crystallinity, i.e. the aromatization of CM and the decrease of defects. In the petroleum domain (where TAI scale, vitrinite and solid bitumen reflectance are used), the term maturity refers not only to chemical and physical properties of CM but also to petroleum potential of CM (or organic matter), i.e. its capacity to generate hydrocarbons (oil and gas).

TAI scale

TAI scale has been traditionally used by palynologists in the petroleum industry to quickly assess the maturity of CM and the temperature that affected CM based on the comparison of palynomorphs present in the samples to a standard color scale, (Fig. A2). Its application can nonetheless be limited as color estimation can be subjective. Moreover, the published scale (Staplin, 1977) was established with laboratory experiments on one or a few types of palynomorphs (mostly spores) and thus is restricted to a certain number of palynomorph types, which are not always present in the investigated sample (Szczepanik, 1997) nor relevant for the Precambrian. Moreover, organic-walled microfossil assemblages commonly include taxa displaying different wall color. Despite their similar taphonomic history, co-occurring taxa may differ in color due to several factors such as the wall thickness, the wall ultrastructure, the wall chemical composition, the wall ornamentation, the intensity of the microscope light, and the overlapping of folds in the specimens darkening the transmitted light. The very simple approach of the TAI permits a practical and quick first assessment of thermal maturity but has strong limitations and does not take into account these effects. To illustrate this idea, a filter with a transparency of 50% applied on the value 2- in the TAI scale correspond to the color of the value 1 (Fig. A2). To use the TAI scale in a more objective way (as much as possible with human eyes), we propose a new pattern of the TAI scale (color codes in Munsell color and RGB systems Fig. A2) showing the different percent of transparency for a same value in the traditional TAI scale (Fig. A2). To use this scale, the observer must determine the value of the TAI scale in an area not displaying folds or inclusions and has to work on a large variety of specimens to obtain a clear overview of the color range of the specimen.

CM Raman spectrum and Raman geothermometry

In an ideal graphite crystal, only one band is Raman active at 1580 cm^{-1}. This band, called G-band, corresponds to in-plane stretching vibration of the aromatic carbon (E_{2g} vibration, e.g. Nemanich and Solin, 1979). In natural CM two additional bands arise. One is centred at 1350 cm^{-1} and another forms a shoulder on the Gband at ca. 1620 cm^{-1}, called D1- and D2-band respectively (Fig. A3, Wopenka and Pasteris, 1993). These two bands correspond to in-plane breathing vibration made possible by the defect in the ideal graphitic structure. Supplementary bands can form shoulders on the D1-band at 1500 cm^{-1} and 1190–1250 cm^{-1}, called D3- and D4-band, respectively, when the crystallinity of the CM is low (Lahfid et al., 2010). The D3-band results from out-of-plane vibration of tetrahedrally coordinated carbons, dangling bonds and heteroatoms (Beyssac et al., 2002; Wopenka and Pasteris, 1993). The D4-band that occurs only in CM with a very low crystallinity has a more discussed origin but could result from the vibration of CeC in polyene structure (Dippel et al., 1999).

CM Raman spectra have been used as proxies to estimate peak metamorphism temperature. The thermal alteration of CM is non-reversible and the evolution of the spectral parameters (Fig. A3) such as peak intensity (I_{D1}, I_{D2}, I_{D3}, I_{D4} and I_G), peak area (A_{D1}, A_{D2}, A_{D3}, A_{D4} and A_G) and peak full width at half maximum (FWHM-D1, FWHM-D2,

FWHM-D3, FWHM-D4, and FWHM-G), as well as the evolution of their ratio, are strongly linked to the crystallinity of the CM (Ferrari and Robertson, 2000; Kouketsu et al., 2014; Wopenka and Pasteris, 1993). Empiric geothermometers, based on the different spectral parameters, have been proposed to estimate peak temperature underwent by CM within metapelites for precise temperature ranges (Beyssac et al., 2002; Rahl et al. (2005); Lahfid et al., 2010; Kouketsu et al., 2014). With the exception of Kouketsu et al. (2014) thermometers, all of the other thermometers have been calibrated for temperature above 200 °C. However, the fitting protocol and the subtraction of baseline due to the background fluorescence are critical parameters for a coherent estimation of the temperature (Lünsdorf et al., 2014). Based on the known geological context of our study sites, we thus decided to apply only the more relevant thermometers established by Kouketsu et al. (2014) based on width of D1-band (FWHM-D1, Eq. 1) or the width of D2-band (FWHM-D2, Eq. 2). Due to the difficulty to identify correctly the D2band, we estimated temperature only with the thermometer based on FWHM-D1 (Eq. 1).

$$T\ (^{\circ}C) = -2.15 * FWHM - +D1\quad 478 \qquad (1)$$

$$T\ (^{\circ}C) = -6.78 * FWHM - +D2\quad 535 \qquad (2)$$

Estimates of temperature from reflectance

Vitrinite is a maceral group derived from terrigenous (woody) CM occurring in post-Silurian sedimentary rocks. Its reflectance, vRo %, (or VR; Taylor et al., 1998) can be used as indicator of the thermal maturity as it increases with temperature (Barker and Pawlewicz, 1994; Jasper et al., 2009; Zieger et al., 2018). It has been widely used to study the thermal evolution of sedimentary basins and for oil and gas exploration (Barker and Pawlewicz, 1994). Barker and Pawlewicz (1994) proposed a calibrated geothermometer, Vitrinite Reflectance Geothermometer (VRG), allowing the estimate of the peak temperature underwent within sedimentary basins in both burial ($T_{peak\ burial}$, Eq. 3) and hydrothermal ($T_{peak\ hydrothermal}$, Eq. 4) settings.

$$T_{peak\ burial}\ (^{\circ}C) = (\ln(vR_0\%) + 1.68)/0.0124 \qquad (3)$$

$$T_{peak\ hydrothermal}\ (^{\circ}C) = (\ln(vR_0\%) + 1.19)/0.00782 \qquad (4)$$

For rocks devoid of vitrinite, the use of solid bitumen reflectance have been proposed ($bR_0\%$; Jacob, 1989; Landis and Castaño, 1995; Riediger, 1993) or Raman reflectance ($RmcR_0\%$; Liu et al., 2013; Sauerer et al., 2017), which can be successively used in the VRG equations (Liu et al., 2013).

Solid bitumen is a residual product of thermal conversion of kerogen in organic-rich mature and post-mature rocks (Landis and Castaño, 1995). Bitumen is part of CM partly migrating in rocks and forming oil, thus it is often not syngenetic to the hosting rock. However, when solidified (sometimes called "pyrobitumen"), it is not mobile anymore and its maturity should reflect the temperature undergone by the hosting rock and co-occurring syngenetic CM such as primary macerals or organic microfossils. Solid bitumen occurs in three optical forms, (1) "anisotropic coked" exhibiting a bright reflective appearance with a strong anisotropy, (2) "granular", and (3) "homogeneous". Only the homogeneous variety is recommended for thermal history studies due to its weak anisotropy and its wider distribution (Landis and Castaño, 1995). In addition, it is extremely difficult to confound this type of solid bitumen with other organic constituents. Different equations have been proposed to obtain an equivalent to vitrinite reflectance (vR_0eq %) from solid bitumen reflectance for different lithologies (Jacob, 1989; Landis and Castaño, 1995; Riediger, 1993; Schoenherr et al., 2007). We used here the equation that has been determined from rocks with a low permeability such as shales and siltstones (Landis and Castaño, 1995, Eq. 5).

$$vR\ eq_0\ \% = (bR_0\% + 0.41)/1.09, \qquad (5)$$

Raman reflectance ($RmcR_0\%$) has been defined as an equivalent of vitrinite reflectance based on the linear correlation of $vR_0\%$ with the distance between the D1- and G- band positions (ωG–ωD1, Eq. 6, Liu et al., 2013) for mature to highly mature samples and with or the intensity ratio of G and D1-bands (I_{D1}/I_G) for post-mature samples (Eq. 7, Liu et al., 2013). We introduced the different vR_0eq % values in the VRG equation defined for burial settings as no evidence for hydrothermalism was observed in our samples.

$$RmcR_0\% \equiv vR\ eq_0\ \% = 0.0537\ (\omega G - \omega D1)^{*} - 11.21 \text{ for mature to highly mature samples} \qquad (6)$$

$$RmcR_0\% \equiv vR\ eq_0\ \% = 1.1659\ (^{*} I_{D1\ G}/I\ ) + 2.7588 \text{ for post} - \text{mature samples} \qquad (7)$$

Illite crystallinity (IC)

Diagenetic clay minerals usually occur as heterogeneous assemblages of submicroscopic layers of different structure types such as illite, smectite, vermiculite and chlorite. The nature of the assemblage and the crystallinity of illite vary as a function of the temperature. Illite crystallinity (IC) has been applied mainly to detect the transition zone between diagenesis and very low-grade metamorphism (Kübler, 1967). The IC currently named Kübler-Index (KI; Guggenheim et al., 2002) corresponds to an indirect measurement of the mean consecutive illite layers contained in coherent scattering domains of mixed-layer illitesmectite (Kübler and Jaboyedoff, 2000). It is obtained by measuring the full width at half maximum height (FWHM) of the 10 Å-illite X-ray peak in the air dried preparation, when for conceptual reasons it is admitted that expandable mixed-layers contain only illite s.s. or that expandable mixed-layers were removed by treatment (Ferreiro Mählmann et al., 2012; Ferreiro Mählmann and Frey, 2012; Kübler and Jaboyedoff, 2000; Warr and Rice, 1994). However, in nature, this representative trend in smectite-free sample is not very frequent (Ferreiro Mählmann et al., 2012). Hence, for samples with discrete smectite content, KI corresponds in fact to FWHM of the 10 Å X-ray diffraction peak of illite/ smectite mixed-layer (I/S) in the ethylene-glycol treated preparation (Jaboyedoff et al., 2000; Jaboyedoff et al., 2001; Kübler and Jaboyedoff, 2000). KI is typically reported in units of Δ°2θ Cu Kα. Its value decreases with rising metamorphic conditions. Several KI values were proposed in the past but, two KI calibrations are recommended (Warr and Ferreiro Mählmann, 2015): (i) from Kübler's original standards (Kübler, 1967) and (ii) from Crystallinity Index Standards (CIS, Warr and Rice, 1994). A correlation was established between these two KI calibrations, for a better compatibility of published data from different laboratories. According to Kübler's original calibration, the diagenesis zone is characterized by KI up to 0.42 Δ°2θ, the anchizone by value between 0.42 and 0.25 Δ°2θ and the epizone by KI lower than 0.25 Δ°2θ. While, for KI values determined using the CIS calibration, the equivalent limits of the anchizone are 0.32 and 0.52°2θ (Warr and Ferreiro Mählmann, 2015). These three metamorphic zones roughly correspond to temperatures lower than 200 °C, 200 to 300 °C, and above 300 °C, respectively. Here we use the Kübler's original scale (also called KF scale, Warr and Ferreiro Mählmann, 2015) to define temperatures ranges undergone by the samples.

Methods

Raman spectroscopy

Samples were prepared at the University of Liège (PPP Laboratory, UR GEOLOGY, Belgium) through two preparation methods prior to Raman measurements: acid maceration (isolated kerogen) and thin section (Fig. 2 and Table 1). Both methods were performed on all samples from Congo (two samples: KN23−123and LU18−312), Taoudeni (two samples: S3−123 and S4−162) and Officer (three samples:

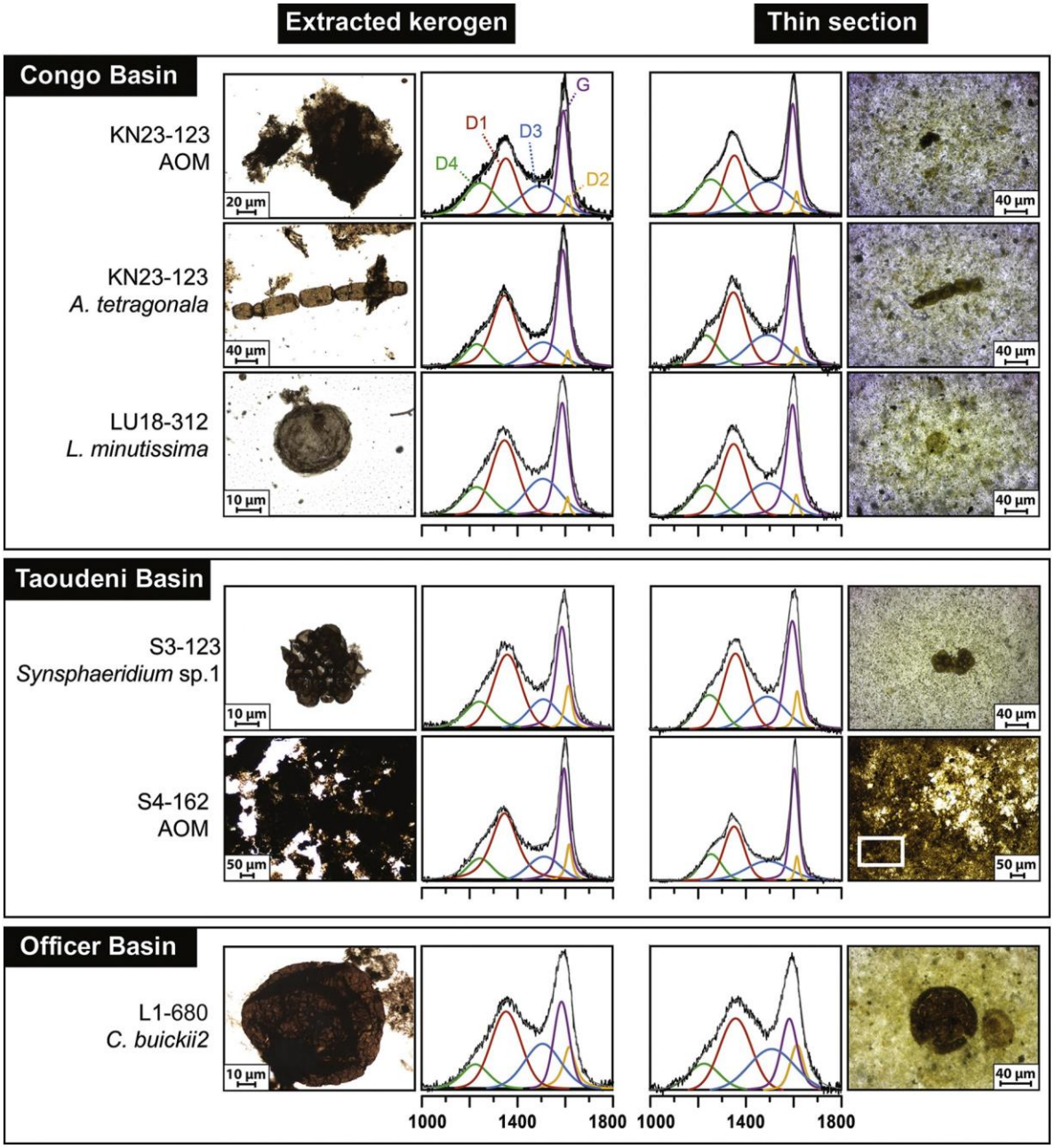

Fig. 2. Photomicrographs of some AOM and microfossils in extracted kerogen (left) and in thin section (right) in studied drill cores from the three basins and corresponding representative Raman deconvoluted spectra.

L1–472, L1–680, L1–955) basins.

The kerogen (microfossils and AOM) was extracted following a modified preparation procedure described by Grey (1999). After cleaning, samples were crushed in a mortar. Carbonates were removed by hydrochloric acid (HCl, 35%) and silicates by hydrofluoric acid (HF, 60%). Neo-formed fluorides were removed by hot HCl. The organic fraction was filtered by hand. Centrifugation that could damage fragile fossilized forms and oxidation that can alter kerogenous wall chemistry and color were avoided. Extracted kerogen was stored in millipore water. For Raman preparation, extracted kerogen was pipetted under an inverted microscope and dropped on standard microscope slides for at least one week drying before Raman analysis.

For preparing the thin sections, a thin sliver parallel to the stratification plane was cut with a diamond saw, allowing the observation of microfossils. This thin sliver was put in an oven at 60 °C for 1 day. After drying, it was mounted on a glass slide by cold bonding with epoxy resin (< 60 °C to not affect the carbonaceous material). The thickness of the sample was reduced to 30 µm with progressively finer abrasive grit (9, 6, 1, ¼ µm) to obtain a mirror polishing.

Raman analyses were performed on a Renishaw Invia Raman microspectrometer at the University of Liège (PPP Laboratory, UR GEOLOGY, Belgium) with an Ar-ion-40 mW monochromatic 514 nm laser source. Laser excitation was focused through a 50× objective to obtain a 1–2 µm spot size and laser power at the sample surface was set at around 2 mW. Acquisitions were made in "Mapping point"-mode, with a 1800 l/mm grating, a 100 cm^{-1} cut-off edge filter and a 1040 × 256 pixel CCD array detector. This allowed the acquisition of Raman spectra with a 2000 cm^{-1} detection range and a 4 cm^{-1} spectral resolution. Beam centering and Raman spectra calibration was

performed on a Si glass with a characteristic Si-band at 520.4 cm^{-1}. In "Mapping-point" mode, the Raman spectrum of each point was acquired in static mode (fixed at 1150 cm^{-1}) for 1 × 1 s running time. To obtain a good estimate of the Raman spectral parameter (Sforna et al., 2014), at least 20 points were measured on each microfossil or AOM. Recorded spectral data were processed with the software "Renishaw Wire 4.1". Out of a total of 1220 spectra acquired, only 914 have been considered (Table 1, Fig. 3). Indeed, some spectra showed a lower resolution due to signal noise and intense fluorescence. To obtain a good estimate for calculated ratios, we excluded these spectra. The baseline subtraction protocol was performed on a truncated spectrum between 1000 and 1800 cm^{-1}. The baseline was subtracted with a third order polynomial fit that was generated using the 'Through chosen points on each spectrum' mode of Wire 4.1 and was constrained by placing anchoring lines each 10 cm^{-1} between 1000 and 1100 cm^{-1} and between 1720 and 1800 cm^{-1}. Following this data processing, D1-, D2-, D3-, D4and G-bands (Fig. 2 and Fig. A3) were fitted by a decomposition based on Gaussian–Lorentzian function with the protocol described in Sforna et al. (2014). This allowed retrieving the position, intensity, area and width of D1-, D2-, D3-, D4- and G-bands (Figs. 2, 3 and Fig. A3).

Solid bitumen reflectance

Only samples from Congo Basin were analyzed (Fig. A4) due to a privacy policies for Taoudeni and Officer samples. Analyses were performed at RWTH Aachen University (Rheinisch-Westfälische Technische Hochschule Aachen). Laboratory protocol matches the guidelines set out in the International Organization for Standardization publications ISO 7404-2, ISO 7404-3 and ISO 7404-5 and in Taylor et al. (1998). Details of sample preparation are described in Sachse et al. (2012). Solid bitumen reflectance measurements were performed on polished core sections under reflected light using a Zeiss microphotometric system, which was calibrated by a Zeiss yttrium–aluminum–garnet standard (R — 0.889%). The photometer was provided with a pinhole aperture to read a spot with a diameter of 5 μm on the sample surface at a wavelength of 546 nm, using a 50×/1.00 n.a. lens in oil immersion (n_e — 1.518). To reach sufficient accuracy of solid bitumen measurements, at least 30 point measurements were taken per polished section. Data processing was performed with Diskus Fossil software (Technisches Büro, Carl H. Hilgers).

Mineralogical analysis and Kübler index (KI)

Mineralogical compositions and clay minerals (Figs. A6, A7 and A8) were determined by X-ray diffraction (XRD) at the University of Liège (AGEs laboratory, UR GEOLOGY, Belgium). For mineralogical composition, 1 g of fresh sample (total rock) was crushed and sieved to 150 μm size particles, installed on a sample holder and then compacted carefully and regularly in order to limit any preferential orientation of minerals (Moore and Reynolds, 1997). The XRD was then performed on a Bruker AXS D8 Advance Eco diffractometer (Cu-Kα radiation, 40 kV and 25 mA), equipped with a linear detector (LINXEYE XE) for the angles between 2 and 70 Δ°2θ, with a step size of 0.02 Δ°2θ. Minerals were first identified using EVA 3.2 software and quantified with Topas (software using the Rietveld method).

In order to identify clay minerals, oriented aggregates (Moore and Reynolds, 1997) were prepared from < 2 μm fraction. This fraction was obtained by decantation from a suspension in distilled water (settling time calculated according to Stoke's law), of 1–2 g of dried bulk sediment previously sieved at 63 μm. For each sample, three X-ray patterns were recorded (Fig. A8): Air-dried (AD), after solvation with ethylene glycol for 24 h (EG) and after heating at 500 °C (H).

The KI values were calibrated to Kübler's original scale. Measurements were made on the EG pattern (Fig. A8) after fitting and deconvolution of three respective peaks (illite, mixed-layers and chlorite, Fig. A5) using Gaussian–Lorentzian function. Clay spectra were deconvoluted with 'Renishaw Wire 4.1' software and executed under the same process as Raman spectral analysis, with the exception that spectra were truncated between 5 and 11Δ°2θ Cu Kα. KI errors are ± 0.06°.

Results and discussion

Thermal Alteration Index

Microfossils from Kanshi sample (KN23–123) have color ranging from medium dark brown to dark-very dark brown corresponding to a TAI scale of 3 to 3^+ (Figs. 4 & A2). The microfossils from Lubi (LU18–312) have a TAI of $3^+/4^-$ as their colors range from dark- very dark brown to very dark brown-black. The CM contained in the Congo samples is thus mature to post-mature and corresponds to a burial temperature between 150 °C and 250 °C. The samples from the three Taoudeni Basin drill cores display acritarchs with wall color ranging from yellow-orange to orange-orange brown for S2–216 sample, and medium dark brown in S3–123 and S4–162 samples. This correspond to TAI values of $2/2^+$, and 3, respectively. The CM preserved in the Taoudeni samples is thus immature in S2 and mature for S3 and S4 and has registered a burial temperature < 60 °C and between 90 and 200 °C, respectively. Acritarchs from the three samples (L1–472; L1–680 and L1–955) of the Officer Basin show wall color ranging from medium light brown to medium dark brown corresponding to a TAI scale of 3^- to 3 (Fig. 4). These TAI values correspond to mature CM and temperatures of burial < 100 °C (Al-Ameri and Wicander, 2008).

Kübler index

Shale samples are mainly characterized by illite, kaolinite, chlorite and a few percent of mixed-layers (illite-vermiculite), and non-clay minerals such as quartz, feldspar and minor phases such as pyrite, carbonate (except sample S2) and gypsum (Fig. A6). In EG spectra, after deconvolution (Fig. A5), excluding the 6.35°2θ chlorite peak, two elementary peaks occur between 5 and 11°2θ. A peak at ca. 8.8°2θ is attributed to illite, whereas a wider peak at 8.5°2θ corresponds to 10–14 mixed layers, interpreted as illite-vermiculite. In the Congo Basin samples, the KI values range from 0.57 to 0.82 Δ°2θ (KN23–123: 0.82, LU18–312: 0.57, Fig. A5, Table 2). In the Taoudeni Basin samples, the KI values vary between 0.48 and 1.98 Δ°2θ (S4–162: 0.48; S3–123: 0.98; S2: 1.48). Finally, in the Officer Basin samples, the KI values show also similar values ranging from 0.87 to 1.23 Δ°2θ (L1–472: 1.23; L1–680: 0.87). All these data suggest that temperatures undergone by the samples are < 200 °C and in the diagenesis domain (Fig. 4). The diagenetic origin of fibrous illite is confirmed by the study of Hamilton (inMory and Haines, 2005) in clays from the Kanpa Formation within the Lancer1 drill core (Officer Basin, Australia). This is also supported by a large content of kaolinite in our samples (until 20%, Fig. A6), indicating temperatures lower than 200 °C (Cathelineau et al., 1985).

Raman spectra and characteristic spectral parameters

Representative spectra from microfossil species and AOM for each sample are shown in Fig. 2. Spectral parameters are displayed in Fig. 3, Table 1 and in Table A. For each of our studied samples from three different basins, the Raman spectra and the spectral parameters for extracted kerogen and thin section within one sample are similar (Fig. 2), even if the spectra acquired on thin section are noisier due to the intrinsic fluorescence of the matrix. AOM and microfossils spectra (Fig. 2) display well-developed D3- and D4-bands, have a D2-band unseparated from the G-band, a broad D1-band (FWHMD1 > 100 cm^{-1}) and an intensity ratio I_{D1}/I_G lower than 1. These characteristics are typical of spectra of poorly ordered CM (Beyssac et al., 2002, 2003; Kouketsu et al., 2014; Lahfid et al., 2010; Sauerer et al., 2017).There is no significant difference in the band positions between spectra acquired on extracted kerogen or on thin section for a given

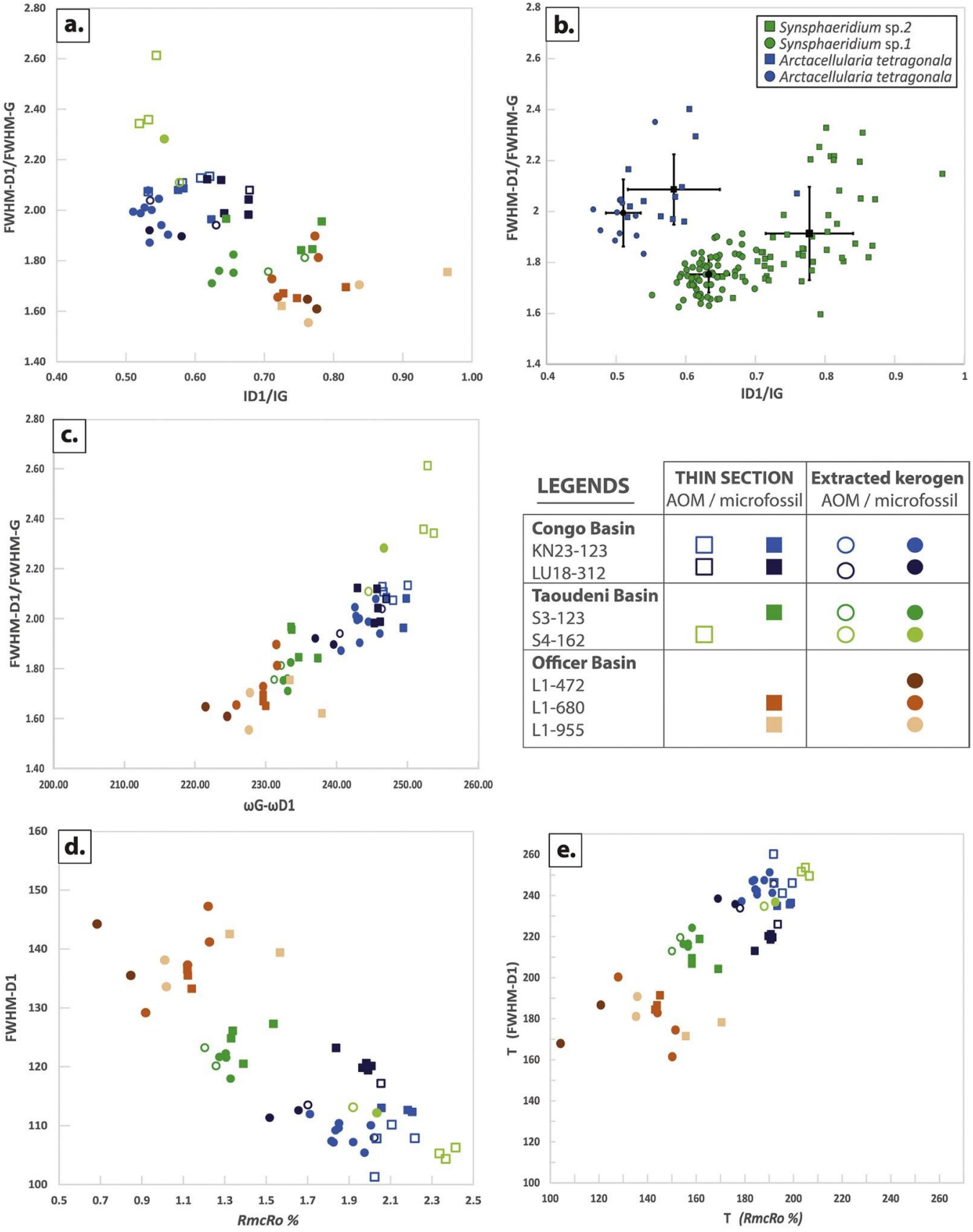

Fig. 3. (a) Average values of FWHM-D1/FWHM-G ratio vs ID1/IG ratio. (b) Analyses for the specimens Synsphaeridium in S3 drill core and Arctacellularia tetragonala in Kanshi drill core (extracted kerogen and thin section). Means and standard deviations are in black. (c) FWHM-D1/FWHM-G ratio vs ωG-ωD1. (d) FWHM-D1 vs $RmcR_o\%$ and (e) T FWHM-D1 (Eq. 5) and T $RmcR_o\%$.

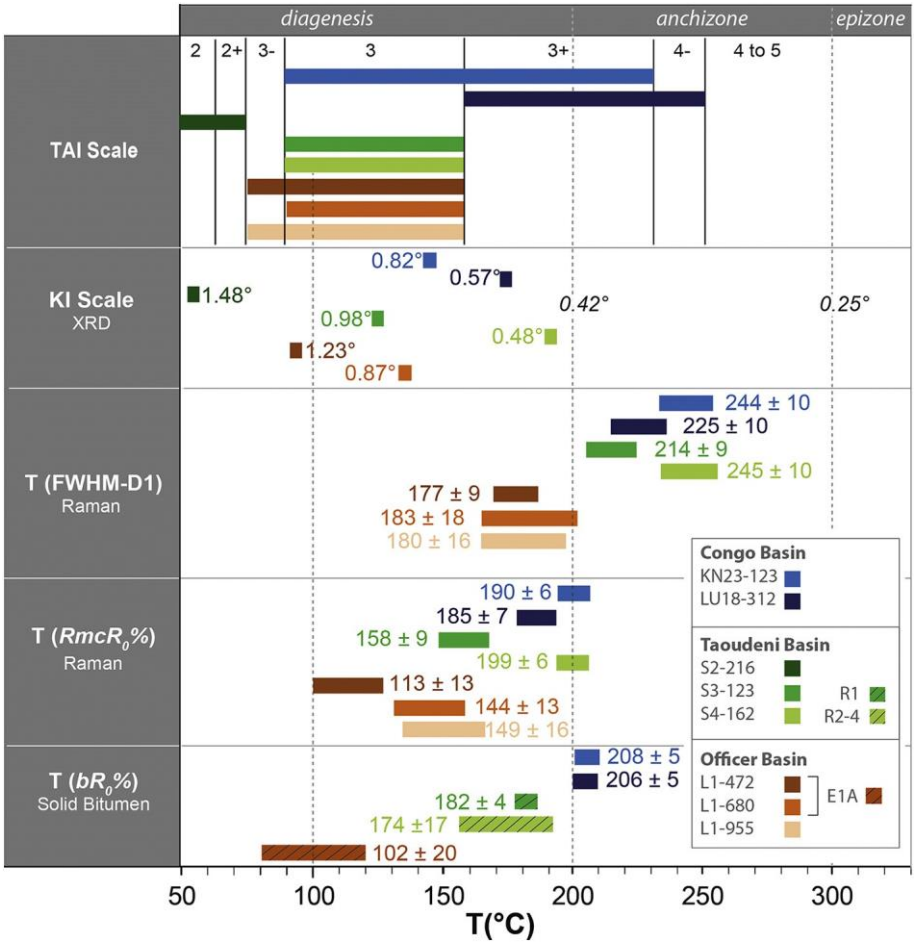

Fig. 4. Compilation of all thermometers used in this study and corresponding mean temperature range. All data come from Table 2. Errors are given in 1σ. Data from dashed boxes are from Martín-Monge et al. (2017) and Ghori (in Stevens and Apak, 1999).

microfossil species (Tables 1 and 2). For example, within spectra acquired on a specimen of Arctacellularia tetragonala isolated from extracted kerogen and other specimen within a thin section, the average position of D1- band are 1350 cm^{-1} and 1351 cm^{-1}, respectively. As for the average positions of G-band, they are 1593 cm^{-1} and 1598 cm^{-1}, respectively (Table 1). There is a slight shift towards lower values for the width and the intensity of the different bands for microfossils from extracted kerogen (Fig. 3b, Table 2 and Table A). These shifts are limited and comprised within two σ range. The dispersion of the data is systematically larger for the thin sections compared to the extracted kerogen whatever the drill core or the microfossil considered (Fig. 3b, Table 2 and Table A). For example, the standard deviation (1σ) on the I_{D1}/I_G ratio for Arctacellularia tetragonala is divided by 3 (thin section: 0.07, extracted kerogen: 0.02, Fig. 3b, Table 1) while it is divided by 2 for Synsphaeridium (thin section: 0.06, extracted kerogen: 0.03, Fig. 3b, Table 1). For the FWHM-D1/FWHM-G, the value for Synsphaeridium is divided by 2 (thin section: 0.17, extracted kerogen: 0.07, Fig. 3b, Table 1) while the values do not change between extracted kerogen and thin section for Arctacellularia tetragonala. This is related to high sensitivity of I_{D1}/I_G to peak fitting and baseline subtraction procedures whereas FWHM-D1/FWHM-G is less sensitive (Beyssac et al., 2003; Kouketsu et al., 2014).

The small differences within the spectra and spectral parameters observed from a species to another species and with the AOM could be explained by a difference in the CM precursors. Despite these minor differences, the uniformity of the Raman spectra and spectral parameters show that microfossils and AOM registered, here, the same thermal history. It often occurs that AOM can be remobilized or inherited, so it is best to make measurement on microfossils for which syngenicity can be evidenced by their distribution in shale: flattened parallel to bedding. The smaller dispersion of data for extracted kerogen leads to better estimates of calculated ratios and thus of the maturity and calculated temperatures. This should be particularly true for low maturity CM that displays high intrinsic fluorescence (Quirico et al., 2005).

D1-band position (ωD1, Tables 1 and Table A) has average values of ~1356 cm^{-1} (L1), ~1354 cm^{-1} (S3–123), ~1352 cm^{-1} (LU18–312), ~1349 cm^{-1} (KN23–123 and S4–162). Conversely, the G-band position (ωG) increases towards higher frequencies with values of ~1580 cm^{-1} (L1–472), ~1584 cm^{-1} (L1–680), ~1587 cm^{-1} (L1–955 and S3–123: ~1587 cm^{-1}), ~1595 cm^{-1} (LU18–312 and KN23–123) and ~1599 cm^{-1} (S4–162). As a consequence, the ωG-ωD1 difference increases (Fig. 3c; Table 1 and Table A), from ~230 cm^{-1} for Lancer samples to ~250 cm^{-1} for S4. FWHM-D1 and FWHM-G are the highest for Lancer samples (FWHM-D1 ~ 138 cm^{-1} and FWHM-G ~ 82 cm^{-1}) and the lowest for S4 (FWHM-D1 ~ 108 cm^{-1} and FWHM-G ~ 47 cm^{-1}). The FWHM-D1/FWHM-G ratio is correlated positively with the ωG-ωD1difference (R^2 = 0.594; Fig. 3c) but negatively with the ID1/IG ratio (R^2 = 0.48; Fig. 3a). The evolution of these parameters and these ratios are coherent with an increasing order of the CM and thus a rise of the maturity degree (Beyssac et al., 2002; Liu et al., 2013; Sauerer et al., 2017).

Raman and solid bitumen reflectance

Raman reflectance derives directly from the ωG-ωD1 difference measured on the Raman spectrum. The full fitting protocol used in this study is difficult to apply when the CM is highly immature (i.e. highly disordered) due to its high fluorescence. As the position of D1- and Gband are almost not sensible to the fitting procedure (Beyssac et al., 2003; Kouketsu et al., 2014), we retrieved, for 30 acquisitions made on one Synsphaeridium specimen from Congo (Table B), the positions of D1and G-bands after application of the full fitting protocol and by directly reading them on the Raman spectra. After calculating the ωG-ωD1 difference with the two extraction protocols, the $RmcR_0$% is the same (Table B). This suggests that for highly immature CM, the Raman Reflectance method is efficient to obtain a good equivalent of the vitrinite reflectance. Values of $RmcR_0$% are presented in Fig. 3e, Tables 1 and 2. Within the same sample, the results are lower for extracted kerogen than in thin section. For example, $RmcR_0$% calculated for KN23–123 ranges in the 1.71–2.02% interval for extracted kerogen while it ranges between 2.02 and 2.22% in thin section. A similar shift of 0.1–0.4% can be observed for all the samples (Tables 1 and 2). However, these $RmcR_0$% values still correspond to the same range of vitrinite reflectance equivalence and thus are not in strong disagreement (Liu et al., 2013). The calculated $RmcR_0$% increases from 0.96 ± 0.18% for Lancer, to 1.27 ± 0.13% for S3–123, 1.64 ± 0.15% for LU18–312, 1.87 ± 0.15% for KN23–123 and 1.97 ± 0.14% for S4–162 (Table 2 and Fig. 3d), suggesting an increase of CM thermal maturity for these samples studied.

Solid bitumen of KN23–123 and LU18–312 samples from Congo Basin occurs as an opaque material of greyish appearance, disseminated in pores and fissures (Fig. A3). Solid bitumen in these samples is either homogeneous, locally elongated and filling fissures or granular. Reflectance histograms of KN23–123 and LU18–312 exhibit a near uniform distribution with bR_0% mean values of 2.28 ± 0.16% and 2.22 ± 0.15%, respectively (Table 2 and Fig. A4). The vR_0eq % obtained from bR_0% ranges from 2.23 to 2.78% and 2.09 to 2.64% for KN23–123 and LU18–312, respectively (Table C). These vR_0eq % are systemically higher than the $RmcR_0$% of ~0.6% (Table 2).

The $RmcR_0$% we obtained for S3 and S4 samples can be compared to the vR_0eq % measured from methylphenanthrene index (Martín-Monge et al., 2017) within the R1 well, equivalent to S3, and within the R2–4 wells, equivalent to S4 drill core (Martín-Monge et al., 2017). Interestingly, the $RmcR_0$% values for S3 (1.20–1.33%) are lower than the vR_0eq % for R1 well (1.72–1.85%; Martín-Monge et al., 2017) while the $RmcR_0$% values for S4 (1.92–2.03%) are higher than the R2–4 wells mean vR_0eq % values (1.17–2.04%, μ = 1.65%; Martín-Monge et al., 2017). These differences could be attributed to a difference in the nature of the CM analyzed or their precursors to obtain these equivalents of vitrinite reflectance (kerogen, solid bitumen, methylphenanthrene index). However, when the maturity degree is considered, the two vR_0eq % fall in the same maturity range (Liu et al., 2013) and can thus be considered equivalent. No data was available for Lancer 1 drill core. However, vR_0eq % obtained from fluorescent lamalginite were reported in the Kanpa Formation within Empress 1A drill core (Ghori inStevens and Apak, 1999). Samples from 516.6 to 830.3 m-depth, equivalent to our Lancer 1 samples, have vR_0eq values between 0.52 and 1.00%. These values are in the same range than our $RmcR_0$% for Lancer 1 (0.76–1.01%). These results indicate that Raman reflectance is a fast, robust and non-destructive tool to evaluate the thermal maturity of carbonaceous material and in particular Proterozoic materials, especially if they are at low maturity levels.

Raman geothermometry

Raman spectra and characteristic ratios, as well as $RmcR_0$% values all show a similar evolution of the thermal maturity of the CM contained in samples from the Congo, Taoudeni and Officer basins (Fig. 4).

There is a progressive increase of thermal maturity from the S2–216 sample to the Lancer 1 samples (L1–472 < L1–680 < L1 955), the S3 sample (S3–123), the Congo samples (LU18–312 ≤ KN23–123) and finally the S4 sample (S4–162). This increasing order of maturity is confirmed with the increasing range of temperature estimates.

Temperatures calculated with Kouketsu geothermometer (T(FWHMD1); Eq. 1) and Raman reflectance (T($RmcR_0$%); Eq. 3) are summarized in Figs. 3e, 4 and in Tables 1, 2. Mean temperatures from Kouketsu geothermometer are ranging from 177 to 245 °C (L1–472: 177 ± 9 °C; L1–955: 180 ± 16 °C; L1–680: 183 ± 18 °C; S3–123: 214 ± 9 °C; LU18–312: 225 ± 10 °C; KN23–123: 244 ± 10 °C and S4–162: 245 ± 10 °C). Mean temperatures from $RmcR_0$% (T $RmcR_0$%) also reflect the same trend, with a range between 113 and 199 °C (L1–472: 113 ± 13 °C; L1–680: 144 ± 13 °C; L1–955: 149 ± 16 °C; S3–123: 158 ± 9 °C; LU18–312: 185 ± 7 °C; KN23–123: 190 ± 6 °C and S4–162: 199 ± 6 °C).

FWHM-D1 and $RmcR_0$% are correlated (R^2 = 0.643, Fig. 3e); as a consequence, the two Raman-based thermometers show the same order of temperature increase (Fig. 3d,e). Nonetheless, T(FWHM-D1) are always ~50 °C higher than the T($RmcR_0$%) (Fig. 3e, 4). However, Kouketsu et al. (2014) gave an empirical error for their thermometer of ± 30 °C. Taking into account this error, the temperature estimate obtained with this thermometer could enter within the diagenesis domain. This suggests that the temperature achieved in the three basins lies certainly in between the two obtained temperature ranges.

Comparison of methods

As summarize in Fig. 4, Kübler index show that all studied samples have been known a thermal evolution restricted to diagenesis domain, i.e. < 200 °C (Kübler, 1967). This is also confirmed by TAI scale values with the exception of samples from Congo Basin for which values extend beyond diagenesis domain (i.e. up to 250 °C). The temperatures obtained from solid bitumen reflectance, for samples from Congo basin, are ca. 207 °C and correspond to the upper range of the T($RmcR_0$%). For samples from Officer and Taoudeni basins, literature data of vitrinite equivalent (vR_0eq %) from methylphenanthrene index (Martín-Monge et al., 2017) and lamalginite (Ghori inStevens and Apak, 1999), respectively, give also temperatures which are in accordance with the diagenesis domain. Overall, whatever the nature of carbonaceous material (solid bitumen, methylphenanthrene or lamalginite), T(vR_0eq %) are consistent with temperatures from Raman Reflectance T($RmcR_0$%). TAI scale and Kübler index from these different Proterozoic sequences are also compatible with T($RmcR_0$%). By contrast, T(FWHM-D1) give temperatures higher than those of the diagenesis domain for Congo and Taoudeni samples. For Officer samples, T(FWHM-D1) falls into the diagenesis domain with an overestimate of ~50 °C. Relative to conventional techniques cited above, results from T($RmcR_0$%) seem more consistent than those from T(FWHM-D1). However, with the possibility of being measured directly on any unambiguous microfossils, Raman Reflectance excludes the risk of disturbance by inherited minerals which restricts sometime the use of Kübler index (Kübler, 1967). In addition, Raman reflectance is more accurate than the subjective TAI (see Section 3.1 above) and also probably easier to use than solid bitumen reflectance, for which only a homogeneous variety is recommended for thermal history studies (see Section 3.3 above). The Raman reflectance thus appears to be a valuable tool to evaluate the thermal maturity of poorly ordered carbonaceous material at various stages of diagenesis.

Conclusions

Raman spectra measured on microfossils and amorphous organic matter in both extracted kerogen and in situ in thin sections allowed to evaluate the thermal maturity of samples from the three studied Proterozoic sedimentary sequences. We obtain estimates temperatures by using Raman Kouketsu

geothermometry, reflectance geothermometers (Raman reflectance and solid bitumen reflectance), illite crystallinity and Thermal Alteration Index. All these techniques provide consistent range of temperatures except for Raman Kouketsu geothermometry, which gives slightly higher estimates. The consistency of results from one method to another validates the use of Raman reflectance as a robust tool to evaluate the thermal maturity of poorlyorganized (disordered) carbonaceous material from Proterozoic rocks. This technique is well suited at low temperatures (< 300 °C). We also demonstrate that extracted kerogen provides accurate estimates for thermal maturity relative to kerogen in thin section. Thus, our study shows that the rapid and non-destructive Raman measurements on dispersed kerogenous material (microfossils and amorphous organic matter) could be used successfully to quantify the thermal evolution of a sedimentary succession.

Supplementary data to this article can be found online at https://doi.org/10.1016/j.coal.2018.03.007.

Acknowledgements

The authors are grateful to K. Grey (Geological Survey of West Australia, Perth, Australia) for access of the Lancer 1 drill core; to JP Houzay, C. Blanpied and Total S.A. (TOTAL Projets Nouveaux, Paris, France), for access to the S2 drill core; to J. J. Brocks (The Australian National University, Canberra, Australia) and S. W. Poulton (University of Leeds, Leeds, United Kingdom) for access to the samples of the S3 and S4 drill cores; and to The Royal Museum for Central Africa (Tervuren, Belgium) for access to the Kanshi S13B and Lubi drill cores. We also thank D. Macherey for sample preparation and for help during solid bitumen reflectance measurements (RWTH Aachen University, Germany), M. Giraldo and J. Laval (University of Liège, Geology Department, Belgium) for sample preparation and E. Pleuger (University of Liège, UR Geology, Belgium) for help during XRD analyses. This work was supported by the European Research Council Stg ELITE FP7/308074 to B.K.B., Y.C., J.-Y.S., E.J.J. (P.I.); the BELSPO IAP PLANET TOPERS to CF, JB, E.J.J. (PI), and the Marie-Curie Cofund program at the University of Liège to M.C.S.

References

Al-Ameri, T., Wicander, R., 2008. An assessment of the gas generation potential of the Ordovician Khabour Formation, Western Iraq. Comun. Geol. 95, 157–166.

Albert-Villanueva, E., Permanyer, A., Tritlla, J., Levresse, G., Salas, R., 2016. Solid hydrocarbons in proterozoic dolomites, taoudeni basin, Mauritania. J. Pet. Geol. 39, 5–27. http://dx.doi.org/10.1111/jpg.12625.

Baludikay, B.K., Storme, J.-Y., Francois, C., Baudet, D., Javaux, E.J., 2016. A diverse and exquisitely preserved organic-walled microfossil assemblage from the MesoNeoproterozoic Mbuji-Mayi Supergroup (Democratic Republic of Congo) and implications for Proterozoic biostratigraphy. Precambrian Res. 281, 166–184. http://dx.doi.org/10.1016/j.precamres.2016.05.017.

Barker, C.E., Pawlewicz, M.J., 1994. Calculation of vitrinite reflectance from thermal histories and peak temperatures. a comparison of methods. ACS Symp. Ser. 570, 216–229.

Begg, G.C., Griffin, W.L., Natapov, L.M., O'Reilly, S.Y., Grand, S.P., O'Neill, C.J., Hronsky, J.M.A., Djomani, Y.P., Swain, C.J., Deen, T., Bowden, P., 2009. The lithospheric architecture of Africa: seismic tomography, mantle petrology, and tectonic evolution The lithospheric architecture of Africa. Geosphere 5, 23–50.

Beghin, J., Storme, J.-Y., Blanpied, C., Gueneli, N., Brocks, J.J., Poulton, S.W., Javaux, E.J., 2017. Microfossils from the late Mesoproterozoic – early Neoproterozoic Atar/El Mreïti Group, Taoudeni Basin, Mauritania, northwestern Africa. Precambrian Res. 291, 63–82. http://dx.doi.org/10.1016/j.precamres.2017.01.009.

Bertrand, R., 1990. Correlations among the reflectances of vitrinite, chitinozoans, graptolites and scolecodonts. Org. Geochem. 15, 565–574.

Bertrand, R., Héroux, Y., 1987. Chitinozoan, graptolite, and scolecodont reflectance as an alternative to vitrinite and pyrobitumen reflectance in Ordovician and Silurian strata, Anticosti Island, Quebec, Canada. Am. Assoc. Pet. Geol. Bull. 71, 951–957.

Beyssac, O., Goffé, B., Chopin, C., Rouzaud, J.N., 2002. Raman spectra of carbonaceous material in metasediments: a new geothermometer. J. Metamorph. Geol. 20, 859–871. http://dx.doi.org/10.1046/j.1525-1314.2002.00408.x.

Beyssac, O., Goffé, B., Petitet, J.P., Froigneux, E., Moreau, M., Rouzaud, J.N., 2003. On the characterization of disordered and heterogeneous carbonaceous materials by Raman spectroscopy. Spectrochim. Acta A Mol. Biomol. Spectrosc. 59, 2267–2276. http://dx.doi.org/10.1016/S1386-1425(03)00070-2.

Cahen, L., Snelling, N.J., Delhal, J., Vail, J.R., Bonhomme, M., Ledent, D., 1984. The Geochronology and Evolution of Equatorial Africa. Clarendon, Oxford, pp. 512.

Camacho, A., Armstrong, R., Davis, D.W., Bekker, A., 2015. Early history of the Amadeus Basin: implications for the existence and geometry of the Centralian Superbasin. Precambrian Res. 259, 232–242. http://dx.doi.org/10.1016/j.precamres.2014.12. 004.

Cathelineau, M., Olivier, R., Nieva, D., Garfias, A., 1985. Mineralogy and distribution of hydrothermal mineral zones in Los Azufres (Mexico) geothermal field. Geothermics 14, 49–57.

Cotter, K.L., 1997. Neoproterozoic microfossils from the Officer Basin, Western Australia. Alcheringa 21, 247–270. http://dx.doi.org/10.1080/03115519708619166.

Delpomdor, F., Blanpied, C., Virgone, A., Préat, A., 2015. Sedimentology and sequence stratigraphy of the late precambrian carbonates of the mbuji-mayi supergroup in the sankuru-mbuji-mayi-lomami- lovoy basin (Democratic Republic of the Congo). In: De Wit, M.J., Guillocheau, F., De Wit, M.C.J. (Eds.), Geology and Resource Potential of the Congo Basin. Springer-Verlag, Berlin Heidelberg, pp. 59–76. http://dx.doi.org/ 10.1007/978-3-642-29482-2.

Delpomdor, F., Bonneville, S., Baert, K., Préat, A., 2018. An introduction to the Precambrian petroleum system in the Sankuru–Mbuji-May–Lomami–Lovoy Basin, South-Central Democratic Republic of Congo. J. Pet. Geol. 41 (I), 5–27.

Delvaux, D., Barth, A., 2010. African stress pattern from formal inversion of focal mechanism data. Tectonophysics 482, 105–128. http://dx.doi.org/10.1016/j.tecto. 2009.05.009.

Delvaux, D., Fernandez, M., 2015. Petroleum potential of the congo basin. In: de Wit, M., Guillochau, F., de Wit, M.C.J. (Eds.), The Geology and Resource Potential of the Congo Basin. Regional Geology Reviews, Springer, Heidelberg, pp. 371–391. http://dx.doi.org/10.1007/978-3-642-29482-2_18.

Dippel, B., Jander, H., Heintzenberg, J., 1999. NIR FT Raman spectroscopic study of flame soot. Phys. Chem. Chem. Phys. 1, 4707–4712. http://dx.doi.org/10.1039/a904529e.

Du, J., Geng, A., Liao, Z., Cheng, B., 2014. Potential Raman parameters to assess the thermal evolution of kerogen from different pyrolysis experiments. J. Anal. Appl. Pyrolysis 107, 242–249. http://dx.doi.org/10.1016/j.jaap.2014.03.007.

Dunoyer de Segonzac, G., 1969. Les minéraux argileux dans la diagenèse — passage au métamorphisme. Mém. Serv. Carte Géol. Als-Lorr. 29, 1–320.

Espitalié, J., Laporte, J.L., Madec, M., Marquis, F., Leplat, P., Paulet, J., Boutefeu, A., 1977. Méthode rapide de caracterisation des roches mères, de leur potential petrolier et de leur degré d'évolution. Revue de l'Institut français du Pétrole 32, 23–42.

Ferrari, A.C., Robertson, J., 2000. Interpretation of Raman spectra of disordered and amorphous carbon. Phys. Rev. B 61, 14095–14107. http://dx.doi.org/10.1103/ PhysRevB.61.14095.

Ferreiro Mählmann, R., Frey, M., 2012. Standardisation, calibration and correlation of the Kübler-index and the vitrinite/bituminite reflectance: an inter-laboratory and field related study. Swiss J. Geosci. 105, 153–170.

Ferreiro Mählmann, R., Bozkaya, Ö., Potel, S., Le Bayon, R., Šegvić, B., Nieto, F., 2012. The pioneer work of Bernard Kübler and Martin Frey in very low-grade metamorphic terranes: paleo-geothermal potential of variation in Kübler-index/organic matter reflectance correlations. A review. Swiss J. Geosci. 105, 121–152.

François, C., Baludikay, B.K., Storme, J.-Y., Baudet, D., Paquette, J.L., Fialin, M., Javaux, E.J., 2017. Contributions of U-Th-Pb dating on the diagenesis and sediment sources of the lower group (BI) of the Mbuji-Mayi Supergroup (Democratic Republic of Congo). Precambrian Res. 298, 202–219. http://dx.doi.org/10.1016/j.precamres.2017.06. 012.

Grey, K., 1999. A modified palynological preparation technique for the extraction of large Neoproterozoic acanthomorph acritarchs and other acid-insoluble microfossils. In: Western Australia Geological Survey, Record 1999/10, pp. 23.

Grey, K., Hill, A.C., Calver, C., 2011. Chapter 8 Biostratigraphy and stratigraphic subdivision of Cryogenian successions of Australia in a global context. Geol. Soc. Lond. Mem. 36, 113–134.

Guggenheim, S., Bain, D.C., Bergaya, F., Brigatti, M.F., Drits, V.A., Eberl, D.D., Formoso, M.L.L., Galán, E., Merriman, R.J., Peacor, D.R., Stanjek, H., Watanabe, T., 2002. Report of the Association Internationale pour L'étude des Argiles (AIPEA) Nomenclature Committee for 2001: Order, disorder and crystallinity in phyllosilicates and the use of the "crystallinity index". Clay Clay Miner. 50, 406–409. http://dx.doi.org/10.1346/000986002760833783.

Hartkopf-Fröder, C., Königshof, P., Littke, R., Schwarzbauer, J., 2015. Optical thermal maturity parameters and organic geochemical alteration at low grade diagenesis to anchimetamorphism: a review. Int. J. Coal Geol. 150-151, 74–119.

Jaboyedoff, M., Kübler, B., Sartori, M., Thélin, P., 2000. Basis for meaningful illite crystallinity measurements: an example from the Swiss Prealps. Bull. suisse Minér. Pétrogr. 80, 75–83.

Jaboyedoff, M., Bussy, F., Kübler, B., Thélin, P., 2001. Illite crystallinity revisited. Clay Clay Miner. 49 (2), 156–167.

Jacob, H., 1989. Classification, structure, genesis and practical importance of natural solid oil bitumen ("migrabitumen"). Int. J. Coal Geol. 11, 65–79. http://dx.doi.org/ 10.1016/0166-5162(89)90113-4.

Jasper, K., Krooss, B.M., Flajs, G., Hartkopf-Fröder, C., Littke, R., 2009. Characteristics of type III kerogen in coal-bearing strata from the Pennsylvanian (Upper Carboniferous) in the Ruhr Basin, Western Germany: comparison of coals, dispersed organic matter, kerogen concentrates ans coal-mineral mixtures. Int. J. Coal Geol. 80, 1–19.

Javaux, E.J., Marshall, C.P., Bekker, A., 2010. Organic-walled microfossils in 3.2-billionyear-old shallow-marine siliciclastic deposits. Nature 463, 934–938.

Kadima, E., Delvaux, D., Sebagenzi, S.N., Tack, L., Kabeya, M., 2011a. Structure and geological history of the Congo Basin: an integrated interpretation of gravity, magnetic and reflection seismic data. Basin Res. 23 (5), 499–527. http://dx.doi.org/10.1111/j.1365-2117.2011.00500.x.

Kadima, E.K., Sebagenzi, S.M.N., Lucazeau, F., 2011b. A Proterozoic-rift origin for the structure and evolution of the cratonic Congo Basin. Earth Planet. Sci. Lett. 304, 240–250. http://dx.doi.org/10.1016/j.epsl.2011.01.037.

Kouketsu, Y., Mizukami, T., Mori, H., Endo, S., Aoya, M., Hara, H., Nakamura, D., Wallis, S., 2014. A new approach to develop the Raman carbonaceous material geothermometer for low-grade metamorphism using peak width. Island Arc 23, 33–50. http://dx.doi.org/10.1111/iar.12057.

Kübler, B., 1964. Les argiles, indicateurs de métamorphisme. 19. Revue de l'Institut Francaise du Petrole, pp. 1093–1112.

Kübler, B., 1967. La cristallinité de l'illite et les zones tout à fait supérieures du métamorphisme. In: Etages tectoniques-Colloques Neuchâtel, 18–21 Avril 1967, pp. 105–122.

Kübler, B., Jaboyedoff, M., 2000. Illite crystallinity. Comptes Rendus l'Académie Sci. Ser. IIa Sci. la Terre des Planétes 331, 75–89.

Lahfid, A., Beyssac, O., Deville, E., Negro, F., Chopin, C., Goffé, B., 2010. Evolution of the Raman spectrum of carbonaceous material in low-grade metasediments of the Glarus Alps (Switzerland). Terra Nova 22, 354–360. http://dx.doi.org/10.1111/j.13653121.2010.00956.x.

Lahondère, D., Thiéblemont, D., Goujou, J.C., Roger, J., Moussine-Pouchkine, A., Le Métour, J., Cocherie, A., Guerrot, C., 2003. Notice explicative des cartes géologiques et gîtologiques à 1/200 000 et 1/500 000 du nord de la Mauritanie. Vol. 1.

Landis, C.R., Castaño, J.R., 1995. Maturation and bulk chemical properties of a suite of solid hydrocarbons. Org. Geochem. 22, 137–149. http://dx.doi.org/10.1016/01466380(95)90013-6.

Littke, R., Urai, J.L., Uffmann, A.K., Risvanis, F., 2012. Reflectance of dispersed vitrinite in Palaeozoic rocks with and without cleavage: implications for burial and thermal history modeling in the Devonian of Rursee area, northern Rhenish Massif, Germany. Int. J. Coal Geol. 89, 41–50.

Liu, D.H., Xiao, X.M., Tian, H., Min, Y.S., Zhou, Q., Cheng, P., Shen, J.G., 2013. Sample maturation calculated using Raman spectroscopic parameters for solid organics: methodology and geological applications. Chin. Sci. Bull. 58, 1285–1298. http://dx. doi.org/10.1007/s11434-012-5535-y.

Lucazeau, F., Armitage, J., Kadima Kabongo, E., 2015. Thermal Regime and Evolution of the Congo Basin as an Intracratonic Basin. In: De Wit, M.J., Guillocheau, F., De Wit, M.C.J. (Eds.), Geology and Resource Potential of the Congo Basin. Springer-Verlag, Berlin Heidelberg, pp. 229–244. http://dx.doi.org/10.1007/978-3-642-29482-12.

Lünsdorf, N.K., Dunkl, I., Schmidt, B.C., Rantitsch, G., von Eynatten, H., 2014. Towards a higher comparability of geothermometric data obtained by Raman spectroscopy of carbonaceous material. Part 1: evaluation of biasing factors. Geostand. Geoanal. Res. 38 (1), 73–94.

Marshall, C.P., Javaux, E.J., Knoll, A.H., Walter, M.R., 2005. Combined micro-Fourier transform infrared (FTIR) spectroscopy and micro-Raman spectroscopy of Proterozoic acritarchs: a new approach to Palaeobiology. Precambrian Res. 138, 208–224. http://dx.doi.org/10.1016/j.precamres.2005.05.006.

Martín-Monge, A., Baudino, R., Gairifo-Ferreira, L.M., Tocco, R., Badali, M., Soriano, S., El Hafiz, N., Hernán-Gómez, J., Chacón, B., Brisson, I., Grammatico, G., Varadé, R., Abdallah, H., 2017. An Unusual Proterozoic Petroleum Play in Western Africa: The Atar Group Carbonates (Taoudeni Basin, Mauritania). 438 Geological Society Special Publications (39pp). https://doi.org/10.1144/SP438.5.

Moore, D.M., Reynolds, R.C., 1997. X-Ray Diffraction and the Identification and Analysis of Clay Minerals, 2nd ed. Oxford University Press, Oxford, New York.

Mory, A., Haines, P., 2005. Gswa Lancer 1 Well Completion Report (Interpretive Papers) Officer and Gunbarrel Basins Western Australia. In: Geological Survey of Western Australia, Theatre Record 2005/4, pp. 90.

Nemanich, R.J., Solin, S.A., 1979. First- and second-order Raman scattering from finitesized crystals of graphite. Phys. Rev. B 20, 392–401.

Pasteris, J.D., Wopenka, B., 2003. Necessary, but not sufficient: Raman identification of disordered carbon as a signature of ancient life. Astrobiology 3, 727–738. http://dx.doi.org/10.1089/153110703322736051.

Peters, K.E., 1986. Guidelines for evaluating petroleum source rock using programmed pyrolysis. Am. Assoc. Pet. Geol. Bull. 70, 318–329.

Peters, K.E., Cassa, M.R., 1994. Applied source rock geochemistry. In: Magoon, L.B., Dow, W.G. (Eds.), The Petroleum System–from Source to Trap: AAPG Memoir. 60. pp. 93–120.

Quirico, E., Rouzaud, J.N., Bonal, L., Montagnac, G., 2005. Maturation grade of coals as revealed by Raman spectroscopy: progress and problems. Spectrochim. Acta - Part A Mol. Biomol. Spectrosc. 61, 2368–2377. http://dx.doi.org/10.1016/j.saa.2005.02. 015.

Radke, M., Welte, D.H., 1983. The Methylphenanthrene Index (MPI): a maturity parameter based on aromatic hydrocarbons. In: Bjorøy, M. (Ed.), Advances in Organic Geochemistry. Wiley, Chichester, pp. 504–512.

Rahl, J.M., Anderson, K.M., Brandon, M.T., Fassoulas, C., 2005. Raman spectroscopic carbonaceous material thermometry of low-grade metamorphic rocks: calibration and application to tectonic exhumation in Crete, Greece. Earth Planet. Sci. Lett. 240, 339–354. http://dx.doi.org/10.1016/j.epsl.2005.09.055.

Raucq, P., 1970. Nouvelles acquisitions sur le Système de la Bushimay. Ann. Mus. Roy. Congo belge, Tervuren (Belgique), série in-8. Sci. Géol. 69, 156.

Riediger, C.L., 1993. Solid bitumen reflectance and Rock-Eval Tmax as maturation indices: an example from the "Nordegg Member", Western Canada Sedimentary Basin. Int. J. Coal Geol. 22, 295–315. http://dx.doi.org/10.1016/0166-5162(93)90031-5. Rooney, A.D., Selby, D., Houzay, J.P., Renne, P.R., 2010. Re-Os geochronology of a Mesoproterozoic sedimentary succession, Taoudeni basin, Mauritania: Implications for basin-wide correlations and Re-Os organic-rich sediments systematics. Earth Planet. Sci. Lett. 289, 486–496. http://dx.doi.org/10.1016/j.epsl.2009.11.039.

Sachse, V.F., Delvaux, D., Littke, R., 2012. Petrological and geochemical investigations of potential source rocks of the Central Congo Basin, Democratic Republic of Congo. Am. Assoc. Pet. Geol. Bull. 96, 245–275. http://dx.doi.org/10.1306/07121111028.

Sauerer, B., Craddock, P.R., Aljohani, M.D., Alsamadony, K.L., Abdallah, W., 2017. Fast and accurate shale maturity determination by Raman spectroscopy measurement with minimal sample preparation. Int. J. Coal Geol. http://dx.doi.org/10.1016/j. coal.2017.02.008.

Schiffbauer, J.D., Wallace, A.F., Hunter, J.L., Kowalewski, M., Bodnar, R.J., Xiao, S., 2012. Thermally-induced structural and chemical alteration of organic-walled microfossils: an experimental approach to understanding fossil preservation in metasediments. Geobiology 10, 402–423. http://dx.doi.org/10.1111/j.1472-4669.2012. 00332.x.

Schoenherr, J., Littke, R., Urai, J.L., Kukla, P.A., Rawahi, Z., 2007. Polyphase thermal evolution in the Infra-Cambrian Ara Group (South Oman Salt Basin) as deduced by maturity of solid reservoir bitumen. Org. Geochem. 38, 1293–1318. http://dx.doi.org/10.1016/j.orggeochem.2007.03.010.

Sforna, M.C., van Zuilen, M.A., Philippot, P., 2014. Structural characterization by Raman hyperspectral mapping of organic carbon in the 3.46 billion-year-old Apex chert, Western Australia. Geochim. Cosmochim. Acta 124, 18–33. http://dx.doi.org/10.1016/j.gca.2013.09.031.

Staplin, F.L., 1969. Sedimentary organic matter, organic metamorphism, and oil and gas occurrence. Bull. Can. Petrol. Geol. 17, 47–66.

Staplin, F.L., 1977. Interpretation of thermal history from color of particulate organic matter: a review. Palynology 1, 9–18. http://dx.doi.org/10.2307/3687312.

Stevens, M.K., Apak, S.N., 1999. GSWA Empress 1 and 1A well completion report Yowalga Sub-basin, Officer Basin Western Australia. In: Geol. Surv. West. Aust. Rec. 1999/4, (118pp).

Szczepanik, Z., 1997. Preliminary results of thermal alteration investigations of the Cambrian acritarchs in the Holy Cross Mts. Geol. Q. 41, 257–264.

Taylor, G.H., Teichmüller, M., Davis, A., Diessel, C.F.K., Littke, R., Robert, P., 1998. Organic Petrology. Borntraeger, Stuttgart (704pp).

Walter, M.R., Veevers, J.J., Calver, C.R., Grey, K., 1995. Neoproterozoic stratigraphy of the Centralian Superbasin, Australia. Precambrian Res. 73, 173–195. http://dx.doi.org/10.1016/0301-9268(94)00077-5.

Warr, L.N., Ferreiro Mählmann, R., 2015. Recommendations for Kübler Index standardization. Clay Miner. 50, 283–286.

Warr, L.N., Rice, A.H.N., 1994. Inter-laboratory standardization and calibration of clay mineral crystallinity and crystallite size data. J. Metamorph. Geol. 12, 141–152.

Weaver, E.W., 1960. Possible uses of clay minerals in search for oil. Bull. Am. Assoc. Pet. Geol. 44, 1505–1518.

Wopenka, B., Pasteris, J.D., 1993. Structural characterization of kerogen to granulitefacies graphite: applicability of Raman microprobe spectroscopy. Am. Mineral. 78, 533–557.

Zieger, L., Littke, R., Schwarzbauer, J., 2018. Chemical and structural changes in vitrinites and megaspores from carboniferous coals during maturation. Int. J. Coal Geol. 185, 91–102. http://dx.doi.org/10.1016/j.coal.2017.10.007.

6.3. Implications sur l'évolution thermique du bassin du Congo

Dans le sondage Kanshi 13B (n = 5) les températures varient de 186°C à 193°C ; de 233°C à 249°C et 206 °C à 208°C, respectivement pour T (*RmcR₀* %), T (FWHM-D1) et T (% *bR₀*). Ces gammes de températures sont globalement similaires dans les sondages Lubi S70 (n = 8) et Kafuku 15 (n = 3). Cependant, l'échantillon LU101-197 du sondage Lubi S70 a enrégistré une température supérieure à 400°C (Table 6.1). Une température aussi élévée au milieu d'une gamme des températures ne dépassant pas 250°C, suggère la présence de matériels carbonés hérités (Figs. 5I et 6.2), des socles encaissants pendant le dépôt de Groupe BI. Le sondage Kanshi 13B recoupe la partie supérieure du Supergroupe de Mbuji-Mayi, tandis que Kafuku 15 et Lubi S70 recoupent la partie inférieure. Si l'on considère un gradient géothermique apparent normal de 25°C/km, la température moyenne déduite de la réflectance Raman enregistrée dans les roches du sondage Kanshi 13B d'environ 190°C correspond à une profondeur d'enfouissement de 7,5 km. Cependant, l'épaisseur maximale de sédiments enregistrée dans le groupe BII est d'environ 1 km. Néanmoins, la présence de particules de vitrinite résédimentées dans le groupe de Lukuga, situées à la limite Est du bassin du Congo, suggère que 3 à 4 km de sédiments carbonifères à dévoniens ont été érodés (*Sachse et al., 2012*) au cours d'une ou deux phases de l'érosion dans la région (*Lucazeau et al., 2015*). Le bassin a connu un affaissement à long terme lié en partie à la relaxation thermique d'une lithosphère épaisse (200–250 km) après le Néoprotérozoïque avec une réactivation possible pendant la période du Karoo (environ 320 Ma). Les sources de chaleur externes pourraient également être prises en compte pour expliquer la différence entre la température enregistrée et celle déduite de l'épaisseur des sédiments. Par exemple, la mise en place de roche volcaniques ave dans les régions de Mbuji-Mayi et de Lomami survenue pendant le Mésoprotérozoïque, aurait pu affecter l'histoire thermique (*Cahen et al., 1984; Delpomdor et al., 2015*). Un métamorphisme de faible intensité enregistré dans la zone de Lomami dans la dolérite (structures SC, faciès des schistes verts à environ 400 km) et dans les laves surmontant le Supergroupe de Mbuji-Mayi (faciès pumpelleyite) doit également être pris en compte. Ainsi, le bassin du Congo a eu une longue histoire d'accumulation de sédiments, d'activités tectoniques et d'érosion depuis le Mésoprotérozoïque (*Kadima et al., 2011* et références y figurant) et est toujours actif sur le plan tectonique (*Delvaux and Barth 2010*), ce qui a fortement perturbée l'histoire thermique.

Table 6.1. Compilation des températures moyennes calculées à partir des paramètres spectraux Raman, de la réflectance du bitume solide ainsi que l'échelle TAI et l'index de Kübler pour tous les échantillons (kérogène isolé et lame mince).

		Données de bitume solide				Températures calculées										Données XRD	
N° éch. - profondeur	**Préparation**	***bR$_o$ %***		***vR$_o$ eq %***		**T*peak vR$_o$ eq %*(°C)**		**T*peak RmcR$_o$ %* (°C)**		**T° FWHMD1 (°C)**		**T° R2 (°C)**		**TOC (wt%)**	**Echelle TAI**	**Kübler index (Δ°2θ)**	**KI domaine**
		$\overline{X}$	**1σ**	$\overline{X}$	**1σ**	$\overline{X}$	**1σ**	$\overline{X}$	**1σ**	$\overline{X}$	**1σ**	$\overline{X}$	**1σ**				
KN31-114	Kérogène isolé	–	–	–	–	–	–	193	4	249	7	–	–			–	–
KN23-123	Kérogène isolé	2.28	0.16	2.46	0.15	208	5	186	7	244	9	–	–	0.4	3 / 3+	0.82	Diagenèse
	lame mince							196	8	243	13	–	–				
KN20a-162	Kérogène isolé	–	–	–	–	–	–	192	5	246	10	–	–			O.86	Diagenèse
KN34-255	Kérogène isolé	–	–	–	–	–	–	187	6	233	9	–	–			0.59	Diagenèse
KN20b-268	Kérogène isolé	–	–	–	–	–	–	192	8	244	11	–	–	1.5			
KA19-16	Kérogène isolé	–	–	–	–	–	–	211	1	254	7	–	–	0.9		0.70	Diagenèse
KA51-23	Kérogène isolé	–	–	–	–	–	–	175	11	215	21	–	–				
KA65A-28	Kérogène isolé	–	–	–	–	–	–	200	20	243	17	–	–			–	–
LU187-73	lame mince	–	–	–	–	–	–	198	7	211	36	–	–	1.1		–	–
LU186-74	Kérogène isolé	–	–	–	–	–	–	194	8	222	16	–	–	1.9		–	–
LU67-83	Kérogène isolé	–	–	–	–	–	–	201	6	228	22	–	–			–	–
LU157-112	Kérogène isolé	–	–	–	–	–	–	173	7	207	12	–	–			–	–
LU57-120	Kérogène isolé	–	–	–	–	–	–	172	7	229	11	–	–			–	–

LU101-197*	Kérogène isolé	–	–	–	–	–	–	–	–	–	–	440*	23	0.2		–	–
LU69-257	lame mince	–	–	–	–	–	–	203	6	220	21			0.1			–
LU18-312	Kérogène isolé	2.22	0.15	2.41	0.14	206	5	185	7	236	7			0.5	3+ / 4-	0.57	Diagenèse
	lame mince							190	8	220	14						

*échantillon avec du matériel carboné graphitisé et pour lequel le géothermomètre de Beyssac (*2002*) a été utilisé pour le calcul des températures.

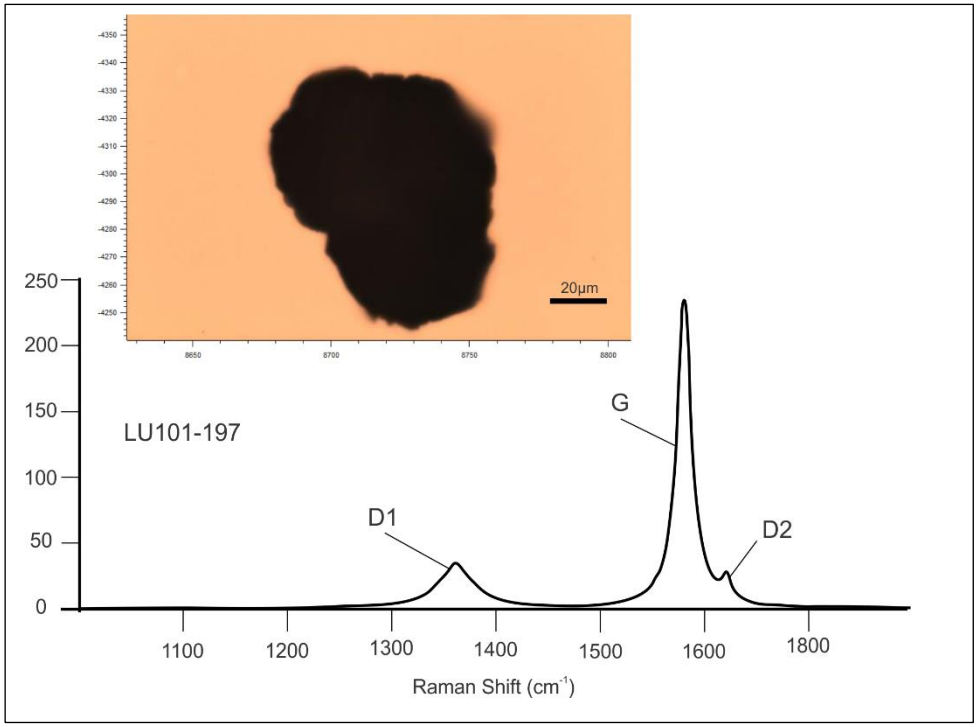

Fig.6.2. Photographie d'un matériel carboné graphitisé contenu dans l'échantillon LU101-19 et son spectre Raman avec trois pics, D1, D2 et G (bien développé)

Chapitre 7 : Conclusions et perspectives

Cette étude avait pour objectif principal de contribuer à notre compréhension de l'évolution des premiers eucaryotes dans la longue histoire de la vie sur notre chère planète Terre. Le choix du Supergroupe de Mbuji-Mayi, situé en Afrique Centrale (en République Démocratique du Congo) et daté de la fin du Mésoprotérozoïque (~ 1065 à ~ 1000 Ma), se justifiait pour deux raisons :

(1) le continent africain, en dépit de l'étendue de ses dépôts précambriens, ne fournissait que des données très éparses qui soient utiles et intéressantes pour la communauté des paléobiogéologues dans leur travail de reconstitution et de compréhension de l'histoire de la vie en général, et des eucaryotes en particulier ;

(2) Daté de la fin du Mésoprotérozoïque, cette séquence sédimentaire s'est mise en place pendant une période charnière où interviennent plusieurs changements environnementaux et biologiques (entre autres, la stratification redox des eaux océaniques, eucaryovorie – prédation des eucaryotes sur les eucaryotes, l'acquisition de la photosynthèse eucaryote) qui permettront et faciliteront la grande diversification des eucaryotes dans le Néoprotérozoïque.

Cet objectif principal a été partitioné en plusieurs objectifs secondaires. La caractérisation de l'assemblage de microfossiles à paroi organique a révélé un état de préservation en général excellent, plus diversifié que le suggéraient les prémiers études (*Baudet, 1987 ; Maithy, 1975*), et comportant 49 taxa, parmi lesquels dominent les procaryotes avec 28 taxa. De plus cet assemblage est semblable aux assemblages contemporains mondiaux, indiquant que le bassin marin dans lequel s'est déposé le Supergroupe de Mbuji-Mayi était connecté aux autres bassins océaniques. Cette étude a également permis de raffiner la distribution stratigraphique de certains taxa, permettant ainsi d'améliorer la biostratigraphie du Protérozoïque. Les eucaryotes unicellulaires et multicellulaires consistent en 11 taxa reconnus ailleurs dans le monde, Il s'agit de *Germinosphaera bispinosa, Jacutianema solubila, Lophosphaeridium granulatum, Pterospermopsimorpha insolita, P. pileiformis, cf. Tappania plana, Trachyhytrichosphaera aimika, T. botula, Valeria elongata, V. lophostriata* et un acanthomorphe non nommé. *Trachyhytrichosphaera aimika* est le fossile index de la transition Méso. –Néoprotérozoïque, dont la présence a été raportée, grâce à ce travail, pour la première fois en Afrique Centrale. Les 10 autres taxa sont soit des eucaryotes soit des procaryotes. La

grande diversification des premiers eucaryotes au début du Néoprotérozoïque est généralement estimée vers 0,8 Ga (*Cohen and Riedman 2018; Knoll et al., 2006a Porter & Knoll, 2000; Porter et al., 2003*), mais ce travail de these et quelques récemment (*Beghin et al., 2017 ; Gibson et al., 2018 ; Javaux and Knoll, 2016 ; Loron et al., 2018a, b*) permettent de la reculer vers 1,2–1,05 Ga (fin Mésoprotérozoïque). L'âge de la prédation (eukaryovry), considérée comme un des facteurs ayant contribué à la diversification des premiers eucaryotes, vient d'être aussi reculé à la fin du Mésoprotérozïque (*Loron et al., 2018b*). Les analyses de la spéciation du fer ont révélé une stratification des eaux, en milieux oxique, anoxique ferrugineux et anaoxique sulfidique (euxinique), bien que le milieu oxique prédominait tant temporellement que spatialement dans les eaux de surface du bassin peu profond. Les eucaryotes semblent prédominer dans les environements proximaux anoxiques, mais sans connaissance de leur métabolisme, il est difficile d'affirmer s'ils étaient anaérobies ou aérobies. Leur présence abondante dans ces milieus anoxiques pourrait tout simplement indiquer de meilleures conditions de préservation.

La chimiostratigraphie du carbone ($\delta^{13}C_{carb}$) a enregistré trois excursions positives et une excursion négative sans lien avec l'anomalie Bitter Springs comme suggéré précédemment dans d'autres travaux, et bien qu'il y ait des échantillons pour lesquels la signature marine a été altérée par des événements post-dépôt, la majorité des carbonates du Supergroupe de Mbuji-Mayi a enregistré le signal isotopique des carbonates du Mésoprotérozoïque. Ces variations semblent semblables avec les variations contemporaines enregistrées ailleurs dans le monde mais des analyses géochimiques supplémentaires sont nécessaires pour permettre une bonne interprétation

La géothermométrie Raman sur les microfossiles et la matière organique amorphe (AOM), à la fois dans le kérogène isolé et in situ en la lame mince, a permis l'évaluation thermique des roches hôtes. Cependant des valeurs de la réflectance Raman ($RmcR_0$ %, équivalent de vitrinite réflectance VR_0 % pour des roches qui en sont dépourvues) supérieures à 1,3% et des températures (T°$RmcR_0$ %) allant jusqu'à 211°C pour quelques échantillons (16) analysés ne permettent pas de donner un avis tranché quant au potentiel pétrolier de ce bassin. Ces analyses ont été cependant utiles pour mieux comprendre la préservation du kérogène, y compris des microfossiles, et ont permis de montrer que l'extraction acide du kérogène ne modifie pas son signal Raman et donc probablement sa chimie.

A l'issue de cette étude, quelques axes qui mériteraient des approfondissements apparaissent. Des analyses géochimiques détaillées (majeurs, mineur et traces) seraient nécessaires pour permettre l'interprétation des résultats de la chimiostratigraphie et leur comparaison aved des événements contemporains dans d'autres succesions. De plus pour élucider l'identité de microfossiles de morphologie simple au sein des procaryotes et eucaryotes, des micro-analyses ultrastructurales et microchimiques (*Javaux and Marshall, 2006*) seraient nécessaires. Idéalement, de nouveaux échantillonnages permettraient de compléter les informations sur les niveaux du Supergroupe de Mbuji-Mayi qui n'étaient pas disponibles dans les sondages. Toutes ces informations complémentaires permettraient de mieux déchiffrer la paléoécologie, la paléobiologie et les causes de la diversification des premiers eucaryotes.

Références bibliographiques

Agić, Heda, Małgorzata Moczydłowska, and Leiming Yin. 2017. “Diversity of Organic-Walled Microfossils from the Early Mesoproterozoic Ruyang Group, North China Craton – A Window into the Early Eukaryote Evolution.” *Precambrian Research* 297: 101–30. doi:10.1016/j.precamres.2017.04.042.

Algeo, T. J., and N. Tribovillard. 2009. “Environmental Analysis of Paleoceanographic Systems Based on Molybdenum-Uranium Covariation.” *Chemical Geology* 268 (3–4). Elsevier B.V.: 211–25. doi:10.1016/j.chemgeo.2009.09.001.

Algeo, Thomas J., and Timothy W. Lyons. 2006. “Mo-Total Organic Carbon Covariation in Modern Anoxic Marine Environments: Implications for Analysis of Paleoredox and Paleohydrographic Conditions.” *Paleoceanography* 21 (1). doi:10.1029/2004PA001112.

Algeo, Thomas J., and Harry Rowe. 2012. “Paleoceanographic Applications of Trace-Metal Concentration Data.” *Chemical Geology* 324–325. Elsevier B.V.: 6–18. doi:10.1016/j.chemgeo.2011.09.002.

Allison, Carol Wagner, and Stanley M Awramik. 1989. “Organic-Walled Microfossils from Earliest Cambrian or Latest Proterozoic Tindir Group Rocks, Northwest Canada.” *Precambrian Research* 43 (4): 253–94. doi:http://dx.doi.org/10.1016/0301-9268(89)90060-0.

Allwood, Abigail C., Malcolm R. Walter, Ian W. Burch, and Balz S. Kamber. 2007. “3.43 Billion-Year-Old Stromatolite Reef from the Pilbara Craton of Western Australia: Ecosystem-Scale Insights to Early Life on Earth.” *Precambrian Research* 158 (3–4): 198–227. doi:10.1016/j.precamres.2007.04.013.

Allwood, Abigail C, John P Grotzinger, Andrew H Knoll, Ian W Burch, Mark S Anderson, Max L Coleman, and Isik Kanik. 2009. “Controls on Development and Diversity of Early Archean Stromatolites.” *Proceedings of the National Academy of Sciences of the United States of America* 106 (24): 9548–55. doi:10.1073/pnas.0903323106.

Allwood, Abigail C, Malcolm R Walter, Balz S Kamber, Craig P Marshall, and Ian W Burch. 2006. “Stromatolite Reef from the Early Archaean Era of Australia.” *Nature* 441 (7094): 714–18. doi:10.1038/nature04764.

Anbar, A. D. 2004. “Molybdenum Stable Isotopes: Observations, Interpretations and Directions.” *Reviews in Mineralogy and Geochemistry* 55 (1): 429–54. doi:10.2138/gsrmg.55.1.429.

Anbar, a D, and a H Knoll. 2002. “Proterozoic Ocean Chemistry and Evolution: A Bioinorganic Bridge?” *Science (New York, N.Y.)* 297 (5584): 1137–42. doi:10.1126/science.1069651.

Anbar, A D, and A H Knoll. 2002. “Proterozoic Ocean Chemistry and Evolution: A Bioionorganic Bridge?” *Science* 297 (January 2017): 1137–42. doi:10.1126/science.1069651.

Anbar, Ariel D., and Olivier Rouxel. 2007. “Metal Stable Isotopes in Paleoceanography.” *Annual Review of Earth and Planetary Sciences* 35 (1): 717–46.

doi:10.1146/annurev.earth.34.031405.125029.

Andreeva, E. M. 1966. “Opisanie Iskopaemykh Spor Predstaviteley Bryophyta, Lycopsida, Sphenopsida, Filicinae i Rastitelnykh Mikrofossily Neyasnogo Sistematicheskogo Polozheniya.” In *Pokorovskaya, I.M (Ed.), Paleopalinologiya, Volume 1. VSEGEI, Trudy*, Nedra, 141:114–35. Leningrad.

Arndt, Nicholas T., and Euan G. Nisbet. 2012. “Processes on the Young Earth and the Habitats of Early Life.” *Annual Review of Earth and Planetary Sciences* 40 (1): 521–49. doi:10.1146/annurev-earth-042711-105316.

Arnold, G L, A D Anbar, J Barling, and T W Lyons. 2004. “Molybdenum Isotope Evidence for Widespread Anoxia in Mid-Proterozoic Oceans Published by : American Association for the Advancement of Science Stable URL : Http://Www.Jstor.Org/Stable/3836616 The Early Evolution of the Tetrapod Humerus.” *Science* 304 (5667): 87–90.

Arouri, Khaled R, Paul F Greenwood, and Malcolm R Walter. 2000. “Biological Affinities of Neoproterozoic Acritarchs from Australia: Microscopic and Chemical Characterisation.” *Organic Geochemistry* 31 (1): 75–89. doi:http://dx.doi.org/10.1016/S0146-6380(99)00145-X.

Asael, Dan, François L H Tissot, Christopher T. Reinhard, Olivier Rouxel, Nicolas Dauphas, Timothy W. Lyons, Emmanuel Ponzevera, Céline Liorzou, and Sandrine Chéron. 2013. “Coupled Molybdenum, Iron and Uranium Stable Isotopes as Oceanic Paleoredox Proxies during the Paleoproterozoic Shunga Event.” *Chemical Geology* 362. Elsevier B.V.: 193–210. doi:10.1016/j.chemgeo.2013.08.003.

Baludikay, B.K., J.-Y. Storme, C. François, D. Baudet, and E.J. Javaux. 2016. “A Diverse and Exquisitely Preserved Organic-Walled Microfossil Assemblage from the Meso–Neoproterozoic Mbuji-Mayi Supergroup (Democratic Republic of Congo) and Implications for Proterozoic Biostratigraphy.” *Precambrian Research* 281. The Authors: 166–84. doi:10.1016/j.precamres.2016.05.017.

Baludikay, Blaise K., Camille François, Marie Catherine Sforna, Jérémie Beghin, Yohan Cornet, Jean-Yves Storme, Nathalie Fagel, et al. 2018. “Raman Microspectroscopy, Bitumen Reflectance and Illite Crystallinity Scale: Comparison of Different Geothermometry Methods on Fossiliferous Proterozoic Sedimentary Basins (DR Congo, Mauritania and Australia).” *International Journal of Coal Geology* 191 (December 2017). Elsevier: 80–94. doi:10.1016/j.coal.2018.03.007.

Barker, Charles E, and M. J. Pawlewicz. 1994. “Calculation of Vitrinite Reflectance from Thermal Histories and Peak Temperatures.” *Vitrinite Reflectance as a Maturity Parameter* 570 (14): 216–29. doi:doi:10.1021/bk-1994-0570.ch014\r10.1021/bk-1994-0570.ch014.

Barling, J. and Anbar, A.D. 2004. “Molybdenum Isotope Fractionation during Adsorption by Manganese Oxides.” *Earth and Planetary Science Letters* 217: 315–29.

Barling, J., G. L. Arnold, and A. D. Anbar. 2001. “Natural Mass-Dependent Variations in the Isotopic Composition of Molybdenum.” *Earth and Planetary Science Letters* 193 (3–4): 447–57. doi:10.1016/S0012-821X(01)00514-3.

Bartley, Julie K., and Linda C. Kah. 2004. “Marine Carbon Reservoir, Corg-Ccarb Coupling, and the Evolution of the Proterozoic Carbon Cycle.” *Geology* 32 (2): 129–32. doi:10.1130/G19939.1.

Bartley, Julie K, Linda C Kah, Julie L McWilliams, and Alice F Stagner. 2007. “Carbon Isotope Chemostratigraphy of the Middle Riphean Type Section (Avzyan Formation, Southern Urals, Russia): Signal Recovery in a Fold-and-Thrust Belt.” *Chemical Geology* 237 (1–2): 211–32. doi:http://dx.doi.org/10.1016/j.chemgeo.2006.06.018.

Bartley, Julie K, Mikhail A Semikhatov, Alan J Kaufman, Andrew H Knoll, Michael C Pope, and Stein B Jacobsen. 2001. “Global Events across the Mesoproterozoic–Neoproterozoic Boundary: C and Sr Isotopic Evidence from Siberia.” *Precambrian Research* 111 (1–4): 165–202. doi:http://dx.doi.org/10.1016/S0301-9268(01)00160-7.

Baudet, D. 1987. “Implications of a Palynological Study in the Upper Precambrian from Eastern Kasai and Northwestern Shaba, Zaire.” *Geological Journal* 22. John Wiley & Sons Ltd: 121–37. http://dx.doi.org/10.1002/gj.3350220611.

Beard, Brian L., Clark M. Johnson, Joseph L. Skulan, Kenneth H. Nealson, Lea Cox, and Henry Sun. 2003. “Application of Fe Isotopes to Tracing the Geochemical and Biological Cycling of Fe.” *Chemical Geology* 195 (1–4): 87–117. doi:10.1016/S0009-2541(02)00390-X.

Beard, Brian L., Clark M. Johnson, Karen L. Von Damm, and Rebecca L. Poulson. 2003. “Iron Isotope Constraints on Fe Cycling and Mass Balance in Oxygenated Earth Oceans.” *Geology* 31 (7): 629–32. doi:10.1130/0091-7613(2003)031<0629:IICOFC>2.0.CO;2.

Beghin, J-Y., Storme, C., Blanpied, N., Gueneli, J., Brocks, S.W.,Poulton, E.J., Javaux. 2017. “Microfossils from the Late Mesoproterozoic – Early Neoproterozoic Atar/El Mreïti Group, Taoudeni Basin, Mauritania, Northwestern Africa.” *Precambrian Research* 291: 63–82. doi:doi.org/10.1016/j.precamres.2017.01.009.

Beghin, Jérémie, Romain Guilbaud, Simon W. Poulton, Nur Gueneli, Jochen J. Brocks, Jean Yves Storme, Christian Blanpied, and Emmanuelle J. Javaux. 2017. “A Palaeoecological Model for the Late Mesoproterozoic – Early Neoproterozoic Atar/El Mreïti Group, Taoudeni Basin, Mauritania, Northwestern Africa.” *Precambrian Research* 299 (July). Elsevier: 1–14. doi:10.1016/j.precamres.2017.07.016.

Bekker, A. Karhu, J.A., and A.J. Eriksson, K.A. and Kaufman. 2003. “Chemostratigraphy of Paleoproterozoic Carbonate Successions of the Wyoming Craton: Tectonic Forcing of Biogeochemical Change?” *Precambrian Research* 120: 279–325.

Bekker, a., J.a. Karhu, and a.J. Kaufman. 2006. “Carbon Isotope Record for the Onset of the Lomagundi Carbon Isotope Excursion in the Great Lakes Area, North America.” *Precambrian Research* 148 (1–2): 145–80. doi:10.1016/j.precamres.2006.03.008.

Bekker, A, H D Holland, P Wang, D Rumble Iii, H J Stein, J L Hannah, L L Coetzee, and N J Beukes. 2004. “Dating the Rise of Atmospheric Oxygen.” *Nature* 427: 117–20.

Bekker, a, a Kaufman, J Karhu, and K Eriksson. 2005. “Evidence for Paleoproterozoic Cap Carbonates in North America.” *Precambrian Research* 137 (3–4): 167–206. doi:10.1016/j.precamres.2005.03.009.

Bertine, Kathe K. and Turekian, Karl K. 1973. “Molybdenum in Marine Deposits.” *Geochimica et Cosmochimica Acta* 37 (6): 1415–34. doi:10.1016/0016-7037(73)90080-X.

Bertrand-Sarfati, J. 1972. “Stromatolites Columnaires de Certaines Formations Carbonatées

Du Précambrien Supérieur Du Bassin Congolais." 74. 8. Tervuren (Belgique).

Bhandari, N. 2002. "A Quest for the Moon." *Current Science* 83 (4): 377–93.

Bobrovskiy, Ilya, Janet M Hope, Andrey Ivantsov, Benjamin J Nettersheim, Christian Hallmann, and Jochen J Brocks. 2018. "Ancient Steroids Establish the Ediacaran Fossil Dickinsonia as One of the Earliest Animals." *Science* 1249 (September): 1246–49.

Bosak, T., A. H. Knoll, and A. P. Petroff. 2013. "The Meaning of Stromatolites." *Annual Review of Earth and Planetary Sciences* 41: 21–44. doi:10.1146/annurev-earth-042711-105327.

Bowring, S.A. and Housh, T. 1995. "The Earth's Early Evolution." *Science* 269 (5230): 1535–40.

Bowring, Samuel A., and Ian S. Williams. 1999. "Priscoan (4.00-4.03 Ga) Orthogneisses from Northwestern Canada." *Contributions to Mineralogy and Petrology* 134 (1): 3–16. doi:10.1007/s004100050465.

Brasier, Martin D, Owen R Green, Andrew P Jephcoat, Annette K Kleppe, Martin J Van Kranendonk, John F Lindsay, Andrew Steele, and Nathalie V Grassineau. 2002. "Questioning the Evidence for Earth ' s Oldest Fossils" 416 (March).

Brocks, Jochen J, Roger Buick, Roger E Summons, and Graham a Logan. 2003. "A Reconstruction of Archean Biological Diversity Based on Molecular Fossils from the 2.78 to 2.45 Billion-Year-Old Mount Bruce Supergroup, Hamersley Basin, Western Australia." *Geochimica et Cosmochimica Acta* 67 (22): 4321–35. doi:10.1016/S0016-7037(03)00209-6.

Butterfield, N.J., Knoll, A.H. and Keene Swett. 1994. "Paleobiology of the Neoproterozoic Svanbergfjellet Formation, Spitsbergen." *Fossils and Strata : An International Monograph Series of Palaeontology and Stratigraphy*, no. 34: 84.

Butterfield, N. J. 2015. "Early Evolution of the Eukaryota." *Palaeontology* 58 (1): 5–17. doi:10.1111/pala.12139.

Butterfield, N J, and F W Chandler. 1992. "Palaeoenvironmental Distribution of Proterozoic Microfossils, with an Example from the Agu Bay Formation, Baffin Island." *Palaeontology*. http://www.scopus.com/inward/record.url?eid=2-s2.0-0027072605&partnerID=40.

Butterfield, Nicholas J. 2004. "A Vaucheriacean Alga from the Middle Neoproterozoic of Spitsbergen: Implications for the Evolution of Proterozoic Eukaryotes and the Cambrian Explosion." *Paleobiology* 30 (2): 231–52. http://www.bioone.org/doi/abs/10.1666/0094-8373%282004%29030%3C0231%3AAVAFTM%3E2.0.CO%3B2.

———. 2005. "Probable Proterozoic Fungi." *Paleobiology* 31 (1): 165–82. doi:10.1666/0094-8373(2005)031<0165:PPF>2.0.CO;2.

———. 2009. "Modes of Pre-Ediacaran Multicellularity." *Precambrian Research* 173: 201–11. doi:10.1016/j.precamres.2009.01.008.

Butterfield, Nicholas J., and Robert H. Rainbird. 1998. "Diverse Organic-Walled Fossils, Including 'possible Dinoflagellates,' from the Early Neoproterozoic of Arctic Canada." *Geology* 26 (11): 963–66. doi:10.1130/0091-7613(1998)026<0963:DOWFIP>2.3.CO;2.

Butterfield, Nicholas J. 2001. "Paleobiology of the Late Mesoproterozoic (ca. 1200 Ma)

Hunting Formation, Somerset Island, Arctic Canada." *Precambrian Research* 111 (1–4): 235–56. http://www.sciencedirect.com/science/article/pii/S0301926801001620.

Cahen, L., Snelling, N.J., Delhal, J. and Vail, J.R. 1984. *Geological and Evolution of Africa*. Clarendon Press, Oxford.

Cahen, L. and Mortelmans, G. 1947. "Le Systeme de La Bushimaie Au Katanga." *Bulletin de La Société Belge de Géologie, Hydrologie, Paléontologie* 56: 217–53.

Cahen, L. 1954. "Résultats Géochronologiques Obtenus Sur Des Minéraux Du Congo Jusqu'en Mai 1954." *Bulletin de La Société Géologique de Belgique* 77: B268–81.

———. 1974. "Geological Background To the Copper Bearing Strata of Southern Shaba." *Annales de La Société Géologique de La Belgique*, 57–77.

Canfield, D. E., Raiswell, R., Westrich, J.T., Reaves, C.M. and Berner, R.A. 1986. "The Use of Chromium Reduction in the Analysis of Reduced Inorganic Sulfur in Sediments and Shales." *Chemical Geology* 54 (1–2): 149–55.

Canfield, D.E, Poulton, S.W. and Narbonne, G.M. 2007. "Late-Neoproterozoic Deep-Ocean Oxygenation and the Rise of Animal Life." *Science* 315: 92–94.

Canfield, D. E. 1998. "A New Model for Proterozoic Ocean Chemistry." *Nature* 396 (6710): 450–53. doi:10.1038/24839.

Canfield, D.E. 2005. "THE EARLY HISTORY OF ATMOSPHERIC OXYGEN: Homage to Robert M. Garrels." *Annual Review of Earth and Planetary Sciences* 33 (1): 1–36. doi:10.1146/annurev.earth.33.092203.122711.

Canfield, Don E, Minik T Rosing, and Christian Bjerrum. 2006. "Early Anaerobic Metabolisms." *Philosophical Transactions of the Royal Society of London. Series B, Biological Sciences* 361 (1474): 1819-34; discussion 1835-6. doi:10.1098/rstb.2006.1906.

Canfield, Donald E, Simon W Poulton, Andrew H Knoll, Guy M Narbonne, Gerry Ross, Tatiana Goldberg, and Harald Strauss. 2008. "Ferruginous Conditions Dominated Later Neoproterozoic Deep-Water Chemistry." *Science (New York, N.Y.)* 321 (5891): 949–52. doi:10.1126/science.1154499.

Cavalier-Smith, T. 1998. "A Revised Six-Kingdom System of Life." *Biological Reviews* 73 (3): 203–66. doi:10.1111/j.1469-185X.1998.tb00030.x.

Clarkson, M. O., S. W. Poulton, R. Guilbaud, and R. A. Wood. 2014. "Assessing the Utility of Fe/Al and Fe-Speciation to Record Water Column Redox Conditions in Carbonate-Rich Sediments." *Chemical Geology* 382. Elsevier B.V.: 111–22. doi:10.1016/j.chemgeo.2014.05.031.

Cohen, Phoebe A., and Francis A. Macdonald. 2015. "The Proterozoic Record of Eukaryotes." *Paleobiology* 41 (4): 610–32. doi:10.1017/pab.2015.25.

Cohen, Phoebe A., and Leigh Anne Riedman. 2018. "It's a Protist-Eat-Protist World: Recalcitrance, Predation, and Evolution in the Tonian–Cryogenian Ocean." *Emerging Topics in Life Sciences* 2 (2): 173–80. doi:10.1042/ETLS20170145.

Combaz, A., Lange, F.W. and Pansart, J. 1967. "Les 'Leiofusidae' Eisenack, 1938." *Review of Palaeobotany and Palynology* 1: 291–307.

Coplen, Tyler B., Willi A. Brand, Matthias Gehre, Manfred Gröning, Harro A J Meijer, Blaza Toman, and R. Michael Verkouteren. 2006. “New Guidelines for Δ13C Measurements.” *Analytical Chemistry* 78 (7): 2439–41. doi:10.1021/ac052027c.

Craig, J, U Biffi, R F Galimberti, K A R Ghori, J D Gorter, N Hakhoo, D P Le Heron, J Thurow, and M Vecoli. 2013. “The Palaeobiology and Geochemistry of Precambrian Hydrocarbon Source Rocks.” *Marine and Petroleum Geology* 40 (0): 1–47. doi:http://dx.doi.org/10.1016/j.marpetgeo.2012.09.011.

Craig, Jonathan, Juergen Thurow, Bindra Thusu, Andy Whitham, and Yousef Abutarruma. 2009. “Global Neoproterozoic Petroleum Systems: The Emerging Potential in North Africa.” *Geological Society, London, Special Publications* 326 (1): 1–25. doi:10.1144/SP326.1.

Cumming, Vivien M., Simon W. Poulton, Alan D. Rooney, and David Selby. 2013. “Anoxia in the Terrestrial Environment during the Late Mesoproterozoic.” *Geology* 41 (5): 583–86. doi:10.1130/G34299.1.

De Waele, B., Johnson, S.P. and Pisarevsky, S.A. 2008. “Palaeoproterozoic to Neoproterozoic Growth and Evolution of the Eastern Congo Craton: Its Role in the Rodinia Puzzle.” *Precambrian Research* 160 (1–2): 127–41.

Delhal, J., Ledent, D. and Pasteels, P. 1975. “L’age Du Complexe Granitique et Migmatitique de Dibaya (Région Du Kasai, Zaire) Par Les Méthodes Rb-Sr et U-Pb.” *Annales de La Société Géologique de La Belgique* 98: 141–54.

Delhal, J. Lepersonne, J and Raucq, P. 1966. “Le Complexe Sédimentaire et Volcanique de La Lulua (Kasaï).” Tervuren (Belgique).

Delpomdor, F., C. Blanpied, A. Virgone, and A. Préat. 2013. “Paleoenvironments in Meso–Neoproterozoic Carbonates of the Mbuji-Mayi Supergroup (Democratic Republic of Congo) – Microfacies Analysis Combined with C–O–Sr Isotopes, Major-Trace Elements and REE + Y Distributions.” *Journal of African Earth Sciences* 88 (3). Elsevier Ltd: 72–100. doi:10.1016/j.jafrearsci.2013.09.002.

Delpomdor, Franck, Christian Blanpied, Aurelien Virgone, and Alain Préat. 2015. “Sedimentology and Sequence Stratigraphy of the Late Precambrian Carbonates of the Mbuji-Mayi Supergroup in the Sankuru-Mbuji-Mayi-Lomami-Lovoy Basin (Democratic Republic of the Congo).” In *Geology and Resource Potential of the Congo Basin*, edited by Maarten J. de Wit, François Guillocheau, and Michiel C. J. de Wit, 59–76. Springer Berlin Heidelberg. doi:10.1007/978-3-642-29482-2-4.

Delpomdor, Franck, Ulf Linnemann, Ariel Boven, Andreas Gärtner, Aleksey Travin, Christian Blanpied, Aurélien Virgone, Hielke Jelsma, and Alain Préat. 2013. “Depositional Age, Provenance, and Tectonic and Paleoclimatic Settings of the Late Mesoproterozoic Middle Neoproterozoic Mbuji-Mayi Supergroup, Democratic Republic of Congo.” *Palaeogeography, Palaeoclimatology, Palaeoecology* 389: 4–34. doi:10.1016/j.palaeo.2013.06.012.

Delpomdor, Franck, and Alain Préat. 2013. “Early and Late Neoproterozoic C, O and Sr Isotope Chemostratigraphy in the Carbonates of West Congo and Mbuji-Mayi Supergroups: A Preserved Marine Signature?” *Palaeogeography, Palaeoclimatology, Palaeoecology* 389 (2): 35–47. doi:10.1016/j.palaeo;2013.07.007.

Delpomdor, Franck R.A., Xavier Devleeschouwer, Simo Spassov, and Alain R. and Préat.

2017. *Stratigraphic Correlations in Mid- to Late-Proterozoic Carbonates of the Democratic Republic of Congo Using Magnetic Susceptibility*. *Sedimentary Geology*. Vol. 351. Elsevier B.V. doi:10.1016/j.sedgeo.2017.02.007.

Delvaux, D and Fernandez-Alonso, M. 2015. "Petroleum Potential of the Congo Basin." In *Geology and Resource Potential of the Congo Basin*, edited by de Wit M de Wit M., Guillocheau F., Springer, 371–91. Berlin, Heidelberg: Springer Berlin Heidelberg. doi:org/10.1007/978-3-642-29482-2_18.

Delvaux, Damien, and Andreas Barth. 2010. "African Stress Pattern from Formal Inversion of Focal Mechanism Data." *Tectonophysics* 482 (1–4). Elsevier: 105–28. doi:10.1016/J.TECTO.2009.05.009.

Deunff, J. 1955. "Un Microplancton Fossile Dévonien a Hystrichosphères Du Continent Nord-Américain." *Bulletin de La Microscopie Appliquée*, 2, 5: 138–49.

Diamond, C. W., N. J. Planavsky, C. Wang, and T. W. Lyons. 2018. "What the ~1.4 Ga Xiamaling Formation Can and Cannot Tell Us about the Mid-Proterozoic Ocean." *Geobiology* 16 (3): 219–36. doi:10.1111/gbi.12282.

Diamond, Charles W., and Timothy W. Lyons. 2018. "Mid-Proterozoic Redox Evolution and the Possibility of Transient Oxygenation Events." *Emerging Topics in Life Sciences*, ETLS20170146. doi:10.1042/ETLS20170146.

Diaz, R.J., and R. Rosenberg. 2008. "Spreading Dead Zones and Consequences Formarine Ecosystems." *Science* 321 (August): 926–29.

Doyle, Katherine A., Simon W. Poulton, Robert J. Newton, Victor N. Podkovyrov, and Andrey Bekker. 2018. "Shallow Water Anoxia in the Mesoproterozoic Ocean: Evidence from the Bashkir Meganticlinorium, Southern Urals." *Precambrian Research* 317 (September). Elsevier: 196–210. doi:10.1016/j.precamres.2018.09.001.

Duda, Jan Peter, Martin J. Van Kranendonk, Volker Thiel, Danny Ionescu, Harald Strauss, Nadine Schäfer, and Joachim Reitner. 2016. "A Rare Glimpse of Paleoarchean Life: Geobiology of an Exceptionally Preserved Microbial Mat Facies from the 3.4 Ga Strelley Pool Formation, Western Australia." *PloS One* 11 (1): e0147629. doi:10.1371/journal.pone.0147629.

Eisenack, A. 1958. "Tasmanites Newton 1875 Und Leiosphaeridia n.g. Als Gattungen Der Hystricosphaeridia." *Palaeontographica* 110: 1–19.

———. 1965. "Mikrofossilien Aus Dem Silur Gotlands. Hystrichosphären, Problematika." *Neues Jahrbuch Für Geologie Und Paläontologie, Abhandlungen* 122: 257–74.

Evitt, W. 1963. "A DISCUSSION AND PROPOSALS CONCERNING FOSSIL DINOFLAGELLATES, HYSTRICHOSPHERES, AND ACRITARCHS,." *National Academy of Sciences* 47. National Academy of sciences, USA: 158–64, 298–302.

Fairchild, I. J., and M. J. Kennedy. 2007. "Neoproterozoic Glaciation in the Earth System." *Journal of the Geological Society* 164 (5): 895–921. doi:10.1144/0016-76492006-191.

Fedonkin, Mikhail a. 2003. "The Origin of the Metazoa in the Light of the Proterozoic Fossil Record." *Paleontological Research* 7 (1): 9–41. doi:10.2517/prpsj.7.9.

François, C, Debaille, V., Paquette, J.L., Baudet, D. and Javaux, J. 2018. "The Earliest Evidence for Modern-Style Plate Tectonics Recorded by HP–LT Metamorphism in the

Paleoproterozoic of the Democratic Republic of the Congo." *Scientific Reports* 8 (15452): 1–10.

François, C., B.K. Baludikay, J.Y. Storme, D. Baudet, J.L. Paquette, M. Fialin, and E.J. Javaux. 2017. "Contributions of U-Th-Pb Dating on the Diagenesis and Sediment Sources of the Lower Group (BI) of the Mbuji-Mayi Supergroup (Democratic Republic of Congo)." *Precambrian Research* 298. doi:10.1016/j.precamres.2017.06.012.

Frank, T. D., L. C. Kah, and T. W. Lyons. 2003. "Changes in Organic Matter Production and Accumulation as a Mechanism for Isotopic Evolution in the Mesoproterozoic Ocean." *Geological Magazine* 140 (4): 397–420. doi:10.1017/S0016756803007830.

Frimmel, Hartwig E. 2010. "On the Reliability of Stable Carbon Isotopes for Neoproterozoic Chemostratigraphic Correlation." *Precambrian Research* 182 (4). Elsevier B.V.: 239–53. doi:10.1016/j.precamres.2010.01.003.

Garcia-Ruiz, J.M., Hyde, S.T., Carnerup, A.M., Christy, A.G., Van Kranendonk, M.J. and Welham, N.J. 2003. "Self-Assembled Silica-Carbonate Structures and Detection of Ancient Microfossils." *Science* 302 (5648): 1194–97.

García-Ruiz, Juan Manuel, Emilio Melero-García, and Stephen T Hyde. 2009. "Morphogenesis of Self-Assembled Nanocrystalline Materials of Barium Carbonate and Silica." *Science (New York, N.Y.)* 323 (5912): 362–65. doi:10.1126/science.1165349.

Gerdes, Gisela. 2007. "CHAPTER TWO STRUCTURES LEFT BY MODERN MICROBIAL MATS IN THEIR HOST SEDIMENTS," 5–38.

German, T.N. and Podkovyrov, V.N. 2009. "New Insights into the Nature of the Late Riphean Eosolenides." *Precambrian Research* 173: 154–62.

Ghori, K.A.R., Craig, J., Thusu, B., Luning, S., Geiger, M. 2009. "Global Infracambrian Petroleum Systems." In *Global Neoproterozoic Petroleum Systems and the Emerging Potential in North Africa.*, edited by Y. Craig, J., Thurow, J., Thusu, B., Whitham, A., Abutarruma, 326:109–36.

Gibson, Timothy M., Patrick M. Shih, Vivien M. Cumming, Woodward W. Fischer, Peter W. Crockford, Malcolm S.W. Hodgskiss, Sarah Wörndle, et al. 2018. "Precise Age of Bangiomorpha Pubescens Dates the Origin of Eukaryotic Photosynthesis." *Geology* 46 (2): 135–38. doi:10.1130/G39829.1.

Gilleaudeau, Geoffrey J., and Linda C. Kah. 2013. "Carbon Isotope Records in a Mesoproterozoic Epicratonic Sea: Carbon Cycling in a Low-Oxygen World." *Precambrian Research* 228 (May). Elsevier B.V.: 85–101. doi:10.1016/j.precamres.2013.01.006.

———. 2015. "Heterogeneous Redox Conditions and a Shallow Chemocline in the Mesoproterozoic Ocean: Evidence from Carbon-Sulfur-Iron Relationships." *Precambrian Research* 257. Elsevier B.V.: 94–108. doi:10.1016/j.precamres.2014.11.030.

Giraldo M., Cornet, Y and Javaux, E.J. 2018. "Isolating Kerogenous Organic-Walled Microfossils from Precambrian Fine-Grained Siliciclastic Rocks." In *COST Workshop , Bertinoro, Italy*.

Giresse, Pierre. 2005. "Mesozoic-Cenozoic History of the Congo Basin." *Journal of African Earth Sciences* 43 (1–3): 301–15. doi:10.1016/j.jafrearsci.2005.07.009.

Goldblatt, C., K. J. Zahnle, N. H. Sleep, and E. G. and Nisbet. 2010. “The Eons of Chaos and Hades.” In *Solid Earth*, 1–3.

Golovenock, V. K. and Belova, M. Yu. 1984. “Riphean Microbiota in Cherts of the Billyakh Group on the Anabar Uplift.” *Paleontological Journal*, no. English translation: 20–30.

———. 1986. “The Riphean Microflora in the Cherts from the Malgin Formation in the Yudoma-Maya Basin.” *Paleontological Journal*, no. English translation: 85–90.

Goodwin, A.M. 1991. *Precambrian Geology. The Dynamic Evolution of the Continental Crust*. Edited by E. G. Nisbet. London: Academic Press.

Grey, K. 1999. “A Modified Palynological Preparation Technique for the Extraction of Large Neoproterozoic Acanthomorph Acritarchs and Other Acid-Insoluble Microfossils.” Record 1999/10. Perth: Geological survey of Western Australia.

———. 2005. “Ediacaran Palynology of Australia.” *Mem. Assoc. Australas. Palaeontol.*

Grey, Kathleen, Malcolm Walter, and Clive Calver. 2003. “Neoproterozoic Biotic Diversification : Snowball Earth or Aftermath of the Acraman Impact ?,” no. 5: 459–62.

Guilbaud, R., B.J. Slater, S.W. Poulton, T.H.P. Harvey, J.J. Brocks, B.J. Nettersheim, and N.J. Butterfield. 2018. “Oxygen Minimum Zones in the Early Cambrian Ocean.” *Geochemical Perspectives Letters*, 33–38. doi:10.7185/geochemlet.1806.

Guilbaud, Romain, Simon W. Poulton, Nicholas J. Butterfield, Maoyan Zhu, and Graham A. Shields-Zhou. 2015. “A Global Transition to Ferruginous Conditions in the Early Neoproterozoic Oceans.” *Nature Geoscience* 8 (6): 1–5. doi:10.1038/NGEO2434.

Guo, Hua, Yuansheng Du, Linda C. Kah, Junhua Huang, Chaoyong Hu, Hu Huang, and Wenchao Yu. 2013. “Isotopic Composition of Organic and Inorganic Carbon from the Mesoproterozoic Jixian Group, North China: Implications for Biological and Oceanic Evolution.” *Precambrian Research* 224. Elsevier B.V.: 169–83. doi:10.1016/j.precamres.2012.09.023.

Halverson, G.P., Wade, B.P., Hurtgen, M.T. and Barovicha, K.M. 2010. “Neoproterozoic Chemostratigraphy.” *Precambrian Research* 182: 337–50.

Halverson, Galen P, Paul F Hoffman, Daniel P Schrag, Adam C Maloof, and A Hugh N Rice. 2005. “Toward a Neoproterozoic Composite Carbon-Isotope Record.” *Geological Society of America Bulletin* 117 (9): 1181. doi:10.1130/b25630.1.

Halverson, Galen P, Adam C Maloof, Daniel P Schrag, Francis Ö Dudás, and Matthew Hurtgen. 2007. “Stratigraphy and Geochemistry of a ca 800 Ma Negative Carbon Isotope Interval in Northeastern Svalbard.” *Chemical Geology* 237 (1–2): 5–27. doi:http://dx.doi.org/10.1016/j.chemgeo.2006.06.013.

Han, T.M. and Runnegar, B. 1992. “Megascopic Eukaryotic Algae from the 2.1-Billion-Year-Old Negaunee Iron-Formation, Michigan.” *Science* 257 (5067): 232–35. doi:DOI: 10.1126/science.1631544.

Hardisty, Dalton S., Timothy W. Lyons, Natascha Riedinger, Terry T. Isson, Jeremy D. Owens, Robert C. Aller, Danny M. Rye, et al. 2018. “An Evaluation of Sedimentary Molybdenum and Iron as Proxies for Pore Fluid Paleoredox Conditions.” *American Journal of Science* 318 (5): 527–56. doi:10.2475/05.2018.04.

Hayes, J.M. 1994. “Global Methanotrophy at the Archean-Proterozoic Transition.” In *Early*

Life on Earth, Nobel Symp, 220–36. New York: Columbia University Press.

Hermann, T. N. 1974. “Nakhodki Massovykh Skopleniy Trikhomov v Rifee.” In *Timofeev, B.V. (Ed.), Mikrofitofossili Proterozoya i Rannego Paleozoya SSSR. Nauka, Leningrad*, 6–10.

———. 1990. *Organic World Billion Year Ago*. Leningrad: Academy of Sciences of the USSR, Instute of Precambrian Geology and Geochronology.

Hermann, T. N., and V. N. Podkovyrov. 2008. “On the Nature of the Precambrian Microfossils Arctacellularia and Glomovertella.” *Paleontological Journal* 42 (6): 655–64. http://link.springer.com/10.1134/S0031030108060117.

Hermann, T N, and V N Podkovyrov. 2007. “Rugosoopsis : A New Group of Upper Riphean Animals.” *Geological Society, London, Special Publications* 286: 429–31.

Hill, A.C, and M.R Walter. 2000. *Mid-Neoproterozoic (~830–750 Ma) Isotope Stratigraphy of Australia and Global Correlation*. *Precambrian Research*. Vol. 100. http://linkinghub.elsevier.com/retrieve/pii/S0301926899000741.

Hoffman, P.F. and, and Z.-X. Li. 2009. “A Palaeogeographic Context for Neoproterozoic Glaciation.” *Palaeogeography, Palaeoclimatology, Palaeoecology* 277 (3–4). Elsevier B.V.: 158–72. http://linkinghub.elsevier.com/retrieve/pii/S0031018209001114.

Hofmann, H.J. and Jackson, G.D. 1994. “Shale-Facies Microfossils from the Proterozoic Bylot Supergroup, Baffin Island, Canada.” *Memoir (The Paleontological Society)* 37 (Supplement to N°4). Paleontological Society: 1–39. http://www.jstor.org/stable/1315579.

Hofmann, H.J. 1999. “Global Distribution of the Proterozoic Sphaeromorph Acritarch Valeria Lophostriata (Jankauskas).” *Acta Micropalaeontologica Sinica* 16 (3): 215–24.

Holmes, A. and Cahen, L. 1955. “African Geochronology.” *Colonial Geology and Mineral Ressources* 5 (1): 3–38.

Isley, A.E. and Abbott, D.H. 1999. “Plume-Related Mafic Volcanism and the Deposition of Banded Iron Formation.” *Journal of Geophysical Research* 104 (B7): 15.461-15.477.

Jacob, H. 1989. “Classification, Structure, Genesis and Practical Importance of Natural Solid Oil Bitumen (‘migrabitumen’).” *International Journal of Coal Geology* 11 (1): 65–79. doi:10.1016/0166-5162(89)90113-4.

Javaux, E.J. 2011. “Early Eukaryotes in Precambrian Oceans.” In *Origins and Evolution of Life:An Astrophisical Perspective*, edited by Hervé Martin Muriel Gargaud, Purificación López-Garcìa, Belin, 525. Cambridge University Press.

Javaux, E J, and A H Knoll. 2016. “Micropaleontology of the Lower Mesoproterozoic Roper Group , Australia , and Implications for Early Eukaryotic Evolution.” *Journal of Paleontology* 91 (2): 199–229. doi:10.1017/jpa.2016.124.

Javaux, E J, and C P Marshal. 2006. “A New Approach in Deciphering Early Protist Paleobiology and Evolution: Combined Microscopy and Microchemistry of Single Proterozoic Acritarchs.” *Review of Palaeobotany and Palynology* 139 (1–4): 1–15. http://www.sciencedirect.com/science/article/pii/S0034666706000145.

Javaux, Emmanuelle J. 2011. “Evolution of Early Eukaryotes in Precambrian Oceans.” In *Origins and Evolution of Life: An Astrobiology Perspective*, edited by H Martin

Gargaud, M, P Lopez-Garcia, 414–49. Cambridge University Press.

Javaux, Emmanuelle J., Andrew H. Knoll, and Malcolm R. Walter. 2001. "Morphological and Ecological Complexity in Early Eukaryotic Ecosystems." *Nature* 412 (6842): 66–69. doi:10.1038/35083562.

Javaux, Emmanuelle J, Andrew H Knoll, and Malcolm Walter. 2003. "Recognizing and Interpreting the Fossils of Early Eucaryotes." *Origins of Life and Evolution of Biospheres* 33 (April 2002): 75–94.

Javaux, Emmanuelle J, Andrew H Knoll, and Malcolm R Walter. 2004. "TEM Evidence for Eukaryotic Diversity in Mid-Proterozoic Oceans." *Geobiology* 2 (3): 121–32. doi:10.1111/j.1472-4677.2004.00027.x.

Javaux, Emmanuelle J, Craig P Marshall, and Andrey Bekker. 2010. "Organic-Walled Microfossils in 3.2-Billion-Year-Old Shallow-Marine Siliciclastic Deposits." *Nature* 463 (7283). Macmillan Publishers Limited. All rights reserved: 934–38. http://www.ncbi.nlm.nih.gov/pubmed/20139963.

Jubb, Aaron M., Palma J. Botterell, Justin E. Birdwell, Robert C. Burruss, Paul C. Hackley, Brett J. Valentine, Javin J. Hatcherian, and Stephen A. Wilson. 2018. "High Microscale Variability in Raman Thermal Maturity Estimates from Shale Organic Matter." *International Journal of Coal Geology* 199 (August). Elsevier: 1–9. doi:10.1016/j.coal.2018.09.017.

Kadima, E, Delvaux, D, Sebagenzi, S.N., Tack, L., Kabeya, S.M. 2011. "Structure and Geological History of the Congo Basin: An Integrated Interpretation of Gravity, Magnetic and Reflection Seismic Data." *Basin Research* 23 (5): 499–527. doi:10.1111/j.1365-2117.2011.00500.x.

Kadima, E, S.S.M. and Ntabwoba, and F. Lucazeau. 2011. "A Proterozoic-Rift Origin for the Structure and the Evolution of the Cratonic Congo Basin." *Earth and Planetary Science Letters* 304 (1–2). Elsevier B.V.: 240–50. doi:10.1016/j.epsl.2011.01.037.

Kah, L. C., Lyons, T.W. and Franck, T. D. 2004. "Low Marine Sulphate and Protracted Oxygenation of the Proterozoic Biosphere." *Nature* 431 (1): 834–38. http://proxy.libraries.smu.edu/login?url=http://search.ebscohost.com/login.aspx?direct=true&db=sih&AN=SM082531&site=ehost-live&scope=site.

Kah, Linda C., and Julie K. Bartley. 2011. "Protracted Oxygenation of the Proterozoic Biosphere." *International Geology Review* 53 (11–12): 1424–42. doi:10.1080/00206814.2010.527651.

Kah, Linda C., Julie K. Bartley, and David a. Teal. 2012. "Chemostratigraphy of the Late Mesoproterozoic Atar Group, Taoudeni Basin, Mauritania: Muted Isotopic Variability, Facies Correlation, and Global Isotopic Trends." *Precambrian Research* 200–203 (April). Elsevier B.V.: 82–103. doi:10.1016/j.precamres.2012.01.011.

Kah, Linda C, Timothy W Lyons, and John T Chesley. 2001. "Geochemistry of a 1.2 Ga Carbonate-Evaporite Succession, Northern Baffin and Bylot Islands: Implications for Mesoproterozoic Marine Evolution." *Precambrian Research* 111 (1–4): 203–34. doi:10.1016/S0301-9268(01)00161-9.

Kampunzu, A.B., Tembo, F., Matheis, G., Kapenda, D. and Huntsman-Mapila, P. 2000. "Geochemistry and Tectonic Setting of Mafic Igneous Units in the Neoproterozoic

Katangan Basin, Central Africa: Implications for Rodinia Break-Up." *Gondwana Research* 3 (2): 125–53.

Kasting, J.F. 1993. "Earth's Early Atmosphere." *Science* 259 (5097): 920–26.

Kerr, R.A. 2003. "Minerals Cooked up in the Laboratory Call Ancient Microfossils Into Question." *Science* 302 (5648): 1134.

Kim, Sang Tae, Alfonso Mucci, and Bruce E. Taylor. 2007. "Phosphoric Acid Fractionation Factors for Calcite and Aragonite between 25 and 75 °C: Revisited." *Chemical Geology* 246 (3–4): 135–46. doi:10.1016/j.chemgeo.2007.08.005.

Knauth, L.P. and Lowe, D.R. 2003. "High Archean Climatic Temperature Inferred from Oxygen Isotope Geochemistry of Cherts in the 3.5 Ga Swaziland Supergroup, South Africa." *The Geological Society of America* 115 (5): 566–80.

Knauth, L Paul, and Martin J Kennedy. 2009. "The Late Precambrian Greening of the Earth." *Nature* 460 (7256). Nature Publishing Group: 728–32. doi:10.1038/nature08213.

Knoll, A. H., Sweet, K. and Mark, J. 1991. "Paleobiology of a Neoproterozoic Tidal Flat/Lagoonal Complex: The Draken Conglomerate Formation, Spitsbergen." *Journal of Paleontology* 65: 531–70.

Knoll, A. H., E J Javaux, D Hewitt, and P Cohen. 2006. "Eukaryotic Organisms in Proterozoic Oceans." *Philosophical Transactions of the Royal Society of London. Series B, Biological Sciences* 361 (June): 1023–38. doi:10.1098/rstb.2006.1843.

Knoll, A.H. 1984. "Microbiotas of the Late Precambrian Hunnberg Formation, Nordaustlandet, Svalbard." *Journal of Paleontology* 58 (1): 131–62.

Knoll, Andrew H. 2014. "Paleobiological Perspectives on Early Eukaryotic Evolution." *Cold Spring Harbor Perspectives in Biology* 6 (1). doi:10.1101/cshperspect.a016121.

Knoll, Andrew H., and Martin A. Nowak. 2017. "The Timetable of Evolution." *Science Advances* 3 (5): 1–14. doi:10.1126/sciadv.1603076.

Knoll, Andrew H. 1994. "Proterozoic and Early Cambrian Protists: Evidence for Accelerating Evolutionary Tempo." *Proceedings of the National Academy of Sciences* 91 (15): 6743–50. doi:10.1073/pnas.91.15.6743.

Knoll, Andrew, Malcolm Walter, Guy Narbonne, and Nicholas Christie-Blick. 2006. "The Ediacaran Period: A New Addition to the Geologic Time Scale." *Lethaia* 39 (1): 13–30. doi:10.1080/00241160500409223.

Koeberl, C. 2003. "THE LATE HEAVY BOMBARDMENT IN THE INNER SOLAR SYSTEM: IS THERE ANY CONNECTION TO KUIPER BELT OBJECTS?" *Earth, Moon, and Planets* 92: 79–87.

Kolosov, P. N. 1982. *Upper Precambrian Paleoalgological Residues from the Siberian Platform*. Nauka. Moscow. [In Russian].

Kouketsu, Yui, Tomoyuki Mizukami, Hiroshi Mori, Shunsuke Endo, Mutsuki Aoya, Hidetoshi Hara, Daisuke Nakamura, and Simon Wallis. 2014. "A New Approach to Develop the Raman Carbonaceous Material Geothermometer for Low-Grade Metamorphism Using Peak Width." *Island Arc* 23 (1): 33–50. doi:10.1111/iar.12057.

Kübler, B. and Jaboyedoff, M. 2000. "Illite Crystallinity." *Earth and Planetary Science*

Letters 331: 75–89.

Lamb, D M, S M Awramik, D J Chapman, and S Zhu. 2009. "Evidence for Eukaryotic Diversification in the ~1800 Million-Year-Old Changzhougou Formation, North China." *Precambrian Research* 173 (1–4): 93–104. doi:http://dx.doi.org/10.1016/j.precamres.2009.05.005.

Landis, Charles R., and John R. Castaño. 1995. "Maturation and Bulk Chemical Properties of a Suite of Solid Hydrocarbons." *Organic Geochemistry* 22 (1): 137–49. doi:10.1016/0146-6380(95)90013-6.

Ledru, P., Johan, V. Milési, J.P. and Tegyey, M. 1994. "Markers of the Last Stages of the Palaeoproterozoic Collision: Evidence for a 2 Ga Continent Involving Circum-South Atlantic Provinces." *Precambrian Research* 69 (1–4): 169–91.

Leiming, Yin, Yuan Xunlai, Meng Fanwei, and Hu Jie. 2005. "Protists of the Upper Mesoproterozoic Ruyang Group in Shanxi Province, China." *Precambrian Research* 141: 49–66. doi:10.1016/j.precamres.2005.08.001.

Lepland, A., Arrhenius, G. and Cornell, D. 2002. "Apatite in Early Archean Isua Supracrustal Rocks, Southern West Greenland: Its Origin, Association with Graphite and Potential as a Biomarker." *Precambrian Research* 118: 221–41.

Lepot, K., Benzerara, K., Brown, G.E. and Philippot, P. 2008. "Microbially Influenced Formation of 2,724-Million-Year-Old Stromatolites." *Nature Geoscience* 1: 118–21.

Li, Z. X., S. V. Bogdanova, A. S. Collins, A. Davidson, B. De Waele, R. E. Ernst, I. C.W. Fitzsimons, et al. 2008. "Assembly, Configuration, and Break-up History of Rodinia: A Synthesis." *Precambrian Research* 160 (1–2): 179–210. doi:10.1016/j.precamres.2007.04.021.

Liu, DeHan H., XianMing M. Xiao, Hui Tian, YuShun S. Min, Qin Zhou, Peng Cheng, and JiaGui G. Shen. 2013. "Sample Maturation Calculated Using Raman Spectroscopic Parameters for Solid Organics: Methodology and Geological Applications." *Chinese Science Bulletin* 58 (11): 1285–98. doi:10.1007/s11434-012-5535-y.

Lopez-Garcia, P. and Moreira, D. 2006. "Selective Forces for the Origin Ofthe Eukaryotic Nucleus." *BioEssays : News and Reviews in Molecular, Cellular and Developmental Biology* 28: 525–33.

López-García, Purificación, Laura Eme, and David Moreira. 2017. "Symbiosis in Eukaryotic Evolution." *Journal of Theoretical Biology* 434: 20–33. doi:10.1016/j.jtbi.2017.02.031.

Loron, Corentin C., Robert H. Rainbird, Elizabeth C. Turner, J. Wilder Greenman, and Emmanuelle J. Javaux. 2018a. "Implications of Selective Predation on the Macroevolution of Eukaryotes: Evidence from Arctic Canada." *Emerging Topics in Life Sciences*, ETLS20170153. doi:10.1042/ETLS20170153.

———. 2018b. "Organic-Walled Microfossils from the Late Mesoproterozoic to Early Neoproterozoic Lower Shaler Supergroup (Arctic Canada): Diversity and Biostratigraphic Significance." *Precambrian Research*. Elsevier B.V. doi:10.1016/j.precamres.2018.12.024.

Lowe, Donald R. 1994. "Accretionary History of the Archean Barberton Greenstone Belt (3.55-3.22 Ga), Southern Africa." *Geology* 22: 1099–1102.

Lucazeau , F. Armitage, J. and Kadima K, and .E. 2015. “Thermal Regime and Evolution of the Congo Basin as an Intracratonic Basin.” In *Geology and Resource Potential of the Congo Basin*, edited by M.J. de Wit et al. (eds.), 229–44.

Lunine, Jonathan I. 1998. *Earth: Evolution of a Habitable World*. New York: Cambridge University Press.

Luo, Q L. 1991. “New Data on the Microplants from Changlongshan Formation of Upper Precambrian in Western Yanshan Range.” *Tianjin Institute of Geology and Mineral Resources, Bulletin* 25: 107–18.

Lyons, Timothy W., Ariel D. Anbar, Silke Severmann, Clint Scott, and Benjamin C. Gill. 2009. “Tracking Euxinia in the Ancient Ocean: A Multiproxy Perspective and Proterozoic Case Study.” *Annual Review of Earth and Planetary Sciences* 37 (1): 507–34. doi:10.1146/annurev.earth.36.031207.124233.

Lyons, Timothy W., and Silke Severmann. 2006. “A Critical Look at Iron Paleoredox Proxies: New Insights from Modern Euxinic Marine Basins.” *Geochimica et Cosmochimica Acta* 70 (23 SPEC. ISS.): 5698–5722. doi:10.1016/j.gca.2006.08.021.

Lyons, Timothy W., Josef P. Werne, David J. Hollander, and R. W. Murray. 2003. “Contrasting Sulfur Geochemistry and Fe/Al and Mo/Al Ratios across the Last Oxic-to-Anoxic Transition in the Cariaco Basin, Venezuela.” *Chemical Geology* 195 (1–4): 131–57. doi:10.1016/S0009-2541(02)00392-3.

Lyons, Timothy W, Christopher T Reinhard, and Noah J Planavsky. 2014. “The Rise of Oxygen in Earth’s Early Ocean and Atmosphere.” *Nature* 506 (7488). Nature Publishing Group: 307–15. doi:10.1038/nature13068.

Maithy, P. K. 1975. “Micro-Organisms from the Bushimay System (Late Pre-Cambrian) of Kanshi, Zaire.” *The Palaeobotanist* 22 (2): 133–49.

Martin, H. 1994. “The Archean Grey Gneisses and the Genesis of Continental Crust.” In *Archean Crstal Evolution*, edited by K.C. Condie, 205–59. doi:doi.org/10.1016/S0166-2635(08)70224-X.

März, C., S. W. Poulton, B. Beckmann, K. Küster, T. Wagner, and S. Kasten. 2008. “Redox Sensitivity of P Cycling during Marine Black Shale Formation: Dynamics of Sulfidic and Anoxic, Non-Sulfidic Bottom Waters.” *Geochimica et Cosmochimica Acta* 72 (15): 3703–17. doi:10.1016/j.gca.2008.04.025.

Mcfadden, Kathleen A, and Amy E Kelly. 2011. “Carbon and Sulfur Stable Isotopic Systems and Their Application in Paleoenvironmental Analysis.” In *Quantifying the Evolution of Early Life*, edited by and Dornbos S. Laflamme M., Schiffbauer J., 36:403–50. Dordrecht: Springer, Dordrecht. doi:10.1007/978-94-007-0680-4.

McManus, James, Thomas F. Nägler, Christopher Siebert, C. Geoffrey Wheat, and Douglas E. Hammond. 2002. “Oceanic Molybdenum Isotope Fractionation: Diagenesis and Hydrothermal Ridge-Flank Alteration.” *Geochemistry, Geophysics, Geosystems* 3 (12): 1–9. doi:10.1029/2002GC000356.

Merdith, Andrew S., Alan S. Collins, Simon E. Williams, Sergei Pisarevsky, John D. Foden, Donnelly B. Archibald, Morgan L. Blades, et al. 2017. “A Full-Plate Global Reconstruction of the Neoproterozoic.” *Gondwana Research* 50 (June). Elsevier B.V.: 84–134. doi:10.1016/j.gr.2017.04.001.

Mikhailova, N. S. and Podkovyrov, V. N. 1992. “New Data on the Organic Wall Microfossils from the Upper Precambrian of Ural.” *Izvestiya Akademiya Nauk SSSR, Seriya Geologicheskaya* 10: 111–23.

Mikhailova, N. S. 1986. “New Finds of Microphytofossils from Upper Riphean Deposits of the Krasnoyar Region.” In *Sokolov, B.S. (Ed.): Aktual’nye Voprosy Sovremennoj Paleoalgologii*, 31–37. [in Russian]. Naukova Dumka, Kiev.

Milesi, J. P., S. F. Toteu, Y. Deschamps, J. L. Feybesse, C. Lerouge, A. Cocherie, J. Penaye, et al. 2006. “An Overview of the Geology and Major Ore Deposits of Central Africa: Explanatory Note for the 1:4,000,000 Map ‘Geology and Major Ore Deposits of Central Africa.’” *Journal of African Earth Sciences* 44 (4–5 SPEC. ISS.): 571–95. doi:10.1016/j.jafrearsci.2005.10.016.

Mojzsis, S.J., Arrhenius, K.D., McKeegan, T.M., Nutman, A.P. and Friend, C.R.L. 1996. “Evidence for Life on Earth before 3,800 Million Years Ago.” *Nature* 384: 55–59.

Nagovitsin, K.E., A.M. Stanevich, and T.a. Kornilova. 2010. “Stratigraphic Setting and Age of the Complex Tappania-Bearing Proterozoic Fossil Biota of Siberia.” *Russian Geology and Geophysics* 51 (11). Elsevier B.V.: 1192–98. http://linkinghub.elsevier.com/retrieve/pii/S1068797110001793.

Nagovitsin, Konstantin. 2009. “Tappania-Bearing Association of the Siberian Platform: Biodiversity, Stratigraphic Position and Geochronological Constraints.” *Precambrian Research* 173: 137–45. doi:10.1016/j.precamres.2009.02.005.

Nagy, Robin M., Susannah M. Porter, Carol M. Dehler, and Yanan Shen. 2009. “Biotic Turnover Driven by Eutrophication before the Sturtian Low-Latitude Glaciation.” *Nature Geoscience* 2 (6). Nature Publishing Group: 415–18. doi:10.1038/ngeo525.

Narbonne, G.M. and Gehling, J.G. 2003. “Life after Snowball : The Oldest Complex Ediacaran Fossils.” *Geology* 31 (1): 27–30.

Narbonne, Guy M. 2005. “THE EDIACARA BIOTA: Neoproterozoic Origin of Animals and Their Ecosystems.” *Annual Review of Earth and Planetary Sciences* 33 (1): 421–42. doi:10.1146/annurev.earth.33.092203.122519.

Naumova, S.N. 1949. “Spory Nizhnego Kembriya. [Spores from the Lower Cambrian].” *Izvestiya Akademiy Nauk* 4: 49–56.

———. 1968. “Zonal Assemblages of Precambrian and Lower Cambrian Plant Microfossils of Eurasia and Their Stratigraphic Significance.” In *Mezhdunarodnyy Geologicheskiy Kongress, XXIII Sessiya, Doklady Sovetskikh Geologov*, 30–39. [in Russian].

Nisbet, E. G., N. V. Grassineau, C. J. Howe, P. I. Abell, M. Regelous, and R. E. R. Nisbet. 2007. “The Age of Rubisco: The Evolution of Oxygenic Photosynthesis.” *Geobiology* 5 (4): 311–35. doi:10.1111/j.1472-4669.2007.00127.x.

Nyberg, A. V. and Schopf, J. W. 1984. “Microfossils in Stromatolitic Cherts from the Upper Proterozoic Min’yar Formation, Southern Ural Mountains.” *Journal of Paleontology* 58: 738–72.

O’Neil, J., Carlson, R.W., Francis, D. and Stevenson, R.K. 2008. “Neodymium-142 Evidence for Hadean Mafic Crust.” *Science* 321: 1828–31.

Owens, Jeremy D., Timothy W. Lyons, Xiaona Li, Kenneth G. MacLeod, Gwenyth Gordon,

Marcel M.M. Kuypers, Ariel Anbar, Wolfgang Kuhnt, and Silke Severmann. 2012. “Iron Isotope and Trace Metal Records of Iron Cycling in the Proto-North Atlantic during the Cenomanian-Turonian Oceanic Anoxic Event (OAE-2).” *Paleoceanography* 27 (3): 1–13. doi:10.1029/2012PA002328.

Pang, Ke, Qing Tang, Xun-Lai Yuan, Bin Wan, and Shuhai Xiao. 2015. “A Biomechanical Analysis of the Early Eukaryotic Fossil Valeria and New Occurrence of Organic-Walled Microfossils from the Paleo-Mesoproterozoic Ruyang Group.” *Palaeoworld* 24 (3): 251–62. doi:https://doi.org/10.1016/j.palwor.2015.04.002.

Pavlov, A.A and Kasting, J.F. 2002. “Mass-Independent Fractionation of Sulfur Isotopes in Archean Sediments: Strong Evidence for an Anoxic Archean Atmosphere.” *Astrobiology* 2 (1): 27–41.

Peacock, C.L., A. Lalonde, and K. Konhauser. 2007. “Geochemical Proxies for Biogeochemical Cycling and Ocean Anoxia.” *Redox-Reactive Minerals: Properties, Reactions and Applications in Clean Technologies* 17: 121–72. doi:10.1180/EMU-notes.17.14.

Pearson, A., And Budin, M., and J.J. Brocks. 2003. “Phylogenetic and Biochemical Evidence for Sterol Synthesis in the Bacterium Gemmata Obscuriglobus.” *Proceedings of the National Academy of Sciences of the United States of America* 100 (26): 15352–57. doi:10.1073/pnas.2536559100.

Pedreira, A.J and De Waele, B. 2008. “Contemporaneous Evolution of the Palaeoproterozoic–Mesoproterozoic Sedimentary Basins of the São Francisco–Congo Craton.” *Geological Society, London, Special Publications* 294: 33–48.

Peng, Y, H Bao, and X Yuan. 2009. “New Morphological Observations for Paleoproterozoic Acritarchs from the Chuanlinggou Formation, North China.” *Precambrian Research* 168 (3–4): 223–32. doi:10.1016/j.precamres.2008.10.005.

Planavsky, Noah J., John F. Slack, William F. Cannon, Brennan O’Connell, Terry T. Isson, Dan Asael, John C. Jackson, Dalton S. Hardisty, Timothy W. Lyons, and Andrey Bekker. 2018. “Evidence for Episodic Oxygenation in a Weakly Redox-Buffered Deep Mid-Proterozoic Ocean.” *Chemical Geology* 483 (August 2017). Elsevier: 581–94. doi:10.1016/j.chemgeo.2018.03.028.

Planavsky, Noah J, Peter McGoldrick, Clinton T Scott, Chao Li, Christopher T Reinhard, Amy E Kelly, Xuelei Chu, Andrey Bekker, Gordon D Love, and Timothy W Lyons. 2011. “Widespread Iron-Rich Conditions in the Mid-Proterozoic Ocean.” *Nature* 477 (7365). Nature Publishing Group: 448–51. doi:10.1038/nature10327.

Porter, S. M., Meisterfeld, R. and Knoll, A. H. 2003. “Vase-Shaped Microfossils from the Neoproterozoic Chuar Group, Grand Canyon: A Classification Guided by Modern Testate Amoebae.” *Journal of Paleontology* 77 (3): 409–29.

Porter, S. M. and, and A.H. Knoll. 2000. “Testate Amoebae in the Neoproterozoic Era: Evidence from Vase-Shaped Microfossils in the Chuar Group, Grand Canyon.” *Paleobiology* 26 (3): 360–85. doi:10.1666/0094-8373(2000)026<0360:TAITNE>2.0.CO;2.

Porter, Susannah M., Heda Agić, and Leigh Anne Riedman. 2018. “Anoxic Ecosystems and Early Eukaryotes.” *Emerging Topics in Life Sciences*, no. July: ETLS20170162. doi:10.1042/ETLS20170162.

Porter, Susannah M. and, and Leigh Anne Riedman. 2016. “Systematics of Organic-Walled Microfossils from the ca. 780–740 Ma Chuar Group, Grand Canyon, Arizona.” *Journal of Paleontology* 90 (05): 815–53. doi:10.1017/jpa.2016.57.

Poulton, S.W. and Raiswell, R. 2002. “THE LOW-TEMPERATURE GEOCHEMICAL CYCLE OF IRON: FROM CONTINENTAL FLUXES TO MARINE SEDIMENT DEPOSITION.” *American Journal of Science* 302: 774–805.

Poulton, S.W. Fralick, P.W. & Canfield, D.E. 2004. “The Transition to a Sulphidic Ocean 1.84 Billion Years Ago.” *Nature* 431: 173–77.

Poulton, Simon W., and Donald E. Canfield. 2005. “Development of a Sequential Extraction Procedure for Iron: Implications for Iron Partitioning in Continentally Derived Particulates.” *Chemical Geology* 214 (3–4): 209–21. doi:10.1016/j.chemgeo.2004.09.003.

———. 2011. “Ferruginous Conditions: A Dominant Feature of the Ocean through Earth’s History.” *Elements* 7 (2): 107–12. doi:10.2113/gselements.7.2.107.

Poulton, Simon W., Philip W. Fralick, and Donald E. Canfield. 2010. “Spatial Variability in Oceanic Redox Structure 1.8 Billion Years Ago.” *Nature Geoscience* 3 (7). Nature Publishing Group: 486–90. doi:10.1038/ngeo889.

Pyatiletov, V.G. 1980. “O Nakhodkakh Mikrofossiliy Roda Navifusa v Lakhandinskoy Svite.” *Paleontologichesky Zhurnal* 3: 143–45.

———. 1988. “Mikrofossili Pozdnego Dokembriya Uchuro-Mayskogo Rayona.” In *Khomentovskiy et Al. (Eds.), Pozdniy Dokembriy i Ranniy Paleozoy Sibiri, Rifey i Vend. Sbornik Nauchnyky Trudov, Akademiya Nauk SSSR, Sibirskoye Otdelenie*, 47–104. Novosibirsk.

Raiswell, R. and Canfield, D.E. 1998. “Sources of Iron for Pyrite Formation in Marine Sediments.” *American Journal of Science* 298: 219–45.

Raiswell, R., R. Newton, and P.B. Wignall. 2001. “An Indicator of Water-Column Anoxia: Resolution of Biofacies Variations in the Kimmeridge Clay (Upper Jurassic, U.K.).” *Journal of Sedimentary Research* 71 (2): 286–94. doi:10.1306/070300710286.

Raiswell, Rob, Dalton S. Hardisty, Timothy W. Lyons, Donald E. Canfield, Jeremy D. Owens, Noah J. Planavsky, Simon W. Poulton, and Christopher T. Reinhard. 2018. “The Iron Paleoredox Proxies: A Guide to the Pitfalls, Problems and Proper Practice.” *American Journal of Science* 318 (5): 491–526. doi:10.2475/05.2018.03.

Ramkumar, Mu. 2015. “Toward Standardization of Terminologies and Recognition of Chemostratigraphy as a Formal Stratigraphic Method.” In *Chemostratigraphy: Concepts, Techniques, and Applications*, 1–21. Elsevier Inc. doi:10.1016/B978-0-12-419968-2.00001-7.

Rasmussen, Birger, Ian R Fletcher, Jochen J Brocks, and Matt R Kilburn. 2008. “Reassessing the First Appearance of Eukaryotes and Cyanobacteria.” *Nature* 455 (7216): 1101–4. doi:10.1038/nature07381.

Raucq Paul. 1957. “Contribution à La Connaissance Du Système de La Bushimay (Congo Belge).” Sciences géologiques, Vol. 18. Annales du. In-8. Tervuren (Belgique).

———. 1970. “Nouvelles Acquisitions Sur Le Système de La Bushimay.” Sciences

géologiques n° 69. In-8. Tervuren (Belgique).

Reinhard, C. T., N. J. Planavsky, L. J. Robbins, C. A. Partin, B. C. Gill, S. V. Lalonde, A. Bekker, K. O. Konhauser, and T. W. Lyons. 2013. "Proterozoic Ocean Redox and Biogeochemical Stasis." *Proceedings of the National Academy of Sciences* 110 (14): 5357–62. doi:10.1073/pnas.1208622110.

Reinhard, Christopher T., Noah J. Planavsky, Stephanie L. Olson, Timothy W. Lyons, and Douglas H. Erwin. 2016. "Earth's Oxygen Cycle and the Evolution of Animal Life." *Proceedings of the National Academy of Sciences* 113 (32): 8933–38. doi:10.1073/pnas.1521544113.

Reitlinger, E. A. 1948. "Cambrian Foraminifera of Yakutia." *Bulletin of Moscow Nature Investigators Society, Geological Section* 23 (2): 77–81.

Riediger, C. L. 1993. "Solid Bitumen Reflectance and Rock-Eval Tmaxas Maturation Indices: An Example from the 'Nordegg Member', Western Canada Sedimentary Basin." *International Journal of Coal Geology* 22 (3–4): 295–315. doi:10.1016/0166-5162(93)90031-5.

Riedman, L. a., S. M. Porter, G. P. Halverson, M. T. Hurtgen, and C. K. Junium. 2014. "Organic-Walled Microfossil Assemblages from Glacial and Interglacial Neoproterozoic Units of Australia and Svalbard." *Geology* 42 (11): 1011–14. doi:10.1130/G35901.1.

Riedman, Leigh Anne, and Peter M. Sadler. 2017. "Global Species Richness Record and Biostratigraphic Potential of Early to Middle Neoproterozoic Eukaryote Fossils." *Precambrian Research*, no. May. Elsevier: 0–1. doi:10.1016/j.precamres.2017.10.008.

Rosenbaum, J, and S.M.F Sheppard. 1986. "An Isotopic Study of Siderites, Dolomites and Ankerites at High Temperatures." *Geochimica et Cosmochimica Acta* 50 (6). Pergamon: 1147–50. doi:10.1016/0016-7037(86)90396-0.

Rosing, M.T. 1999. "13C-Depleted Carbon Microparticles in >3700-Ma Sea-Floor Sedimentary Rocks from West Greenland." *Science* 283: 674–76.

Rouxel, O.J, Bekker, A. and Edwards, K.J. 2005. "Paleoproterozoic Ocean Redox State Iron Isotope Constraints on the Archean and Paleoproterozoic Ocean Redox State." *Science* 307: 1088–91. doi:10.1126/science.1105692.

Rouxel, Olivier, Wayne C. Shanks, Wolfgang Bach, and Katrina J. Edwards. 2008. "Integrated Fe- and S-Isotope Study of Seafloor Hydrothermal Vents at East Pacific Rise 9-10°N." *Chemical Geology* 252 (3–4): 214–27. doi:10.1016/j.chemgeo.2008.03.009.

Rouxel, Olivier, Edward Sholkovitz, Matthew Charette, and Katrina J. Edwards. 2008. "Iron Isotope Fractionation in Subterranean Estuaries." *Geochimica et Cosmochimica Acta* 72 (14): 3413–30. doi:10.1016/j.gca.2008.05.001.

Russel, M.J. & Arndt, N.T. 2005. "Geodynamic and Metabolic Cycles in the Hadean." *Biogeosciences* 2: 97–111.

Ryder, Graham. 2003. "Bombardment of the Hadean Earth: Wholesome or Deleterious?" *Astrobiology* 3 (1): 3–6.

Sachse, Victoria F., Damien Delvaux, and Ralf Littke. 2012. "Petrological and Geochemical Investigations of Potential Source Rocks of the Central Congo Basin, Democratic Republic of Congo." *AAPG Bulletin* 96 (2): 245–75. doi:10.1306/07121111028.

Samuelsson, Joakim, and Nicholas J Butterfield. 2001. “Neoproterozoic Fossils from the Franklin Mountains, Northwestern Canada: Stratigraphic and Palaeobiological Implications.” *Precambrian Research* 107 (3–4): 235–51.

Sansjofre, P., Ader, M., R.I.F. Trindade, Cartigny Elie, M., Lyons, J., and A.C.R. P. and Nogueira. 2011. “A Carbon Isotope Challenge to the Snowball Earth.” *Nature* 478: 93–96.

Sauerer, Bastian, Paul R. Craddock, Mohammed D. AlJohani, Khalid L. Alsamadony, and Wael Abdallah. 2017. “Fast and Accurate Shale Maturity Determination by Raman Spectroscopy Measurement with Minimal Sample Preparation.” *International Journal of Coal Geology* 173. Elsevier B.V: 150–57. doi:10.1016/j.coal.2017.02.008.

Schidlowski, M. and Aharon, P. 1992. “Carbon Cycle and Carbon Isotope Record: Geochemical Impact of Life over 3.8 Ga of Earth History.” In *Early Organic Evolution*, edited by Trudinger P.A. (eds) Schidlowski M., Golubic S., Kimberley M.M., McKirdy D.M., 147–75. Springer, Berlin, Heidelberg. doi:doi.org/10.1007/978-3-642-76884-2_11.

Schito, Andrea, Claudia Romano, Sveva Corrado, Domenico Grigo, and Brent Poe. 2017. “Diagenetic Thermal Evolution of Organic Matter by Raman Spectroscopy.” *Organic Geochemistry* 106. Elsevier Ltd: 57–67. doi:10.1016/j.orggeochem.2016.12.006.

Schmidt, J. S., R. Hinrichs, and C. V. Araujo. 2017. “Maturity Estimation of Phytoclasts in Strew Mounts by Micro-Raman Spectroscopy.” *International Journal of Coal Geology* 173 (2016). Elsevier B.V: 1–8. doi:10.1016/j.coal.2017.02.003.

Schneider, D.A., Bickford, M.E., Cannon, W.F., Schulz, K.J. and Hamilton, M.A. 2002. “Age of Volcanic Rocks and Syndepositional Iron Formations, Marquette Range Supergroup: Implications for the Tectonic Setting of Paleoproterozoic Iron Formations of the Lake Superior Region.” *Canadian Journal of Earth Sciences* 39: 999–1012.

Schopf, J.W. and Packer, B.M. 1987. “Early Archean (3.3-Billion to 3.5-Billion-Year-Old) Microfossiles from Warrawoona Group, Australia.” *Science* 237: 70–73.

Schopf, J. W. 1993. “Microfossils of the EarlyArchean Apex Chert: New Evidence of the Antiquity of Life.” *Science* 260: 640–46.

Schopf, J. William. 1968. “Microflora of the Bitter Springs Formation, Late Precambrian, Central Australia.” *Journal of Paleontology* 42 (3): 651–88.

Scott, C., T. W. Lyons, A. Bekker, Y. Shen, S. W. Poulton, X. Chu, and A. D. Anbar. 2008. “Tracing the Stepwise Oxygenation of the Proterozoic Ocean.” *Nature* 452 (7186): 456–59. doi:10.1038/nature06811.

Sergeev, V. N. 2009. “The Distribution of Microfossil Assemblages in Proterozoic Rocks.” *Precambrian Research* 173: 212–22. doi:10.1016/j.precamres.2009.04.002.

Sergeev, Vladimir N, Andrew H Knoll, and Natalya G Vorob Eva. 2011. “Ediacaran Microfossils from the Ura Formation, Baikal-Patom Uplift, Siberia: Taxonomy and Biostratigraphic Significance.” *Journal of Paleontology* 85 (5): 987–1011.

Sergeev, Vladimir N, and J William Schopf. 2010. “Taxonomy, Paleoecology and Biostratigraphy of the Late Neoproterozoic Chichkan Microbiota of South Kazakhstan : The Marine Biosphere on the Eve of Metazoan Radiation.” *Journal of Paleontology* 84 (3): 363–401.

Severmann, S., C. M. Johnson, B. L. Beard, C. R. German, H. N. Edmonds, H. Chiba, and D. R.H. Green. 2004. "The Effect of Plume Processes on the Fe Isotope Composition of Hydrothermally Derived Fe in the Deep Ocean as Inferred from the Rainbow Vent Site, Mid-Atlantic Ridge, 36°14′N." *Earth and Planetary Science Letters* 225 (1–2): 63–76. doi:10.1016/j.epsl.2004.06.001.

Sharma, Mukund, and Yogmaya Shukla. 2009. "Taxonomy and Affinity of Early Mesoproterozoic Megascopic Helically Coiled and Related Fossils from the Rohtas Formation, the Vindhyan Supergroup, India." *Precambrian Research* 173 (1–4). Elsevier B.V.: 105–22. http://www.sciencedirect.com/science/article/pii/S0301926809001120.

Shen, Yanan, Andrew H Knoll, and Malcolm R Walter. 2003. "Evidence for Low Sulphate and Anoxia in a Mid-Proterozoic Marine Basin" 423 (June): 632–35. doi:10.1038/nature01663.1.

Shen, Yanan, Tonggang Zhang, and Paul F Hoffman. 2008. "On the Coevolution of Ediacaran Oceans and Animals." *Proceedings of the National Academy of Sciences of the United States of America* 105 (21): 7376–81. doi:10.1073/pnas.0802168105.

Shepeleva, E. D. 1960. "Nakhodki Sinezelenykh Vodoroslej v Nizhnekembrijskikh Otlozheniyakh Leningradskoj Oblasti." In *Problemy Neftyanoj Geologii i Voprosy Metodiki Laboratornykh Issledovanij*, Nauka, 170–72. Moscow.

———. 1974. "Stratigraficheskoe Raschlenenie Vendskikh Otlozheniy Tzentralnyky Rayonov Russkoy Platformy Po Akritarkham." In *Vozzhennikova, T.F., Timofeev, B.V. and Sheshegova, L.I. (Eds), Mikrofossili SSSR. Transactions of the Instute of Geology and Geophysics, Issue 81, Nauka, Siberian Branch, Novosibirsk*, 13–23.

Siebert, Christopher, thomas F Nagler, and Jan D Kramers. 2001. "Determination of Mo Isotope Fractionation by Double-Spike Multicollector Inductively Coupled Plasma Mass Spectrometry." *Geochemistry Geophysics Geosystems* 2: 2000GC000124. doi:http://dx.doi.org/10.1029/2000GC000124.

Simonetti, C. and, and Thomas R Fairchild. 2000. "Proterozoic Microfossils from Subsurface Siliciclastic Rocks of the São Francisco Craton, South-Central Brazil." *Precambrian Research* 103 (1–2): 1–29. http://www.sciencedirect.com/science/article/pii/S0301926800000711.

Simpson, E.H. 1949. "Measurement of Diversity." *Nature* 163: 688.

Spang, Anja, Jimmy H. Saw, Steffen L. Jørgensen, Katarzyna Zaremba-Niedzwiedzka, Joran Martijn, Anders E. Lind, Roel Van Eijk, Christa Schleper, Lionel Guy, and Thijs J.G. Ettema. 2015. "Complex Archaea That Bridge the Gap between Prokaryotes and Eukaryotes." *Nature* 521 (7551): 173–79. doi:10.1038/nature14447.

Srivastava, Purnima. 2009. "Trachyhystrichosphaera : An Age-Marker Acanthomorph from the Bhander Group , Upper Vindhyan , Rajasthan," no. 5: 575–82.

Stern, R.A. and Bleeker, W. 1998. "Age of the World's Oldest Rocks Refined Using Canada's SHRIMP: The Acasta Gneiss Complex, Northwest Territories, Canada." *Geoscience Canada* 25 (1): 27–31.

Sugitani, Kenichiro, Kevin Lepot, Tsutomu Nagaoka, Koichi Mimura, Martin Van Kranendonk, Dorothy Z Oehler, and Malcolm R Walter. 2010. "Biogenicity of Morphologically Diverse Carbonaceous Microstructures from the ca. 3400 Ma Strelley

Pool Formation, in the Pilbara Craton, Western Australia." *Astrobiology* 10 (9): 899–920. doi:10.1089/ast.2010.0513.

Summons, Roger E, Alexander S Bradley, Linda L Jahnke, and Jacob R Waldbauer. 2006. "Steroids, Triterpenoids and Molecular Oxygen." *Philosophical Transactions of the Royal Society of London. Series B, Biological Sciences* 361 (1470): 951–68. doi:10.1098/rstb.2006.1837.

Swanson-Hysell, N. L., a. C. Maloof, D. J. Condon, G. R. T. Jenkin, M. Alene, M. M. Tremblay, T. Tesema, a. D. Rooney, and B. Haileab. 2015. "Stratigraphy and Geochronology of the Tambien Group, Ethiopia: Evidence for Globally Synchronous Carbon Isotope Change in the Neoproterozoic." *Geology* 43 (4): 1–4. doi:10.1130/G36347.1.

Tack, Luc, Franck Delpomdor, Valentin Kanda Nkula, and Alain Préat. 2010. "The Neoproterozoic West Congo and Katanga Supergroups : Similarites and Differences," 76–82.

Tang, H. and Chen, Y. 2013. "Global Glaciations and Atmospheric Change at ca. 2.3 Ga." *Geoscience Frontiers* 4: 583–96.

Tang, Qing, Nigel C. Hughes, N. Ryan McKenzie, Paul M. Myrow, and Shuhai Xiao. 2017. "Late Mesoproterozoic – Early Neoproterozoic Organic-Walled Microfossils from the Madhubani Group of the Ganga Valley, Northern India." *Palaeontology* 60 (6): 869–91. doi:10.1111/pala.12323.

Tang, Qing, Ke Pang, Shuhai Xiao, Xunlai Yuan, Zhiji Ou, and Bin Wan. 2013. "Organic-Walled Microfossils from the Early Neoproterozoic Liulaobei Formation in the Huainan Region of North China and Their Biostratigraphic Significance." *Precambrian Research* 236 (0): 157–81. http://www.sciencedirect.com/science/article/pii/S0301926813002301.

Tang, Qing, Ke Pang, Xunlai Yuan, Bin Wan, and Shuhai Xiao. 2015. "Organic-Walled Microfossils from the Tonian Gouhou Formation, Huaibei Region, North China Craton, and Their Biostratigraphic Implications." *Precambrian Research*. Elsevier B.V. doi:10.1016/j.precamres.2015.05.025.

Thomazo, Christophe, M. Ader, J. Farquhar, and P. Philippot. 2009. "Methanotrophs Regulated Atmospheric Sulfur Isotope Anomalies during the Mesoarchean (Tumbiana Formation, Western Australia)." *Earth and Planetary Science Letters* 279 (1–2). Elsevier B.V.: 65–75. doi:10.1016/j.epsl.2008.12.036.

Tice, Michael M, and Donald R Lowe. 2004. "Photosynthetic Microbial Mats in the 3 , 416-Myr-Old Ocean Fluorescence at the Geoanalytical Laboratory , Washington State University (Pullman ," 431 (September): 549–52. doi:10.1038/nature02920.1.

Timofeev, B.V., Hermann, T.N. and Mikhailova, N.S. 1976. *Microphytofossils from the Precambrian, Cambrian and Ordovician*. Nauka, Leningrad. [in Russian].

Timofeev, B.V. and Hermann, T.N. 1979. "Precambrian Microbiota of the Lakhanda Formation." In *Sokolov, B.S. (Ed.): Paleontology of the Precambrian and Early Cambrian. Nauka, Leningrad,* 137–147. [in Russian].

Timofeev, B.V. 1959. *Drevneyshaya Flora Pribaltiki i Ee Stratigraficheskoe Znachenie.* Vol. 129. Trudy Vesesoyuznogo Neftyanogo Nauchno-Issledovatel'skogo Geologorazvedochnogo Instituta (VNIGRI).

———. 1966. *Micropaleophytological Investigations of Ancient Suites*. Nauka. Moscow. [In Russian].

Trail, D., Mojzsis, S.J. & Harrison, T.M. 2007. "Thermal Events Documented in Hadean Zircons by Ion Microprobe Depth Profiles." *Geochimica et Cosmochimica Acta* 71: 4044–65.

Tribovillard, N., T. J. Algeo, F. Baudin, and A. Riboulleau. 2012. "Analysis of Marine Environmental Conditions Based Onmolybdenum-Uranium Covariation-Applications to Mesozoic Paleoceanography." *Chemical Geology* 324–325. Elsevier B.V.: 46–58. doi:10.1016/j.chemgeo.2011.09.009.

Tribovillard, Nicolas, Thomas J. Algeo, Timothy Lyons, and Armelle Riboulleau. 2006. "Trace Metals as Paleoredox and Paleoproductivity Proxies: An Update." *Chemical Geology* 232 (1–2): 12–32. doi:10.1016/j.chemgeo.2006.02.012.

Tynni, R. and J. Donner. 1980. "A Microfossil and Sedimentation Study of the Late Precambrian Formation of Hailuoto, Finland." *Geological Survey of Finland, Bulletin 311*, 27.

Tyson, R.V. 1995. *Sedimentary Organic Matter: Organic Facies and Palynofacies*. Edited by Richard V. Tyson. London: Chapman & Hall. doi:10.1007/978-94-011-0739-6.

Valley, J. W., Lackey, J.S., Cavoise, A.J., Clechenko, C.C., Spicuzza, M.J., Basei, M.A.S., Bindeman, I.N., Ferreira, V.P., Sial, A.N., King, E.M., Peck, W.H., Sinha, A.K. & Wei, C.S. 2005. "4.4 Billion Years of Crustal Maturation: Oxygen Isotope Ratios of Magmatic Zircon." *Contrib Mineral Petrol* 150: 561–80.

Valley, J.W., Cavoise, A.J., Ushikubo, T., D.A. Reinhard, D.F. Lawrence, D.J. Larson, P.H Clifton, T.F. Kelly, S.A. Wilde, D.E. Moser, and M.J. and Spicuzza. 2014. "Hadean Age for a Post-Magma-Ocean Zircon Confirmed by Atom-Probe Tomography." *Nature Geoscience* 7: 219–23.

Van Kranendonk, M.J., Contributors:Altermann, W., Beard, B.L., Hoffman, P.F., Johnson, C.M., Kasting, J.F., Melezhik, V.A., Nutman, A.P., Papineau, D. and Pirajno, F. 2012. "A Chronostratigraphic Division of the Precambrian: Possibilities and Challenges." In *The Geologic Time Scale*, 299–392. Elsevier. doi:doi.org/10.1016/B978-0-444-59425-9.00016-0.

van Loon, A.J. 2007. "The Nature of Mawsonites (Ediacara Fauna)." *Gondwana Research* 14: 175–82.

Van Zuilen, M.A., Lepland, A. and, and G. Arrhenius. 2002. "Reassessing the Evidence for the Earliest Traces of Life." *Nature* 418 (6898): 627–30. doi:10.1038/nature00934.

Veis, A. F., N. G. Vorob'eva, and E. Yu. Golubkova. 2006. "The Early Vendian Microfossils First Found in the Russian Plate: Taxonomic Composition and Biostratigraphic Significance." *Stratigraphy and Geological Correlation* 14 (4): 368–85.

Veizer, Ján, K. A. Plumb, R. N. Clayton, R. W. Hinton, and J. P. Grotzinger. 1992. "Geochemistry of Precambrian Carbonates: V. Late Paleoproterozoic Seawater." *Geochimica et Cosmochimica Acta* 56 (6): 2487–2501. doi:10.1016/0016-7037(92)90204-V.

Vidal, Gonzalo. 1976. "Late Precambrian Microfossils from the Visingsö Beds in Southern Sweden." *Fossils and Strata* 9: 57.

Vidal, Gonzalo, and Andrew H Knoll. 1983. “Proterozoic Plankton.” *Geological Society of America Memoirs* 161: 265–78. http://memoirs.gsapubs.org/content/161/265.abstract.

Vorob’eva, N. G., V. N. Sergeev, and A. H. Knoll. 2009. “Neoproterozoic Microfossils from the Margin of the East European Platform and the Search for a Biostratigraphic Model of Lower Ediacaran Rocks.” *Precambrian Research* 173 (1–4): 163–69. doi:10.1016/j.precamres.2009.04.001.

Vorob’eva, Natalya G., Vladimir N. Sergeev, and Peter Yu. Petrov. 2015. “Kotuikan Formation Assemblage: A Diverse Organic-Walled Microbiota in the Mesoproterozoic Anabar Succession, Northern Siberia.” *Precambrian Research* 256. Elsevier B.V.: 201–22. doi:10.1016/j.precamres.2014.11.011.

Wacey, David, Martin Saunders, and Charlie Kong. 2018. “Remarkably Preserved Tephra from the 3430 Ma Strelley Pool Formation, Western Australia: Implications for the Interpretation of Precambrian Microfossils.” *Earth and Planetary Science Letters* 487 (April). Elsevier: 33–43. doi:10.1016/J.EPSL.2018.01.021.

Waldbauer, Jacob R., Laura S. Sherman, Dawn Y. Sumner, and Roger E. Summons. 2009. “Late Archean Molecular Fossils from the Transvaal Supergroup Record the Antiquity of Microbial Diversity and Aerobiosis.” *Precambrian Research* 169 (1–4). Elsevier B.V.: 28–47. doi:10.1016/j.precamres.2008.10.011.

Waldbauer, Jacob R, Dianne K Newman, and Roger E Summons. 2011. “Microaerobic Steroid Biosynthesis and the Molecular Fossil Record of Archean Life.” *Proceedings of the National Academy of Sciences of the United States of America* 108 (33): 13409–14. doi:10.1073/pnas.1104160108.

Wedepohl, K. H. 1971. “Environmental Influences on the Chemical Composition of Shales and Clays.” *Physics and Chemistry of the Earth* 8 (C): 305–33. doi:10.1016/0079-1946(71)90020-6.

Westall, Frances, Cornel E J de Ronde, Gordon Southam, Nathalie Grassineau, Maggy Colas, Charles Cockell, and Helmut Lammer. 2006. “Implications of a 3.472-3.333 Gyr-Old Subaerial Microbial Mat from the Barberton Greenstone Belt, South Africa for the UV Environmental Conditions on the Early Earth.” *Philosophical Transactions of the Royal Society of London. Series B, Biological Sciences* 361 (1474): 1857–75. doi:10.1098/rstb.2006.1896.

Wilde, Simon A., John W. Valley, William H. Peck, and Colin M. & Graham. 2001. “Evidence from Detrital Zircons for the Existence of Continental Crust and Oceans on the Earth 4.4 Gyr Ago.” *Nature* 409: 175–78.

Willman, Sebastian, and Małgorzata Moczydłowska. 2008. “Ediacaran Acritarch Biota from the Giles 1 Drillhole, Officer Basin, Australia, and Its Potential for Biostratigraphic Correlation.” *Precambrian Research* 162 (3–4): 498–530. doi:10.1016/j.precamres.2007.10.010.

Willman, Sebastian, Małgorzata Moczydłowska, and Kathleen Grey. 2006. “Neoproterozoic (Ediacaran) Diversification of Acritarchs—A New Record from the Murnaroo 1 Drillcore, Eastern Officer Basin, Australia.” *Review of Palaeobotany and Palynology* 139 (1–4): 17–39. doi:10.1016/j.revpalbo.2005.07.014.

Woese, C. R., O. Kandler, and M. L. Wheelis. 1990. “Towards a Natural System of Organisms: Proposal for the Domains Archaea, Bacteria, and Eucarya.” *Proceedings of*

the National Academy of Sciences 87 (12): 4576–79. doi:10.1073/pnas.87.12.4576.

Wood, B.J &Halliday, A.N. 2005. “Cooling of the Earth and Core Formation after the Giant Impact.” *Nature* 437: 1345–48.

Xiao, Shuhai, and L I N Dong. 2006. “On the Morphological and Ecological History of Proterozoic Macroalgae,” 57–90.

Xiao, Shuhai, and Qing Tang. 2018. “After the Boring Billion and before the Freezing Millions: Evolutionary Patterns and Innovations in the Tonian Period.” *Emerging Topics in Life Sciences*, ETLS20170165. doi:10.1042/ETLS20170165.

Yankauskas, T.V., Mikhaylova, N.S. and German, T.N. 1989. *Precambrian Microfossils of the USSR*. Nauka. Leningrad [in Russian].

Yankauskas, T.V. 1980. “On the Micropaleontological Characteristics of the Middle and Upper Cambrian in the Northwest of the East European Platform.” *Izvestiya Akademiya Nauk Estonskoyi SSSR, Geology* 19 (4): 131–135. [in Russian].

———. 1982. “Mikrofossilii Rifeya Yuzhnogo Urala.” In *B. M. Kelleri (Ed.): Stratotyp Rifeya-Paleontologiya Paleomagnetism. Akademiya Nauk SSSR*, 84–120 [in Russian].

Yin, L.M. and Li, Z. 1978. “Precambrian Microfloras of Southwest China, with Reference to Their Stratigraohic Significance.” *Geol. Palaeontol.* 10: 41–102. [in chinese].

Zang, Wen-long. 1995. “Early Neoproterozoic Sequence Stratigraphy and Acritarch Biostratigraphy, Eastern Officer Basin, South Australia.” *Precambrian Research* 74: 119–75.

ANNEXES